

Satellite-based monitoring of environmental related factors affecting rural livelihoods, food security, and health risks in Africa



Dissertation an der Fakultät für Biologie
der Ludwig-Maximilians-Universität München

vorgelegt von
Maximilian Schwarz

München, 17. Oktober 2022

Erstgutachter: Prof. Dr. Florian Siegert

Zweitgutachterin: Prof. Dr. Silke Werth

Tag der Abgabe: 17. Oktober 2022

Tag der mündlichen Prüfung: 25. Januar 2023

ACKNOWLEDGEMENTS

I would like to thank Prof. Dr. Florian Siegert for allowing me to realize the dissertation at hand at the Remote Sensing Solutions GmbH, Munich. As my supervisor, Prof. Dr. Siegert supported me and provided helpful ideas and thoughts to my work. I would also like to thank Dr. Jonas Franke, with who I closely worked on many projects. Thank you for being able to take part in all these different, interesting projects and for all your support, guidance, insights, and motivation. Even though it was not always easy during the Covid-19 pandemic, I want to thank both of you for the opportunities to visit and speak at conferences and for being able to participate in business trips.

I thank Prof. Dr. Karl-Friedrich Wetzel very much for his support during my Master's degree, for being part of my TAC, and for motivating me to graduate. I am thankful that Prof. Dr. Silke Werth agreed on being the second referee of my thesis and also for being part of my TAC and her support and valuable opinions.

Furthermore, I would like to express my gratitude to my colleagues and former colleagues Anna, Tobi, Yannic, Abhi, Liz, Natalie, Helle, Isabel, Werner, Anna, Sandra, Kevin, and Stefan for being always helpful and supportive. Thank you all for being part of my time at RSS and for the good working environment. Especially, I would like to thank Anna, Sandra, Tobi, and Jonas, who were always helpful from the beginning. Thanks for the motivation to graduate, for all the proofreading, and for answering all my questions regardless of whether they were of scientific or non-scientific nature. Thank you all for accompanying me through this whole time.

I also want to thank all my partners in the various research projects that I worked in. It was a pleasure to work with and learn from you.

This dissertation would not have been possible without my family and friends. I want to thank my family for believing in me and supporting me during all the years of my studies. Thank you to all my friends, who accompanied me during my doctoral studies. Very special thanks to my girlfriend Janine for her support and especially her patience with me.

ABSTRACT

Increasingly frequent extreme weather and climate events, such as droughts or floods, represent one of the greatest global risks of the future. They have already led to acute food insecurity and water shortages. While droughts occur more frequently and also expand in area, strong inter-annual fluctuations in precipitation and more frequent extreme precipitation can occur. Africa is severely affected by the impacts of climate change, both on its environment and population. Examples range from lower agricultural yields, livestock health to malnutrition among the most vulnerable population. In this regard, rural households are more vulnerable and thus more affected by the impacts of climate change. They are heavily dependent on natural resources such as water and land. Most rural African communities depend on yields from rain-fed agriculture, while agriculture is one of Africa's most important economic sectors, accounting for more than half of the continent's gross domestic product. Not only have negative impacts of climate change already been identified in the past, but they are equally projected into the future. Communities in arid and semi-arid areas in sub-Saharan Africa are particularly vulnerable, where lower yields reflect one of the main causes of food shortages and malnutrition. Similarly, transhumance with its seasonally migrating pastoralists is directly affected by the increasing climatic variability. Herders with their livestock are dependent on natural resources such as water and pasture and thus highly vulnerable to droughts. A correlation between droughts and livestock deaths has been noted in the past. Armed conflicts between local smallholder farmers and pastoralists over natural resources, which are further exacerbated by drought-induced water scarcity, represent an already increasing risk.

These climate change related risks and their impacts highlight the need for large-scale monitoring of the environmental aspects in support of local communities. In this regard, remote sensing with its recent technological advances, mainly through high-resolution data with shorter revisit cycles of satellites and global data availability, plays a crucial role.

This thesis investigates how Earth Observation can be used to assess risks to food security, health, and livelihoods from different perspectives. Droughts, surface water availability, and analyses of transhumance and smallholder farmers are discussed. In my first paper, a spatially transferable drought model to detect regional drought conditions for rangelands and croplands is presented, reflecting local drought probability, vulnerability, and risk. Water is one of the most important natural resources for agriculture and transhumance, so reliable monitoring and detection of water surfaces is crucial. Another study therefore compared different surface water detection algorithms to

provide an assessment of their performances and to identify the most promising methods, including their limitations and advantages. In the third paper of my thesis, a monitoring system for the environmental suitability of transhumance is presented. A conceptual framework was created to support prevention and mitigation of conflicts between pastoralists and local farmers and to better plan and manage transhumance. In addition, a remote sensing-based crop yield model at the field level was developed as presented in my last paper. The high-resolution crop yield estimates show variability within and between individual fields and are based on a unique three-year training dataset. The study provides important results for public health studies and adaptation options.

Overall, this work has developed, tested and demonstrated satellite-based monitoring systems that support livelihoods, through analyzing aspects of food security among local populations and environmental resources in Africa. It highlights potential decision support tools for policy makers and it demonstrates how satellite data can be linked and effectively being used for multiple applications in the future.

ZUSAMMENFASSUNG

Die in ihrer Häufigkeit steigenden extremen Wetter- und Klimaereignisse wie Dürren oder Überflutungen stellen global eines der größten Risiken der Zukunft dar. Sie führten bereits zu akuter Ernährungsunsicherheit und Wasserknappheit. Während Dürren häufiger auftreten werden und sich auch flächenmäßig ausdehnen, treten starke zwischenjährliche Schwankungen des Niederschlags und häufigere Extremniederschläge auf. Große Teile Afrikas sind dabei besonders von den Auswirkungen des Klimawandels auf seine Umwelt und Bevölkerung betroffen. Beispiele führen von geringeren Erträgen in der Landwirtschaft, über die Gesundheit der Nutztiere zu Unterernährung in der Bevölkerung. Dabei sind ländliche Haushalte anfälliger und somit stärker von den Auswirkungen des Klimawandels betroffen. Sie sind stark abhängig von natürlichen Ressourcen wie Wasser und Land und in hohem Maße von Erträgen des Regenfeldbaus abhängig. Landwirtschaft ist einer der wichtigsten wirtschaftlichen Sektoren Afrikas und stellt mehr als die Hälfte des mittleren Bruttoinlandproduktes des Kontinents dar. Dabei wurden nicht nur bereits in der Vergangenheit negative Auswirkungen des Klimawandels festgestellt, sondern sie werden auch gleichermaßen in die Zukunft prognostiziert. Dabei sind speziell Bevölkerungsgruppen in ariden und semiariden Gebieten in Sub-Sahara Afrika betroffen, wo niedrigere Erträge einen der Hauptgründe für Nahrungsknappheit und Unterernährung darstellen. Gleichermaßen ist die Transhumanz mit den saisonal migrierenden Hirten direkt von den Auswirkungen des Klimawandels betroffen, da sie hochgradig abhängig von natürlichen Ressourcen wie Wasser und Weideland sind. In der Vergangenheit wurde bereits eine Korrelation zwischen Dürren und Tiersterblichkeit festgestellt. Ein weiteres Risiko stellen bewaffnete Konflikte zwischen lokalen Kleinbauern und wandernden Pastoralisten dar, die um natürliche Ressourcen konkurrieren, was durch die von Dürren verursachte Wasserknappheit weiter verstärkt wird.

Die durch den Klimawandel verursachten Risiken und deren Auswirkungen auf die Lebensgrundlagen der Bevölkerung im ländlichen Afrika machen deutlich, dass ein großflächiges Monitoring umweltrelevanter Aspekte nötig ist. Dabei stellt die Fernerkundung zusammen mit ihren jüngsten technologischen Fortschritten ein wichtiges Instrument dar. Hoch aufgelöste Daten in hoher zeitlicher Frequenz und deren globale Verfügbarkeit spielen dabei eine entscheidende Rolle.

In dieser Arbeit sollen die betrachteten Risiken in Bezug auf Nahrungssicherung, Gesundheit und Lebensgrundlagen mittels Methoden der Erdbeobachtung betrachtet werden. Dabei stehen Dürren, die Verfügbarkeit von Oberflächenwasser und Analysen der Transhumanz sowie die landwirtschaftlichen Erträge von Kleinbauern im Fokus. In

meiner ersten Publikation, wird ein räumlich übertragbares Dürremodell zur Erkennung von regionalen Dürren vorgestellt, das die örtliche Dürrewahrscheinlichkeit, -vulnerabilität und das Dürrierisiko wiedergibt. Wasser ist eine der wichtigsten natürlichen Ressourcen für die Landwirtschaft und Transhumanz, weshalb ein zuverlässiges Monitoring und Erkennen von Wasserflächen von entscheidender Bedeutung ist. Daher wurden in einer weiteren Studie verschiedene Algorithmen zur Erkennung von Oberflächenwasser verglichen, um einen Überblick über deren Aussagekraft zu erhalten. Die dritte Publikation stellt ein Monitoringsystem der umweltbedingten Eignung für Transhumanz vor, welches ein Tool sowohl zur Unterstützung der Konfliktvorbeugung und -minderung als auch zur Planung und zum Management von Transhumanz darstellen kann. In der letzten hier vorgestellten Studie wurden Ernteertragsmodelle der Hauptfruchtarten für kleinste landwirtschaftliche Flächen entwickelt. Die hochaufgelösten Ernteertragsabschätzungen zeigen die teilschlagspezifische Variabilität sowie die Variabilität der Erträge zwischen verschiedenen Feldern, wobei die Modelle auf einem einzigartigen dreijährigen Trainingsdatensatz basieren. Die Studie liefert wichtige Ergebnisse für Studien der Ernährungssicherung, der Gesundheit und zu Anpassungsmöglichkeiten.

Insgesamt konnten in dieser Arbeit satellitenbasierte Monitoringsysteme entwickelt, getestet und demonstriert werden, die die Lebensgrundlagen der lokalen Bevölkerung verbessern können, da sie Aspekte der Ernährungssicherung und der natürlichen Ressourcen in Afrika beleuchten. Die Arbeit stellt neue Möglichkeiten potentieller Entscheidungshilfen für politische Entscheidungsträger vor und diskutiert wie Satellitendaten in Zukunft verknüpft werden und effektiv für mehrere Anwendungsbereiche genutzt werden können.

LIST OF ORIGINAL ARTICLES

CHAPTER I

Schwarz, M., Landmann, T., Cornish, N., Wetzel, K.-F., Siebert, S., Franke, J. (2020) A Spatially Transferable Drought Hazard and Drought Risk Modeling Approach Based on Remote Sensing Data. *Remote Sensing*, 12(2), 237. DOI: <https://doi.org/10.3390/rs12020237>

CHAPTER II

Schwarz, M., Landmann, T., Jusselme, D., Zambrano, E., Danzeglocke, J., Siegert, F., Franke, J. (2022) Assessing the Environmental Suitability for Transhumance in Support of Conflict Prevention in the Sahel. *Remote Sensing*, 14(5), 1109. DOI: <https://doi.org/10.3390/rs14051109>

CHAPTER III

Tottrup, C., Druce, D., Meyer, R.P., Christensen, M., Riffler, M., Dulleck, B., Rastner, P., Jupova, K., Sokoup, T., Haag, A., Cordeiro, M.C.R., Martinez, J.-M., Franke, J., **Schwarz, M.**, Vanthof, V., Liu, S., Zhou, H., Marzi, D., Rudiyanto, R., Thompson, M., Hiestermann, J., Alemohammad, H., Masse, A., Sannier, C., Wangchuk, S., Schumann, G., Giustarini, L., Hallowes, J., Markert, K., Paganini, M. (2022) Surface Water Dynamics from Space: A Round Robin Intercomparison of Using Optical and SAR High-Resolution Satellite Observations for Regional Surface Water Detection. *Remote Sensing*, 14(10), 2410. DOI: <https://doi.org/10.3390/rs14102410>

CHAPTER IV

Schwarz, M., Ouédraogo, A. W., Traoré, I., Müller, C., Sié, A., Barteit, S., Mank, I., Siegert, F., Sauerborn, R., Franke, J. (2022) Satellite-based multi-annual yield models for major food crops at the household field level for nutrition and health research: a case study from the Nouna HDSS, Burkina Faso. *International Journal of Applied Earth Observation and Geoinformation*. Manuscript submitted for publication.

CONTRIBUTION OF THE AUTHORS

CHAPTER I

Maximilian Schwarz, Dr. Tobias Landmann, Natalie Cornish, Prof. Dr. Karl-Friedrich Wetzel, and Dr. Jonas Franke conceived and designed the experiments. The methodology was designed by **Maximilian Schwarz**, Dr. Tobias Landmann, and Dr. Jonas Franke, while **Maximilian Schwarz** performed the data processing, experiments, and analysis of the data. **Maximilian Schwarz** performed the validation of the results and wrote the original paper draft. Dr. Tobias Landmann, Natalie Cornish, Prof. Dr. Karl-Friedrich Wetzel, Prof. Dr. Stefan Siebert, and Dr. Jonas Franke reviewed and edited the manuscript. The work was supervised by Prof. Dr. Karl-Friedrich Wetzel and Dr. Jonas Franke, while Prof. Dr. Stefan Siebert was in charge of the project administration.

CHAPTER II

Dr. Jonas Franke, Dr. Tobias Landmann, Jens Danzeglocke, and Damien Jusselme conceptualized the study. **Maximilian Schwarz** and Dr. Jonas Franke designed the methodology, while **Maximilian Schwarz** handled all software tasks. The formal analysis was done by **Maximilian Schwarz**, Prof. Dr. Florian Siegert, Damien Jusselme, and Eduardo Zambrano, while **Maximilian Schwarz** was in charge of the visualization. **Maximilian Schwarz** wrote the original paper draft and Dr. Jonas Franke, Dr. Tobias Landmann, Damien Jusselme, Jens Danzeglocke, Eduardo Zambrano and Prof. Dr. Florian Siegert reviewed and edited the manuscript. All authors discussed the results and provided critical feedback. The work was supervised by Prof. Dr. Florian Siegert and Dr. Jonas Franke. Dr. Jonas Franke also handled the project administration and the funding acquisition.

CHAPTER III

Christian Tottrup, Marc Paganini, and Mads Christensen conceptualized the study, Christian Tottrup and Tomas Sokoup designed the methodology, while Katerina Jupova, Rasmus Probst Meyer, and Christian Tottrup performed the validation of the results. The formal analysis and investigation were done by Daniel Druce, Dr. Micheal Riffer, Bjoern

Dulleck, Dr. Jonas Franke, **Maximilian Schwarz**, Dr. Sonam Wangchuk, Suxia Liu, Haowei Zhou, Dr. Guy Schumann, Dr. Laura Guistarini, Dr. Antoine Masse, Dr. Christophe Sannier, Victoria Vanthof, Arjen Haag, Kel Markert, Mauricio C. R. Cordeiro, Dr. Jean-Michel Martinez, David Marzi, Rudiyanto Rudiyanto, Mark Thompson, Dr. Hamed Alemohammad, Jens Hiestermann, and Jason Hallows. As this study exploits an intercomparison of different algorithms for surface water detection, all of these authors (or teams of authors) performed the same analysis with their methodology over different study sites. **Maximilian Schwarz** performed the formal analysis and investigation for our team, while Dr. Jonas Franke supervised the work. Data curation was done by Dr. Philipp Rastner and Rasmus Probst Meyer. The original draft was written by Christian Tottrup and Daniel Druce, while Dr. Jonas Franke, **Maximilian Schwarz**, Dr. Sonam Wangchuk, Suxia Liu, Haowei Zhou, Dr. Guy Schuman, Dr. Laura Guistarini, Dr. Antoine Masse, Dr. Christophe Sannier, Victoria Vanthof, Arjen Haag, Kel Markert, Mauricio C. R. Cordeiro, Dr. Jean-Michel Martinez, David Marzi, Rudiyanto Rudiyanto, Mark Thompson, Dr. Hamed Alemohammad, Jens Hiestermann, Jason Hallows, Mads Christensen and Marc Paganini reviewed and edited the manuscript. All authors discussed the results, provided critical feedback, and helped shape the research, analysis, and manuscript. The work was supervised by Christian Tottrup, while Christian Tottrup and Marc Paganini were in charge of the funding acquisition.

CHAPTER IV

Dr. Jonas Franke and Prof. Dr. Rainer Sauerborn conceptualized the study. Windpanga Aristide Ouédraogo, Dr. Issouf Traoré, and Isabel Mank did the investigation, prepared the field data protocol, and were in charge of the field sampling. The different datasets used were curated by **Maximilian Schwarz**, Windpanga Aristide Ouédraogo, Dr. Issouf Traoré, Dr. Sandra Barteit, and Isabel Mank. **Maximilian Schwarz** designed the methodology of the modeling approach and was in charge of software tasks and the formal analysis. **Maximilian Schwarz** also performed the validation, while the visualization was done by **Maximilian Schwarz**, Windpanga Aristide Ouédraogo, and Dr. Issouf Traoré. The original draft was written by **Maximilian Schwarz**, Windpanga Aristide Ouédraogo, Dr. Issouf Traoré and Charlotte Müller while Dr. Sandra Barteit, Isabel Mank, Prof. Dr. Florian Siegert, Prof. Dr. Rainer Sauerborn, and Dr. Jonas Franke

CONTRIBUTION OF THE AUTHORS

reviewed and edited the manuscript. The work was supervised by Alie Sié, Prof. Dr. Florian Siegert, Prof. Dr. Rainer Sauerborn, and Dr. Jonas Franke. Prof. Dr. Rainer Sauerborn was in charge of the project administration and the funding acquisition. All authors discussed the results and provided critical feedback to shape the research and the final manuscript.

I hereby confirm the above statements.

Munich,

Maximilian Schwarz

Prof. Dr. Florian Siegert

TABLE OF CONTENTS

ACKNOWLEDGEMENTS..... i

ABSTRACT.....iii

ZUSAMMENFASSUNG v

LIST OF ORIGINAL ARTICLES.....vii

CONTRIBUTION OF THE AUTHORSviii

TABLE OF CONTENTSxi

LIST OF FIGURES.....xiii

LIST OF ACRONYMSxiv

I. Introduction 1

 1. Climate change and its effects on livelihoods in Africa 1

 2. Droughts and water availability.....3

 2.1. Definition of droughts3

 2.2. Drought as a natural hazard4

 2.3. Drought risk and drought vulnerability.....6

 3. Transhumance.....7

 3.1. Definition and economic value in the Sahel region7

 3.2. Transhumance at risk9

 4. Small-scale and subsistence farming 11

 4.1. Definition and the economic value of smallholder farmers in Sub-Saharan Africa 11

 4.2. Risks for small-scale and subsistence farming 12

 5. Remote Sensing 14

 5.1. Introduction to remote sensing: History, definition, and basics 14

 5.2. Passive sensors (optical) and remote sensing of environmental factors 17

 5.3. Active systems (radar) and remote sensing of environmental factors 20

 5.4. Applications and remote sensing-based modeling.....23

 5.4.1. Droughts23

 5.4.2. Remote sensing for transhumance25

 5.4.3. Remote sensing-bases yield estimations at different scales27

 6. Objectives and structure of the thesis30

TABLE OF CONTENTS

II. Spatially transferable modeling framework for regional drought assessment in Southern Africa (Chapter I)	33
III. Environmental suitability for transhumance and conflict prevention (Chapter II) ...	57
IV. Intercomparison of satellite-based algorithms for regional surface water detection (Chapter III)	77
V. Multi-annual yield model at the field level for subsistence farming in Burkina Faso (Chapter IV)	99
VI. Synthesis	127
1. General Discussion	127
2. Future research	132
REFERENCES.....	cxxxv
STATEMENT AND DECLARATION OF HONOR	cli
CURRICULUM VITAE.....	clii

LIST OF FIGURES

Figure 1: Transhumance and nomadism in Sahelian countries (OECD/SWAC, 2014)....	8
Figure 2: Smallholder farmers in Ghana (FAO, 2021).....	12
Figure 3: The electromagnetic spectrum, including wavelength, energy, and a detailed excerpt of the visible subdivision (Verhoeven, 2017).....	15
Figure 4: Spectral characteristics of atmospheric transmittance and common remote sensing systems (Lillesand et al., 2015).	16
Figure 5: Spectral signatures of green vegetation, dry vegetation, and soil across the spectra measured by passive sensors (Maisongrande et al., 2007).	18
Figure 6: Exemplary false color Sentinel-2 image in Burkina Faso during the crop growing season (06.09.2021). Color representation: Red: SWIR, Green: NIR, Blue: Red. The black square in the inset represents the location of the image in Burkina Faso. Background: ESRI Basemaps.....	19
Figure 7: Exemplary preprocessed Sentinel-1 image in the border area of Chad, Cameroon and Nigeria during the wet season (19.09.2022). The black square in the inset represents the location of the image. Background: ESRI Basemaps.	21
Figure 8: Schematic overview of the different scattering mechanisms surface scattering, volume scattering, and double-bounce, arrows simulate directions of energy (Berninger, 2020).....	22

LIST OF ACRONYMS

ACLED	Armed Conflict Location and Events Data
ADCI	Agricultural dry condition index
APAR	Absorbed Photosynthetically Active Radiation
CAD	Canadian Dollar
CAR	The Central African Republic
CCI	Climate Change Initiative
CCKP	Climate Change Knowledge Portal
CDI-E	Combined Drought Indicator for Ethiopia
CFS	United Nations Committee on World Food Security
CHIRPS	Climate Hazards Group InfraRed Precipitation with Station data
CIRAD	French Agricultural Research Centre for International Development
CNN	Convolutional Neural Network
DEM	Digital Elevation Model
DSI	Drought Severity Index
DTM	Displacement Tracking Matrix
DVI	Drought Vulnerability Index
ECOWAS	Economic Community for West African States
EDM	Ensemble Distribution Modeling
EO	Earth observation
ESA	European Space Agency
EVI	Enhanced Vegetation Index
FAO(STAT)	Food and Agriculture Organization (Corporate Statistical Database)
FEWS NET	Famine Early Warning Systems Network
GEOBIA	Geographic Object-Based Image Analysis
GDO	Global Drought Observatory
GDP	Gross domestic product
GLAD-GSWD	Global Land Analysis and Discovery Group's Global Surface Water Dynamics
GPS	Global Positioning System
H	Horizontal
ha	Hectare
HAND	Height Above Nearest Drainage
HDMSI	High-resolution soil moisture index
(N)HDSS	(Nouna) Health and Demographic Surveillance System
HOA	Horn of Africa
IOM	International Organization for Migration
IPCC	Intergovernmental Panel on Climate Change
IR	Infrared
JRC(-GSWE)	Joint Research Center (- Global Surface Water Explorer)
kg	Kilogram
LAI	Leaf Area Index
LASSO	Least Absolute Shrinkage and Selection Operator
LCP	Least Cost Path
LiDAR	Light Detection and Ranging

LST	Land surface temperature
LSWI	Land Surface Water Index
m	Meter
MIR	Mid-wave infrared
MODIS	Moderate Resolution Imaging Spectroradiometer
MrVBF	Multi-resolution Valley Bottom Flatness Index
(d)NBR	(difference) normalized burn ratio
NDII	Normalized Difference Infrared Index
NDMC	National Drought Mitigation Center (at the University of Nebraska, Lincoln, USA)
NDRE	Normalized Difference Red Edge Index
NDSI	Normalized Difference Snow index
NDVI	Normalized Difference Vegetation Index
NDWI	Normalized Difference Water Index
NIR	Near-infrared
NLDC	National Land Cover Database
NPV	Non-photosynthetic vegetation
O	Optical
OA	Overall accuracy
PA	Producer accuracy
PPVI	Probabilistic Precipitation Vegetation Index
R ²	Coefficient of determination
RADAR	Radio Detection and Ranging
RCP	Representative Concentration Pathway
(n)RMSE	(normalized) Root mean square error
SAR	Synthetic Aperture Radar
SDG	Sustainable Development Goal
Sen2Agri	Sentinel-2 for Agriculture
SIPSA	Système d'information sur le Pastoralisme au Sahel
SMA	Spectral unmixing analysis
SPI	Standardized Precipitation Index
SRTM	Shuttle Radar Topography Mission
SSA	Sub-Saharan Africa
SWB	Small water bodies
SWIR	Short wave infrared
t	Ton
TIR	Thermal infrared
TRMM	Tropical Rainfall Measuring Mission
TTT	Transhumance Tracking Tool
UA	User accuracy
USA	United States of America
USD	United States Dollar
USDM	United States Drought Monitor
UV	Ultraviolet
V	Vertical
VHI	Vegetation Health Index
VI	Vegetation index
VIS	Visible radiation
WASDI	Web Advanced Space Developer Interface

I. Introduction

1. Climate change and its effects on livelihoods in Africa

Climate change and its far-reaching consequences represent one of the most significant current and future problems for the Earth. Emerging changes in climate patterns and increased frequency of extreme weather events are just two future projections of the effects (IPCC, 2013). These increasing weather and climate extreme events have already been observed and have led to acute food insecurity and reduced water security (IPCC, 2022; Myers et al., 2017). Africa represents one of the places with the largest impact of climate change on locations and communities. Changes in ecosystem structures, especially terrestrial ecosystems and freshwater, have already taken place. They resulted in water scarcity, reductions in crop production and livestock health, increased malnutrition, and damage to key economic sectors, which has additionally worsened due to floods and drought (IPCC, 2022). Drought areas in East Africa will likely increase according to simulations based on Representative Concentration Pathways (RCPs). Area growths of 16 %, 36 %, and 54 % (RCPs 2.6, 4.5, and 8.5 respectively) are predicted towards the end of the 21st century, while areas with extreme drought are set to increase more rapidly than severe and moderate droughts (Haile et al., 2020). West Africa is similarly exposed to climate change through strong inter-annual precipitation variability, an increased frequency of rainfall extremes, and prolonged droughts (Salack et al., 2016; Sultan et al., 2019). Climate change projections show a continuing warming trend with increasing aridity and frequent occurrences of extreme heat events (Serdeczny et al., 2017). Heat-related child mortality has already doubled in 2009 in comparison to a scenario without climate change (Chapman et al., 2022). According to the Intergovernmental Panel on Climate Change (IPCC) (2022), mid- to long-term risks (2041 - 2100) include increasing pressure on food production and access as well as food security risks resulting in more severe malnutrition in Sub-Saharan Africa (SSA) with 2°C or higher global warming levels (Grolleaud, 2020; IPCC, 2022; Myers et al., 2017). Additional future risks for Africa are freshwater loss, loss of livelihoods due to reduced food production from crops and livestock, reduced economic output and growth, and an increased risk to water security due to drought and heat (IPCC, 2022).

While facing all these risks, Africa and especially West-, Central-, and East Africa are the hotspots most vulnerable to climate change (IPCC, 2014, 2022). A study in South

Africa furthermore showed that rural households are more susceptible to climate change than urban households (Leocadia Zhou et al., 2022). While poverty has been identified as the greatest limit to adaptation, rural areas are more vulnerable in contrast to urban areas in all three vulnerability aspects: exposure, sensitivity, and adaptive capacity. People living in rural environments rely more heavily on climate-sensitive resources, as agriculture for example (crops and livestock combined) needs natural resources like land and water (Leocadia Zhou et al., 2022). Rainfed agriculture, which is dominant in West Africa, is therefore highly vulnerable to Climate Change (Carr et al., 2022).

Agriculture, in general, is one of the most important economic sectors in Africa as it adds up to 55% of Africa's Gross Domestic Product (GDP) (AGRA, 2017). It is the base for food security and livelihood as 85 % of the population relies on rain-fed agriculture (Shah et al., 2008). The IPCC states with a high level of confidence, that the overall effect of climate change on yields of the major cereal crops in the African region is very likely to be negative, with a strong regional variation (Niang et al., 2014). Edame et al. (2011) also stated that agriculture is a vulnerable sector, that is exposed to the impacts of climate change and climate variability. Seasonal changes in precipitation and temperature in addition to their varying severity will negatively impact crop production and food security also due to the overreliance on rainfed agriculture (Kogo et al., 2021). Especially vulnerable are communities in arid and semi-arid areas (Kogo et al., 2021). Carr et al. (2022) revealed that yields declined by 6 % (median) for all major staple crops they analyzed due to climate change in all considered scenarios. Lower crop yields are also a prominent driver of food insecurity and child malnutrition, especially among rural smallholder farmers in SSA (FAO et al., 2019; Grolleaud, 2020; Myers et al., 2017). Common adaptation strategies like optimized planting dates or cultivars, however, could increase yields that are affected by climate change by 13 % (Carr et al., 2022). Carr et al. (2022) also state that a combination of fertilizers and adopted cropping practices is needed to enhance future crop production. Kogo et al. (2021) support this statement by saying that crop production and food security systems need more adaptation as future projections show a high population growth and urbanization rate. Together with higher climate variability this will lead to the altering of cropping patterns and yield.

Pastoral systems are also highly affected by climate change. The pastoral systems of the drylands in the Sahel, for example, are highly dependent on natural resources including pasture, fodder, forest products, and water, all of which are directly affected by climate

variability (Djouidi et al., 2013). Livestock is also vulnerable to drought, particularly where it depends on local biomass production (Masike & Ulrich, 2018). Thornton et al. (2009) already found a strong correlation between drought and animal death in the past. Adding to these climate risks, conflicts over natural resources arose between farmers and herders and have increased over the past two decades (Ayana et al., 2016). Especially conflicts due to drought and water tensions have become widespread in the Sahel (Ayana et al., 2016; Puig Cepero et al., 2021). These conflicts represent an additional health risk to all the climate change-related risks above.

2. Droughts and water availability

Droughts are affecting livelihoods in Africa in many different ways - from a lack of drinking water to damaged crops and food insecurity. In the following, some definitions of droughts are provided and their aspects are described in more detail.

2.1. Definition of droughts

A missing accurate and universally accepted drought definition led to confusion and disagreement in drought research in the past (Dracup et al., 1980). Even in recent years, there was no single definition of drought. Mishra and Singh (2010) define droughts as natural hazards that create problems for activities, groups, and environmental sectors through water deficits over an extended period of time. Sheffield and Wood (2007), on the other hand, describe a drought as a continuous period in which soil moisture remains below the twentieth percentile on a monthly scale. Heim (2002) states that droughts are viewed by the remote sensing community as a period of abnormally low precipitation that alters vegetation conditions. Defining the beginning and end of droughts is additionally problematic because the effects of droughts often accumulate slowly over a considerable period of time (Tannehill, 1949). In the process, economic, social, and natural impacts occur, which is why droughts can be characterized by economic, social, and environmental bifurcation (Owringi et al., 2011). In general, drought can be described as a recurrent climatic process that affects all climatic regions of the world (Sivakumar et al., 2011; Wilhite, 2000a) and is the consequence of a natural reduction in precipitation over an extended period of time. In this context, the severity of droughts can be influenced by the interaction with other climate factors (Sivakumar et al., 2011).

Despite the difficulty of defining droughts universally, they can be divided into four broad categories. In 1997, the American Meteorological Society (Heim, 2002) divided them into meteorological, agricultural, hydrological, and socio-economic droughts. These four types have become established in drought science (FAO & NDMC, 2008; Wilhite et al., 2007). Here, meteorological drought is defined as a negative rainfall deviation, relative to the normal or expected value, over an extended period of time (Sivakumar et al., 2011). Agricultural droughts are characterized by prolonged deficits in soil moisture leading to crop losses (Mishra & Singh, 2010; Sivakumar et al., 2011). Deficits in surface and subsurface water supply are expressed by the term "hydrologic drought" (Sivakumar et al., 2011). All these types of droughts have an impact on society and the economy, so they are referred to as social and economic droughts.

For a better understanding of droughts, three essential elements are differentiated – intensity, duration, and spatial extent (Sivakumar et al., 2011). Drought intensity is defined by the degree of rainfall deficit and/or the severity of its impact as well as by the deviation of climatic indices (e.g., Standardized Precipitation Index (SPI)) from normal. In determining drought impacts, intensity is closely related to duration. Droughts usually take two to three months to develop. However, they can also last for several months and years, such as in arid regions where successive years of drought are not uncommon. Prolonged droughts over several seasons or years produce more drastic effects due to greater depletion of surface and subsurface water supplies. In addition, the longer duration affects a greater number of users. For vulnerable arid and semi-arid ecosystems, frequently recurring and prolonged droughts are a particularly critical problem, as they result in both natural and managed systems having no opportunity to recover. In general, droughts naturally are regional events that affect millions of square kilometers. Due to their long duration, the drought's epicenter, the location of maximum severity, shifts from season to season and year to year (Sivakumar et al., 2011).

2.2. Drought as a natural hazard

According to the IPCC (2013), the frequency and severity of droughts are expected to increase due to global warming. In recent decades, this trend has already been noted (Hulme & Kelly, 1993) as the effects of weather extremes worsened due to population growth, environmental degradation, industrial development, and fragmented government authority over water and resource management, which is for example reflected in large

annual vegetation losses (Wilhite, 2000b). Because of the socially, economically, and environmentally relevant aspects (Owringi et al., 2011) with enormous potential damage to the economy, society, and environment, the monitoring of droughts is very important (Gulácsi & Kovács, 2015; J. Wu et al., 2012; Lei Zhou et al., 2013; Zhuo et al., 2016). For example, the occurrence of droughts correlates with wildfires in the western United States (Westerling et al., 2006), Canada (Flannigan & Harrington, 1988), and southeastern Australia (Bradstock et al., 2009). The interplay of severe, prolonged droughts and elevated temperatures has also had a tremendous impact on terrestrial ecosystems over the past several decades (Kaptué et al., 2015; Overpeck & Udall, 2010; Zhao & Running, 2010). Thus, successive drought years also affect forests (Anderegg et al., 2015; McDowell & Allen, 2015). Recent mega-droughts, as in 2005 and 2010 in the Amazon Basin (Gatti et al., 2014; Saleska et al., 2007), substantially reduced forest productivity and ecosystem services. This has already been demonstrated in Europe (Ciais et al., 2005), Africa (Liming Zhou et al., 2014), Australia (van Dijk et al., 2013), and East Asia (Saigusa et al., 2010). For humans, agriculture represents the most vulnerable sector affected by droughts (Di Wu et al., 2015). Recent large-scale droughts in Europe, Asia, Africa, and throughout the Americas resulted in large crop and monetary losses (Hazaymeh & Hassan, 2016). According to the IPCC (Bates & Kundzewicz, 2008), rice, corn, and wheat production in Asia have already declined in the past. Between 1980 and 2003, droughts in the U.S. caused 144 billion USD in monetary damages, which is about 41% of the estimated total cost of weather/climate-related disasters. 3.6 billion CAD were lost by Canada in agricultural production due to drought between 2001 and 2002 (Hazaymeh & Hassan, 2016). However, the consequences of droughts amount not only to monetary damages but also to humanitarian damages as drinking water and food shortages can occur. Between 1981 and 2010, 253 million people in Africa were affected by drought, of which half a million died as a result (Rojas et al., 2011). These figures make it clear that droughts, like other natural hazards, can have enormous damage to the environment, economy, and society (J. Wu et al., 2012).

Because of their drastic consequences, the designation of droughts as natural hazards is obvious. Natural hazards are associated with geophysical processes - an integral part of the environment - that have the potential for damage or loss in the presence of a vulnerable society, while posing an unexpected threat to humans or their property (Bobrowsky, 2013). Geophysical natural hazards are preceded by geological, geomorphological,

climatic, or meteorological reasons (Bobrowsky, 2013). Thus, a drought is a geophysical natural hazard because of its meteorological origin. Furthermore, there are four reasons why droughts are different from other natural hazards and why early warning systems in the form of accurate, reliable temporal estimates of their severity and impacts, as well as so-called drought preparedness plans, are of enormous importance (Sivakumar et al., 2011).

One of these reasons is that drought impacts accumulate slowly over a considerable period of time and can persist for years after the natural disaster has ended. In addition, the beginning and end are difficult to determine. Third, there is no precise and universally accepted drought definition. The fourth reason is that impacts are described over a larger geographic area than, for example, floods, hurricanes, and most other natural hazards making quantification of impacts much more difficult (Sivakumar et al., 2011).

2.3. Drought risk and drought vulnerability

Drought risk represents the interaction of the exposure of the geographic region and the vulnerability of society (Sivakumar et al., 2011). Exposure varies regionally, so there is almost no opportunity for action to reduce or prevent recurrence, frequency, or occurrence. Therefore, climatic understanding of droughts and their frequency, severity, and duration is necessary, as these aspects vary spatially. Further, identifying the regions most likely to experience drought is critical (Sivakumar et al., 2011).

Vulnerability is reflected in the interaction of social factors, such as population growth and the shift of society from humid to arid and rural to urban areas. Population growth increases pressure on natural resources and people are pushed to settle in regions more vulnerable to drought. Urbanization has a similar effect, putting pressure on water resources and contributing to the conflict between agricultural and urban water use. Progressive technologization though can reduce vulnerability. On the other hand, there are natural factors, such as environmental degradation (e.g., desertification), which positively and negatively affect drought vulnerability (Sivakumar et al., 2011).

Studies on drought vulnerability have already been conducted in the past. Dabanli (2018), for example, includes population density and the proportion of artificially irrigated fields for his vulnerability analysis. However, the latter data are not available with sufficient accuracy and over large areas. In contrast, Naumann et al. (2014) considered the economic factor of GDP per capita as an indirect indicator of well-being and attested to

a correlation with drought vulnerability. Other factors such as pasture animal density were also sometimes included in vulnerability analyses (Carrão et al., 2016). Climate change and increased greenhouse gas concentrations could also increase the occurrence and severity of meteorological droughts in some regions (IPCC, 2007). Thus, drought vulnerability is highly dynamic and ideally needs to be evaluated periodically. Furthermore, it is influenced by many variables, which makes it difficult to quantify and evaluate vulnerability uniformly across different regions. Because of this dynamic occurrence, current and spatially explicit data, such as remote sensing imagery, are needed.

3. Transhumance

Droughts severely affect transhumance, which has established itself as one of the most important lifeforms in several regions of the world, including the Sahel region in Africa. Pastoralists need grazing land as forage for their animals and have to tackle several risks to maintain their livelihoods. In the following, transhumance, its economic value, and its risks in the Sahel are described in more detail.

3.1. Definition and economic value in the Sahel region

Different descriptions of transhumance can be found in the literature. Oteros-Rozas et al. (2014) described transhumance partly as a farming practice shaping cultural landscapes, but also as an adaptive strategy, that overcomes the growing challenges of environmental change due to mobility. Brottem (2014) states, that transhumance consists of regular patterns of herd movements along persistent corridors between key pastoral sites. Jones (2005) mentioned that transhumance separates from pastoral nomadism in several ways. Transhumance, therefore, is not only based on mobile livestock herding, that adjusts to environmental conditions, but parts of the groups also have permanent village residents with arable agriculture. Here, several definitions from the IOM (International Organization for Migration) (Leonhardt, 2017) help to draw boundaries between several terms, that are often used as synonyms. Following, pastoralism generally describes an economic system based on livestock production with different degrees of mobilities and therefore includes nomadism, transhumance, and semi-transhumance. Furthermore, transhumance features a seasonal movement of herds and a return to a fixed origin with

I. Introduction

a permanent place of residence, in contrast to nomadism. The migration schedule is dependent on the onset of the wet and dry seasons, while routes and destination pastures are generally well-known. Semi-transhumance on the other hand has one family responsible for agriculture, while the other part practices seasonal migration. Transhumance can furthermore be divided into long transhumance, where herders travel several hundred kilometers, and short transhumance, which is only limited to a small local area. Cross-border transhumance then describes seasonal movements, during which national borders are being crossed in search of natural resources like water and pasture (ECOWAS, 1998). Transhumance also displays the importance of livestock mobility across various spatio-temporal scales, as it is flexible in response to ecological variability. This reduces the vulnerability to climatic change and also the likelihood of overgrazing (Brottem et al., 2014; Fernandez-Gimenez & Le Febre, 2006). Movement patterns generally consist of north-south movements in the Sahel zone (Figure 1), while movements north take place during the rainy season (April – October) (Brottem et al., 2014). The movement starts at the beginning of the green-up period and the beginning of senescence (Brottem et al., 2014).

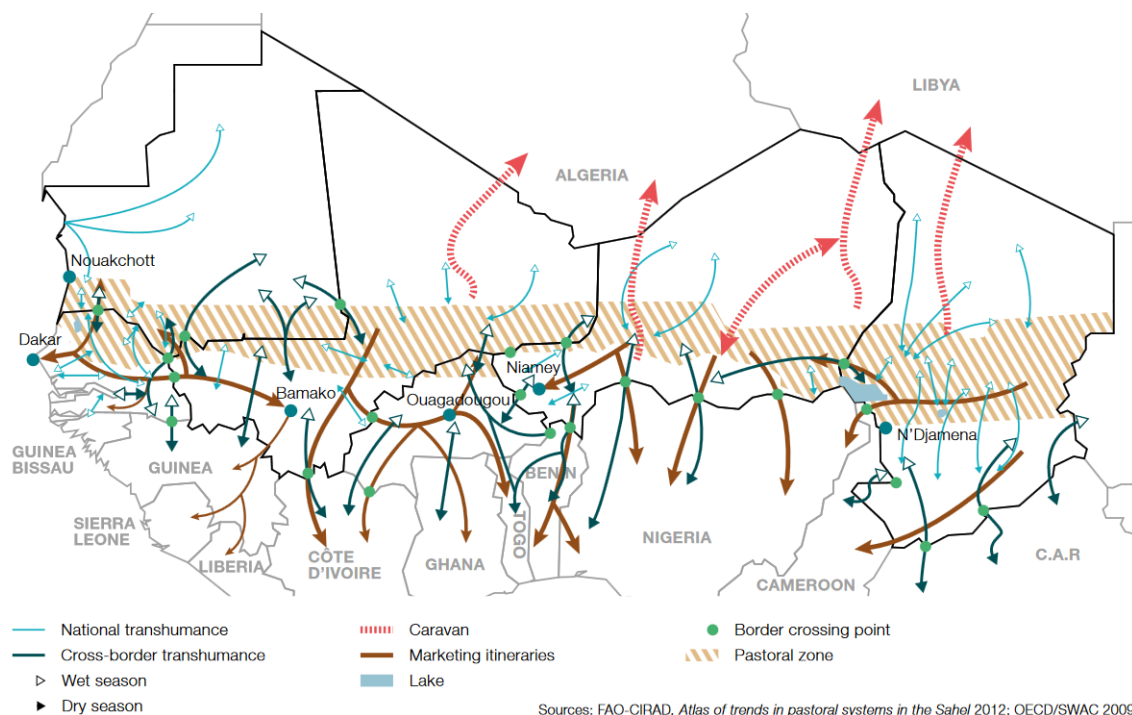


Figure 1: Transhumance and nomadism in Sahelian countries (OECD/SWAC, 2014).

Rates of movement also differ between the two movement times. While herders move faster at the end of the rainy season due to the good nutritional status of the livestock,

movements at the end of the dry season are much slower (Diallo, 1978). Another reason for that is, that the annual grasses further north provide higher nutritional content (Penning de Vries & Djitéye, 1982). Routes or corridors of transhumance are generally well known by the herders as they often have fixed reliable resting points each year. Verified information about locations and the legal status of the corridors and resting points though is mainly not available. Resting points describe key locations along the transhumant corridors between origin and destination areas and are often located along water sources (Brottem et al., 2014). The transhumant movement generally follows the same trajectories each year with a highly varying length of stay at the origin and destination areas as well as at resting points (Brottem et al., 2014).

Transhumance has a high economic value in the Sahelian countries of the ECOWAS (Economic Community for West African States) region. Livestock production is estimated at around 40 % of the GDP and can reach up to 50 % with animal traction, manure, and the transformation of animal products like butter or leather (Leonhardt, 2017). 38 % of West Africa consists of unfavorable land for agriculture (OECD/SWAC, 2014), where livestock production is the only way of using these arid zones. Livestock production not only employs millions of people but is also an important source of food and income, especially in fragile ecological zones like the Sahel. Rural inhabitants here are especially vulnerable to food insecurity, where livestock makes up about half of their capital. Large parts of the cattle, camels, goats, and sheep are held in transhumant production systems in the Sahel zone. Transhumance is well adapted to ecological and economic realities in West Africa and holds 70-90 % of the Sahel's cattle, 30-49 % of its sheep and goats, and produces around 65 % of cattle meat and 70 % of milk (Leonhardt, 2017).

3.2. Transhumance at risk

Despite their economic value, transhumant pastoralists also face several risks and challenges. These consist of population growth, climate change, expansion of agricultural areas, and the privatization of formerly shared resources (Leonhardt, 2017). This includes policies, that are favoring agriculture. In Mali for example big pastures have been converted to rice fields (Benjaminsen & Ba, 2009). The neglect and lack of governance in rural areas also contribute to the competition for natural resources. Conflicts and violence arising from that competition, lead to a negative perception of pastoralists and

reinforces marginalization. Transhumance is therefore often seen as a security issue instead of a development issue. Back in time, subsistence farmers and pastoralists complemented each other in how agroecological systems were used. Increasing competition for natural resources (Ikhuoso et al., 2020), increases in herd sizes, cropland expansion, poor governance, and extreme weather events have exacerbated these conflicts (Inter-resaux, 2017; Touré et al., 2012). All this leads to a contrary, where rights to secure fixed territories and social boundaries are needed to protect pastoralists and their pasture, and on the other side the spatio-temporal variability of resources for livestock (Marty, 1993; Painter et al., 1994). Fernandez-Gimenez (2002) describes this as the “paradox of pastoral land tenure”. Accompanied is a confusion of policymakers and incoherent policy frameworks, that limited the progress in improving pastoral management and the securing of rights to key resources (Fernandez-Gimenez & Le Febre, 2006; Turner et al., 2011). The complexity arose from a highly variable and low predictable spatio-temporal distribution of pastoral resources. A step in the right direction was the ECOWAS Protocol on Transhumance in 1998 and the supporting regulation in 2003, where ECOWAS Member states recognized cross-border pastoralist transhumance as a valuable economic activity. Regional regulatory frameworks for cross-border transhumance were set in place to provide free movement of persons, services, and goods (Leonhardt, 2017). Agricultural expansion nevertheless is a pressing challenge for transhumances as it leads to restricted movements and a reduced number of paths, as well as paths under conditions of heavy cultivation pressure (Brottem et al., 2014). Brottem (2014) described the extension of the cropland area as the most vulnerable aspect for transhumance and not climate change. The extension of cultivated areas leads to blocks, where movements between areas with water and pastures are not possible anymore and therefore result in lower viability for transhumance. Drought-related farmer-herder conflicts and water tensions with both fighting for the same natural resources are widespread in the Sahel and East Africa (Benjaminsen et al., 2009; Cabot, 2017). The fight for limited resources was also the main reason for recent conflicts in Nigeria (Ikhuoso et al., 2020). While conflicts have increased over the past two decades (Ayana et al., 2016), it became apparent that environmental factors act in tandem with many socioeconomic and political factors to trigger conflicts (Detges, 2016; Scheffran et al., 2019; Shettima & Tar, 2008). The understanding of the drivers of transhumance patterns as well as possible sources and

locations of conflicts is limited due to the lack of information on spatio-temporal migratory movements, grazing locations, or resting points (Motta et al., 2018).

4. Small-scale and subsistence farming

Transhumance is not the only form of agriculture that faces the previously described risks. Small-scale and subsistence farmers represent another form of livelihood in rural Africa and are at least equally important as transhumant herders. Therefore, this chapter focuses on smallholder farmers and outlines their economic value along with the risks they are facing.

4.1. Definition and the economic value of smallholder farmers in Sub-Saharan Africa

Small-scale farmers belong to the group of smallholders that also contain pastoralists, forest keepers, and fishers (FAO, 2012). Smallholders in general are managing small areas of less than one hectare up to ten hectares and are focused on the stability of the farm household. Mainly family labor is used for production and a part of the produce is for family consumption (FAO, 2012). Subsistence and small-scale farming are sometimes interchangeably used (e.g., Michael Aliber et al., 2005; Moeletsi et al., 2013). Small-scale farmers grow subsistence crops on small plots of land plus one or more cash crops while relying almost exclusively on family labor (Lidzhegu & Kabanda, 2022). Smallholder farmers also vary in activities they are engaged in, assets and resources available to them (e.g., land area or water), land tenure (e.g., rental or share-cropping arrangements), the control of the natural resources used, the scale of production, the share of family labor utilized, the degree of market integration and the distance of the holding farms from their family residence (Maass Wolfenson, 2013). So, despite being grouped under the same definition, there can be huge differences between individual smallholder farmers. Smallholder farmers in SSA also face some barriers as low nutrient inputs, insufficient control of weeds, pests, and diseases, and inadequate labor puts them into a category of low input systems (Sheahan & Barrett, 2017). The agricultural sector in Africa and especially in SSA is underdeveloped with an over-reliance on primary agriculture. Within that, the minimal use of external farm inputs, significant pre- and post-harvest food crop losses, minimal value addition, and product differentiation play a huge role (Assefa et al., 2020; Tilman et al., 2011; van Ittersum et al., 2016).



Figure 2: Smallholder farmers in Ghana (FAO, 2021).

Nevertheless, agriculture plays an important role in the economy and food security in Africa. In SSA agriculture employs 51.6 % of the population and generates 20 % of the GDP in 2016 (The Global Economy, 2019). Recent estimates found 33 million farms in SSA (IFC, 2013) with a contribution of up to 90 % of agricultural production in the same countries of SSA (Wiggins, 2009). Nearly 80 % of the farmland in SSA is managed by smallholder farmers with an average size of agricultural holdings below 3 ha which together produce up to 80 % of the total food supply in SSA (FAO, 2012). Still, the consumption of self-produced food crops represents only 20 % of the food needed for SSA smallholder households (Frelat et al., 2016). Despite actions to achieve the “Zero-Hunger” Sustainable Development Goal (SDG) by 2030, food security in SSA is still far away (FAO et al., 2020). In recent years, yields of staple crops such as maize, wheat, or sorghum have decreased across Africa, widening food security gaps and leaving open challenges besides other risks for small-scale farmers (Ketiemi et al., 2017).

4.2. Risks for small-scale and subsistence farming

This food security risk is additionally amplified in the future by the projected population growth. 1.02 billion people lived in SSA in 2017 and 2.17 billion inhabitants are projected for 2050 (United Nations, 2017). This population expansion will lead to an increased food demand (Kim et al., 2021). Subsistence farmers are also one of the most vulnerable groups to climate variability. It is difficult for them to cope with climate-related hazards as they have no capital for adaptive strategies (Thompson et al., 2007). Especially vulnerable are households relying on rain-fed agriculture (Thorlakson & Neufeldt, 2012). The worsening

food situation though is only partly related to climate change as poor and weakening market situations also play a role (Abdul Mumin & Abdulai, 2022). Prohibitive transaction costs by underdeveloped market systems and infrastructure as well as market failures, inadequate access to finance and technologies hinder the efficiency of food market systems and lead to limited potential of agricultural marketing (Abdulai & Birachi, 2009; Abdul-Rahaman & Abdulai, 2020; Fafchamps, 1992). An additional risk to smallholder farmers is the loss of land as a decline in land/labor ratios shows (Jayne et al., 2010). The amount of arable land under cultivation has only risen marginally while the population of households in agriculture tripled between 1960 and 2000 (Jayne et al., 2010). The bottom quartile of small-scale farmers in Ethiopia and Rwanda for example control less than 0.02 to 0.03 ha of land (Jayne et al., 2003). Another example is Malawi, where 70 % of smallholders possess less than one ha of land (Chirwa, 2006), which shows the risk of landlessness (Jayne et al., 2010). Rural communities heavily depend on access to land and natural resources while agricultural land on communal lands is one of the major land uses that supports the livelihood of millions of people (Shackleton, 2020). While facing adverse conditions like inadequate access to production resources (Mpandeli & Maponya, 2014) or poor access to markets (Loeper et al., 2016), the most alarming challenge in South Africa for rural communities is the access to and ownership of arable land (Loeper et al., 2016; Mpandeli & Maponya, 2014; Shackleton, 2020). In South Africa, 87% of agricultural land is used by commercial farms leaving only 13% for small-scale subsistence farmers (M. Aliber & Hart, 2009). Ineffective land use management that is less protective of smallholder farmers in rural areas led to a decline in land under agricultural fallow from 26% to 8% with a 69% decline in extent in South Africa as many areas were converted to built-up land (Lidzhegu & Kabanda, 2022). Besides the economic viability and the contribution to a diversified landscape and culture, small-scale farming faces additional risks. The competitive pressure from globalization and the integration into common economic communities only leaves two choices: either to be purely self-subsistent or to grow into larger units, that can compete with large industrialized farms (FAO, 2012). Another problem and risk for future food security is the stagnant food crop productivity in SSA in contrast to the risen productivity in the rest of the world since 1960 (Jayne et al., 2010). For example, while global maize production has increased with increasing yields, maize production in most countries of SSA only increased with increasing areas (Cairns et al., 2021). This expansion-based production

growth though is not sustainable in the long run (Cairns et al., 2021) pointing to the need for adaptation strategies.

5. Remote Sensing

Remote sensing, through its large spatial coverage and high revisiting frequency, allows us to analyze various processes on the Earth surface in a spatiotemporal way. Before providing an overview of the status of current remote sensing applications for droughts, transhumance, or agriculture, the principles of remote sensing together with its different sensors to monitor environmental factors are described in the following.

5.1. Introduction to remote sensing: History, definition, and basics

The term “remote sensing” was first used between 1960 and 1970 (Campbell & Wynne, 2011). Over time, there were many different definitions surrounding one central concept – the gathering of information at a distance. The closest definition for this thesis explains remote sensing as “the practice of deriving information about the earth’s land and water surfaces using images acquired from an overhead perspective, using electromagnetic radiation in one or more regions of the electromagnetic spectrum, reflected or emitted from the Earth’s surface” (Campbell & Wynne, 2011). Regarding this thesis, the definition needs to be a bit broader as meteorology for example is not included, but is a factor in this work primarily in the form of rainfall. Satellite remote sensing designed for the observation of land surfaces started in 1972 with the launch of Landsat 1 providing systematic and repetitive observations for the first time. Rapid advances in technologies like hyperspectral remote sensing in the 1980s, the first satellite systems designed to collect data of the entire earth in the 1990s, and public remote sensing, which was made available through the advances of the internet in the first decade of the 21st century lead to today's standards of long time series archives of satellite data with varying spatial and temporal resolutions dependent on the applications (Campbell & Wynne, 2011). Remote sensing itself represents a process that starts with physical objects on the earth’s surface (e.g., buildings or vegetation). Subsequently, sensor data is collected by viewing the objects with instruments and recording electromagnetic radiation, that is either emitted or reflected. To use these types of sensor data, analyses and interpretation are necessary to convert this data to information that can be used to address practical problems (e.g.,

identifying burned areas). Finally, the extracted information can be used in combination with other data for specific applications like land use planning or drought monitoring (Campbell & Wynne, 2011). Remote sensing additionally consists of several key concepts – the spectral differentiation where different features on the earth reflect or emit different energy, the radiometric differentiation where differences in brightness of the objects are measured, the spatial differentiation which is limited to the smallest area that can be separately recorded by a sensor (minimal units: pixels), and the temporal dimension where constant repetition of observations over years allow change detections (Campbell & Wynne, 2011).

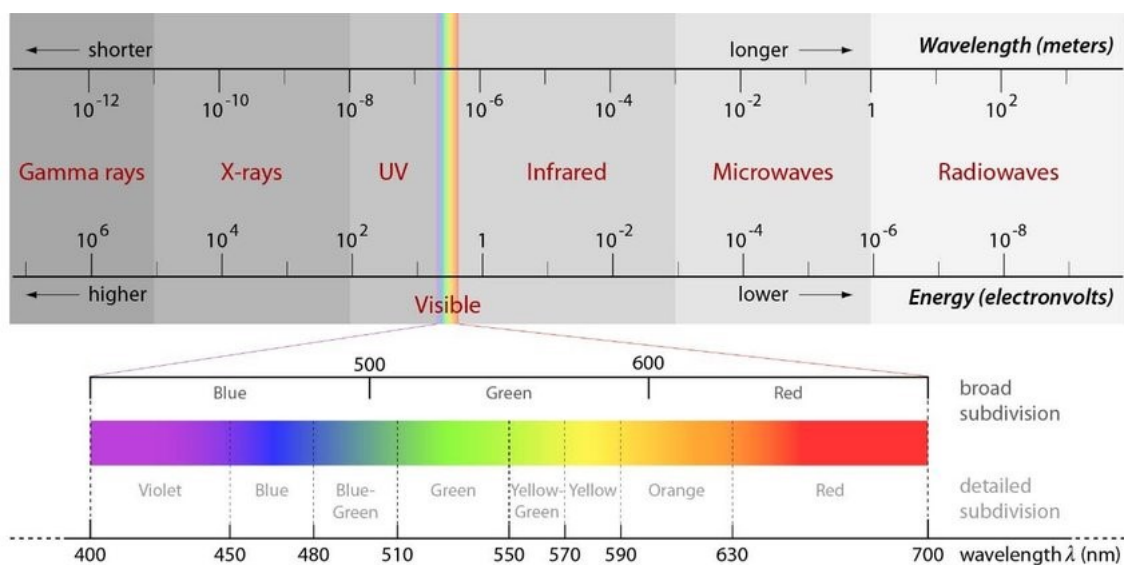


Figure 3: The electromagnetic spectrum, including wavelength, energy, and a detailed excerpt of the visible subdivision (Verhoeven, 2017).

All these concepts rely on the basis that all objects on the earth's surface emit or reflect electromagnetic radiation. The emitted and/or reflected radiation can be measured by sensors and different characteristics of features such as vegetation, structures, soils, rock, or water bodies can then be identified. Each electromagnetic wave consists of one electric (vertical) and one magnetic (horizontal) field, which are orthogonal to each other and the direction of the wave propagation (Lo, 1987). Each wave has several properties, which include the wavelength (λ) representing the distance of separation between adjacent wave peaks, the frequency (f) describing the number of wave peaks passing a fixed point in a given period of time, the amplitude as the height of each peak, and the phase, which shows the extent to which peaks of one waveform align with those of another (Campbell & Wynne, 2011; Lo, 1987). As the speed of electromagnetic energy is constant, the

frequency and wavelength are related inversely proportional and the characteristics of electromagnetic radiation can be described through either one of them (Campbell & Wynne, 2011; Lillesand & Kiefer, 1994). The most common way to categorize waves uses their wavelength location in the electromagnetic spectrum (Figure 3) (Lillesand & Kiefer, 1994). The electromagnetic spectrum consists of several subdivisions including gamma rays, X-rays, ultraviolet radiation (UV), visible light (VIS), infrared radiation (IR), microwave radiation, and radio waves (Figure 3) (Campbell & Wynne, 2011).

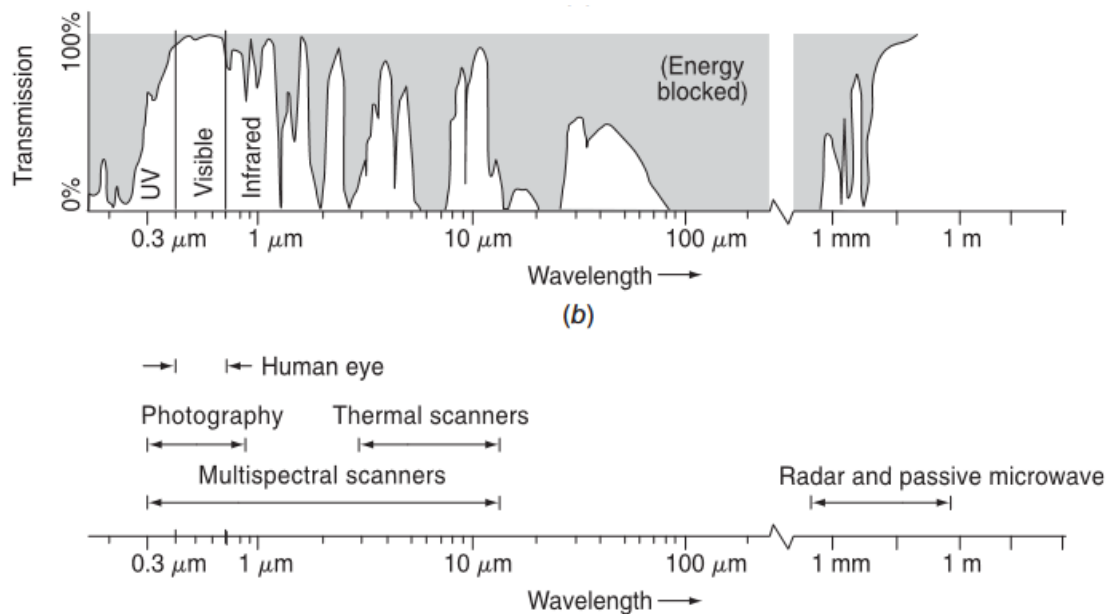


Figure 4: Spectral characteristics of atmospheric transmittance and common remote sensing systems (Lillesand et al., 2015).

While the radiation travels through the atmosphere, its energy is altered in intensity and wavelength by particles and gases (Campbell & Wynne, 2011). Interactions in the atmosphere include scattering, which describes an unpredictable diffusion of radiation by particles in the atmosphere, and absorption which is an effective loss of energy to atmospheric constituents (Lillesand & Kiefer, 1994). While the effect of scattering on sensor data can be reduced through atmospheric correction, the effect of absorption cannot be corrected and leaves so-called “atmospheric windows” where remote sensing systems can receive transmissive energy (Figure 4) (Lillesand & Kiefer, 1994). Therefore, remote sensing systems operate on several wavelengths to gather information about features on the earth’s surface. These features can be differentiated by their spectral signature, which represents the spectral response of a feature over a range of wavelengths. The spectral responses of objects on the earth’s surface in different wavelengths can be

observed through several satellite-based remote sensing systems. In the field of remote sensing, active and passive systems are distinguished based on the same physical principles as explained above. Different passive and active remote sensing systems as well as their physics and exemplary application fields, which are related to the topic of this thesis, are described in the following two sections.

5.2. Passive sensors (optical) and remote sensing of environmental factors

Passive sensors are based on the principle of measuring radiation, which is reflected or emitted by objects, and depend on external energy sources. The main external energy source is the sun, but also thermal energy emitted by fires can be measured (Schowengerdt, 2007). Passive sensors measure radiation in the visible, near-infrared (NIR), mid-infrared (MIR), and thermal infrared (TIR) parts of the electromagnetic spectrum ranging from 0.4 – 14 μm (Figure 3) (Schowengerdt, 2007). Objects on earth react differently to incoming radiation, as they reflect, emit, absorb or transmit the energy. Reflection is defined by the change of the radiation's direction without emitting or absorbing energy and is divided into diffuse and specular (direct) reflectance. Absorption describes the intake of energy by an object, emission in this context is defined through outgoing secondary heat radiation. Energy can also transit through the object without changing, which is called transmission (Borengasser et al., 2008). These properties vary for features on the earth's surface and are dependent on the material, shape, and size as well as their physical and chemical characteristics (e.g. moisture content) while the most important properties are color, structure, and surface condition. Features on the earth's surface have unique properties and can therefore be identified through their spectral signature, as described in the previous section (Campbell & Wynne, 2011). Passive sensors in this work were mainly used for vegetation monitoring. Vegetation monitoring is also based on the spectral signature principle, where mostly healthy and dry vegetation, as well as soil, are differentiated.

In the optical wavelength region, vegetation absorbs much of the solar radiation for photosynthesis through pigments in the leaf tissue - particularly chlorophyll a and b, carotenoids, and anthocyanins (Chang et al., 2017). Plant greenness is influenced by the fact that healthy vegetation is greener and absorbs more incident visible light, such as that of the red and blue spectrums, and reflects a significant amount of near-infrared energy as well as a small reflectance peak for the green part of the visible spectrum (Figure 5).

Less vital and sparse vegetation, on the other hand, reflects more visible light without a green reflectance peak and less near-infrared (NIR) energy (Hazaymeh & Hassan, 2016). To evaluate vegetation and soil status, the wavelength range 0.4-2.5 μm (Red Spectrum, NIR, Shortwave Infrared (SWIR)) is most used due to the clear response from vegetation greenness and vegetation moisture (Hazaymeh & Hassan, 2016).

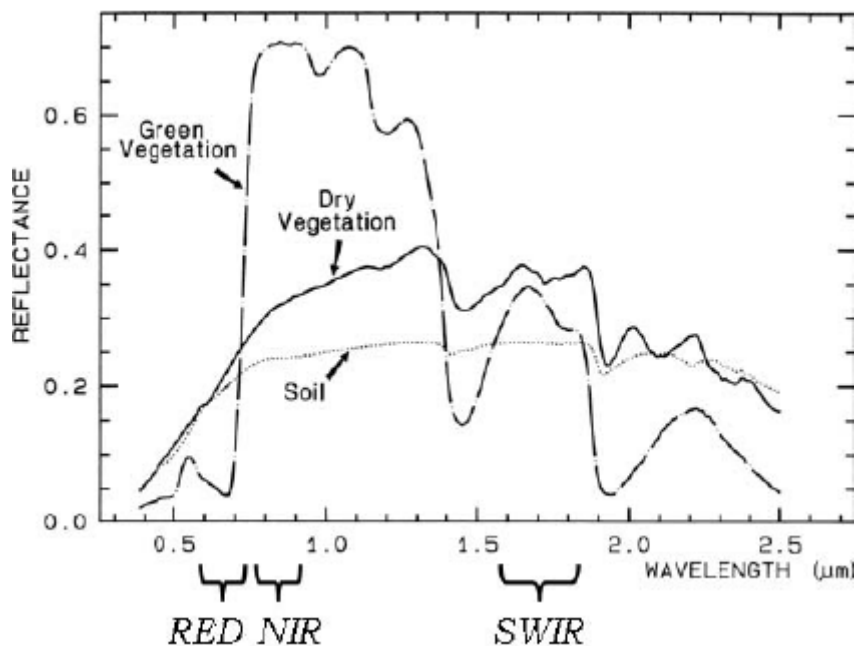


Figure 5: Spectral signatures of green vegetation, dry vegetation, and soil across the spectra measured by passive sensors (Maisongrande et al., 2007).

For moisture, the NIR is less sensitive than the SWIR, which has a significant absorption peak for vegetation water content (Zhang et al., 2013). In general, surface reflectance increases with higher levels of water deficits, especially in the spectrum of the SWIR (Hazaymeh & Hassan, 2016).

Vegetation monitoring is mostly done by exploiting the described properties of vegetation throughout their spectral signatures. An example is given in Figure 6, where a false color composite is shown. Here, green vegetation appears green as it shows high reflectance values in the NIR (Figure 5), which are displayed as the green band of image. Differences can also be seen between agricultural areas (light green to yellow) with partly dryer vegetation and forests (darker green). Healthy, green vegetation, therefore, can be clearly distinguished from other land cover types like for example bare soil, which is represented by purple and white to rosa coloring depending on the soil type (e.g., built up land (pink)

or sandy soil (light rosa)) as well as sparse vegetation cover or the moisture content. By calculating vegetation indices like the NDVI or the NDRE (Normalized Difference Red Edge Index) as well as water indices, e.g., the NDWI (Normalized Difference Water Index) (Gao, 1996; Lambert et al., 2017) vegetation monitoring takes advantage of the spectral signatures. Water indices that use the NIR and SWIR regions of the electromagnetic spectrum are more suitable for the evolution of drought for example than indices that use the visible and near-infrared wavelength spectrum. This is because water

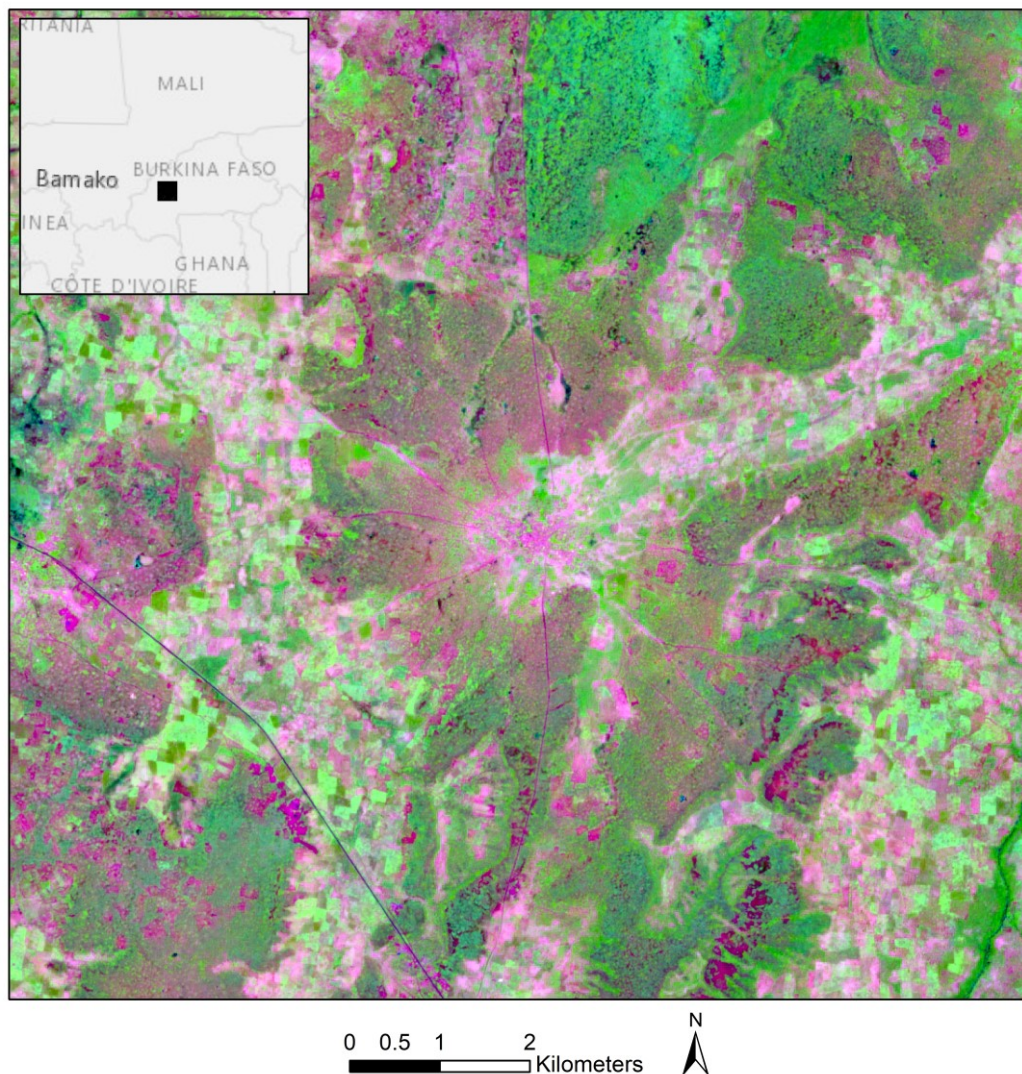


Figure 6: Exemplary false color Sentinel-2 image in Burkina Faso during the crop growing season (06.09.2021). Color representation: Red: SWIR, Green: NIR, Blue: Red. The black square in the inset represents the location of the image in Burkina Faso. Background: ESRI Basemaps.

indices are more sensitive to changes in drought conditions than vegetation indices (Chang et al., 2017; Gulácsi & Kovács, 2015). Vegetation health for crop yield models is

also often based on water indices together with vegetation indices (Groten, 1993; Lambert et al., 2017). Optical remote sensing indices can be divided into different groups for drought monitoring. There are indices describing soil drought and those describing vegetation drought (Hazaymeh & Hassan, 2016). In this context, for example, soil drought indices have uncertainties about vegetation areas because vegetation reacts consistently to short-term drought conditions in leaves and roots, which leads to delayed identification of drought and uncertainties in results (Farooq et al., 2009). Similarly, vegetation indices have uncertainties over areas of sparse vegetation. Another way of vegetation monitoring is called spectral unmixing analysis (SMA) (Roberts et al., 2003; Yebra et al., 2013). In contrast to indices, it does not only use specific bands recorded by remote sensing sensors but all vegetation-related bands throughout the measured spectrum. Spectral mixture analyses are suitable to assess the fractional green photosynthetic vegetation versus per pixel non-photosynthetic vegetation, and bare substrate (soil) abundances from satellite data (Asner et al., 2005; Franke et al., 2018; Roberts et al., 1993).

Examples of passive remote sensing systems, that are used in this work are the Moderate Resolution Imaging Spectroradiometer (MODIS) and Sentinel-2. MODIS provides different products about surface reflectance or the albedo on a spatial resolution of 500m since the year 2000, while also delivering global coverage (Schaaf & Wang, 2015; Vermote et al., 2015). Sentinel-2 also operates on a global level but has a much finer resolution of 10 – 20m, which makes it extremely important for yield estimations for small fields of rural smallholder farmers (ESA, 2022; Karst et al., 2020).

5.3. Active systems (radar) and remote sensing of environmental factors

Active remote sensing systems actively emit electromagnetic energy and measure the part of this energy that is reflected and backscattered by objects. Therefore, the sensors are independent of other energy sources like the sun and can also operate at night. Examples are radar and LiDAR (light detection and ranging). As only radar satellites were used in this thesis, only this methodology will be elaborated on in more detail.

Radar originates from radio detection and ranging (Lillesand & Kiefer, 1994) and transmits short bursts or pulses of microwave energy (Figure 3). Sensors record the strength and origin of echoes or reflections of objects. Spaceborne instruments only use

Synthetic Aperture Radar (SAR) as real aperture systems would have an insufficient resolution (Lillesand & Kiefer, 1994). SAR instruments transmit microwave pulses at a

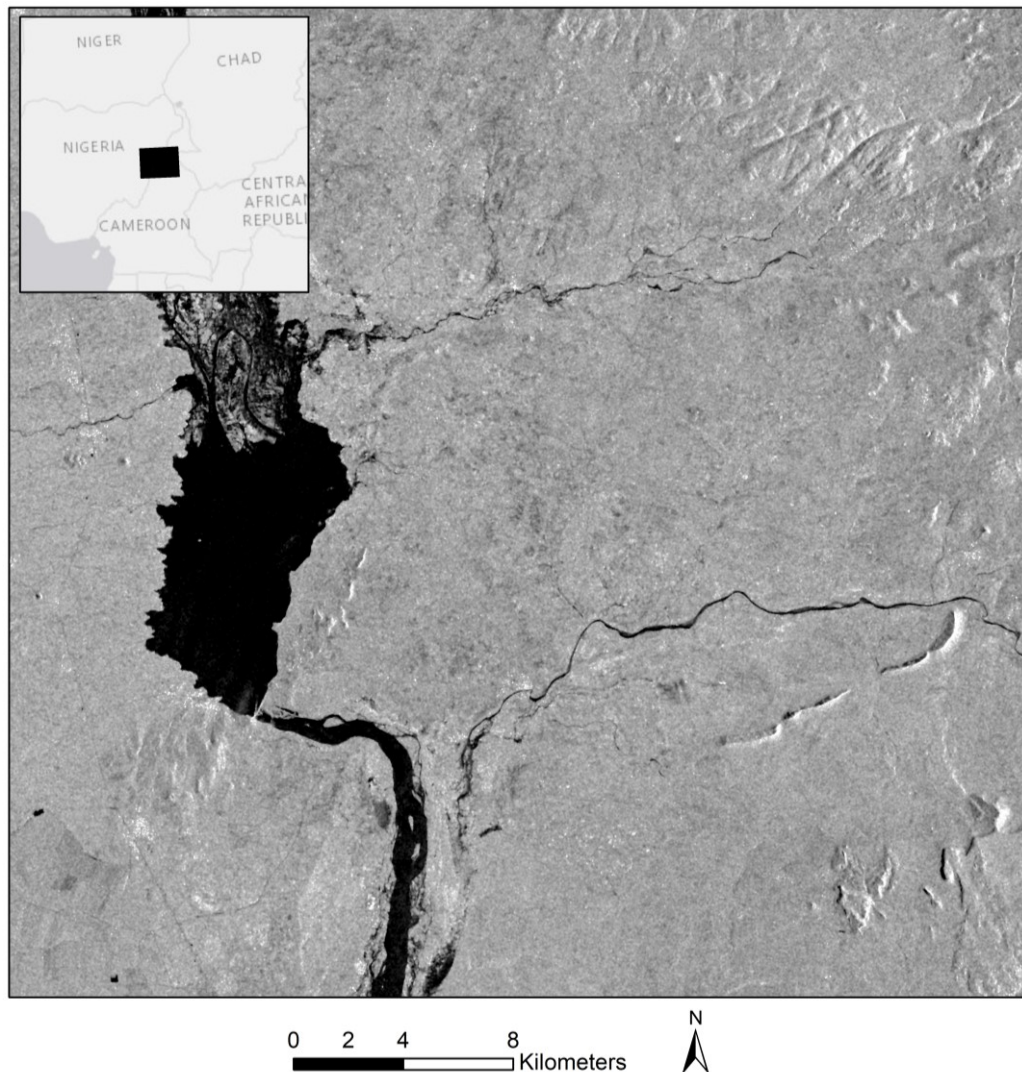


Figure 7: Exemplary preprocessed Sentinel-1 image in the border area of Chad, Cameroon and Nigeria during the wet season (19.09.2022). The black square in the inset represents the location of the image. Background: ESRI Basemaps.

given frequency and measure the backscattered energy in form of magnitude and phase (Campbell & Wynne, 2011). These relatively long wavelengths (1 mm – 1 m) (Figure 3) can penetrate clouds making SAR instruments weather-independent in contrast to optical platforms (Richards, 2009). Radar systems primarily measure the time it takes for the transmitted microwave pulses to return to the sensor. By doing so, the distance of the target can be calculated (Richards, 2009). The side-looking angles of the instruments and the terrain geometry result negative in phenomenons including radar shadows,

foreshortening, and the layover effect (Lillesand & Kiefer, 1994). As relief, e.g., mountains can slope perpendicular towards the sensor, the backside of the mountain cannot be reached by the transmitted microwave pulses resulting in zero energy measured. This is called radar shadow. Foreshortening exists when the size of the sloped surface is compressed on the recorded image and layover effects occur when the signal of the top of a vertical feature reaches the sensor before the signal of the base of the feature. Both of them are severe (layover) or less severe (foreshortening) relief displacements in the resulting image (Lillesand & Kiefer, 1994). Figure 7 shows a preprocessed Sentinel-1 SAR image where one of these phenomena can be clearly seen. Terrain effects have been reduced during preprocessing with a terrain correction, but radar shadows cannot be removed as they represent no data areas. This is shown by the black areas on the backside (left) of the elevated features in lower right corner of the image.

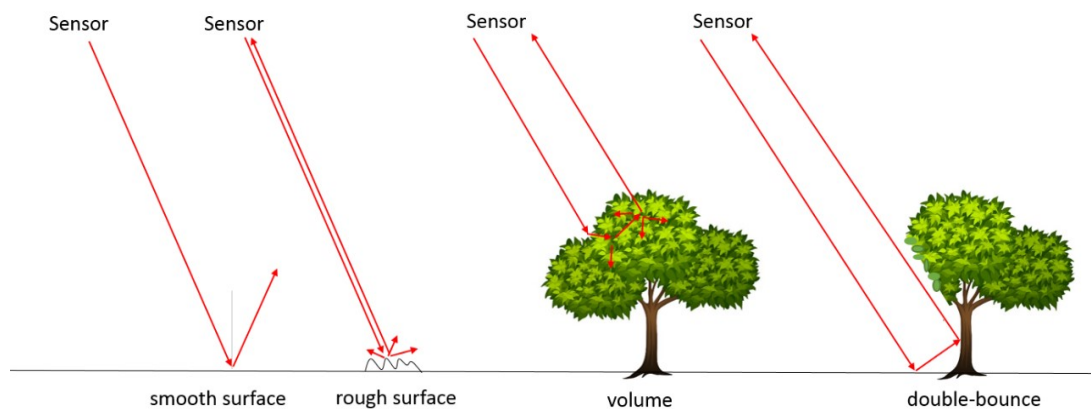


Figure 8: Schematic overview of the different scattering mechanisms surface scattering, volume scattering, and double-bounce, arrows simulate directions of energy (Berninger, 2020)

The transmitted electromagnetic waves have a geometrical orientation of the oscillations, that are specified by their polarization (Campbell & Wynne, 2011). The energy is transmitted in simple linear polarization either horizontal (H) or vertical (V). Both polarizations can be received in different channels as scattering by the objects on the earth's surface can change the polarization (Cloude, 2010). Therefore, four different combinations are possible – HH, VV, HV, and VH, where the first letter stands for the transmitted polarization and the second letter for the received polarization. HH and VV are called like- or co-polarized while HV and VH are called cross-polarized (Campbell & Wynne, 2011). Horizontally polarized waves are more sensitive to horizontally oriented features and vertically polarized waves to vertically oriented features while cross-

polarized waves are more influenced by volume scattering and co-polarization is strongly affected by surface properties like moisture (Le Toan et al., 1992). These different polarizations allow the differentiation of land cover types and properties (Campbell & Wynne, 2011). As radar systems emit energy in varying frequencies and wavelengths, their differentiation is based on bands. Sentinel-1 for example operates with the C-Band with a wavelength between 5.2 and 7.1 cm (European Space Agency, 2022). Bands and wavelength differ in the penetration depth of the signal into soil or vegetation, as in dry conditions the penetration depth increases with increasing wavelength (Campbell & Wynne, 2011). The sensor measured energy is scattered by objects, which means the redirection of energy (Campbell & Wynne, 2011) and is dependent on different properties like roughness or moisture. Different kinds of scattering are distinguished. Surface scattering represents the backscatter without interaction with other objects and depends on the roughness of the surface (Richards, 2009), volume scattering consists of numerous scattering elements in 3D bodies like trees (Campbell & Wynne, 2011), and double-bounce describes scattering resulting from two relatively smooth surfaces perpendicular to each other (Figure 8) (Richards, 2009).

In this context, smooth water surfaces are specular reflectors, that return no signals to the antenna, whereas rough water results in signal returns of varying strengths due to waves (Lillesand & Kiefer, 1994). On the basis of water as an almost specular reflector, surface water classifications can be done for example with radar data as for example in Steinbach et al. (2021). Surface water classifications in this work also followed this principle. This is also demonstrated in Figure 7, where large black areas and streamlines represent rivers and reservoirs.

5.4. Applications and remote sensing-based modeling

By using these different sensors and monitoring techniques, remote sensing can be used in various applications together with other datasets. In the following section, applications of remote sensing for drought monitoring, yield modeling, and the support of transhumance are described in more detail.

5.4.1. Droughts

Satellite data have been used for drought detection and monitoring since the 1980s (Kogan, 1997). The advantages of remote sensing-based drought indices are the large

spatial coverage and the almost continuous data availability. In contrast, difficulties and challenges arise with small areas, data gaps, consistent historical datasets, integration of recent satellite missions, and the development of a standard for a validation scheme (Hazaymeh & Hassan, 2016). The usability of data depends on its availability, cost, quality, pre-processing, and post-processing requirements (Hazaymeh & Hassan, 2016). Nevertheless, remote sensing is the most effective way to detect and analyze the impacts of droughts on ecosystems (Zhang et al., 2013).

Droughts are usually triggered by a precipitation deficit in combination with increased solar radiation and a temperature rise (Zhang et al., 2013). Using remote sensing to map this phenomenon is based on the fact that droughts affect the biophysical and chemical properties of soils and plants, such as soil moisture, organic matter content, vegetation biomass, chlorophyll content, canopy cover, and soil temperature (Anjum et al., 2011). Droughts can alter the spectral or thermal responses of ecosystems, from which indicators of their occurrence can be derived (Hazaymeh & Hassan, 2016). Remotely sensed drought indices depend primarily on the characteristics of energy reflected or emitted from the Earth's surface (Hazaymeh & Hassan, 2016). They are based on individual spectral signatures of the ground surface and tree canopy characteristics (Hazaymeh & Hassan, 2016). These signatures vary with changes in vegetation. For example, photosynthetic barriers are the result of declines in evapotranspiration and stomatal closure, leading to a reduction in absorbed photosynthetically active radiation (APAR). This is a defensive response of plants, leading to slower growth under stress - triggered, for example, by water deficits. Droughts also reduce enzyme activity in plants, which can cause damage to biomolecules and chlorophyll (H. G. Jones & Corlett, 1992; Reddy et al., 2004). This causes the leaves to dry out, fall off, and the plant dies (Zhang et al., 2013). Plant death and growth are mainly controlled by the three environmental factors of temperature, water, and sunlight, all of which are interrelated (Zhang et al., 2013). The temperature increase can be measured in the thermal wavelength range of the measurement instruments on the satellites (Zhang et al., 2013). In the optical wavelength region, the green of the plants can be inferred (Chang et al., 2017), and in the infrared region, the water content of the leaves can be inferred (Zhang et al., 2013).

The primary goal of drought research is to reduce the negative impacts of drought through improvements in water management, drought management, and agricultural practices (Di Wu et al., 2015). For proper drought strategies, temporal information on the onset,

severity, and duration is very important (Di Wu et al., 2015). Moreover, a comprehensive understanding of the causes and consequences of historical and current droughts is essential for food production and crop planning/management (Hazaymeh & Hassan, 2016). Studies aimed at better drought management exist, for example, by Bachmair et al. (2017), who modeled probabilities of drought impacts from drought reports. More consistent methods are presented by Diermanse et al. (2018) and Towler and Lazarus (2016), who conduct general drought risk analyses at regional and local scales based on meteorological and hydrological data. Going into more detail, Rojas et al. (2011) use the Vegetation Health Index (VHI) to calculate drought probabilities of agricultural land during the growing season in Africa. Even more specific are Wu and Wilhite (2004), who model drought risks for individual crops. Regional droughts were observed for example by Shen et al. (2019) who used multi-source remote sensing data with MODIS NDVI and EVI (Enhanced Vegetation Index) as well as TRMM (Tropical Rainfall Measuring Mission) data. Their deep learning model for drought showed good applicability in monitoring regional droughts. Monteleone et al. (2020) on the other hand successfully developed a new composite index for agricultural drought (PPVI (Probabilistic Precipitation Vegetation Index) in Haiti by combining the SPI and the VHI. By only using globally available remote sensing data sets their methods could also be transferred to and applied in other areas. Also, global drought models are available, but mostly on a lower resolution and therefore they often lack precise regional information. Examples are the Global Drought Observatory (Vogt et al., 2018) and Climate Engine data (Huntington et al., 2017).

5.4.2. Remote sensing for transhumance

In contrast to droughts, remote sensing related to transhumance is not as established. Most studies and analyses have been conducted based on fieldwork, like interviews or participatory mapping studies. Nevertheless, there has been some research in this field. Butt et al. (2011) for example used MODIS (Moderate Resolution Imaging Spectroradiometer) NDVI data with 1km resolution for vegetation analysis, to detect green-up and senescence times at the beginning and end of the rainy season at a higher resolution than before. Although green-up and senescence are very important for transhumant mobility, the detection of yearly varying times was not as beneficial as assumed, because the difference between green-up at the dry season homes and the wet

season destinations further north was only marginal (Butt et al., 2011). Therefore, they conclude that more spatially defined information about particular locations of vegetation green-up or the lack of senescence would be of use. Brottem et al. (2014) also used 1km MODIS NDVI data to analyze the spatiotemporal variability of forage availability which is important as green-up and senescence determine the timing of transhumance movements. They used NDVI data as a proxy for green forest and looked for inter-annual variability, seasonal changes in the connectivity of forage patches, and key locations with consistently early green-up or late senescence of the vegetation (Brottem et al., 2014). By doing so, they found information about specific locations of quality fodder and water at higher resolutions together with place names recognizable to local people. They also highlight the necessity of protecting sites with early green-up or late senescence from competing land use. Ellison et al. (2021) analyzed Landsat data from 1986 to 2017 for changes in land cover and found that rangeland transformations had negative impacts on transhumant herds' mobility and forage availability. Consequently, the rangeland stability and consent between agricultural and pastoral land users is a tipping point (Ellison et al., 2021). They further state that informed policies, land use planning, and compromises among all stakeholders will be needed in the future. Therefore, research was not only conducted on movements based on vegetation, but also on the connections between farmer-herder conflicts and climate change. McGuirk and Nunn (2020) conducted their research based on the assumption that droughts can disrupt the cooperative relationship between pastoralists and farmers, where arable land is used for crop farming during the wet season and animal grazing in the dry season. During droughts, pastoralists would migrate to agricultural land before the dry season, which causes conflicts (McGuirk & Nunn, 2020). Therefore, they analyzed a time series from 1989 to 2018 by connecting ethnographic information on traditional locations of pastoralists and sedentary agriculturalists, with rainfall data and satellite-based data on the vegetation status. Their results showed conflicts in neighboring areas of the pastoralists' territories that were affected by drought and revealed that conflicts are concentrated in agricultural areas due to the rainfalls' impact on plant biomass growth. This mechanism explains a sizable proportion of conflicts in Africa (McGuirk & Nunn, 2020). Ayana et al. (2016) demonstrate that environmental stressors are only partly predictive of conflicts. They analyzed NDVI and rainfall time series data together with conflict location data. Efforts to directly support pastoralists were also made in the past. The French Agricultural

Research Centre for International Development (CIRAD) therefore developed the “système d’information sur le pastoralisme au Sahel” (SIPSA) in 2012. Within this system satellite data was used to derive a set of biophysical indicators relating to rangeland productivity, the state of the vegetation, and the extent of surface water and burned areas (Touré et al., 2012). Furthermore, Mertz et al. (2016) stated that improved information on weather and natural resources as a support for transhumance would help to reduce the level of conflicts if communicated together with multiple options for herd movements. The modeling of movement paths or movement options concerning transhumance is still a largely unexplored field. An example can be seen in D’Abramo et al. (2021). They used GPS locations of the pastoralists’ winter and summer camps in Argentina and connected these data with terrain indices derived from a Digital Elevation Model (DEM), environmental parameters like vegetation status from 30m Landsat data, and river networks. They conducted a Least Cost Path (LCP) analysis on cost surfaces based on Ensemble Distribution Modelling (EDM) and found a good concordance with some ethnographic routes. The appropriate locations of the ethnographic routes though could not be predicted. Nevertheless, they conclude that modeling can contribute to a deeper understanding of transhumance and that human mobility is not only driven by environmental factors. Cultural and social factors (e.g., fences or paved roads) or specific herd characteristics, like size and composition, also play a role (D’Abramo et al., 2021). Modeling in general, however, allows for the identification of critical areas for seasonal mobility, which is the basis for maintaining traditional practices and developing information-based policies to regulate sustainable environmental management strategies (D’Abramo et al., 2021).

Concluding this chapter, it is evident that more research needs to be done, especially in the Sahel zone. Not only is satellite data helpful to monitor environmental conditions, but also to determine alternate grazing locations, and can serve as a basis for modeling transhumant routes. Even though exact routes cannot be predicted, modeled routes with the right input parameters can be helpful for policymakers to support transhumance itself and to minimize conflicts.

5.4.3. Remote sensing-bases yield estimations at different scales

While remote sensing for transhumance and pastoralists is not as widespread as in the drought context, remote sensing for agricultural purposes is already widely used. Past

examples include numerous studies in Europe or the US for example, as Bolton and Friedl (2013) did crop predictions on county-level based MODIS data. This section though focuses on remote sensing applications in Africa, where timely monitoring of cropland is important to ensure food security and to make agricultural activities more sustainable (Huang et al., 2019). Several challenges for remote sensing come into play in Africa. Smallholder fields are often characterized by high spatial and temporal heterogeneities, which are enhanced by intercropping and the presence of trees within plots (Bégué et al., 2020). Unfavorable weather conditions for optical remote sensing in the rainy season represent an additional challenge as for example a revisit time period of 1 – 3 days in August would be needed to get 8-day image composites with clear sky conditions of 70% of agricultural land in SSA (Bégué et al., 2020). The paucity of ground databases also causes problems as ground data are critical for developing and assessing the accuracy of remote sensing-based indicators and methods (Bégué et al., 2020). Ground data though has some limitations as they come with labor-intensive surveys and are not easily scalable. For that reason, high-resolution earth observation data is needed for crop production estimates in heterogeneous smallholder farming systems (Lambert et al., 2018). Despite recent advances in remote sensing and crop modeling for assessing agricultural conditions, reliably and cheaply assessing production losses is still challenging in complex landscapes and also points out the need for the improved collection and accessibility of reliable ground-reference data on crop types and production (Benami et al., 2021). Major uncertainties in large-scale crop modeling also arise from the lack of information on the spatiotemporal variability of crop sowing dates, which can be reduced through remote sensing (Rezaei et al., 2021). Rezaei et al. (2021) did multiple simulations of maize yields for four provinces in South Africa with previously defined scenarios of sowing dates from 2001 to 2016 and found differences of 48% of the mean yield in the long-term at the province level. Therefore, they conclude that remote sensing could help to gain a better representation of sowing dates. Samasse et al. (2018) additionally state that accurate estimates of cultivated areas and crop yield are critical to further the understanding of agricultural production and food security, especially for semi-arid regions like the Sahel, where agriculture is mainly rainfed. Accurate estimations of agricultural areas could also outline abandoned cropland. Olsen et al. (2021) for example found that conflicts in South Sudan led to a reduction of 16% in cultivated cropland and that the abandoned croplands could have supported food for

around 25% of the population in the southern states of South Sudan. This shows that it is also important to identify land where agricultural production can be practiced to support food security. Studies on yield estimations have also been conducted by Leroux et al. (2019), who forecasted yields by two months with a combination of remote sensing, crop modeling, and machine learning. They also found that more research on the spatial variability of yields is needed to strengthen agricultural monitoring systems. Petersen (2018) used MODIS data to predict yields at the country level in Africa based on NDVI, EVI, and NDWI anomalies for vegetation health. The predictions were done for each of the countries' main crops while finding errors of less than 2% for 20% of the predictions and errors of less than 5% for 40% of the predictions. To support food security on the household level in rural areas though, high-resolution satellite data is needed. Therefore, Lambert et al. (2018) used Sentinel-2 and ground data to estimate individual crop production at farm-to-community scales. Through Sen2-Agri (Sentinel-2 for Agriculture) estimates of the LAI (Leaf Area Index), they got correlations between 0.48 and 0.8 with an uncertainty of 0.3% of the total production for the main crops in Mali. Karst et al. (2020) went further by producing yield predictions at the field level for smallholder farmers. They used Sentinel-2 data together with ground observations to build a linear regression model based on different vegetation indices for crop yield estimations. While only having one year of training data, they state that yield predictions of smallholder fields provide crucial information for food security and health-related issues like malnutrition.

6. Objectives and structure of the thesis

The climate change-related risks on livelihoods in Africa make it evident, that large-scale monitoring measures are needed to help local and especially rural communities in adapting to climate change and to improve health and livelihood outlooks.

Therefore, the overarching aims of this thesis, are:

- the development of satellite-based approaches to support livelihoods, food security, and studies on natural resources
- the demonstration of satellite-based monitoring as precursors decision support tools for policymakers,
- the support of prevention measures regarding health risks, conflicts, and food insecurity in Africa through remote sensing-based evidence, and
- providing an outlook on how satellite data and derivative products can be used efficiently in multiple domains.

This thesis is divided into four chapters based on stand-alone publications, which are surrounded by a general introduction including theory and background that provides detailed information on the different topics, as well as a synthesis including a discussion of the four studies in the context of the overarching aims of this thesis together with an outlook over future research.

The first study (Chapter I) describes a regional transferable drought modeling framework based on satellite data and national yield statistics. After being trained in a ‘data-rich’ area, the modeling framework was transferred to southern Africa to provide monthly drought monitoring measures on a regional scale.

In Chapter II, environmental suitability maps for transhumance were developed through remote sensing data, survey data, and other geospatial data sources. Theoretical optimal movement paths of pastoralists along the highest environmental suitability scores were additionally modeled. By combining the suitability maps and modeled movement paths with other data sets, for example on conflicts, a potential decision support and planning tool is presented to support conflict prevention in the Sahel.

Chapter III consists of an intercomparison of remote sensing-based algorithms to detect surface water. It provides a systematic evaluation of different existing algorithms and

points out the pros and cons of different sensors and models for surface water detection and monitoring.

The last study (Chapter IV) describes a high-resolution, satellite-based modeling approach for yield estimates at the smallholder field level. By using for the first time an in-situ dataset of three years of field measurements, this study examines if it is possible to make the time- and cost-consuming field measurements obsolete. Therefore, models based on one year of training data are compared to the general crop yield model based on three years of training data.

The results of the studies support the conceptualization of monitoring systems, prevention measures, and decision support tools, that are essential to maintain livelihoods in Africa, which face several health risks, food insecurity, and conflicts. The analyses are partly nested in research units like the DFG research unit “Climate Change and Health in Sub-Saharan Africa” and partly depend on close cooperations with institutions such as the International Organization for Migration.

II. Spatially transferable modeling framework for regional drought assessment in Southern Africa (Chapter I)

Schwarz, M., Landmann, T., Cornish, N., Wetzel, K.-F., Siebert, S., Franke, J. (2020) A Spatially Transferable Drought Hazard and Drought Risk Modeling Approach Based on Remote Sensing Data. *Remote Sensing*, 12(2), 237. DOI: <https://doi.org/10.3390/rs12020237>



Article

A Spatially Transferable Drought Hazard and Drought Risk Modeling Approach Based on Remote Sensing Data

Maximilian Schwarz ^{1,2,*} , Tobias Landmann ¹, Natalie Cornish ¹, Karl-Friedrich Wetzel ², Stefan Siebert ³  and Jonas Franke ¹

¹ Remote Sensing Solutions GmbH, Dingolfinger Str. 9, 81673 Munich, Bavaria, Germany; landmann@rsggmbh.de (T.L.); cornish@rsggmbh.de (N.C.); franke@rsggmbh.de (J.F.)

² Institute of Geography, University of Augsburg, Alter Postweg 118, 86159 Augsburg, Bavaria, Germany; karl-friedrich.wetzel@geo.uni-augsburg.de

³ Institute for Crop Sciences, University of Göttingen, Von-Siebold-Str. 8, 37075 Göttingen, Lower Saxony, Germany; stefan.siebert@uni-goettingen.de

* Correspondence: schwarz@rsggmbh.de; Tel.: +49-89-48954765

Received: 30 October 2019; Accepted: 8 January 2020; Published: 9 January 2020



Abstract: Drought adversely affects vegetation conditions and agricultural production and consequently the food security and livelihood situation of the often most vulnerable communities. In spite of recent advances in modeling drought risk and impact, coherent and explicit information on drought hazard, vulnerability and risk is still lacking over wider areas. In this study, a spatially explicit drought hazard, vulnerability, and risk modeling framework was investigated for agricultural land, grassland and shrubland areas. The developed drought hazard model operates on a higher spatial resolution than most available drought models while also being scalable to other regions. Initially, a logistic regression model was developed to predict drought hazard for rangelands and croplands in the USA. The drought hazard model was cross-verified for the USA using the United States Drought Monitor (USDM). The comparison of the model with the USDM showed a good spatiotemporal agreement, using visual interpretation. Subsequently, the explicit and accurate USA model was transferred and calibrated for South Africa and Zimbabwe, where drought vulnerability and drought risk were assessed in combination with drought hazard. The drought hazard model used time series crop yields data from the Food and Agriculture Organization Corporate Statistical Database (FAOSTAT) and biophysical predictors from satellite remote sensing (SPI, NDVI, NDII, LST, albedo). A McFadden's Pseudo R^2 value of 0.17 for the South African model indicated a good model fit. The plausibility of the drought hazard model results in southern Africa was evaluated by using regional climate patterns, published drought reports and a visual comparison to a global drought risk model and food security classification data. Drought risk and vulnerability were assessed for southern Africa and could also be spatially explicit mapped showing, for example, lower drought vulnerability and risk over irrigated areas. The innovative aspect of the presented drought hazard model is that it can be applied to other countries at a global scale, since it only uses globally available data sets and therefore can be easily modified to account for country-specific characteristics. At the same time, it can capture regional drought conditions through a higher resolution than other existing global drought hazard models. This model addressed the gap between global drought models, that cannot spatially and temporally explicitly capture regional drought effects, and sub-regional drought models that may be spatially explicit but not spatially transferable. Since we used globally available and spatially consistent data sets (both as predictors and response variables), the approach of this study can potentially be used globally to enhance existing modelling routines, drought intervention strategies and preparedness measures.

Keywords: drought; hazard; vulnerability; risk; modelling; MODIS; USA; South Africa; Zimbabwe; agriculture

1. Introduction

Drought is a recurring, extreme, climatic event [1,2] that is generally defined as an extended period with abnormal low rainfall relative to the statistical multi-year average. Furthermore, droughts can be categorized into meteorological, hydrological, agricultural and socioeconomic droughts. This study focuses on agricultural droughts that appear when rainfall deficits lead to impacts on crops that cause yield losses [3]. According to the Intergovernmental Panel on Climate Change (IPCC), drought is set to increase globally in both frequency and severity due to climate change [4]. Drought frequency and severity increased notably in the previous decades [5], while drought risk is amplified by numerous factors such as population growth, environmental degradation, industrial development and fragmented governance in water and resource management [6]. Monitoring drought hazard and impact is highly critical due to the widespread effects of drought on various sectors of the agro-ecological system [7], the potential for enormous damage to the economy, society, and the environment [8–11]. For humans, agriculture is the most vulnerable sector impacted by drought [12].

Spatially explicit drought monitoring can ensure drought preparedness and help to provide preventive measures in particular vulnerable areas. Remote sensing has the ability to measure biophysical vegetation properties over larger areas, making it an effective way to assess the impact of drought on terrestrial ecosystems [13]. For more than 30 years, remote sensing technology allows to cover a large spatial footprint with near-continuous data availability [14], and benefits analyses of agricultural droughts [15]. In previous studies, multiple earth observation approaches for agricultural droughts have been developed. For example, a high-resolution soil moisture index (HDMSI) was correlated with rainfall data and crop yields over the Korean peninsula and showed good results for monitoring meteorological and agricultural droughts [16]. A Drought Severity Index (DSI) was computed for China to analyze drought trends and correlations with crop yields in the past, which allows monitoring agricultural droughts in space and time [17]. Bayissa et al. [18] created a combined Drought Indicator for Ethiopia (CDI-E) and correlated it with rainfall and crop yield data. The CDI-E showed good correlation results with the rainfall data, but the correlation with crop yield data showed to be highly area-dependent. Zhang et al. [19] analyzed droughts from multiple perspectives from 1981 to 2013 in India and established a relationship between droughts and crop yield anomalies. While this is a comprehensive multi-perspective approach, the analysis was conducted for a determined period of time and to our knowledge, has not been developed for near-real time monitoring. Furthermore, only wheat was used as a crop type for crop type anomalies, while we focus on total country yield that inherently accounts for multiple crop type. Sur et al. [20] developed the agricultural dry condition index (ADCI) based on MODIS satellite data in South Korea by combining weighted indices on soil moisture, vegetation health and land surface temperature. The results showed a good correlation with crop yield data from potatoes and soybeans, which showed that the ADCI is capable of monitoring droughts in East Asia. Qu et al. [21] also used MODIS satellite data to derive indicators on vegetation health over the Horn of Africa (HOA) and monitored extreme droughts by analyzing trends of rainfall and vegetation health data. Additionally, the Vegetation Health Index (VHI) showed a high correlation with rainfall data over the 2015–2016 drought, but was not compared to agricultural yield data. Other research analyzed drought hazard by using remote sensing derived indicators on vegetation health (NDVI, NDII) [22], rainfall anomalies (SPI), LST [23,24] and albedo [2,25]. We followed these research approaches, but additionally combined these explicit (pixel-based) drought occurrence measures with globally available yields and socioeconomic data to better capture drought hazard, vulnerability and risk. Moreover, these previous studies have either not been tested in other geographic areas or did not show a robust correlation with crop yields over the whole study area, which limits a wider application

II. Spatially transferable modeling framework for regional drought assessment in Southern Africa (Chapter I)

of these approaches. In contrast to these regional analyses, some global drought models are available at lower spatial resolution which are often lacking precise regional information like for example the Global Drought Observatory [26] or Climate Engine data [27].

Producing spatially explicit information on drought hazard, vulnerability and risk has thus multiple challenges. Whereas global models do not allow for characterization of regional drought events due to low spatial resolution, regional models are often not transferable to other countries or regions.

In the present study, a satellite-based drought hazard model for agricultural and rangeland at a spatial resolution of 0.01° using independent socioeconomic time series data as reference data was developed. Additionally, a simplified drought risk indicator was calculated through combining drought hazard and vulnerability. Pertaining to drought hazard modeling, this study exploits the unprecedented potential of a longer observation period to statistically identify individual or several drought years for robust model parametrization and model drought hazard, given the availability of nearly 18 years of biophysical time-series from MODIS currently (2001–2019). We aimed to produce a drought modeling framework reflecting regional conditions while also potentially being globally transferable since the model only bases on globally available data for parametrization and modeling. With this model we addressed the gap between global models, that work with a low spatial resolution and cannot capture regional droughts, and local and regional drought models that either do not use globally available consistent data or have not been tested in other geographical regions. Our drought model works on a moderate spatial resolution that can capture regional droughts and is potentially spatially transferable due to the use of globally available data (i.e., the FAO crop stats yields data). In order to test the transferability of the hazard modeling framework, it was applied in three countries and cross-evaluated with other reference data such as the United States Drought Monitor (USDM) in the USA, a global drought model, food security classification data as well as published drought reports.

2. Materials and Methods

The overall approach entailed to first develop the drought hazard model for the Missouri Basin in the USA using a statistical logistic regression model based on time series data of remote sensing-based predictors. The results were then evaluated through a comparison with the USDM. Subsequently, the model was transferred and applied to Zimbabwe and South Africa where the model results were verified with reports in newspapers and regional climate patterns. The developed model for southern Africa was additionally compared to the Global Drought Observatory (GDO) and to food security classification data from the Famine Early Warning Systems Network (FEWS NET) and subsequently discussed. This will show how our model benefits compared to global drought models and why it is spatially transferable. Lastly, drought vulnerability was assessed for South Africa and Zimbabwe based on data on population and livestock density, the gross domestic product (GDP) and farming systems (rain fed or irrigated). Drought hazard and drought vulnerability were then combined to determine drought risk for Zimbabwe and South Africa, respectively (more in Section 2.3). In creating a spatial modelling framework that uses socio-ecological data relevant to risk and vulnerability (i.e., yields) as well as spatially explicit yet wide-areas' remote sensing predictors, drought effects and impacts of droughts can be explicitly and feasibly predicted.

2.1. Study Area

The study areas encompassed cropland and rangeland areas within dry and mild temperate agro-meteorological biomes in the United States of America (USA), South Africa and Zimbabwe [28]. The American site was limited to the Missouri Basin, an area with widespread cropland and rangeland. In comparison to other agricultural areas in the USA such as the 'Corn Belt', the Missouri Basin is a less examined area regarding droughts. The Missouri Basin was also chosen as being a data-rich study site with an established drought monitoring system (the U.S. Drought Monitor), which ensured that the model could be developed and evaluated with good quality reference data. South Africa

II. Spatially transferable modeling framework for regional drought assessment in Southern Africa (Chapter I)

represents a country with widespread, diverse agriculture (commercial and subsistence) and data availability on vulnerability at scales finer than administrative boundaries. Zimbabwe, on the other hand, can be considered a data-poor country with only limited data available on administrative scales and widespread small scale and subsistence farming.

2.2. Geo-Data

Existing land use data for the USA and southern Africa (National Land Cover Database (NLDC) for the USA, Climate Change Initiative Landcover—S2 prototype land cover of Africa (CCI)) was aggregated to mask out irrelevant land use and land cover classes (Table 1). Only agricultural land, grass- and bushland were considered in the analysis. To identify historical drought years and non-drought years, crop yield data from the Food and Agriculture Organization of the United Nations [29] was used. Within the three study areas, the FAO yield data for the crop types maize, green maize, soybeans, wheat, and sorghum was analyzed. Subsequently, MODIS and CHIRPS (Climate Hazards Group InfraRed Precipitation with Station data) data were used to produce predictors for the logistic regression modelling drought probabilities. In order to assess drought vulnerability and drought risk as a combination of drought probability and vulnerability, gridded data for population density (product: Gridded Population of the World v4 (GPWv4)), the gross domestic product (GDP) (product: GDP_PPP_30arcsec_v2), farming systems (irrigated or non-irrigated) and livestock density was furthermore used as predictors for both the drought risk and drought vulnerability. Each of these products was resampled to a harmonized spatial resolution of 0.01° before including it in the analysis. The loss of information through resampling is considered neglectable, since drought is a regional or larger-scale phenomenon and drought information is needed for the whole region but not for single agricultural fields.

Table 1. Summary of the data used in this study.

Data	Product	Spatial Resolution	Period	Spatial Coverage	Data Source
<i>Land use classification</i>					
Land use	NLCD	30 m	2011	USA	[30]
Land use	CCI	20 m	2016	Africa	[31]
<i>Definition of drought periods</i>					
Crop yield	FAOSTAT	National statistics	2001–2016	Global	[29]
<i>Predictors for logistic regression model</i>					
Precipitation	CHIRPS	0.05°	1981–2018	50°S–50°N	[32]
Surface reflectance	MOD09A1	500 m	2000–today	Global	[33]
LST	MOD11A2	1 km	2000–today	Global	[34]
Albedo	MOD43A3	500 m	2000–today	Global	[35]
<i>Data for drought vulnerability and drought risk analysis</i>					
Population density	GPWv4	30 arc-sec	2015	Global	[36]
Gross domestic product	GDP_PPP_30arcsec_v2	30 arc-sec	2015	Global	[37]
Farming systems	Farming Systems	30 m	2017	Zimbabwe	[38]
Livestock density	-	~0.08°	2010	Global	[39]

2.3. Methodology

The input data for the drought hazard analysis (bold box), including land use data, SPI, and MODIS-derived index anomalies, were processed to obtain standardized anomalies as input variables for the logistic regression model (Figure 1). Subsequently, the drought and non-drought years were extracted and used as training data for the hazard model. During the model optimization autocorrelation and multicollinearity was tested as well as the relevance of each individual predictor variable. Relationships between the predictor variables and their importance for the model outcome can change regionally and therefore have to be assessed. After model optimization, the input predictors for the modeling were determined and pixel-level drought hazard probabilities were predicted.

II. Spatially transferable modeling framework for regional drought assessment in Southern Africa (Chapter I)

Remote Sens. 2020, 12, 237

5 of 22

The drought hazard analysis was first carried out in the Missouri Basin. After being evaluated by a comparison with the USDM, the model was transferred to southern Africa. Subsequently, a drought vulnerability index was generated by combining relevant indicators, which was then used together with the drought probability to assess drought risk (dashed box) in southern Africa. The individual steps are described in detail below.

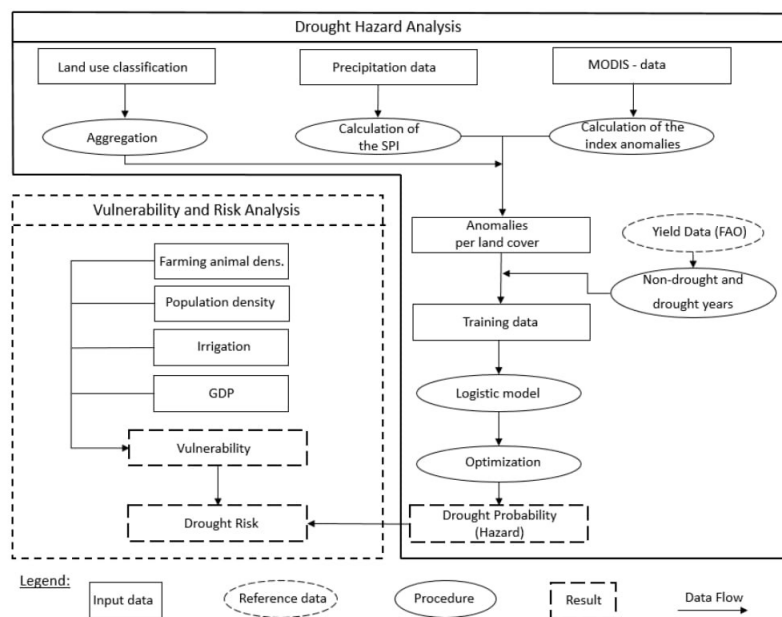


Figure 1. Workflow of the drought hazard, vulnerability and risk analysis.

2.3.1. Drought Hazard Analysis

(1) Processing and Calculation of the Model Predictors

The precipitation data was used to produce the Standardized Precipitation Index (SPI), with the methodology from Mckee et al. [40]. The study at hand used the three-monthly SPI. For each month, rainfall data from the present month and the two previous months was accumulated from 1981 to 2017 before the SPI was calculated.

The MODIS data was processed differently for each product. The 8-day composites of the MOD09A1 product were corrected with the quality state flags to remove cloudy pixels. Subsequently, the Normalized Difference Vegetation Index (NDVI) [41] and the Normalized Difference Infrared Index (NDII) [22] were produced from the cloud masked MODIS bands between 2001 and 2017 at its original spatial resolution of 500 m. The indices were processed by calculating their monthly maxima and thus further reducing cloud influence [42]. The 8-day composites of the MOD11A2 product, on the other hand, were not corrected for clouds since the land surface temperature (LST) was only produced for cloud-free pixels [43]. Monthly maxima were also calculated for the LST. The 16-day composite MOD43A3 albedo product was selected on the 15th of each month and was assumed to be the monthly mean. From the MODIS albedo product, the mean of all three albedo bands (visual, near infrared, short wave infrared) was calculated and used as an input variable in this study.

In addition, index anomalies were produced to develop a normalized and spatially invariant measure that reduces the influence of spatially varying vegetation and land cover types. This was done for all MODIS-based indices used as model predictors (NDVI, NDII, LST, mean albedo). The anomalies

II. Spatially transferable modeling framework for regional drought assessment in Southern Africa (Chapter I)

were calculated as the deviation of the long-term mean standardized with the standard deviation (“z-score”) [22]:

$$Z_{kxy} = \frac{(DI_{kxy} - \alpha_{kx})}{\sigma_{kx}}, \quad (1)$$

Z_{kxy} represents the anomaly value for kernel k during the time span x , which was 2001–2017 in this study, for a given month y . DI_{kxy} stands for the drought index value for kernel k during the time span x in month y and α_{kx} and σ_{kx} represent the mean and standard deviation of kernel k over the time span x . The index anomalies were then used as predictors for the logistic regression model.

(2) Identification of Drought Periods

After the vegetation and rainfall index anomalies were derived, they were masked with the aggregated land use classification (Figure 1). Subsequently, drought and non-drought periods were determined within the growing periods of the main crops maize, green maize, sorghum, soybean, and wheat. For the USA, the growing season was assumed to last from May to September and for southern Africa from November to March. Drought periods were identified as drought seasons or drought years, using a segmented regression of the FAO’s annual yield data [29]. Long term shifts in the total yield are possible for example due to advances in technologization, widespread use of fertilizers or the implementation of irrigation. To consider these shifts in the modeling framework, the regression divided the time series into several segments and assigned a stable regression relationship to each segment [44]. Considering a standardized linear regression model

$$y_i = x_i * \beta_i + u_i \quad (i = 1, \dots, n), \quad (2)$$

where y_i represents the estimate of the linear relationship of the response to x_i that includes the yield observations sorted by time i after applying ordinary least squares to the linear regression model. β_i represents the linear parameter estimates and u_i the constant. Assuming that there are m breakpoints, this model changes to

$$y_i = x_i * \beta_j + u_i \quad (i = i_{j-1} + 1, \dots, i_j, \quad j = 1, \dots, m + 1), \quad (3)$$

where j represents the segment index. Zeileis et al. [44] developed an algorithm in “R”, a software environment for statistical computing, to automatically determine these breakpoints, which was used in this study. It was assumed that a segment would last a minimum of four years. This limits the total number of breakpoints for each crop type in each study area to three, given the assessed time period spans 2001 to 2017. Muggeo [45] transcribed the segmented regression model as a function in R that could be applied to the data using the breakpoints defined from the breakpoint analysis. In each study area, the residuals of the model for each crop type were subsequently determined individually and then accumulated. The five crops used in this study stand as representatives for the total agricultural yield in the three study areas. The standard deviation was calculated from the summed residuals in each region. The growing periods where residuals fell below one negative standard deviation were defined as drought years or periods. Non-drought years were periods in which the residuals exceeded one positive standard deviation. Any growing periods with values with a standard deviation between -1 and 1 were not considered, in order to ensure clean and distinctive training classes for the model. As a result, the drought years identified for model parametrization were only those years where a large-scale drought caused yield deficits and which affected the entire country during each respective growing period. A potential effect of yield losses caused by floods, pests or diseases (other than drought effects) in the training data was minimized by considering not only one crop type to determine drought, but rather five crop types. Since national yearly yield statistics for five crop types were used to identify a drought year, potential effects from small scale yield losses of non-drought causes on the training data are minimized. The drought and non-drought periods identified between 2001 and 2010 served as training data for the logistic regression model described in the following section.

II. Spatially transferable modeling framework for regional drought assessment in Southern Africa (Chapter I)

(3) Logistic Regression Model

Binary logistic modeling has been successfully proven in numerous studies using remote sensing variables as predictors. Such models are also known to render robust variable relevancies, when correlation among variables is accounted for [46,47].

For the identified drought and non-drought years, monthly anomaly data from the NDVI, NDII, LST, albedo and 3-month SPI data were extracted for the relevant land use classes in the 2001–2010 training period for all months of the growing season. 2011 to 2017 was used to test the model. The anomalies were resampled to a spatial resolution of 0.01° and used as predictors for the logistic regression model (Figure 1). Thus, each pixel classified as agricultural, grass or bushland was defined as either a drought or a non-drought observation within the entire study area over the entire respective crop growing season. A random sample of 100,000 pixels (=observations) was taken per class (drought or non-drought) as training data.

Subsequently, the five input indices were tested for autocorrelation and multicollinearity using a Pearson correlation matrix and the condition index. Dormann et al. [48] suggest that a threshold of 0.7 in the pairwise Pearson correlation matrix indicates variables that strongly influence the model. For the condition index, values that exceed a value of 30 are considered critical and indicate strong multicollinearity [48]. Only variables that exhibited no multicollinearity according to the Pearson correlation and the condition index were included in the model as predictors. A logistic model was used to predict a binary classification of the dependent variable y (drought or non-drought). The probability produced by the logistic model with values between 0 and 1 were considered to be drought hazard. The calculation of the probability values $p(X)$, that are translated into drought hazard, are defined using the logistic function [49]:

$$p(X) = \frac{e^{\beta_0 + \beta_1 X}}{1 + e^{\beta_0 + \beta_1 X}}, \quad (4)$$

with a linear regression function as basis [49]:

$$p(X) = \beta_0 + \beta_1 X \quad (5)$$

After setting up the model, the z and p values of the individual predictors were analyzed. High z values ($>|+/-2|$) indicate a decisive influence of the variable on the modeling results. This finding can be confirmed with significant p values (<0.01) [49].

To evaluate the goodness of fit for the logistic regression model McFadden's Pseudo R^2 was used [50]:

$$R_{MF}^2 = 1 - \frac{l_M}{l_0}, \quad (6)$$

l_M represents the log-likelihood of the estimated model and l_0 the log-likelihood of the zero model, which consists of only one constant. Values greater than 0 indicate predictive qualities of the model, while 1 reflects a perfect predictive power [50]. The values of McFadden's Pseudo R^2 are generally much lower than those of the R^2 of general linear regression models. Values between 0.2 and 0.4 indicate an excellent model fit for McFadden's Pseudo R^2 [51].

(4) Verification of the model results

In addition to the statistical evaluation described above, the model was also checked for plausibility. The Missouri Basin study area in the USA was the only site, where an operational drought model (USDM) was available. The USDM is recognized as an advanced tool for drought monitoring in science (e.g., [12]). The data is produced by the National Drought Mitigation Center of the University of Nebraska-Lincoln, the United States Department of Agriculture, and the National Oceanic and Atmospheric Administration and is available on the USDM's homepage (<http://droughtmonitor.unl.edu/Data/Download/ComprehensiveStatistics.aspx>). A visual comparison between the USDM maps and those produced by the logistic regression model provided a qualitative assessment of the model's plausibility.

II. Spatially transferable modeling framework for regional drought assessment in Southern Africa (Chapter I)

Due to the lack of spatial drought information besides global drought models, the verification in South Africa and Zimbabwe was based on newspaper reports and reports from aid agencies published in the World Wide Web (e.g., BBC News) about time periods and areas affected by drought. In addition, model results were compared against occurrence information of El Niño events, as teleconnections of the El Niño phenomenon are known to cause drought in southern Africa [52]. By comparing the data to the teleconnections caused by the El Niño and the drought reports, the model plausibility was assessed for Zimbabwe and South Africa. Finally, the model output was also compared to the Global Drought Observatory provided by the Joint Research Center (JRC) with the key input variables derived from meteorological, soil moisture and vegetation greenness data for drought hazard, population data and baseline water stress for drought exposure and social, economic and infrastructural factors like the level of well-being of individuals for vulnerability. Additionally, we used food security classification data from the Famine Early Warning Systems Network (FEWS NET) for Zimbabwe as a cross-verification source for the drought hazard model.

2.3.2. Vulnerability and Risk Analysis

A simplified drought risk analysis was performed by calculating a drought risk indicator, where risk is the product of vulnerability and hazard [53]. Drought hazard is defined as the probability of a drought occurring, which was calculated by the logistic regression model, while the vulnerability is a relative measure that indicates the degree to which a system is susceptible to damage from the onset of the harmful phenomenon (e.g., drought) [54].

The factors influencing the drought vulnerability in this study were the proportion of irrigated land, the gross domestic product per area, the population density and the density of grazing animals (cattle, sheep, goats). Areas with a higher gross domestic product indicate a lower drought vulnerability. Population density above 300 inhabitants per km² [55], urban areas and pixels immediately adjacent to urban areas were excluded from the analysis since we were only looking at crop- and rangeland. Each individual variable was normalized for each study area as follows:

$$y_i = \frac{x_i - x_{min}}{x_{max} - x_{min}}, \quad (7)$$

whereby y_i is the focused standardized value, x_i is the observed value and x_{min} and x_{max} are the minimum and maximum of all observation values, respectively. Once the mean is calculated for these standardized variables, the drought vulnerability index (DVI) can be calculated using the following equation:

$$DVI_i = \frac{(1 - IL_i) + (1 - GDP_i) + PD_i + GAD_i}{4}, \quad (8)$$

where IL , GDP , PD and GAD represent the mean of irrigated land, gross domestic product, population density and grazing animal density, respectively. The DVI represents the drought vulnerability and was used as a relative, spatial comparison to identify vulnerable areas. The different input variables for DVI can also be differently weighted if necessary. Drought risk was also just used as a relative measure assessed by the multiplication of DVI and drought hazard. This is due to the fact, that drought vulnerability and drought risk are highly complex and cannot be investigated in detail by including every aspect affecting them within this study. A future combination of the drought hazard model with other existing methods and models on drought vulnerability is possible.

3. Results

3.1. Drought Hazard Analysis in the USA, South Africa and Zimbabwe

3.1.1. Drought Hazard in the Missouri Basin (USA)

As stated, the development of the logistic modeling and the construction of the method was first performed in the USA before they were transferred and adapted to South Africa and Zimbabwe.

II. Spatially transferable modeling framework for regional drought assessment in Southern Africa (Chapter I)

The segmented regression (see Section 2.3.1) showed that 2002 was the only drought year detected in the USA for the training data period from 2001 to 2010, and that 2004 and 2009 were non-drought years. The pairwise autocorrelation (Table 2) showed a critical Pearson correlation coefficient of 0.71 between the NDVI and NDII. Due to a slightly higher value in the explained variance for the highest condition index (Table 3) the NDVI was excluded as an input variable for the model.

Table 2. Pairwise Pearson correlation of the model input variables for the model in the USA.

	SPI3	NDII	NDVI	Albedo
NDII	0.41	-	-	-
NDVI	0.45	0.71	-	-
Albedo	-0.3	-0.07	-0.24	-
LST	-0.56	-0.53	-0.49	0.22

Table 3. Decomposed variances of the condition index for the model in the USA (only values >0.3 are shown).

Condition Index	Albedo	LST	NDII	NDVI	SPI3
1	-	-	-	-	-
1.75	-	-	-	-	-
3.15	0.49	0.57	-	-	-
4.23	-	-	-	-	0.96
10.66	-	-	0.93	0.94	-

The summary of the model output (Table 4) shows z-values higher than |2| for all predictors with a confidence level of 99%, indicating that all variables have a significant influence and should be included in the logistic regression model. Moreover, McFadden’s Pseudo R^2 was found to be 0.16, which suggests a good fit.

Table 4. Summary of the logistic regression model for the USA.

	Coefficient	z-Value
(constant)	-0.20	-35.6
Albedo	0.13	22.6
LST	0.43	66.6
NDII	-0.83	-111.7
SPI3	-0.12	-17.6

2012 was identified as a drought year for the model application after the training data period (Figure 2). The maps of the calculated probabilities for 2012 showed increasing drought intensity while the affected area was also growing, finally covering almost the entire area of the Missouri Basin except for the southeast and northwest parts in September. In 2016, drought probabilities decreased over the course of the growing season. Towards the end of the crop cultivation period, high drought probabilities can only be seen in smaller areas in the center and south of the Missouri Basin. On the contrary, low drought probabilities, i.e., normal conditions for agricultural land, grass- and shrubland, were spread over most of the study area. Although not identical, both the model results and the US Drought Monitor indicate large areas affected by drought in 2012 that spatially match. Differences between the two drought models were more pronounced in the 2016 non-drought year.

II. Spatially transferable modeling framework for regional drought assessment in Southern Africa (Chapter I)

Remote Sens. 2020, 12, 237

10 of 22

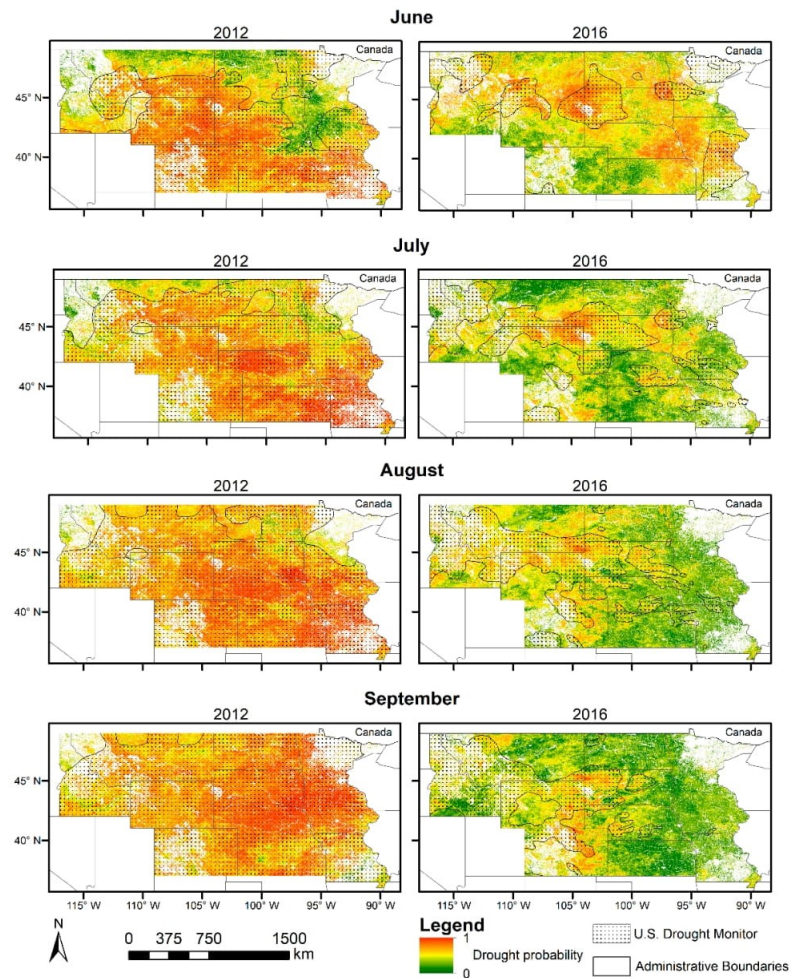


Figure 2. Modeled drought hazard in the Missouri Basin (USA) compared to the U.S. Drought Monitor (dotted polygons) for agricultural, grass- and shrubland in a drought (2012, left) and non-drought year (2016, right).

3.1.2. Applicability of the Developed Hazard Model for South Africa

The analysis over South Africa identified 2007 as a drought year and the years 2002 and 2009 as non-drought years over a time period from 2001 to 2010. The pairwise autocorrelation in South Africa does not show any Pearson correlation values higher than 0.7 and the Condition Index is also well below the critical value. As such, all variables were used to model drought probabilities in South Africa. As with the model results for the USA, all predictors showed z-values greater than |2| on a significance level of 99% (Table 5). The model for South Africa also showed a good model fit, with a McFadden's Pseudo R^2 value of 0.17.

In order to exemplarily compare the hazard model prediction for a drought and a non-drought year for South Africa, the 2013/2014 growing period (hereinafter referred to as 2014) was chosen as the non-drought period and 2015/2016 (hereinafter referred to as 2016) as the drought period (Figure 3). A comparison of the individual months clearly showed that high drought probability areas were more widespread and frequent in 2016. In the non-drought year, higher probabilities were only found in the

II. Spatially transferable modeling framework for regional drought assessment in Southern Africa (Chapter I)

center of the country in January 2014. Low to medium probability ranges were distributed over the entire growing season. During the drought period, one can see that high drought probabilities were prevalent over most of the country in December 2015, followed by a decrease over the subsequent months. In February 2016, artefacts caused by errors in the MODIS cloud mask can be seen in the center and south of South Africa.

Table 5. Summary of the logistic regression model for South Africa.

	Coefficient	z-Value
(constant)	−0.17	−31.5
Albedo	0.25	40.0
LST	0.48	59.8
NDII	−0.35	−40.2
NDVI	0.61	70.0
SPI3	−0.93	−118.1

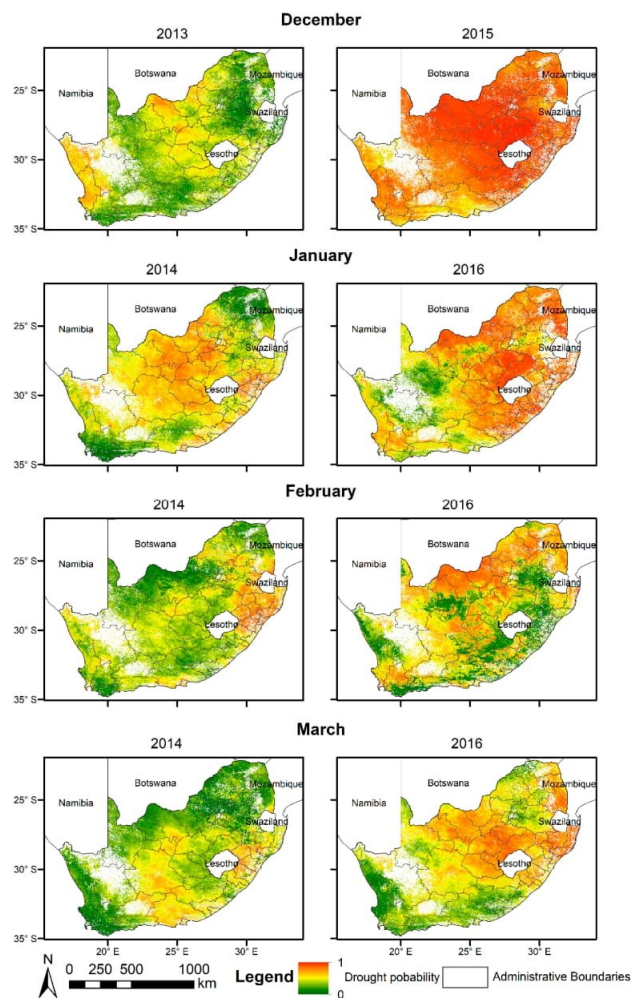


Figure 3. Modeled drought hazard in South Africa for agricultural, grass- and shrubland in a non-drought year (2013/2014, left) and a drought year (2015/2016, right).

II. Spatially transferable modeling framework for regional drought assessment in Southern Africa (Chapter I)

3.1.3. Applicability of the Developed Hazard Model in Zimbabwe

In Zimbabwe, 2003, 2005 and 2008 were identified as drought years, while 2004 and 2006 were identified as non-drought years. Neither the pairwise autocorrelation nor the Condition Index showed critical values and all predictors had a high and significant impact on the model results according to their z-values (Table 6). In contrast to the results for South Africa and the USA, the Pseudo R^2 values obtained for Zimbabwe was 0.06, which indicates a moderate predictive quality.

Table 6. Summary of the logistic regression model in Zimbabwe.

	Coefficient	z-Value
(constant)	−0.03	−6.3
Albedo	0.19	−35.4
LST	0.07	−10.1
NDII	−0.46	−67.4
NDVI	0.10	18.2
SPI3	−0.38	−57.3

The drought probabilities calculated for the 2013/2014 (non-drought) and 2015/2016 (drought) growing periods in Zimbabwe reveal differing climatic conditions (Figure 4). Similar to the conditions seen in South Africa, the latter period is a drought year while the model clearly identified 2014 as a non-drought year. In general, drought probability in Zimbabwe was higher in 2016 than in 2014 and the probabilities decreased over the growing periods of both years.

3.1.4. Evaluation of the Logistic Regression Model for South Africa and Zimbabwe

The advanced monitoring system of the USDM is not available in other countries like South Africa or Zimbabwe. Therefore, both, newspaper articles and drought reports, as well as data on the past El Niño event in 2015/2016 were used for evaluation. The known teleconnections of El Niño are hot and dry conditions between December and February in the southeastern part of Africa [56]. The Oceanic Niño Index (ONI) registered a strong El Niño event during the 2015/2016 season [57] and its effect can be seen in the model results of South Africa and Zimbabwe. The drought probabilities predicted by the logistic regression model were highest during this event, as seen prominently in the North and East of South Africa. In Zimbabwe it seems, that all areas were equally affected in the same period. A decrease in drought probabilities was also observed at the beginning of 2016 in both countries which complies with ONI's reported maximum at the end of 2015, followed by a steadily decreasing trend thereafter.

Newspapers also reported on the 2015/2016 drought in South Africa. According to BBC News [58] and Al Jazeera [59], all provinces in the East of the country like Free State, KwaZulu-Natal and Limpopo, were severely affected. These reports were consistent with the known teleconnections of an El Niño event. The hazard model results for South Africa corroborates both the reports and the climate patterns in these regions (Figure 3). The conditions in Free State and KwaZulu-Natal also lasted longer than in other regions, which is consistent with the newspaper reports claiming that these two provinces were the most affected. News24 [60] also reported extreme drought on the South African West Coast in January 2016, along with a high fire risk. This coincides with the high drought probabilities predicted for the end of 2015 and the beginning of 2016. Overall, the newspaper reports on the 2015/2016 drought and the El Niño data during the same period provide qualitative evidence that the model results resemble true conditions on the ground.

II. Spatially transferable modeling framework for regional drought assessment in Southern Africa (Chapter I)

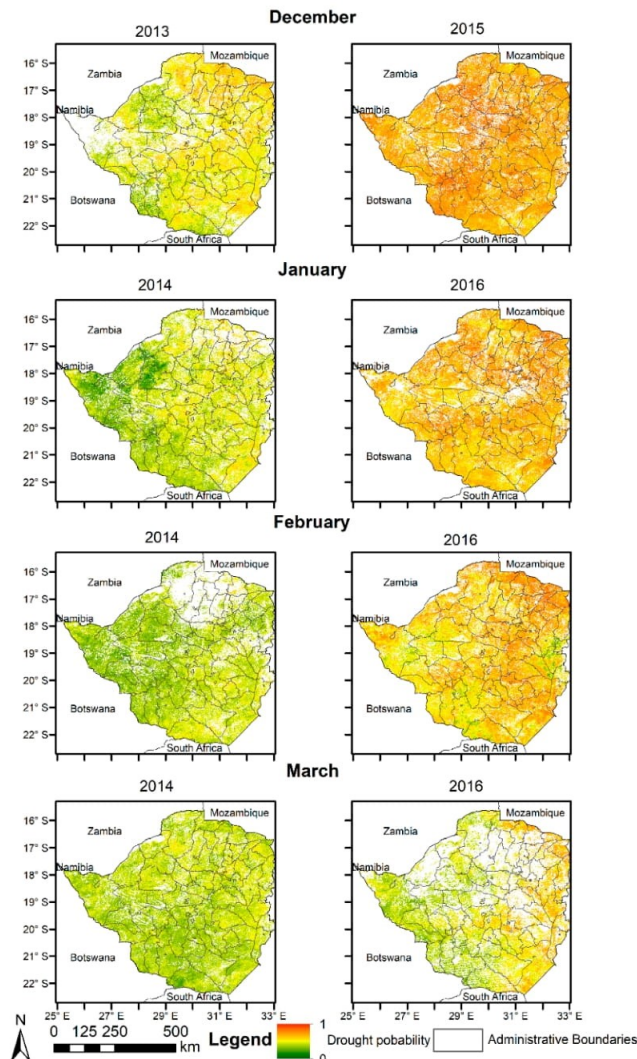


Figure 4. Modeled drought hazard in Zimbabwe for agricultural, grass- and shrubland in a non-drought year (2013/2014, left) and a drought year (2015/2016, right).

In Zimbabwe, BBC News [61] and ReliefWeb [62] both reported prevailing drought conditions in the months prior to February 2016. They cited various provinces and regions that were particularly affected, such as Hwange, Masvingo or Matabeleland South and Matabeleland North, concluding that most of the country was affected by drought. The modeled drought probability maps predicted herein corroborate this, showing high drought probabilities across the country over the same period. The results of the drought hazard model for February 2016 were also compared to FEWS NET food security classification data and drought risk data from the Global Drought Observatory (Figure 5). The visual comparison shows high drought hazard patterns across the country going along with middle to high food insecurity and middle to high drought risk. The visual agreement within this cross-verification shows the plausibility of the drought hazard model.

II. Spatially transferable modeling framework for regional drought assessment in Southern Africa (Chapter I)

Remote Sens. 2020, 12, 237

14 of 22

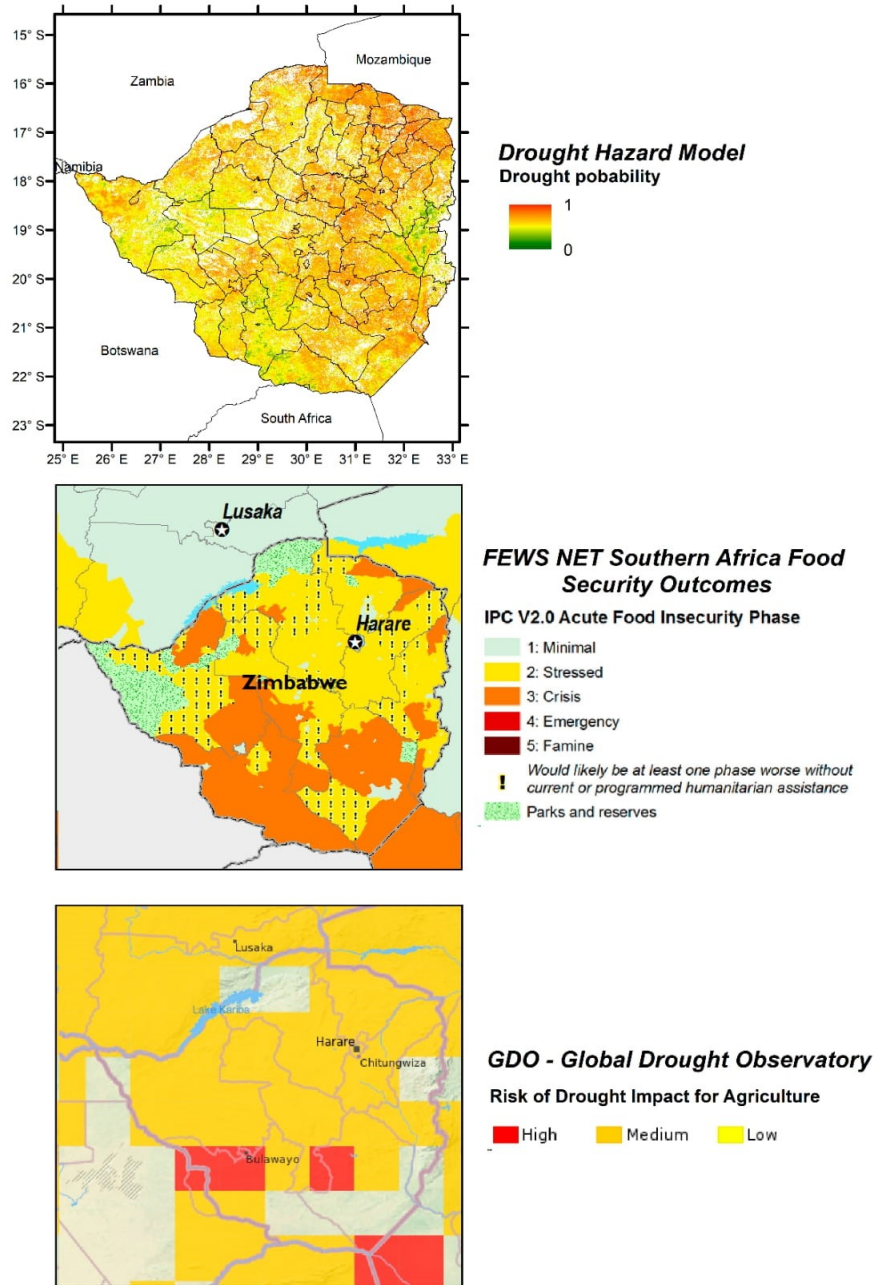


Figure 5. Comparison of the drought hazard model results (**top**) with food security classification data from FEWS NET (http://shapefiles.fews.net.s3.amazonaws.com/HFIC/SA/southern-africa201602_CS.png) (**center**) and the Global Drought Observatory (<https://edo.jrc.ec.europa.eu/gdo/php/index.php?id=2001>) (**bottom**) for the month February in 2016.

II. Spatially transferable modeling framework for regional drought assessment in Southern Africa (Chapter I)

In the observation period from 2011 to 2017, there were only reports for one wide spread drought event (2015–2016). Accordingly, the other years were considered as years with no widespread drought in both countries. Overall, the model output proved to be well suited to predict drought probabilities for agro-ecological landscapes in southern Africa.

3.1.5. Comparison between the Drought Hazard Model and the Global Drought Observatory of the Joint Research Center (JRC)

Currently, there is no known approach that utilizes remote sensing variables to predict drought hazard and has been validated against a state-of-the-art drought monitoring system. A method to predict drought hazard, vulnerability and risk in data scarce areas like Zimbabwe is also missing. However, the model presented does share similarities with the GDO's Risk of Drought Impacts for Agriculture (RDrI-Agri) product which combines drought hazard, vulnerability and exposure [26].

The comparison with the RDrI-Agri was done visually (see Figure 5 for an example) since the difference in the spatial resolution thus not allow for a pixel by pixel analysis. Both datasets predicted similar results for the 2013/2014 and the 2015/2016 growing seasons in South Africa and Zimbabwe. The 2013/2014 season showed low RDrI-Agri and low modeled hazard values while the 2015/2016 season displayed high RDrI-Agri and high hazard values. For 2016 there was, however, a slight discrepancy in drought risk and hazard intensity values that may be due to the differences in input model variables and areas under consideration.

3.2. Drought Vulnerability and Risk Analysis in South Africa and Zimbabwe

Figure 5 shows low drought vulnerabilities along the southern coast of Africa and parts of eastern South Africa, as well as in western Zimbabwe. The southeastern part of Zimbabwe also showed some isolated areas with lower drought vulnerabilities over the observation period which could be due to irrigated croplands. The most vulnerable regions were Free State and KwaZulu-Natal in South Africa and the provinces around Masvingo like Chivi and Buhera in Zimbabwe.

A comparison of the two growing periods for South Africa and Zimbabwe showed clear differences in drought risk. In 2013/2014, low drought risk values were visible over larger areas in South Africa and Zimbabwe while the vulnerability was constant over the full observation period. On the contrary, for the drought within 2015/2016, a greater drought risk could be predicted over a larger area. The most vulnerable regions in both countries are also clearly discernable in the risk maps for both years.

4. Discussion

The model produced spatially explicit information on drought hazard, drought vulnerability and drought risk that performed well according to the quantitative and plausibility checks.

In the comparison with the Global Drought Observatory, there were some discrepancies in the intensity of drought risk and drought hazard which could be due to the diverging methods used. In the RDrI-Agri model, the risk of drought impact on agriculture is predicted while the model presented here predicts drought hazard probabilities on agricultural and rangeland. This presented model also runs on a spatial resolution of 0.01° which is more detailed than the RDrI-Agri model's 1° . On the other hand, the RDrI-Agri model offers a higher temporal resolution, producing maps every 10 days instead of each month. The drought risk product presented here, could not be compared to the RDrI-Agri model because our drought risk model result only considers crop growing seasons'. Due to the complexity of drought effects and impacts, validation of drought models is difficult in general. The presented quantitative figures of model's McFadden's Pseudo R^2 , p values, however, demonstrated the plausibility of the results. Hagenlochner et al. [54] stated that less than 20% of their reviewed drought studies have conducted any form of validation or evaluation of their results. Considering that lack of validation methods and the lack of reference data we used a variety of available information and data to cross-verify our results. Even though this could not be done in a quantitative way, this alternative cross-verification approach showed to be effective for model plausibility checks.

II. Spatially transferable modeling framework for regional drought assessment in Southern Africa (Chapter I)

The spatial transferability of our approach is generally possible since we are using globally available FAO yield response data (as response variables) combined with globally available remote sensing data as predictors. However, the method should be used with care for regions where strong and large-scale yield anomalies are caused by factors different from drought. The logistic regression model that was developed (trained) for the Missouri Basin, could be successfully applied to South Africa and Zimbabwe, thus further demonstrating the transferability of the hazard modeling approach. The application of the model should run at country level, since the FAO yield data is only available at this spatial unit. It is also important to mention that the model itself needs to be country-specifically calibrated and set up when being transferred but always based on the same input data. When setting up the model, multicollinearity should also be checked and minimized during the model optimization process. The final model equation can also contain different variable relevancies depending on the country or region. The need for a country-specific set up becomes apparent when comparing drought and non-drought years using the FAO stats yield data. When considering the three countries USA, Zimbabwe and South Africa, the same crops could be used for the analysis due to their similar agricultural use and responses to water stress in the three countries. However, this may not be the case in other areas, such as Asia, where different reference crops should be selected that better mimic water stress responds. Kogan [63] analyzed the relationship between vegetation health and crop yields in different countries around the world and found, that yield modeling with the help of the vegetation health indices differs regionally for different crops. Thus, regarding the global applicability of our modeling framework, geographical location, climate zone and crop type differences must be considered, specifically when selecting drought and non-drought years in the time line reference yields data. The segmented regression, which mainly accounts for effects of technological advances on yields, can be simply transferred to other crop yields data or other regions. Due to regional differences in climate and plant characteristics, the herein considered variables Albedo, LST, NDII, NDVI and SPI3 vary in importance in terms of their relevance to drought hazard. This results in different model equations for every region when applying the model after a country-specific set-up. The changing relevance of the input variables per country also relates to the autocorrelation and the z-values of the model variables. In South Africa and Zimbabwe, for example, no critical values were found in the pairwise autocorrelation in contrast to the USA. This is due to regional deviating plant characteristics leading to changes in the indices and their interplay [64]. For example, the SPI3 with a z-value of 17.6 is significantly less influential for the model in the USA than it is in South Africa (118.1) and Zimbabwe (57.3). One possible explanation is that the dependence of plants on precipitation could be more distinct in South Africa and Zimbabwe due to, for instance, the lower spatial coverage of irrigation croplands in these two countries [38]. This becomes clearer when looking at the importance of the NDII in the model of the three countries. Di Wu et al. [12] stated that the NDII in its analysis is sensitive to the detection of droughts over irrigated fields. In a country like the USA, where a large part of the agricultural area is under irrigation [12], this index thus plays a decisive role in modeling the probability of drought. The comparison of the z values for the NDII suggests a similar trend. In the USA this was 111.7 and was thus significantly higher than the values of 40.2 and 67.4 in South Africa and Zimbabwe, respectively. Concluding this section, the model showed to be spatially transferable while also capturing regional drought relevant impacts and effects and thus providing spatially more precise information compared to global drought models.

In contrast to existing country statistics on income, poverty or food availability, the vulnerability analysis presented here is simplified but spatially explicit while helping to support drought preparedness or water resource management of more vulnerable regions or communities [26]. As apparent in Figure 6, the administrative units at which level population, GPD and animal density data are reported for Zimbabwe and South Africa, are clearly visible in the vulnerability analysis results. These data that are aggregated information at administrative unit level, can cause under- or overestimation of drought risk in some areas. For instance, in the Kruger National Park (KNP) in northeastern South Africa on the border to Mozambique, this becomes apparent. Within the KNP, high per pixel vulnerability scores

II. Spatially transferable modeling framework for regional drought assessment in Southern Africa (Chapter I)

Remote Sens. 2020, 12, 237

17 of 22

are predicted although the Kruger Park can be considered a ‘no vulnerability’ area with regard to GDP, population, livestock or irrigation. Moreover, if one compares South Africa and Zimbabwe, the spatial patterns in Zimbabwe are more easily delineated than in South Africa (Figure 5). This is probably due to the fact that spatially explicit data availability in South Africa regarding to population density, GDP and livestock density is generally much better than in Zimbabwe.

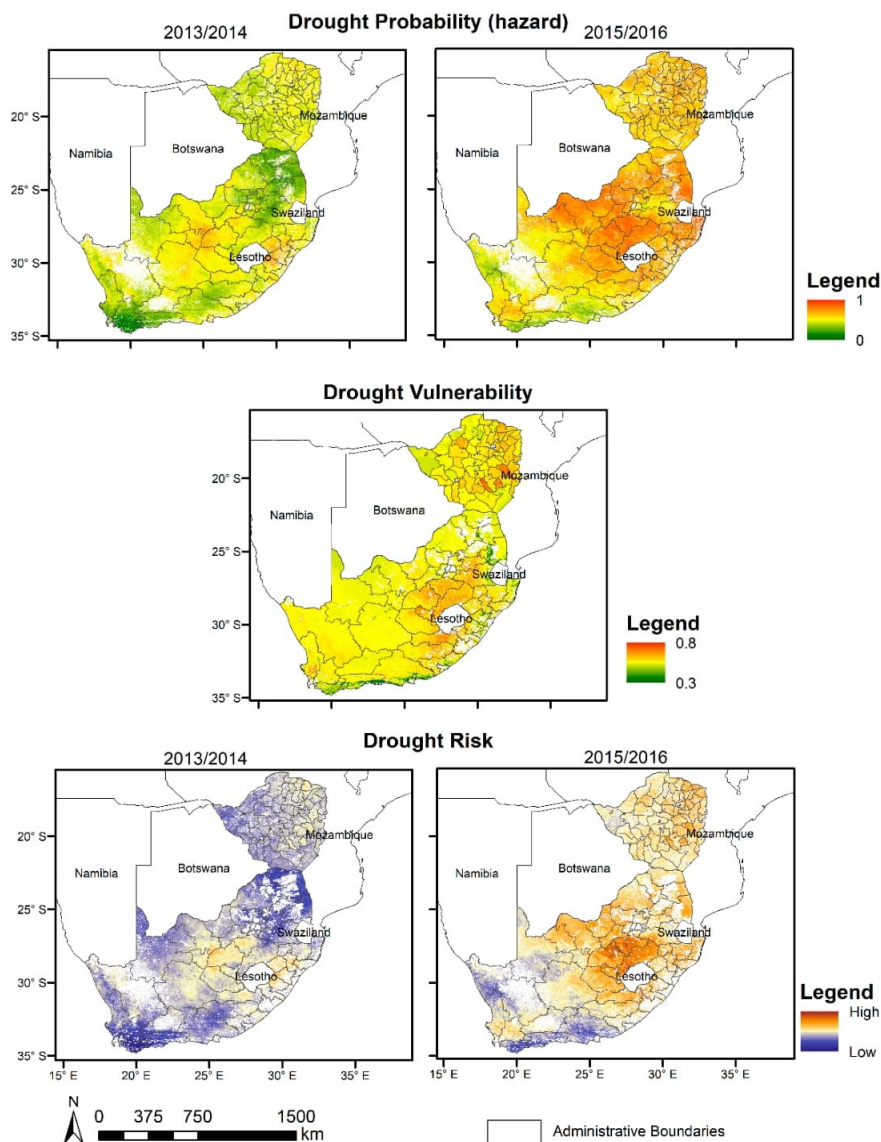


Figure 6. Drought hazard, vulnerability and risk for South Africa and Zimbabwe for the growing seasons December to March 2013/14 and 2015/16. Drought hazard is only presented for crop-, grass- and shrubland, drought vulnerability excludes urban areas and drought risk is presented for crop-, grass- and shrubland additionally excluding urban areas.

II. Spatially transferable modeling framework for regional drought assessment in Southern Africa (Chapter I)

To support drought preparedness and interventions, the vulnerability and simplified risk modeling framework allows for spatial comparisons between regions and can be most useful to identify drought prone regions that are in danger of damages or economic losses [65]. Ebi & Bowen [66] noted that the increase in drought exposure is accompanied by a decline in the Human Development Index. This suggests the need for an approach that allows for a comparison of vulnerability and risk between countries. A disadvantage of this analysis approach is essentially that no absolute degree of vulnerability and risk can be determined. Other studies on regional vulnerability incorporate a wide spectrum of variables to determine drought vulnerability and thus better reflect the absolute drought vulnerability. Vulnerability dimensions are mentioned by Hagenlochner et al. [54] in their review article on drought assessment. The main obstacle is the availability of global spatially explicit data sets. Since only a few useful data sets are available for some countries in this form, water supply and availability could not be included. In our models, the separate analysis of grazing animals offers additional variable weighting possibilities. All input index variables can be weighted differently and the vulnerability index can be easily extended with new data sets that may be available in the future. This allows a better understanding of the region-specific significance of the individual factors for agriculture and pasture management and a more appropriate calculation of drought vulnerability and risk. In this context, it was demonstrated that the simplified analysis of vulnerability and risk can be feasibly calculated at the country level.

5. Conclusions

This paper presented a satellite data-driven logistic regression model that can model drought hazard for agriculture, grass- and shrubland biomes while being spatially transferable. The model showed a good spatial agreement with the U.S. Drought Monitor when compared in the Missouri study site in both drought and non-drought years. The subsequent evaluation in South Africa and Zimbabwe with the help of drought reports and data on the last major El Niño event in 2015/2016 proved the predictive quality of the model. Considering the goodness of fit for the logistic regression model, McFadden's Pseudo R^2 showed a good predictive quality for the USA and for South Africa, but only a moderate predictive quality for Zimbabwe. However, not only quantitative measurements are in need to assess the model performance, but also qualitative analyses regarding plausibility of results. The comparison to the Global Drought Observatory developed by the JRC and to the food security classification data provided by FEWS NET also showed a good match with the results obtained herein.

Overall, the logistic regression model shown here combines the advantage of global models with their global applicability with the strengths of regional models that allow for assessing drought hazard at a regional level through improved spatial resolution. This might require changing various input variables, weights and crop types affected by drought depending on different characteristics of the area. Although it has shown its potential for global transferability, further research on the suitability of the model to predict drought hazard in other geographic regions needs to be done. The drought hazard model can also be seen as a first step towards near real-time drought hazard monitoring since it is exclusively based on near real-time satellite data and thus reflects current conditions. This study could demonstrate a consistent way of analyzing drought hazard, risk and vulnerability within a country. In order to advance this methodology, new global and spatially explicit time series data is needed to support and provide a more comprehensive vulnerability analysis.

Author Contributions: Conceptualization: M.S., T.L., N.C., K.-F.W. and J.F.; Investigation: M.S.; Methodology: M.S., T.L. and J.F.; Project administration: S.S.; Supervision: K.-F.W. and J.F.; Validation: M.S.; Writing—original draft: M.S.; Writing—review & editing: T.L., N.C., K.-F.W., S.S. and J.F. All authors have read and agreed to the published version of the manuscript.

Funding: We sincerely thank the Federal Ministry of Education and Research (BMBF, Germany) for funding this work through the GlobeDrought project (project ID: 02WGR1457D, 02WGR1457F) which is part of the Global Resource Water (GRoW) funding scheme.

Conflicts of Interest: The authors declare no conflict of interest.

II. Spatially transferable modeling framework for regional drought assessment in Southern Africa (Chapter I)

References

1. Wilhite, D.A. (Ed.) *Drought: A Global Assessment*, 2nd ed.; Routledge: London, UK, 2000; ISBN 9780415168335.
2. Sivakumar, M.V.K.; Motha, R.P.; Wilhite, D.A.; Wood, D.A. Agricultural Drought Indices. In Proceedings of the WMO/UNISDR Expert Group Meeting on Agricultural Drought Indices, Murcia, Spain, 2–4 June 2010.
3. UN-Spider. Drought. 2019. Available online: <http://www.un-spider.org/risks-and-disasters/natural-hazards/drought> (accessed on 3 December 2019).
4. IPCC (Ed.) Summary for Policymakers. In *Climate Change 2013: The Physical Science Basis. Contribution of Working Group I to the Fifth Assessment Report of the Intergovernmental Panel on Climate Change*; Cambridge University Press: Cambridge, UK, 2013.
5. Pachauri, R.K.; Mayer, L. (Eds.) *Climate Change 2014, Synthesis Report*; Intergovernmental Panel on Climate Change: Geneva, Switzerland, 2015; ISBN 978-92-9169-143-2.
6. Wilhite, D.A. (Ed.) Preparing for Drought: A Methodology. In *Drought: A Global Assessment*, 2nd ed.; Routledge: London, UK, 2000; pp. 89–104, ISBN 9780415168335.
7. Owrangi, M.A.; Adamowski, J.; Rahnamaei, M.; Mohammadzadeh, A.; Sharifan, R.A. Drought Monitoring Methodology Based on AVHRR Images and SPOT Vegetation Maps. *JWARP* **2011**, *3*, 325–334. [[CrossRef](#)]
8. Wu, J.; Zhou, L.; Liu, M.; Zhang, J.; Leng, S.; Diao, C. Establishing and assessing the Integrated Surface Drought Index (ISDI) for agricultural drought monitoring in mid-eastern China. *Int. J. Appl. Earth Obs. Geoinf.* **2012**, *23*, 397–410. [[CrossRef](#)]
9. Zhou, L.; Wu, J.; Zhang, J.; Leng, S.; Liu, M.; Zhang, J.; Zhao, L.; Zhang, F.; Shi, Y. The Integrated Surface Drought Index (ISDI) as an Indicator for Agricultural Drought Monitoring: Theory, Validation, and Application in Mid-Eastern China. *IEEE J. Sel. Top. Appl. Earth Obs. Remote Sens.* **2013**, *6*, 1254–1262. [[CrossRef](#)]
10. Gulácsi, A.; Kovács, F. Drought Monitoring With Spectral Indices Calculated From Modis Satellite Images in Hungary. *J. Environ. Geogr.* **2015**, *8*. [[CrossRef](#)]
11. Zhuo, W.; Huang, J.; Zhang, X.; Sun, H.; Zhu, D.; Su, W.; Zhang, C.; Liu, Z. Comparison of five drought indices for agricultural drought monitoring and impacts on winter wheat yields analysis. In Proceedings of the 2016 Fifth International Conference on Agro-Geoinformatics (Agro-Geoinformatics), Tianjin, China, 18–20 July 2016; pp. 1–6. [[CrossRef](#)]
12. Di, W.; Qu, J.J.; Hao, X. Agricultural drought monitoring using MODIS-based drought indices over the USA Corn Belt. *Int. J. Remote Sens.* **2015**, *36*, 5403–5425. [[CrossRef](#)]
13. Zhang, Y.; Peng, C.; Li, W.; Fang, X.; Zhang, T.; Zhu, Q.; Chen, H.; Zhao, P. Monitoring and estimating drought-induced impacts on forest structure, growth, function, and ecosystem services using remote-sensing data: Recent progress and future challenges. *Environ. Rev.* **2013**, *21*, 103–115. [[CrossRef](#)]
14. Hazaymeh, K.; Hassan, Q.K. Remote sensing of agricultural drought monitoring: A state of art review. *AIMS Environ. Sci.* **2016**, *3*, 604–630. [[CrossRef](#)]
15. Peng, C.; Deng, M.; Di, L. Relationships between Remote-Sensing-Based Agricultural Drought Indicators and Root Zone Soil Moisture: A Comparative Study of Iowa. *IEEE J. Sel. Top. Appl. Earth Obs. Remote Sens.* **2014**, *7*, 4572–4580. [[CrossRef](#)]
16. Park, S.; Im, J.; Park, S.; Rhee, J. Drought monitoring using high resolution soil moisture through multi-sensor satellite data fusion over the Korean peninsula. *Agric. For. Meteorol.* **2017**, *237–238*, 257–269. [[CrossRef](#)]
17. Zhang, Q.; Yu, H.; Sun, P.; Singh, V.P.; Shi, P. Multisource data based agricultural drought monitoring and agricultural loss in China. *Glob. Planet. Chang.* **2019**, *172*, 298–306. [[CrossRef](#)]
18. Bayissa, Y.A.; Tadesse, T.; Svoboda, M.; Wardlow, B.; Poulsen, C.; Swigart, J.; van Andel, S.J. Developing a satellite-based combined drought indicator to monitor agricultural drought: A case study for Ethiopia. *GIScience Remote Sens.* **2019**, *56*, 718–748. [[CrossRef](#)]
19. Zhang, X.; Obringer, R.; Wei, C.; Chen, N.; Niyogi, D. Droughts in India from 1981 to 2013 and Implications to Wheat Production. *Sci. Rep.* **2017**, *7*, 44552. [[CrossRef](#)] [[PubMed](#)]
20. Sur, C.; Park, S.-Y.; Kim, T.-W.; Lee, J.-H. Remote Sensing-based Agricultural Drought Monitoring using Hydrometeorological Variables. *KSCE J. Civ. Eng.* **2019**, *23*, 5244–5256. [[CrossRef](#)]
21. Qu, C.; Hao, X.; Qu, J.J. Monitoring Extreme Agricultural Drought over the Horn of Africa (HOA) Using Remote Sensing Measurements. *Remote Sens.* **2019**, *11*, 902. [[CrossRef](#)]

II. Spatially transferable modeling framework for regional drought assessment in Southern Africa (Chapter I)

22. Caccamo, G.; Chisholm, L.A.; Bradstock, R.A.; Puotinen, M.L. Assessing the sensitivity of MODIS to monitor drought in high biomass ecosystems. *Remote Sens. Environ.* **2011**, *115*, 2626–2639. [CrossRef]
23. Chang, C.-T.; Wang, H.-C.; Huang, C.-Y. Assessment of MODIS-derived indices (2001–2013) to drought across Taiwan's forests. *Int. J. Biometeorol.* **2017**, 1–14. [CrossRef] [PubMed]
24. Wan, Z.; Wang, P.; Li, X. Using MODIS Land Surface Temperature and Normalized Difference Vegetation Index products for monitoring drought in the southern Great Plains, USA. *Int. J. Remote Sens.* **2004**, *25*, 61–72. [CrossRef]
25. Wang, S.; Davidson, A.; Latifovic, R.; Trishchenko, A. The impact of drought on land surface albedo. *Am. Geophys. Union* **2004**, 85.
26. Vogt, J.V.; Naumann, G.; Masante, D.; Spinoni, J.; Cammalleri, C.; Erian, W.; Pischke, F.; Pulwarty, R.; Barbosa, P. *Drought Risk Assessment. A Conceptual Framework*; Publications Office of the European Union: Luxembourg, 2018; ISBN 978-92-79-97469-4.
27. Huntington, J.L.; Hegewisch, K.C.; Daudert, B.; Morton, C.G.; Abatzoglou, J.T.; McEvoy, D.J.; Erickson, T. Climate Engine: Cloud Computing and Visualization of Climate and Remote Sensing Data for Advanced Natural Resource Monitoring and Process Understanding. *Bull. Am. Meteorol. Soc.* **2017**, *98*, 2397–2410. [CrossRef]
28. Chen, D.; Chen, H.W. Using the Köppen classification to quantify climate variation and change: An example for 1901–2010. *Environ. Dev.* **2013**, *6*, 69–79. [CrossRef]
29. FAO. Faostat. 2019. Available online: <http://www.fao.org/faostat/en/#data> (accessed on 10 January 2019).
30. Homer, C.; Dewitz, J.; Yang, L.; Jin, S.; Danielson, P.; Xian, G.; Coulston, J.; Herold, N.; Wickham, J.; Megown, K. Completion of the 2011 National Land Cover Database for the Conterminous United States—Representing a Decade of Land Cover Change Information. *Photogramm. Eng. Remote Sens.* **2015**, *81*, 345–354.
31. ESA Climate Change Initiative—Land Cover project 2017. CCI Land Cover—S2 Prototype Land Cover 20M Map of Africa. 2016. Available online: <http://2016africallandcover20m.esrin.esa.int/> (accessed on 14 March 2019).
32. Funk, C.; Peterson, P.; Landsfeld, M.; Pedreros, D.; Verdin, J.; Shukla, S.; Husak, G.; Rowland, J.; Harrison, L.; Hoell, A.; et al. The climate hazards infrared precipitation with stations—A new environmental record for monitoring extremes. *Sci. Data* **2015**, *2*, 150066. [CrossRef] [PubMed]
33. Vermote, E.F.; Roger, J.C.; Ray, J.P. MODIS Surface Reflectance User's Guide—Collection 6. 2018. Available online: http://modis-sr.ltdri.org/guide/MOD09_UserGuide_v1.4.pdf (accessed on 20 April 2018).
34. Wan, Z.; Hook, S.; Hulley, G. MOD11A2 MODIS/Terra Land Surface Temperature/Emissivity 8-Day L3 Global 1 km SIN Grid V006 [Data]; NASA EOSDIS Land Processes DAAC; U.S. Geological Survey: Reston, VA, USA, 2015. [CrossRef]
35. Schaaf, C.; Wang, Z. MCD43A3 MODIS/Terra + Aqua BRDF/Albedo Daily L3 Global—500 m V006; NASA EOSDIS Land Processes DAAC; U.S. Geological Survey: Reston, VA, USA, 2015. [CrossRef]
36. CIESIN. Gridded Population of the World, Version 4 (GPWv4): Population Density, Revision 10. Available online: <https://catalog.data.gov/dataset/gridded-population-of-the-world-version-4-gpwv4-population-density-revision-10> (accessed on 10 January 2019).
37. Kummu, M.; Taka, M.; Guillaume, J.H.A. Gridded global datasets for Gross Domestic Product and Human Development Index over 1990–2015. *Sci. Data* **2018**, *5*, 180004. [CrossRef]
38. Landmann, T.; Eidmann, D.; Cornish, N.; Franke, J.; Siebert, S. Optimizing harmonics from Landsat time series data: The case of mapping rainfed and irrigated agriculture in Zimbabwe. *Remote Sens. Lett.* **2019**, *10*, 1038–1046. [CrossRef]
39. Gilbert, M.; Nicolas, G.; Cinardi, G.; van Boeckel, T.P.; Vanwambeke, S.O.; Wint, G.R.W.; Robinson, T.P. Global distribution data for cattle, buffaloes, horses, sheep, goats, pigs, chickens and ducks in 2010. *Sci. Data* **2018**, *5*, 180227. [CrossRef]
40. Mckee, T.B.; Doesken, N.J.; Kleist, J. The Relationship of Drought Frequency and Duration to Time Scales. *Eighth Conf. Appl. Climatol.* **1993**, *22*, 179–184.
41. Rouse, J.W.; Hass, R.H.; Schell, J.A.; Deering, D.W. Monitoring Vegetation Systems in the Great Plains with ERTS. In Proceedings of the 3rd Earth Resources Technology Satellite-1 Symposium, Greenbelt, MD, USA, 10–14 December 1973; pp. 309–317.

II. Spatially transferable modeling framework for regional drought assessment in Southern Africa (Chapter I)

42. Huete, A.; Didan, K.; Miura, T.; Rodriguez, E.P.; Gao, X.; Ferreira, L.G. Overview of the radiometric and biophysical performance of the MODIS vegetation indices. *Remote Sens. Environ.* **2002**, *83*, 195–213. [CrossRef]
43. Wan, Z. MODIS Land Surface Temperature Products Users' Guide: Collection-6. 2019. Available online: https://ices.eri.ucsb.edu/modis/LstUsrGuide/MODIS_LST_products_Users_guide_Collection-6.pdf (accessed on 26 March 2019).
44. Zeileis, A.; Kleiber, C.; Krämer, W.; Hornik, K. Testing and dating of structural changes in practice. *Comput. Stat. Data Anal.* **2003**, *44*, 109–123. [CrossRef]
45. Muggeo, V.M.R. Segmented: An R package to fit regression models with broken-line relationships. *R News* **2008**, *8*, 20–25.
46. Abdel-Rahman, E.; Landmann, T.; Kyalo, R.; Ong'amo, G.; Mwalusepo, S.; Sulieman, S.; Le Ru, B. Predicting stem borer density in maize using RapidEye and generalized linear models. *Int. J. Appl. Earth Obs. Geoinf.* **2017**, *57*, 61–74. [CrossRef]
47. Mosomtai, G.; Evander, M.; Sandström, P.; Ahlm, C.; Sang, R.; Hassan, O.A.; Affognon, H.; Landmann, T. Association of ecological factors with Rift Valley fever occurrence and mapping of risk zones in Kenya. *Int. J. Infect. Dis.* **2016**, *46*, 49–55. [CrossRef] [PubMed]
48. Dormann, C.F.; Elith, J.; Bacher, S.; Buchmann, C.; Carl, G.; Carré, G.; Marquéz, J.R.G.; Gruber, B.; Lafourcade, B.; Leitão, P.J.; et al. Collinearity: A review of methods to deal with it and a simulation study evaluating their performance. *Ecography* **2013**, *36*, 27–46. [CrossRef]
49. James, G.; Witten, D.; Hastie, T.; Tibshirani, R. *An Introduction to Statistical Learning. With Applications in R*, 6th ed.; Springer: New York, NY, USA, 2015; ISBN 978-1-4614-7137-0.
50. Veall, M.R.; Zimmermann, K.F. Pseudo-R² Measures for Some Common Limited Dependent Variable Models. *J. Econ. Surv.* **1996**, *10*, 241–259. [CrossRef]
51. McFadden, D. *Quantitative Methods for Analyzing Travel Behavior of Individuals: Some Recent Developments*; Institute of Transportation Studies, University of California: Berkeley, CA, USA, 1977.
52. Baldenhofer, K.G. Das ENSO-Phänomen: Der El Niño von 2015/16. 2015. Available online: http://www.enso.info/anhang/El_Nino_2015_16.pdf (accessed on 10 January 2019).
53. Zhong, S.; Wang, C.; Yang, Y.; Huang, Q. Risk assessment of drought in Yun-Gui-Guang of China jointly using the Standardized Precipitation Index and vulnerability curves. *Geomat. Nat. Hazards Risk* **2018**, *9*, 892–918. [CrossRef]
54. Hagenlocher, M.; Meza, I.; Anderson, C.C.; Min, A.; Renaud, F.G.; Walz, Y.; Siebert, S.; Sebesvari, Z. Drought vulnerability and risk assessments: State of the art, persistent gaps, and research agenda. *Environ. Res. Lett.* **2019**, *14*, 83002. [CrossRef]
55. Dijkstra, L.; Poelman, H. Regional Working Paper 2014: A harmonised definition of cities and rural areas: The new degree of urbanisation. In *European Commission's Directorate General (DG) for Regional and Urban Policy: Working Papers*; European Commission: Brussels, Belgium, 2014; pp. 1–24.
56. NOAA Climate Government. El Niño Climate Impacts. 2019. Available online: <https://www.climate.gov/news-features/featured-images/global-impacts-el-ni%C3%B1o-and-la-ni%C3%B1a> (accessed on 14 March 2019).
57. Baldenhofer, K.G. Das ENSO-Phänomen: ENSO-Lexikon. 2019. Available online: <http://www.enso.info/enso-lexikon/index.html> (accessed on 23 January 2019).
58. BBC News. South Africa Grapples with Worst Drought in 30 Years. 2019. Available online: <https://www.bbc.com/news/world-africa-34884135> (accessed on 23 January 2019).
59. Al, J. South Africa in Midst of 'Epic Drought'. 2019. Available online: <https://www.aljazeera.com/news/2015/11/south-africa-midst-epic-drought-151104070934236.html> (accessed on 23 January 2019).
60. News24. Extreme Drought Persists Across SA. 2019. Available online: <https://www.news24.com/SouthAfrica/News/extreme-drought-persists-across-sa-20160117> (accessed on 23 January 2019).
61. BBC News. Zimbabwe's Robert Mugabe Declares Drought Disaster. 2019. Available online: <https://www.bbc.com/news/world-africa-35500820> (accessed on 23 January 2019).
62. ReliefWeb. Zimbabwe: 2016–2017 Drought Disaster Domestic and International Appeal for Assistance. 2019. Available online: <https://reliefweb.int/report/zimbabwe/zimbabwe-2016-2017-drought-disaster-domestic-and-international-appeal-assistance> (accessed on 23 January 2019).

II. Spatially transferable modeling framework for regional drought assessment in Southern Africa (Chapter I)

Remote Sens. **2020**, *12*, 237

22 of 22

63. Kogan, F. *Remote Sensing for Food Security*; Springer International Publishing: Cham, Switzerland, 2019; ISBN 978-3-319-96255-9.
64. Onyia, N.; Balzter, H.; Berrio, J.-C. Normalized Difference Vegetation Vigour Index: A New Remote Sensing Approach to Biodiversity Monitoring in Oil Polluted Regions. *Remote Sens.* **2018**, *10*, 897. [[CrossRef](#)]
65. Wilhelmi, O.V.; Wilhite, D.A. Assessing Vulnerability to Agricultural Drought: A Nebraska Case Study. *Nat. Hazards* **2002**, *25*, 37–58. [[CrossRef](#)]
66. Ebi, K.L.; Bowen, K. Extreme events as sources of health vulnerability: Drought as an example. *Weather Clim. Extrem.* **2016**, *11*, 95–102. [[CrossRef](#)]



© 2020 by the authors. Licensee MDPI, Basel, Switzerland. This article is an open access article distributed under the terms and conditions of the Creative Commons Attribution (CC BY) license (<http://creativecommons.org/licenses/by/4.0/>).

III. Environmental suitability for transhumance and conflict prevention (Chapter II)

Schwarz, M., Landmann, T., Jusselme, D., Zambrano, E., Danzeglocke, J., Siegert, F., Franke, J. (2022) Assessing the Environmental Suitability for Transhumance in Support of Conflict Prevention in the Sahel. *Remote Sensing*, 14(5), 1109. DOI: <https://doi.org/10.3390/rs14051109>

A PDF of this article is available at:
<https://www.mdpi.com/2072-4292/14/5/1109>

Article

Assessing the Environmental Suitability for Transhumance in Support of Conflict Prevention in the Sahel

Maximilian Schwarz^{1,2,*} , Tobias Landmann^{1,3}, Damien Jusselme⁴, Eduardo Zambrano⁴, Jens Danzeglocke⁵, Florian Siegert^{1,2} and Jonas Franke¹

¹ Remote Sensing Solutions GmbH, Dingolfinger Str. 9, 81673 Munich, Germany; tlandmann@icipe.org (T.L.); siegert@rsggmbh.de (F.S.); franke@rsggmbh.de (J.F.)

² Department of Biology, Ludwig-Maximilians-University Munich, Großhaderner Str. 2, 82152 Planegg-Martinsried, Germany

³ International Centre of Insect Physiology and Ecology (ICIPE), Nairobi P.O. Box 30772-00100, Kenya

⁴ Displacement Tracking Matrix, International Organization for Migration, Route de Morillons 17, CH-1218 Geneva, Switzerland; djusselme@iom.int (D.J.); ezambrano@iom.int (E.Z.)

⁵ German Aerospace Center (DLR), Space Agency, Koenigswinterer Str. 522-524, 53227 Bonn, Germany; jens.danzeglocke@dlr.de

* Correspondence: schwarz@rsggmbh.de; Tel.: +49-89-48954765

Abstract: Increasing conflicts between farmers and pastoralists continue to be a major challenge in the Sahel. Political and social factors are in tandem important underlying determinants for conflicts in the region, which are amplified by the variability and scarcity of natural resources, often as a result of climate variability and climate change. This study aimed at holistically assessing the main environmental parameters that influence the patterns of seasonal migratory movements (transhumance) in a transboundary area in the southern Republic of Chad and northern Central African Republic through a broad set of Earth observation (EO) data and data from the Transhumance Tracking Tool. A spatial model was applied to the datasets to determine the spatiotemporal dynamics of environmental suitability that reflects suitable areas and corridors for pastoralists. A clear difference in environmental suitability between the origin and destination areas of herders was found in the dry season, proving the main reason for pastoralists' movements, i.e., the search for grazing areas and water. Potential conflict risk areas could be identified, especially along an agricultural belt, which was proven by conflict location data. The results demonstrate the potential and innovation of EO-derived environmental information to support the planning of transhumance corridors and conflict prevention in the Sahel. In the future, a combination of real-time tracking of herders and EO-derived information can eventually lead to the development of an early warning system for conflicts along transhumance corridors in the Sahel.

Keywords: Central African Republic; Chad; Copernicus; famer; herder; migration



Citation: Schwarz, M.; Landmann, T.; Jusselme, D.; Zambrano, E.; Danzeglocke, J.; Siegert, F.; Franke, J. Assessing the Environmental Suitability for Transhumance in Support of Conflict Prevention in the Sahel. *Remote Sens.* **2022**, *14*, 1109. <https://doi.org/10.3390/rs14051109>

Academic Editor: Conghe Song

Received: 14 January 2022

Accepted: 22 February 2022

Published: 24 February 2022

Publisher's Note: MDPI stays neutral with regard to jurisdictional claims in published maps and institutional affiliations.



Copyright: © 2022 by the authors. Licensee MDPI, Basel, Switzerland. This article is an open access article distributed under the terms and conditions of the Creative Commons Attribution (CC BY) license (<https://creativecommons.org/licenses/by/4.0/>).

1. Introduction

Conflicts between farmers and semi-nomadic livestock herders (transhumance) have increased over the past two decades [1], and continue to be a major challenge in sub-Saharan Africa [2,3]. In particular, farmer–herder conflicts concerning drought and water tensions have become widespread in the Sahel and eastern Africa [4,5]. Livestock farming strongly contributes to the regional states' gross domestic product (GDP) in the Sahel, with up to 15% of the total GDP coming from this sector. In some countries (e.g., Burkina Faso, Mali and Niger), products originating from pastoral farming represent the third largest export product [6]. Complex ecological, climatic, anthropogenic and underlying socio-political factors affect agro-ecological production systems in the Sahelian countries [7]. In particular, subsistence farmers and pastoralists, who traditionally complement one another in how agro-ecological systems are used, are increasingly competing for the same natural

resources, such as water and grazing land [8]. Conflicts concerning natural resources and herd mobility have increased in both number and severity. In particular, increases in herd sizes, cropland expansion and extreme weather events have exacerbated these conflicts [6,7]. The complementarity between farmers and herders has also been disrupted by mismanagement due to poor governance, misguided land tenure policies such as large-scale conversions of dry season pastures to rice fields [9], or extending cropland areas for subsistence farming [10]. Currently, there is limited information on spatio-temporal migratory movements, grazing locations, overlay areas, home ranges and nomadic herding practices adopted by pastoralists. This inevitably limits our understanding of the drivers of transhumance patterns and possible sources and locations of conflicts and with that forced population displacement [11].

The reasons behind farmer–herder conflicts have been analyzed from different perspectives, leading to a general assumption that infrastructural, socio-economic and political factors act in tandem with environmental factors and that environmental stressors are only partly predictive of conflict events [1,12–14]. Other studies on conflict resolution have also been conducted, stating the need for addressing climate change-related impacts and the root causes of risks for food security [8] or identifying policy options to address challenges in drought-prone regions [15]. Mbih [16] recently used surveys to collect expert and indigenous agro-ecological knowledge to derive solutions for alternative farmer–herder conflict management and sustainable development. Other studies focused on supporting herders with environmental information. The French Agricultural Research Centre for International Development (CIRAD) therefore developed the “système d’information sur le pastoralisme au Sahel” (SIPSA) in 2012. On a regional level, a certain number of biophysical indicators relating to rangeland productivity, the state of the vegetation, and the extent of surface water and of burned areas were developed using satellite images and subsequently tested and validated by AGRHYMET [7]. Since then, new satellite technology has evolved fast and has not yet been exploited in the context of conflict prevention and mitigation. A participatory mapping study with pastoralists was conducted, where the pastoralists’ rankings of suitable grazing areas matched the vegetation assessment results of the same area [17]. This leads to the assumption that information tools for herders based on environmental information can point out alternative grazing areas and thus could minimize conflicts. Mertz et al. [18] stated that improved weather and natural resource information as well as multiple options for herd movements, if communicated to herders, may reduce the level of conflict.

The present study focuses on (1) developing a geospatial tool to improve the understanding and planning of transhumance migratory movements and corridors and (2) on identifying potential risk areas for conflicts by using a wide range of Earth observation (EO) data to derive various environmental parameters relevant for transhumance. A spatial model was developed that compiles the EO-derived information products into environmental suitability maps for transhumance. Data from the Armed Conflict Location and Events Data (ACLED) set and data from the Transhumance Tracking Tool (TTT) provided by the International Organization for Migration (IOM) were analyzed together with the suitability maps to identify potential risk areas. This study aimed at developing a new conceptual EO framework in direct support of the conflict prevention activities of the International Organization for Migration’s (IOM) in the Sahel.

2. Materials and Methods

2.1. Study Area

The study area (Figure 1), with a total size of 268,193 km², is located in the border area between the Republic of Chad and the Central African Republic (CAR). The climate zone and vegetation differ between the northern and southern parts. While the northern area is located in the semiarid Sahelian zone, dominated by bare areas and sparse grassland vegetation, the southern part is located in the humid tropical zone, dominated by denser vegetation and tropical forests. The north–south gradient in climate and vegetation season-

III. Environmental suitability for transhumance and conflict prevention (Chapter II)

ality (stronger in the north of the study area) is the main reason for seasonal transhumance migratory movements from north to south during the dry season.



Figure 1. Regional map of the study area (red) between Chad and the Central African Republic (green). Source: ESRI Basemaps.

In this area (Figure 1), pastoral livestock farming, or transhumance, plays a key economic role in food and nutritional security. In Chad, around 80% of the national herd, which holds a total of 94 million heads of cattle, comprises the livelihood of ~40% of the population and accounts for 30% of exports [19]. Pastoral livestock farming is closely dependent on environmental conditions resulting in a typical north–south movement at the onset of the dry season and vice versa at the onset of the rainy season. Over the last few decades, these movements have stretched further south, even leading to cross-border movements between Chad and the Central African Republic. Competitions with other groups, especially crop farmers, add to the already existing environmental challenges for pastoralists during their movements [7].

2.2. Data

The data analysis for this study was exemplarily performed for the year 2019. Already existing and freely available geodata such as those from the Copernicus Land Monitoring Service [20] were used as much as possible. For environmental parameters that did not exist in the required coverage and frequency, Sentinel-1 and Sentinel-2 data from the Copernicus programme (Copernicus Sentinel data 2019) were processed to produce the relevant geoinformation products (Table 1). These open satellite data with high temporal resolutions allow large-scale studies and open up new possibilities for systematic monitoring. These data were used to derive dynamic environmental parameters that are important determinants for transhumance migratory movements such as farming systems, rangeland productivity, vegetation cover, burned areas and surface water occurrence. The input data were complemented by geospatial data on urban settlements, spatial data for protected areas [21] and survey data for transhumance movement patterns provided by IOM through the Transhumance Tracking Tool (TTT) [22] and from the ACLED conflict location and event database [23]. The ACLED conflict database contains information about the exact reported location and date of “battle events”, transfers of military control, headquarter establishment, violence against civilians along with riots [23].

The geospatial information products used are listed in Table 1. Accordingly, various map layers were derived from these products as inputs to the spatial modelling of environmental suitability for transhumance (Table 2).

III. Environmental suitability for transhumance and conflict prevention (Chapter II)

Table 1. Overview of the EO products and its data sources.

Geospatial Products	Time Period	Data Type/Source
Surface water occurrence	2017–2019	Sentinel-1
Farming systems	Static 2019	Sentinel-2
Vegetation greenness	Monthly for 2019	Sentinel-2
Vegetation cover	Monthly for 2019	Sentinel-2
Burned areas	Monthly for 2019	Sentinel-2
Urban areas	Static for 2019	Copernicus Land Monitoring Service
Forest type	Static for 2019	Copernicus Land Monitoring Service
Protected areas with access restrictions	Static for 2019	World Database on Protected Areas (WDPA)

Table 2. Input data used for the calculation of the environmental suitability maps for transhumance. The four datasets below the line were used as “mask” areas in which a suitability of 0 was assigned.

Input Layer Name	Spatial Resolution	From Geospatial Product
Distance to water body	10 m	Surface water occurrence
Distance to urban areas	10 m	Urban areas
Monthly rangeland productivity	10 m	Vegetation greenness
Monthly vegetation cover	10 m	Vegetation cover
Monthly burned areas	10 m	Burned areas
Forest type	30 m	Forest type
Agricultural fields	10 m	Farming systems
Water	10 m	Surface water dynamics
Urban areas	30 m	Urban areas
Protected areas with access restrictions		Protected areas with access restrictions

IOM, through its Displacement Tracking Matrix (DTM), works with the Bilital Maroobe Network (RBM) and its branches of pastoralist organizations to map the movements of transhumance herders along main transhumance corridors in West and Central Africa in order to better understand the dynamics and characteristics of internal and cross-border movements. In brief, data collection is conducted in key seasonal transhumant movements locations (such as cattle markets and water points). This tool aims to quantify these movements through direct observations and head counts the cattle and pastoralists. The Transhumance Tracking Tool (TTT) is a set of data collection modalities intended to provide the information needed for the implementation of support programs for populations involved in transhumance. It is composed of an early warning system tool, a mapping tool and flow counting tool that may be implemented in parallel or separately depending on the data needs. The data used for this document were extracted from the Flow Counting tool that quantified the movements and directions of herders and their cattle along main transhumance corridors.

2.3. Methods

2.3.1. Generation of Earth Observation Products

(1) Surface water occurrence

Level-1 ground range detection data from Sentinel-1 in VV polarization from the descending orbit over three years from 2017 to 2019 were used as input data. Both the presence and variability of water are very useful parameters to identify potential watering areas for the livestock as important points of interest for herders. Sentinel-1 satellite data are often used in inundation mapping, because of their sensitivity to water. The data were preprocessed into calibrated, topographically normalized backscatter images. The preprocessed images were classified into binary water body maps by using a threshold identified through zonal statistics over permanent water bodies and defining a 3% percentile

as a variable threshold for each scene. From the individually classified images, a surface water occurrence map was produced, which represents the pixel-wise number of surface water occurrences relative to the number of valid image acquisitions in the observation period of 2017 to 2019 in percent. The product represents a measure for the changing spatial extent of water bodies (permanent vs. seasonal water bodies) and has a spatial pixel resolution of 10 m. The method followed Steinbach et al. [24]. False-positive water detection can occur especially over sparse sandy or bare areas. To remove these false positives, an additional spectral unmixing of multispectral Sentinel-2 data from June 2019 to September 2019 was performed for the endmember's vegetation, soil and water. This period was used in order to cover the maximum extent of the water during the wet season. Pixels that were not covered by water according to the spectral unmixing during the rainy season were eliminated as false positives.

(2) Farming systems

The extent and type of cropland constitute important information in regard to transhumance patterns, since areas occupied by crop production limit the space for migratory movements of herds and also pose a potential risk for conflicts. Agricultural farming systems, i.e., irrigated and rainfed cropland, were differentiated by the use of Sentinel-2 data from 2017 to 2019. The agricultural farming systems were mapped using the methodology developed by Landmann et al. [25], which was modified to Sentinel-2 data. Postprocessing was used to generalize the farming systems by eliminating very small areas (single separated pixels) using a majority filter. For limits of this remote sensing-based classification and the accuracy of the method, see Landmann et al. [25].

(3) Vegetation cover and condition

The spectral properties of vegetation with decreasing water content or senescence are well-known and can be observed using remote sensing [26,27]. Spectral mixture analysis (SMA) holds great potential for estimating biomass condition and moisture content at a subpixel level [28,29], also representing the rangeland productivity (green vegetation cover and abundance). In contrast to vegetation indices, spectral mixture analyses make use of all vegetation-relevant spectral bands and are suitable to assess the fractional green photosynthetic vegetation (GV) versus per pixel non-photosynthetic vegetation (NPV), and bare substrate (soil) abundances from satellite data [30–32]. Sentinel-2 data were used to derive a spectrally unmixed dataset with cover fractions for “green vegetation”, “dry vegetation” and “bare soil”. Green vegetation abundance was used directly as an indicator for rangeland productivity, while the bare soil fraction was subtracted from 1 to indicate the total vegetation cover (green vegetation + dry vegetation). The product was generated on a monthly basis from January 2019 to December 2019 to account for temporal changes in grazing land and vegetation conditions.

(4) Burned areas

Wildfires are common in the study area, and the majority of the fires occur in the dry season (November–March). Since recently burned areas are not suitable for herders and their cattle, due to the unavailability of fodder, burned areas are considered in this analysis as areas temporarily less suitable for transhumance. Burned areas were mapped for each month using all available Sentinel-2 images in the dry season. For every month, a best pixel composite was produced, whereby the composite for the previous month was used as a pre-fire image and the composite of the current month was used as the post-fire image. For each Sentinel-2 scene of the current month as well as for the monthly composites, the normalized burn ratio (NBR) was calculated. Each NBR image was then subtracted from the NBR of the composite of the previous month (pre-fire) to calculate the difference normalized burn ratio (dNBR) following [33]. Every scene was classified using the two highest burn severity levels with a threshold of <440 (scaled by 10^3) according to [34]. To generate monthly burned area composites for the dry season from November to March, all burned areas were cumulated per month.

2.3.2. Model Input Layers

Using the geospatial products described above, two types of input data for the environmental suitability modelling were generated, i.e., binary mask layers with zero suitability assigned (0,1) and environmental suitability layers with scaled values (between 0 and 1).

Mask layers were generated for all areas that represent non-suitable/non-accessible areas for herders, such as inner urban areas, permanent water bodies, and cropland as well as protected areas with access restrictions. To differentiate forests suitable for transhumance (open forests) and forests less suitable (dense forests), all land cover classes that are related to forests were aggregated to “closed forest” and “open forest” according to their legend description [35].

Distance to permanent water (as derived from the surface water dynamics product) was calculated by using the Euclidean distance. The same approach was used for the distance to urban areas, where the class urban was extracted from the land cover data. While urban areas are points of interest for the herders (e.g., livestock markets, veterinary stations, health centers, wells, etc.), which is reflected through the distance to urban areas in the model, the inner urban areas are considered as non-suitable areas for transhumance corridors (applied through zero suitability masking as described above). While the above-described layers were considered as static for the observation year 2019, more dynamic environmental parameters such as the rangeland productivity, vegetation cover and burned areas were generated on a monthly basis for 2019.

Each environmental suitability input layer was standardized to a range from 0 to 1, where 1 indicates the highest suitability for the respective environmental variable. The layers rangeland productivity and vegetation cover are represented in percent and were simply divided by 100. The forest type layer was classified by assigning the value 0.2 to all pixels covering “closed forest” and 0.7 for “open forest”, since herders prefer rather open areas. For both distance layers, local expert knowledge from IOM was incorporated for scaling. Thereby, a maximum distance of two walking days (50 km) was considered as a maximum suitable distance to water bodies and to urban areas. Distances greater than 50 km were set to zero suitability values, while all distances between 0 and 50 km were scaled to a range between 0 and 1. The monthly burned areas were marked with the value 0 (zero suitability).

2.3.3. Spatial Modelling of Environmental Suitability for Transhumance

Figure 2 shows the schematic workflow diagram of the spatial modelling procedure. For each month in 2019, a set of static as well as dynamic environmental variables were used to calculate the environmental suitability maps for transhumance migratory movements. The monthly maps (TS) were calculated using an unweighted mean in the statistical software R as follows:

$$TS = (D. \text{ water} + D. \text{ urban} + \text{Veg. cover} + \text{Veg. green.} + \text{Forest type} + \text{BA}) / ND \quad (1)$$

where TS is the transhumance suitability score, D. refers to “distance to” and BA represents the burned areas. ND is the per pixel denominator, indicating the number of valid input parameters. Since Sentinel-2 data were used to derive vegetation cover and rangeland productivity, persistent clouds in some months led to data gaps in these products, which have to be considered in ND, where 6 indicates that all layers would have valid observations. In this case, the assumption was made that all these parameters can influence the transhumance movement at the same magnitude. To differentiate the magnitude of influence of the different parameters, more detailed research would be needed, as all parameters also act in tandem. This approach was also discussed with experts by IOM and was found the most feasible at this stage of research. However, the model allowed us to change the weights of the input layers, in case adjustments to specific regional conditions were required (e.g., by incorporating local expert knowledge). The resulting TS score ranged from 0 to 1, where

III. Environmental suitability for transhumance and conflict prevention (Chapter II)

1 reflects highly suitable areas for migratory movements and 0 unsuitable areas. The TS score was then masked by using the following equation:

$$TS_{final} = TS * urban\ mask * water\ mask * cropland\ mask * protected\ areas\ mask. \quad (2)$$

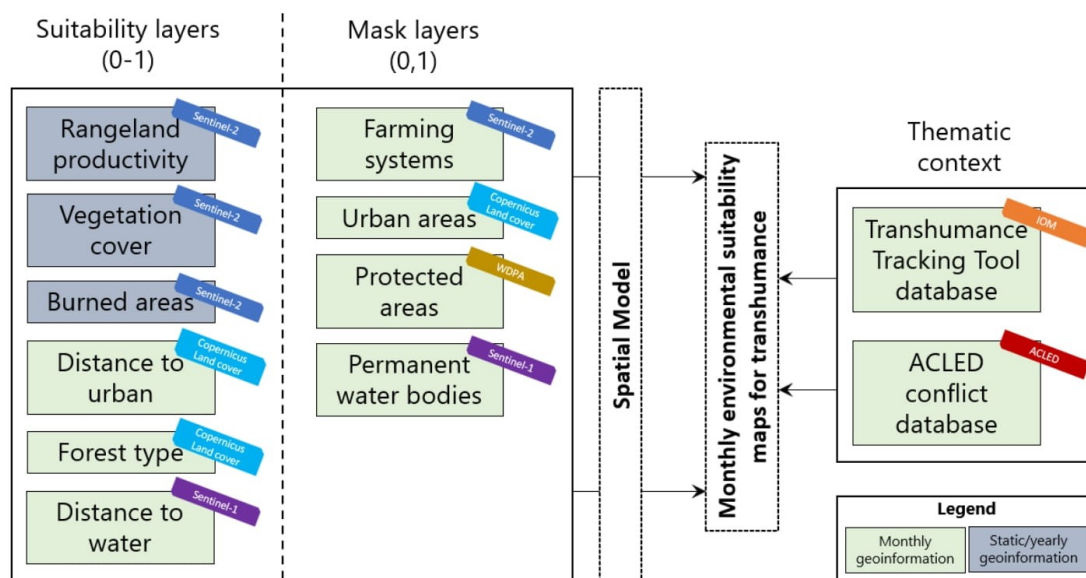


Figure 2. Workflow diagram.

2.3.4. Combining Suitability Maps with Transhumance Tracking Tool and Conflict Data

Additional data of conflict events (ACLED) and data from the transhumance tracking tool (TTT) were used together with the environmental suitability for transhumance maps to interpret the results. The locations for the origin areas of herders, TTT survey locations and destination areas of herders as indicated in the TTT data were mainly analyzed to assess the seasonal mean environmental suitability scores at origin and destination locations (663 data points per location). A radius of 1 km around each origin and destination location was considered. Points with a north–south movement from origin to destination during the dry season were used to compare the situation at origin and destination locations monthly, in order to get a better understanding of the environmental conditions during transhumance movement and to check the plausibility of the suitability values.

A few example points (40 per each origin and destination) were also used to calculate least-cost paths as the theoretical optimal path through areas with the highest suitability values. The input environmental suitability values were average suitability maps for the two periods of movement—from the origin to the TTT survey locations and from the TTT survey to the destination locations. The mean suitability maps were resampled to a spatial resolution of 100 m to provide faster and easier data processing. The TTT data were then analyzed regarding the number of people in each area per month to determine the two movement timespans. The mean suitability for the journey from an origin to a destination was then calculated from June to October (movement timespan one) and from November until January (movement timespan two) for the routes from the survey location to the destination. The environmental suitability raster layers were converted into graphs connecting each cell centers with each other, which then become nodes. The Moore neighborhood approach—comprising eight orthogonal and diagonal nearest neighbors—was used. The nodes were mostly weighted with calculations using

cost, frictions, resistance values or with probabilities of transition. These graphs represent the 'transition matrix' [36]. In this analysis, the transition matrix was calculated using the maximum suitability values between connected cells to follow the highest environmental suitability. A geo-correction was needed to correct geometric distortions of distances, through dividing each conductance matrix value by the distance results in the corrected values [36]. The corrected transition matrix was then used to determine the shortest path along the highest suitability values between the two points of origin and destination (least-cost path) [36]. The results represent the theoretical optimum transhumance paths along the highest environmental suitability values. Alongside these results, the ACLED conflict data are displayed on the environmental suitability maps as additional information to identify potential high-risk areas for conflicts. The ACLED data were filtered for farmer and herder-related conflicts from 2011 to 2019.

3. Results

The used Earth observation products (input for the environmental suitability maps), namely farming systems, rangeland productivity, surface water dynamics, vegetation cover, burned areas and the Copernicus land cover, are displayed exemplarily for a small subset of the study area in Figure 3a–e. Cropland was distinguished between rainfed and irrigated cropland within the product framing systems (Figure 3a). This information is important for transhumance movements, since rainfed cropland may be available as grazing land for herders during the dry season, in contrast to irrigated cropland. Water availability plays a crucial role for humans and animals in general, and was herein described by surface water dynamics (Figure 3c), where low to mid-percentages indicate seasonal water bodies mainly available in the wet season. For the environmental suitability maps, distance to water was calculated from the surface water dynamics for all permanent or near-permanent water bodies. Other seasonal varying factors include vegetation availability and vegetation greenness as an indicator for rangeland productivity (Figure 3b,d). Dry vegetation is an additional factor that was included in the analysis and is incorporated in the vegetation cover layer. Dry and green vegetation abundance varies significantly during the season, as shown in Figure 4a–d, where rangeland productivity (green vegetation cover and abundance) is displayed for four months as an example. The availability of green vegetation shifts southwards during the dry season (January and April) and northwards in the wet season (July and October). This example demonstrates the importance of the rangeland productivity for the monthly assessment of transhumance suitability. Additionally, burned areas were included in the analysis with a low suitability score to represent the absence of grazing land due to recent fire activities (Figure 3d). Burned areas were also analyzed on a monthly basis, but only during the dry season (fire season). The Copernicus land cover data (Figure 3e) were used as a static input product in this analysis, where urban areas were extracted and all forest classes were aggregated to open and closed forest.

III. Environmental suitability for transhumance and conflict prevention (Chapter II)

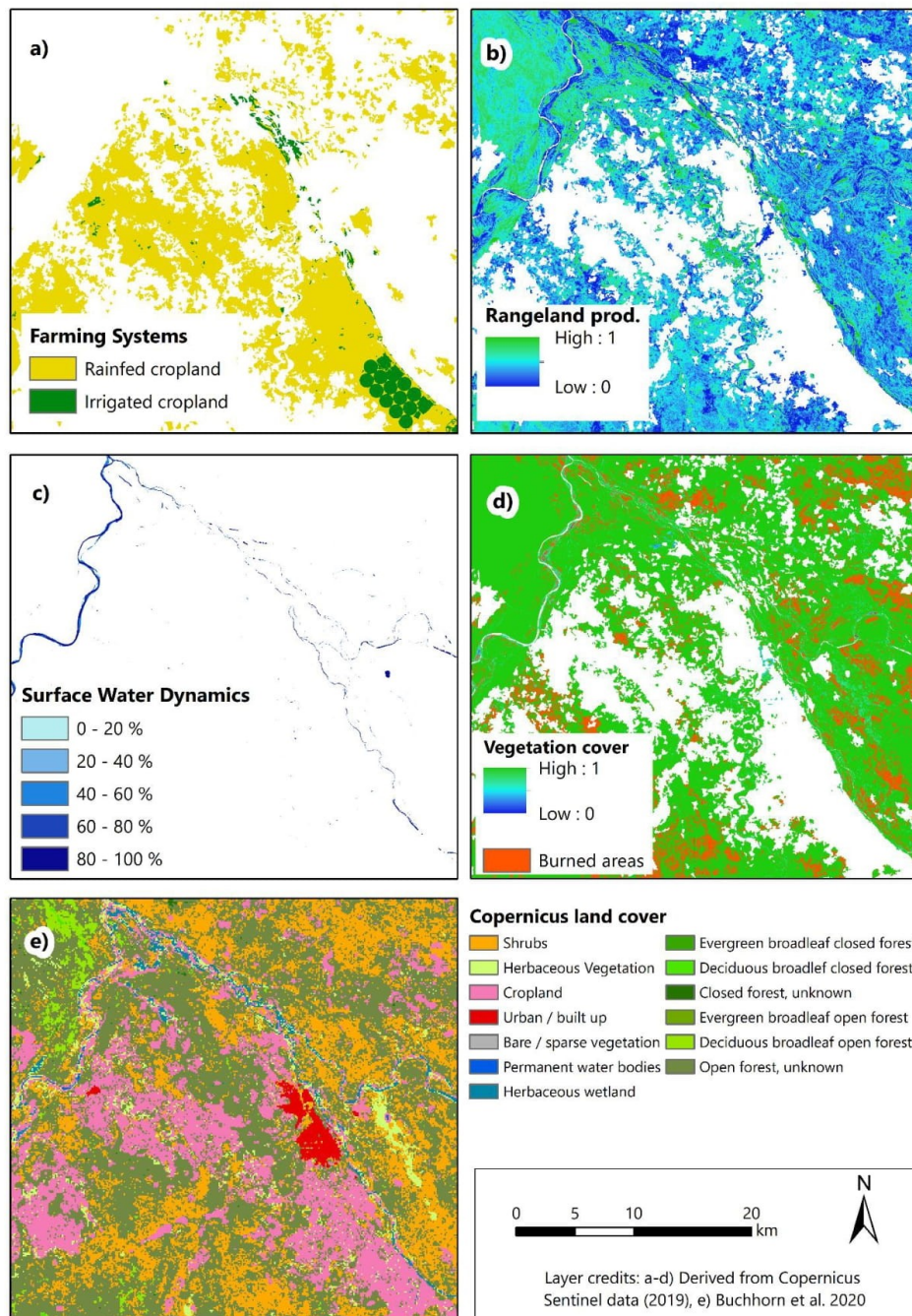


Figure 3. Examples of the different earth observation products for December 2019 for a subset of the study area. (a) Farming systems, (b) rangeland productivity (masked with urban areas, water, and farming systems), (c) surface water dynamics, (d) vegetation cover and burned areas (masked with urban areas, water, and farming systems), and (e) Copernicus land cover.

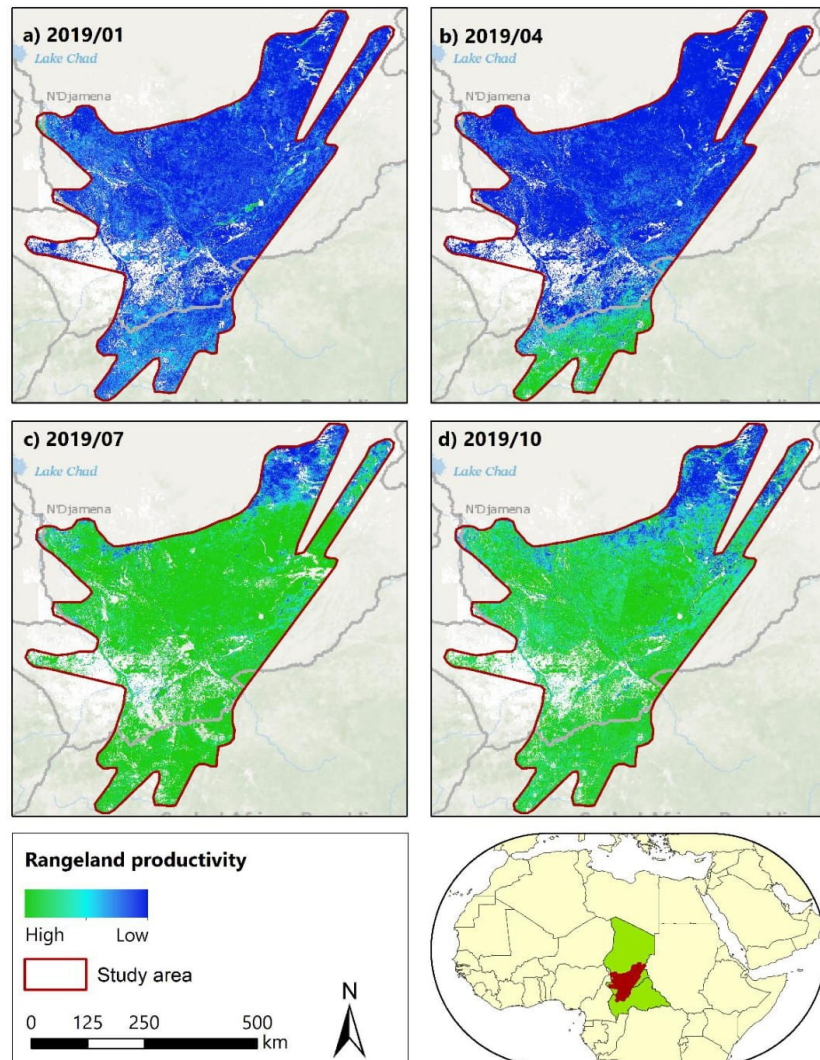


Figure 4. Rangeland productivity displayed for four months in 2019 for the study area: (a) January 2019, (b) April 2019, (c) July 2019, (d) October 2019. Water, urban areas and farming systems are masked out. Some no-data artefacts occur during the wet season due to persistent cloud cover. (Sources: Derived from Copernicus Sentinel data (2019); Background: ESRI Basemaps).

Figure 5a–d demonstrates that the environmental suitability for transhumance is mainly driven by seasonality over most parts of the study area; red colors indicate high suitability scores, while blue colors indicate low environmental suitability for transhumance. While the northern part of the study area is dominated by an arid to semi-arid climate with very distinct wet and dry seasons, the southern part has a humid climatic regime. This directly translates into continuous changes in environmental suitability for transhumance in the northern part, with decreasing resources for the herds in the dry season, which is the main reason for the north to south movement in this period. High suitability remains in only a few northern parts, mainly where water availability in wetlands and along rivers favors vegetation. In the central and southern parts, an agricultural belt extends westwards

III. Environmental suitability for transhumance and conflict prevention (Chapter II)

and eastwards through the study area, indicated by zero suitability scores. This agricultural belt only leaves a few narrow corridors for north–south migrating pastoralists, indicating a high-risk area for farmer–herder conflicts.

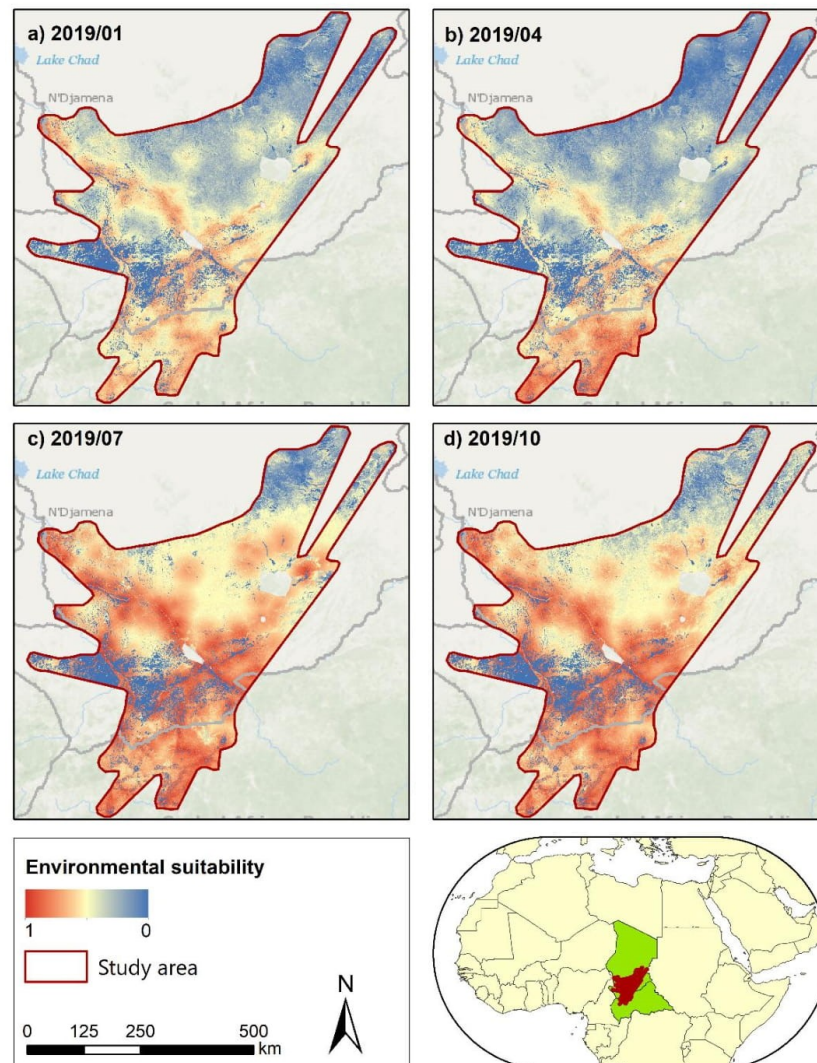


Figure 5. Environmental suitability for transhumance displayed for four timesteps in 2019 for the study area: (a) January 2019, (b) April 2019, (c) July 2019, (d) October 2019. One indicates the highest environmental suitability scores, and zero indicates a low suitability score—the layer for farming systems was assigned the value 0 (sources: derived from Copernicus Sentinel data (2019); background: ESRI Basemaps).

To analyze the environmental suitability in the context of transhumance-related conflicts, the maps were combined with the ACLED conflict data that were filtered for farmer–herder conflicts. Since the farmer–herder conflicts suffer from poor reporting [10], many conflicts may not be covered in the spatial analysis. Figure 6 shows an example for De-

III. Environmental suitability for transhumance and conflict prevention (Chapter II)

ember 2019 (middle of the dry season), when many conflicts occurred in the agricultural belt and close to agricultural areas in the very northeastern part of the study area. Most conflicts occurred in areas with high environmental suitability for transhumance, reflecting the fact that farmers and herders are competing for the same natural resources. Protected areas can also lead to conflicts [37], but must be differentiated regarding their relevance for transhumance. Enclosed protected areas can be seen as “no-go” areas in this context, while protected areas, in general, can still be accessed as grazing land by migratory herders depending on their protection status. During the dry season, the national parks are subject to significant pressure due to the presence of pastoralists, where strong tensions and violent conflicts can also occur between safari operators and pastoralists [37].

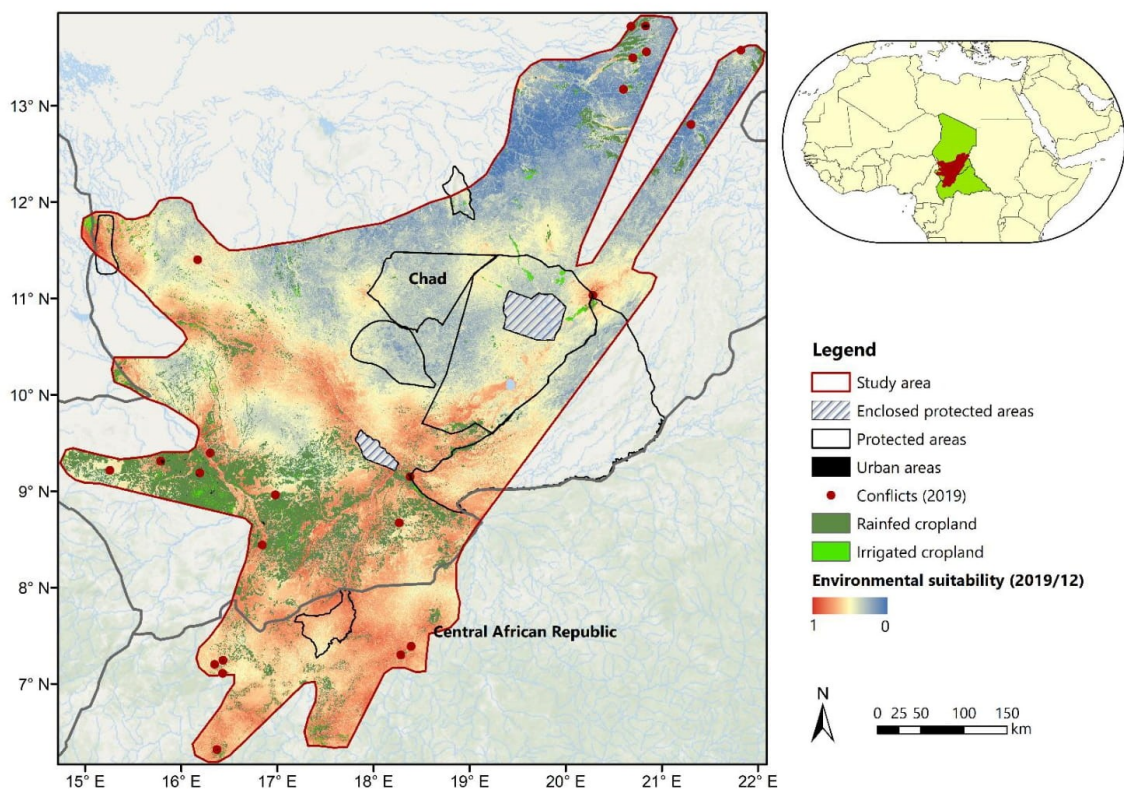


Figure 6. Environmental suitability for transhumance (December 2019) with overlaid ACLED conflict data from 2019, farming systems, urban areas, and protected areas (sources: derived from Copernicus Sentinel data (2019); background: ESRI Basemaps).

The comparison of the environmental suitability between the 663 origin and destination locations of herders in 2019 is displayed in Figure 7, alongside longterm mean precipitation data from 1991 to 2020. While the environmental suitability in the destination areas was higher throughout the year, a drop in suitability scores can be seen from the end of the wet season (October) in both the origin and destination areas (Figure 7). The higher suitability scores during the dry season in the destination areas, with the widest difference between March and May, lead to southward movements of pastoralists.

III. Environmental suitability for transhumance and conflict prevention (Chapter II)

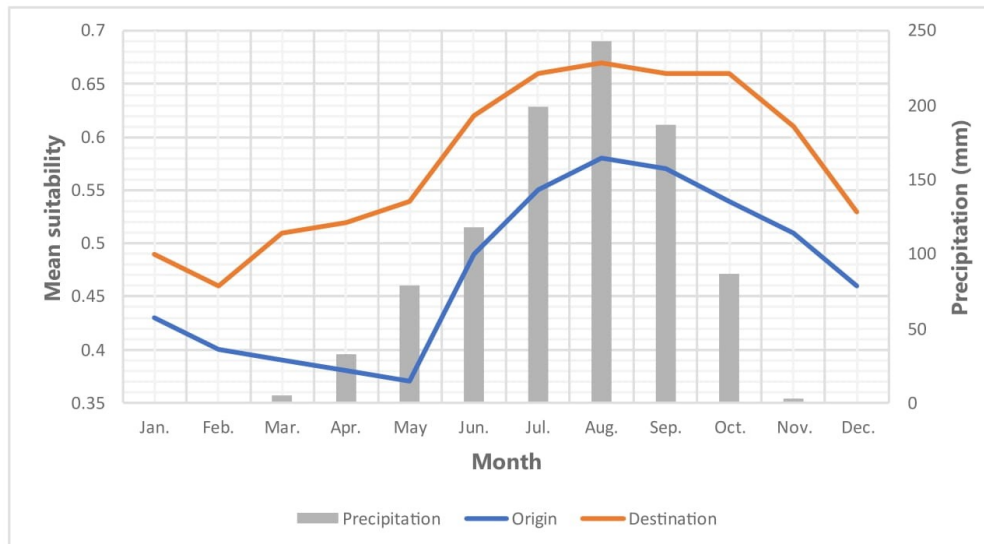


Figure 7. Monthly mean environmental suitability for transhumance for all origin and destination locations within a 1 km radius of the TTT data (663 observations). Only points with a north–south movement were considered for this analysis. Data source: Precipitation data from the Climate Change Knowledge Portal (CCKP) [38].

The results of the least-cost path analysis show theoretical optimal paths for transhumant herders exemplarily displayed for December 2019 (Figure 8). Long distances have to be covered by herders during their southward movements in order to reach their destination areas with enough grazing land in the dry season. These theoretical paths also highlight the need for passing through the agricultural belt to reach the destination areas in the southern part of the study area, or even within the agricultural areas. The dense agricultural belt only allows for narrow corridors accessible to the herders. Here, the challenges with regard to the competition for natural resources lead to a high conflict potential in these areas, as seen in Figure 6.

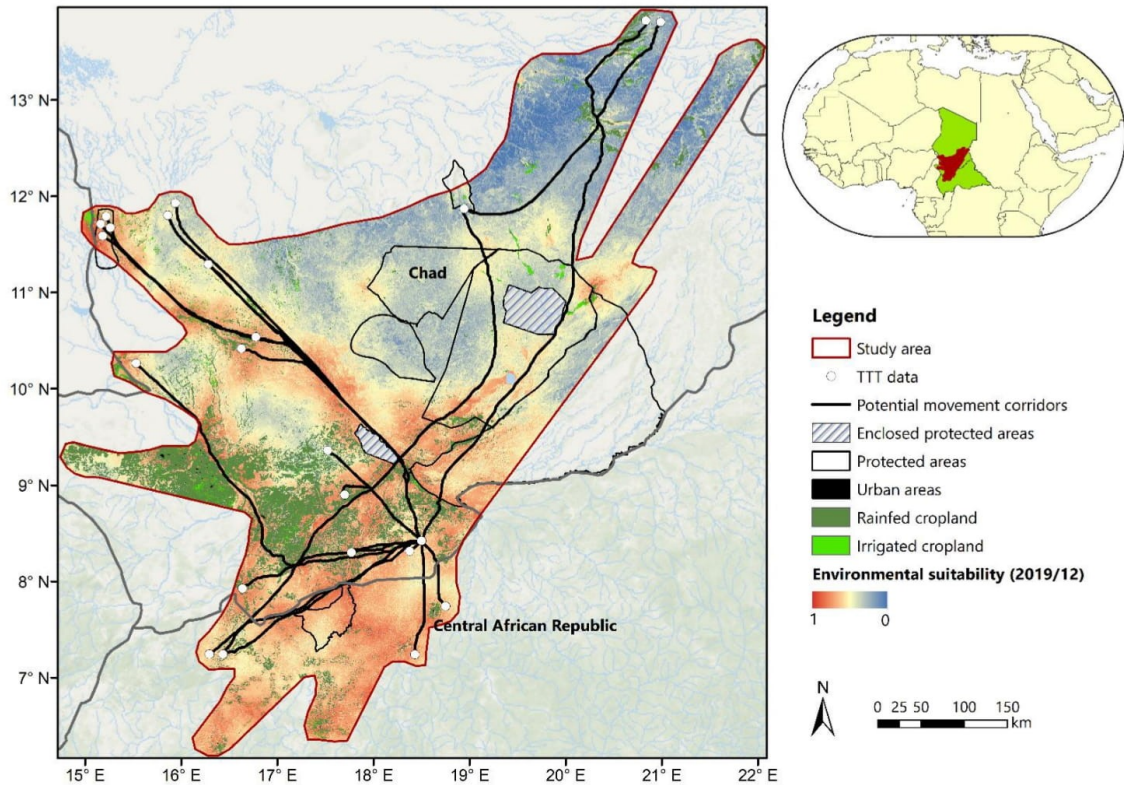


Figure 8. Environmental suitability for December 2019 overlaid with point data from the transhumance tracking tool, potential movement corridors, protected areas, farming systems and urban areas. One represents a high and zero a low suitability score.

4. Discussion

The monthly Earth observation-based environmental suitability maps developed in this study indicate areas favorable for transhumance as well as high-risk areas for conflicts with local subsistence farmers. These can help to understand and potentially manage seasonal movement patterns of pastoralists as they move southwards in the dry season to find enough resources for their livestock. The spatial model is flexible to incorporate additional information layers that might be of interest in some regions, such as distance to wells (additional watering locations) or other fenced areas with access restrictions. In addition, the weighing of the information layers can be adjusted in accordance with expert knowledge. For example, ‘distance to water’ and ‘distance to urban’ was set to a maximum of two walking days through expert knowledge, since this distance is in a range that could influence the routes of pastoralists. This assumption can be changed by manipulating the input layer.

The environmental suitability maps for transhumance do not allow the determination of exact migration routes and locations of herders, as there are many other social, economic and political factors working in tandem with environmental suitability that influence transhumance patterns and also trigger conflicts [9]. However, they may be a good tool to be used in negotiations of transhumance routes and corridors with local, regional and national authorities. Additional research is needed to directly link the environmental suitability maps with the actual or specific routes and migration velocity of pastoralists. To

III. Environmental suitability for transhumance and conflict prevention (Chapter II)

achieve this, location data must be collected along the migratory routes, for example via GPS collars attached to livestock. GPS collars have enhanced research in livestock grazing behavior over the past 20 years while becoming more accurate and cost-effective [39], with no long-term effects on animal activity or behavior [40]. The main limiting factors of GPS collars remain logging frequency, the precision of travel distances and battery lifetime [41], while still providing important information on seasonal variations in movement patterns with seasonal water shortage and feed availability as key factors [42].

Additional research is also needed to analyze the temporal variability of environmental suitability, since this study only focuses on 2019. Additionally, movement paths could either change per year or season or follow traditional routes that may not be favorable in certain years. Laying out this research over multiple years could not only provide a better understanding of the connection between migration routes and temporally varying environmental conditions, but also give more information about varying numbers and locations of conflicts between farmers and herders.

The missing tracking information about the actual movement also hinders the direct quantitative validation of the results. A comparison of the environmental suitability at the different locations from the TTT data allowed a plausibility check of the study results. When calculating mean suitability values for origin and destination areas (Figure 7), the differences in the suitability scores explain the north–south movement patterns at the onset of the dry season and thus prove the plausibility of the values. The extracted environmental suitability values at origin and destination locations may have some uncertainty, since the 663 locations were located via location names in the TTT database. In the future, various plausibility checks could be set as part of the IOM TTT activities to detail missing information about the exact routes used by herders. Local participatory mapping activities conducted along the main transhumance corridors could support a more precise identification of main routes used by herders and cattle. This could be conducted with GPS walk-through activities to draw existing routes using GPS trackers. Similar activities would have to be conducted along each locality of a transhumance corridor to be complete. Focus group discussions with herders in key transit along transhumance routes could also provide detailed maps of transhumance corridors. Finally, during the transhumance season, regular phone checks with herders could also be an option to draw more precise maps of transhumance routes.

While many studies focus on explaining the farmer–herder conflicts by local case studies [9] or use field studies to provide conflict-management strategies [16], few studies addressed spatial tools to improve the understanding of migration movements. In contrast to research on policy options to resolve conflicts [8,15], the present study aimed at providing a range of environmental geospatial information that can help to plan transhumance corridors and passing times and mitigate conflicts with local farmers. However, it must be stated that environmental factors are only partly predictive of conflicts [1]. A study by Mertz et al. [18] showed that weather and resource information can prevent but also increase the level of conflict. A survey of key stakeholders led to the assumption that the communication of information must also include different options for herd movements as well as potential conflict areas [18]. By combining environmental suitability for transhumance with up-to-date conflict data and, e.g., agricultural areas, an early warning system could be established. The benefits of this spatially explicit and large-scale analysis of environmental suitability help to provide information on multiple options for migration routes.

To do so, these additional datasets—ACLED conflict data, TTT data, farming systems, urban areas and protected areas—were considered in the present study to provide a broader context. These data, however, come with some limitations, as the ACLED conflict data are gained through national and international media. Besides only covering incidents that make it to the news, ACLED still provides the largest database on conflicts in Africa [10]. Conflicts may not be covered in the ACLED dataset due to the fact that violence against pastoralists suffers from poor reporting [10]. Overall, the conflict data still help to understand the spatial patterns of conflicts. Comparing the environmental suitability for transhumance

and the ACLED conflict data for the year 2019, a relationship between high environmental suitability, the presence of agriculture and conflicts was found. This conforms with all of the research findings on the presence of farmer–herder conflicts in the Sahel zone [9], showing the information gain of the spatial combination of environmental suitability for herders and the layers for farming systems and conflict data at a high spatial resolution.

The results of the least-cost path analysis can indicate possible transhumance corridors with enough natural resources for herders. These potential movement corridors can help to identify areas with a lower conflict potential, but also determine corridors where limited environmental conditions could occur that cannot hold a large number of moving livestock.

Combining all these datasets can help to provide a possible planning tool together with local experts to not only better plan and manage transhumance, but also to plan agricultural expansion that leaves corridors for seasonal movements, with the overall goal to mitigate conflicts. It was found that traditional transhumance corridors have changed in the last decade, due to changing climatic conditions [3]. With such a spatial tool as that developed in the present study, areas that provide enough natural resources for livestock can be identified to also improve the efficiency of livestock farming along the migratory routes, which increases the productivity of this agricultural production system, and in turn directly contributes to food security. Providing this information regularly to the herders could pilot transhumance through low-risk areas with a high abundance of the main natural resources required. Since transhumance can flexibly and quickly adapt to major seasonal and interannual variations in resources [6], the tool can provide new options for herders to find optimal routes as an alternative for traditional routes. This would help transhumance to adapt to climate change and security issues. Secured and easier transhumance paths might help herders to continue their activity, since more and more herders are choosing to settle down.

5. Conclusions

This study presents an Earth observation data-driven monitoring system of environmental conditions for transhumance, in direct support of IOM’s activities in the Sahel. Through the combination of the suitability maps with data from the Transhumance Tracking Tool and conflict data from ACLED, a new concept for a spatial decision support and future early warning system is demonstrated in direct support of farmer–herder conflict prevention. With the apparent challenges of climate change regarding the fight for natural resources, such a tool can support the planning and managing of transhumance by local stakeholders. The Earth observation data that indicate the environmental suitability for transhumance can thus not only help to mitigate conflicts, but also to increase the productivity of this important agricultural production system in the region and thus promote food security. By using only cost-free datasets with a global coverage, this methodology can be easily transferred to other areas. The flexibility of the spatial model also allows it to be adopted to specific conditions in other regions. Future research is suggested to investigate real-time tracking data of migrating herds which would further promote the development of an early warning system for conflicts with the long-term perspective of a peaceful coexistence between local subsistence farmers and seasonally migrating pastoralists.

Author Contributions: Conceptualization, J.F., T.L., J.D. and D.J.; methodology, J.F. and M.S.; software, M.S.; validation, E.Z. and D.J.; formal analysis, F.S., D.J., E.Z. and M.S.; writing—original draft preparation, M.S.; writing—review and editing, J.F., T.L., F.S., D.J., J.D. and E.Z.; visualization, M.S.; supervision, J.F. and F.S.; project administration, J.F.; funding acquisition, J.F. All authors have read and agreed to the published version of the manuscript.

Funding: This research was funded by the German Space Agency at DLR, via grants from the German Federal Ministry for Economic Affairs and Climate Action (BMWK) under the grant number 50EE1902 and the project title “CoExist—Monitoring environmental-related transhumance patterns and assessing the risk for population displacement”.

III. Environmental suitability for transhumance and conflict prevention (Chapter II)

Data Availability Statement: The data from the Transhumance Tracking Tool were provided through the IOM. All other datasets used in this study are publicly available as listed in the text: Sentinel-1 and Sentinel-2 imagery is available from <http://scihub.copernicus.eu/> (accessed between September 2019 and December 2020), the Copernicus landcover is available from <https://land.copernicus.eu/global/products/lc> (accessed in June 2020), the World database on protected areas (WDPA) is available from <https://www.protectedplanet.net/en> (accessed in February 2021), and the ACLED conflict database is available from <https://acleddata.com/#/dashboard> (accessed in February 2021).

Conflicts of Interest: The authors declare no conflict of interest.

References

1. Ayana, E.K.; Ceccato, P.; Fisher, J.; DeFries, R. Examining the relationship between environmental factors and conflict in pastoralist areas of East Africa. *Sci. Total Environ.* **2016**, *557–558*, 601–611. [CrossRef] [PubMed]
2. Brottem, L.V. Environmental Change and Farmer–Herder Conflict in Agro-Pastoral West Africa. *Hum. Ecol.* **2016**, *44*, 547–563. [CrossRef]
3. Puig Cepero, O.; Desmidt, S.; Detges, A.; Tondel, F.; van Ackern, P.; Foong, A.; Volkholz, J. Climate Change, Development and Security in the Central Sahel. Available online: <https://www.cascades.eu/wp-content/uploads/2021/06/Climate-Change-Development-and-Security-in-the-Central-Sahel.pdf> (accessed on 19 November 2021).
4. Benjaminsen, T.A.; Maganga, F.P.; Abdallah, J.M. The Kilosa Killings: Political Ecology of a Farmer–Herder Conflict in Tanzania. *Dev. Chang.* **2009**, *40*, 423–445. [CrossRef]
5. Cabot, C. Climate Change and Farmer–Herder Conflicts in West Africa. In *Climate Change, Security Risks and Conflict Reduction in Africa*; Springer: Berlin/Heidelberg, Germany, 2016; pp. 11–44. [CrossRef]
6. Inter-Resaux. Pastoral Livestock Farmin in Sahel and West Africa: 5 Preconceptions Put to the Test. Available online: <https://www.inter-reseaux.org/wp-content/uploads/int-17-broch-pastoralismeuk-bd.pdf> (accessed on 9 June 2021).
7. Touré, I.; Ickowicz, A.; Wane, A.; Garba, I.; Gerber, P.; Atte, I.; Cesaro, J.-D.; Diop, A.T.; Djibo, S.; Ham, F.; et al. *Atlas des Évolutions des Systèmes Pastoraux au Sahel: 1970–2012*; United Nations Food and Agriculture Organization of the United Nations (FAO)-Centre for International Cooperation in Agricultural Research for Development (CIRAD): Rome, Italy, 2012; ISBN 978-92-5-107152-6.
8. Ikhuoso, O.A.; Adegbeye, M.; Elghandour, M.; Mellado, M.; Al-Dobaib, S.; Salem, A. Climate change and agriculture: The competition for limited resources amidst crop farmers–livestock herding conflict in Nigeria—A review. *J. Clean. Prod.* **2020**, *272*, 123104. [CrossRef]
9. Benjaminsen, T.A.; Ba, B. Farmer–herder conflicts, pastoral marginalisation and corruption: A case study from the inland Niger delta of Mali. *Geogr. J.* **2009**, *175*, 71–81. [CrossRef]
10. Krätli, S.; Toulmin, C. *Farmer–Herder Conflict in Sub-Saharan Africa?* International Institute for Environment and Development (IIED): London, UK, 2020.
11. Motta, P.; Porphyre, T.; Hamman, S.M.; Morgan, K.L.; Ngwa, V.N.; Tanya, V.N.; Raizman, E.; Handel, I.G.; Bronsvort, B.M. Cattle transhumance and agropastoral nomadic herding practices in Central Cameroon. *BMC Veter. Res.* **2018**, *14*, 214. [CrossRef]
12. Detges, A. Local conditions of drought-related violence in sub-Saharan Africa. *J. Peace Res.* **2016**, *53*, 696–710. [CrossRef]
13. Shettima, A.G.; Tar, U.A. Farmer–Pastoralist Conflict in West Africa: Exploring the Causes and Consequences. *Inf. Soc. Justice* **2008**, *1*, 163–184. [CrossRef]
14. Scheffran, J.; Link, P.M.; Schilling, J. Climate and Conflict in Africa. In *Oxford Research Encyclopedia of Climate Science*; Scheffran, J., Link, P.M., Schilling, J., Eds.; Oxford University Press: London, UK, 2019; ISBN 9780190228620.
15. Adaawen, S.; Rademacher-Schulz, C.; Schraven, B.; Segadlo, N. Drought, migration, and conflict in sub-Saharan Africa: What are the links and policy options? *Curr. Dir. Water Scarcity Res.* **2019**, *2*, 15–31.
16. Mbih, R.A. The politics of farmer–herder conflicts and alternative conflict management in Northwest Cameroon. *Afr. Geogr. Rev.* **2020**, *39*, 324–344. [CrossRef]
17. Wario, H.T.; Roba, H.G.; Kaufmann, B. Shaping the Herders’ “Mental Maps”: Participatory Mapping with Pastoralists’ to Understand Their Grazing Area Differentiation and Characterization. *Environ. Manag.* **2015**, *56*, 721–737. [CrossRef]
18. Mertz, O.; Rasmussen, K.; Rasmussen, L.V. Weather and resource information as tools for dealing with farmer–pastoralist conflicts in the Sahel. *Earth Syst. Dyn.* **2016**, *7*, 969–976. [CrossRef]
19. Guinde, M.; Mahamat, O.; Abdallah, M. The importance of pastoralism in Chad. *Bull. de l’OIE* **2018**, *2018*, 1–5. [CrossRef]
20. Buchhorn, M.; Smets, B.; Bertels, L.; Roo, B.D.; Lesiv, M.; Tsendbazar, N.-E.; Herold, M.; Fritz, S. Copernicus Global Land Service: Land Cover 100m: Collection 3: Epoch 2018: Globe. Available online: <https://library.wur.nl/WebQuery/wurpubs/580265> (accessed on 21 February 2022).
21. UNEP-WCMC; IUCN. Protected Planet: The World Database on Protected Areas (WDPA) and World Database on Other Effective Area-based Conservation Measures (WD-OECM). Available online: www.protectedplanet.net (accessed on 16 June 2021).
22. International Organization for Migration. *Displacement Tracking Matrix Transhumance Tracking Tool*; International Organization for Migration: Geneva, Switzerland, 2021.
23. Raleigh, C.; Linke, A.; Hegre, H.; Karlsen, J. Introducing ACLED: An Armed Conflict Location and Event Dataset. *J. Peace Res.* **2010**, *47*, 651–660. [CrossRef]

III. Environmental suitability for transhumance and conflict prevention (Chapter II)

24. Steinbach, S.; Cornish, N.; Franke, J.; Hentze, K.; Strauch, A.; Thonfeld, F.; Zwart, S.J.; Nelson, A. A New Conceptual Framework for Integrating Earth Observation in Large-scale Wetland Management in East Africa. *Wetlands* **2021**, *41*, 93. [CrossRef]
25. Landmann, T.; Eidmann, D.; Cornish, N.; Franke, J.; Siebert, S. Optimizing harmonics from Landsat time series data: The case of mapping rainfed and irrigated agriculture in Zimbabwe. *Remote Sens. Lett.* **2019**, *10*, 1038–1046. [CrossRef]
26. Knipling, E.B. Physical and physiological basis for the reflectance of visible and near-infrared radiation from vegetation. *Remote Sens. Environ.* **1970**, *1*, 155–159. [CrossRef]
27. Qi, Y.; Dennison, P.E.; Jolly, W.M.; Kropp, R.C.; Brewer, S.C. Spectroscopic analysis of seasonal changes in live fuel moisture content and leaf dry mass. *Remote Sens. Environ.* **2014**, *150*, 198–206. [CrossRef]
28. Roberts, D.; Dennison, P.; Gardner, M.; Hetzel, Y.; Ustin, S.; Lee, C. Evaluation of the potential of hyperion for fire danger assessment by comparison to the airborne visible/infrared imaging spectrometer. *IEEE Trans. Geosci. Remote Sens.* **2003**, *41*, 1297–1310. [CrossRef]
29. Yebra, M.; Dennison, P.E.; Chuvieco, E.; Riaño, D.; Zylstra, P.M.; Hunt, E.R., Jr.; Danson, F.M.; Qi, Y.; Jurdao, S. A global review of remote sensing of live fuel moisture content for fire danger assessment: Moving towards operational products. *Remote Sens. Environ.* **2013**, *136*, 455–468. [CrossRef]
30. Asner, G.P.; Knapp, D.E.; Cooper, A.N.; Bustamante, M.M.C.; Olander, L.P. Ecosystem Structure throughout the Brazilian Amazon from Landsat Observations and Automated Spectral Unmixing. *Earth Interact.* **2005**, *9*, 1–31. [CrossRef]
31. Roberts, D.; Smith, M.; Adams, J. Green vegetation, nonphotosynthetic vegetation, and soils in AVIRIS data. *Remote Sens. Environ.* **1993**, *44*, 255–269. [CrossRef]
32. Franke, J.; Barradas, A.C.; Borges, M.A.; Costa, M.M.; Dias, P.A.; Hoffmann, A.A.; Filho, J.C.O.; Melchiori, A.E.; Siegert, F. Fuel load mapping in the Brazilian Cerrado in support of integrated fire management. *Remote Sens. Environ.* **2018**, *217*, 221–232. [CrossRef]
33. Delcourt, C.; Combee, A.; Izbicki, B.; Mack, M.; Maximov, T.; Petrov, R.; Rogers, B.; Scholten, R.; Shestakova, T.; van Wees, D.; et al. Evaluating the Differenced Normalized Burn Ratio for Assessing Fire Severity Using Sentinel-2 Imagery in Northeast Siberian Larch Forests. *Remote Sens.* **2021**, *13*, 2311. [CrossRef]
34. Lutes, D.C.; Keane, R.E.; Caratti, J.F.; Key, C.H.; Benson, N.C.; Sutherland, S.; Gangi, L.J. *FIREMON: Fire Effects Monitoring and Inventory System*; General Technical Report RMRS-GTR-164-CD; US Department of Agriculture, Forest Service, Rocky Mountain Research Station: Fort Collins, CO, USA, 2006.
35. Buchhorn, M.; Smets, B.; Bertels, L.; Roo, B.D.; Lesiv, M.; Tsendbazar, N.-E.; Li, L.; Tarko, A. Copernicus Global Land Service: Land Cover 100m: Version 3 Globe 2015–2019: Product User Manual. Available online: <https://land.copernicus.eu/global/products/lc> (accessed on 21 February 2022).
36. Van Etten, J. RPackage gdistance: Distances and Routes on Geographical Grids. Available online: <https://cran.microsoft.com/snapshot/2014-12-09/web/packages/gdistance/vignettes/gdistance.pdf> (accessed on 7 October 2021).
37. UICN/PACO. Evaluation de L'efficacité de la Gestion des Aires Protégées: Aires Protégées du Tchad. 2008. Available online: <https://www.iucn.org/fr/content/evaluation-de-lefficacite-de-la-gestion-des-aires-protégees-parcs-et-reserves-du-tchad> (accessed on 21 February 2022).
38. World Bank Group. Climate Change Knowledge Portal (CCKP): Current Climate: Climatology: Precipitation data. Available online: <https://climateknowledgeportal.worldbank.org/country/chad/climate-data-historical> (accessed on 19 November 2021).
39. Bailey, D.W.; Trotter, M.G.; Knight, C.W.; Thomas, M.G. Use of GPS tracking collars and accelerometers for rangeland livestock production research1. *Transl. Anim. Sci.* **2018**, *2*, 81–88. [CrossRef] [PubMed]
40. Stabach, J.A.; Cunningham, S.A.; Connette, G.; Mota, J.L.; Reed, D.; Byron, M.; Songer, M.; Wachter, T.; Mertes, K.; Brown, J.L.; et al. Short-term effects of GPS collars on the activity, behavior, and adrenal response of scimitar-horned oryx (*Oryx dammah*). *PLoS ONE* **2020**, *15*, e0221843. [CrossRef]
41. McGranahan, D.A.; Geaumont, B.; Spiess, J.W. Assessment of a livestock GPS collar based on an open-source datalogger informs best practices for logging intensity. *Ecol. Evol.* **2018**, *8*, 5649–5660. [CrossRef]
42. Feldt, T.; Schlecht, E. Analysis of GPS trajectories to assess spatio-temporal differences in grazing patterns and land use preferences of domestic livestock in southwestern Madagascar. *Pastoralism* **2016**, *6*, 5. [CrossRef]

IV. Intercomparison of satellite-based algorithms for regional surface water detection (Chapter III)

Tottrup, C., Druce, D., Meyer, R.P., Christensen, M., Riffler, M., Dulleck, B., Rastner, P., Jupova, K., Sokoup, T., Haag, A., Cordeiro, M.C.R., Martinez, J.-M., Franke, J., **Schwarz, M.**, Vanthof, V., Liu, S., Zhou, H., Marzi, D., Rudiyanto, R., Thompson, M., Hiestermann, J., Alemohammad, H., Masse, A., Sannier, C., Wangchuk, S., Schumann, G., Giustarini, L., Hallowes, J., Markert, K., Paganini, M. (2022) Surface Water Dynamics from Space: A Round Robin Intercomparison of Using Optical and SAR High-Resolution Satellite Observations for Regional Surface Water Detection. *Remote Sensing*, 14(10), 2410. DOI: <https://doi.org/10.3390/rs14102410>

A PDF of this article is available at:

<https://www.mdpi.com/2072-4292/14/10/2410%20>

Article

Surface Water Dynamics from Space: A Round Robin Intercomparison of Using Optical and SAR High-Resolution Satellite Observations for Regional Surface Water Detection

Christian Tottrup ^{1,*}, Daniel Druce ¹, Rasmus Probst Meyer ¹, Mads Christensen ¹, Michael Riffler ², Bjoern Dulleck ², Philipp Rastner ², Katerina Jupova ³, Tomas Sokoup ³, Arjen Haag ⁴, Mauricio C. R. Cordeiro ⁵, Jean-Michel Martinez ⁵, Jonas Franke ⁶, Maximilian Schwarz ⁷, Victoria Vanthof ⁸, Suxia Liu ⁹, Haowei Zhou ¹⁰, David Marzi ¹¹, Rudiyanto Rudiyanto ¹², Mark Thompson ¹³, Jens Hiestermann ¹³, Hamed Alemohammad ¹⁴, Antoine Masse ¹⁵, Christophe Sannier ¹⁵, Sonam Wangchuk ¹⁶, Guy Schumann ¹⁷, Laura Giustarini ¹⁷, Jason Hallowes ¹⁸, Kel Markert ¹⁹ and Marc Paganini ²⁰

Citation: Tottrup, C.; Druce, D.; Meyer, R.P.; Christensen, M.; Riffler, M.; Dulleck, B.; Rastner, P.; Jupova, K.; Sokoup, T.; Haag, A.; et al. Surface Water Dynamics from Space: A Round Robin Intercomparison of Using Optical and SAR High-Resolution Satellite Observations for Regional Surface Water Detection. *Remote Sens.* **2022**, *14*, 2410. <https://doi.org/10.3390/rs14102410>

Academic Editor: Vito Pascazio

Received: 7 April 2022

Accepted: 10 May 2022

Published: 17 May 2022

Publisher's Note: MDPI stays neutral with regard to jurisdictional claims in published maps and institutional affiliations.



Copyright: © 2022 by the authors. Licensee MDPI, Basel, Switzerland. This article is an open access article distributed under the terms and conditions of the Creative Commons Attribution (CC BY) license (<http://creativecommons.org/licenses/by/4.0/>).

- ¹ DHI A/S, 2970 Hørsholm, Denmark; dadr@dhigroup.com (D.D.); rame@dhigroup.com (R.P.M.); madc@dhigroup.com (M.C.)
 - ² GeoVille GmbH, 6020 Innsbruck, Austria; riffler@geoville.com (M.R.); dulleck@geoville.com (B.D.); rastner@geoville.com (P.R.)
 - ³ Gisat s.r.o., 170 00 Praha, Czech Republic; katerina.jupova@gisat.cz (K.J.); tomas.sokoup@gisat.cz (T.S.)
 - ⁴ Deltares, 2629 HV Delft, The Netherlands; arjen.haag@deltares.nl
 - ⁵ Géosciences Environnement Toulouse (GET), Unité Mixte de Recherche 5563, IRD/CNRS/Université, 31400 Toulouse, France; mauricio@ana.gov.br (M.C.R.C.); jean-michel.martinez@ird.fr (J.-M.M.)
 - ⁶ Remote Sensing Solutions GmbH, 81673 München, Germany; franke@rssgmbh.de
 - ⁷ Department of Biology, Ludwig-Maximilians-University Munich, 82152 Planegg-Martinsried, Germany; schwarz@rssgmbh.de
 - ⁸ Faculty of Environment, University of Waterloo, Waterloo, ON N2L 3G1, Canada; vrvantho@uwaterloo.ca
 - ⁹ Key Laboratory of Water Cycle and Related Land Surface Processes, Institute of Geographic Sciences and Natural Resources Research, Chinese Academy of Sciences, Beijing 100101, China; liusx@igsnr.ac.cn
 - ¹⁰ College of Resources and Environment, Sino-Danish Center, University of Chinese Academy of Sciences, Beijing 100049, China; zhouhw.18b@igsnr.ac.cn
 - ¹¹ Department of Electrical, Computer and Biomedical Engineering, University of Pavia, 27100 Pavia, Italy; david.marzi01@universitadipavia.it
 - ¹² Program of Crop Science, Faculty of Fisheries and Food Science, Universiti Malaysia Terengganu, Kuala Nerus 21030, Terengganu, Malaysia; rudiyanto@umt.edu.my
 - ¹³ GeoTerraImage (Pty) Ltd., Pretoria 0184, South Africa; mark.thompson@geoterraimage.com (M.T.); jens.hiestermann@geoterraimage.com (J.H.)
 - ¹⁴ Radiant Earth Foundation, Washington, DC 20005, USA; hamed@radiant.earth
 - ¹⁵ Group CLS, 31400 Toulouse, France; amasse@groupcls.com (A.M.); csannier@groupcls.com (C.S.)
 - ¹⁶ Faculty of Science, Vrije Universiteit Amsterdam, 1081 HV Amsterdam, The Netherlands; s.wangchuk@vu.nl
 - ¹⁷ RSS-Hydro SARLS, 3593 Dudelange, Luxembourg; gschumann@rss-hydro.lu (G.S.); lgiustarini@rss-hydro.lu (L.G.)
 - ¹⁸ EkoSource Insight (Pty) Ltd., Johannesburg 2196, South Africa; jhallowes@ekosource.co.za
 - ¹⁹ SERVIR-Mekong, Bangkok 10400, Thailand; kel.markert@nasa.gov
 - ²⁰ European Space Agency, ESRIN, 00044 Frascati, Italy; marc.paganini@esa.int
- * Correspondence: cto@dhigroup.com

Abstract: Climate change, increasing population and changes in land use are all rapidly driving the need to be able to better understand surface water dynamics. The targets set by the United Nations under Sustainable Development Goal 6 in relation to freshwater ecosystems also make accurate surface water monitoring increasingly vital. However, the last decades have seen a steady decline in in situ hydrological monitoring and the availability of the growing volume of environmental data from free and open satellite systems is increasingly being recognized as an essential tool for largescale monitoring of water resources. The scientific literature holds many promising studies on satellite-based surface-water mapping, but a systematic evaluation has been lacking. Therefore, a round robin exercise was organized to conduct an intercomparison of 14 different satellite-based

approaches for monitoring inland surface dynamics with Sentinel-1, Sentinel-2, and Landsat 8 imagery. The objective was to achieve a better understanding of the pros and cons of different sensors and models for surface water detection and monitoring. Results indicate that, while using a single sensor approach (applying either optical or radar satellite data) can provide comprehensive results for very specific localities, a dual sensor approach (combining data from both optical and radar satellites) is the most effective way to undertake largescale national and regional surface water mapping across bioclimatic gradients.

Keywords: surface water dynamics; SAR and optical data; data fusion; water resource management; Sustainable Development Goal 6

1. Introduction

Water is key to sustainable development, being critical for socioeconomic development, energy and food production, and healthy ecosystems. Today water scarcity affects more than 40 percent of the world's population and is projected to rise further, exacerbated by climate change [1]. As the global population grows, there is an increasing need to balance the competing demands for water resources and have more efficient ways to manage water supply. The importance of ensuring the availability and sustainable management of water for all has been increasingly addressed in the global political agenda, as seen with the Sixth Sustainable Development Goal (SDG) of the United Nations 2030 Agenda for Sustainable Development [2] and the adoption of an International Decade 2018-2028 for Action on 'Water for Sustainable Development' by the UN General Assembly [3]. As the demand for freshwater increases, the importance of monitoring changes in surface waters is gaining more attention, but many countries are still lacking data to monitor the extent of their inland waters and their intra- and interannual changes.

Earth Observation (EO) is an essential source of information, which can complement national hydrometric data and services and support countries to operationally monitor changes to their surface waters. Ever since the launch of the first Earth observation satellites in the early 1970s, the mapping and monitoring of surface water has been a subject that attracts interest from researchers and practitioners in hydrology, environmental conservation, and water resource management. The field has gradually evolved and been incentivized by the steady buildup of long-term archives of global satellite data and computer resources for analyzing those data. A significant breakthrough in the adoption of EO solutions for water-related topics has been the European Commission Joint Research Center's Global Surface Water Explorer [JRC-GSWE] [4] and the Global Land Analysis and Discovery Group's Global Surface Water Dynamics [GLAD-GSWD] [5]. Despite these developments and the long track record of related successful case studies on surface water mapping, there is still a lack of clear, robust, efficient, user-oriented methods and guidelines that allow for the use of EO data at scale and on an operational basis for surface water mapping and monitoring.

The mapping of surface water with either optical or Synthetic Aperture Radar (SAR) data has been reviewed in several papers (e.g., [6,7]) and with a series of more recent papers focusing on the combined use of optical and SAR data [8–11]. This development is directly related to the Sentinel program under the European Copernicus initiative [12]. Through the Copernicus Sentinel mission, optical and SAR data in high resolution (10 m) have become globally available free of charge and with a short latency of a few days or less. The next leap in EO-based surface water detection will need to take full advantage of this enhanced observation capacity, which offers unprecedented opportunities to develop robust and cost-effective EO methods to monitor the seasonal and annual variations of surface waters. These EO methods and associated information products can be embedded in national processes for more evidence-based water policies and efficient reporting on the global water agenda. This is why the European Space Agency (ESA) has launched the

WorldWater project with a principal aim of strengthening EO capacities in countries to better monitor their inland waterbodies (lakes, reservoirs, rivers, and estuaries) and, consequently, better fulfil their commitments on water resource management and water security in the different water-related global agendas such as the 2030 Agenda on Sustainable Development [2], the 2015 Paris Agreement on climate change [13] and the Sendai Framework for Disaster Risk Reduction [14].

The overarching goal of the WorldWater project is to develop robust and scalable EO solutions for inland surface water monitoring, which can be exploited by a large community of stakeholders involved in water management from local water supplies to national water strategies, including transboundary river basin management plans and global assessment of surface water changes. As part of the project goal, a round robin exercise has been organized to conduct an intercomparison of EO algorithms for surface water detection, using the latest generation of free and open satellite data from Sentinel-1, Sentinel-2, and Landsat 8. The round robin was open to researchers, companies, and other developers of satellite-based algorithms for surface water detection. The precondition for participating in the round robin was a peer-reviewed algorithm for surface water detection based on (or adaptable to) Sentinel-1, Sentinel-2, and/or Landsat 8. Non-peer reviewed algorithms were accepted provided that adequate supplementary documentation and justification could be provided. In this paper, we present the results of the WorldWater round robin intercomparison and use them as the basis for discussing the pros and cons of different approaches to detect and monitor surface waters from Earth observation data. By using various statistical tests, we evaluate the quantitative performance of the individual algorithms and use the findings to draw some qualitative considerations about their performance. The focus is not on the algorithms themselves, as they have already proved themselves (cf. peer-reviewed or in an operational setting), but rather, on the underlying data model, that is, whether the algorithms are relying on single sensor inputs or whether they are using a dual sensor approach. Ideally, the best performing algorithms can provide spatially and temporally consistent timeseries of surface water extent dynamics that meet the user requirements, not only in terms of accuracy but also in terms of transparency, cost, and transferability. The aim is to contribute to the development of a new set of best practices for surface water monitoring, as well as identifying shortfalls and areas of further research.

2. Materials and Methods

2.1. Test Sites and Input Data

All participants in the round robin were required to produce monthly maps of inland, open surface waters at 10-m spatial resolution for 2 consecutive years over three test sites (100 × 100 km) located in 3 different countries: Colombia, Mexico, and Zambia. Optionally, participants could also submit results for an additional two test sites located in Gabon and Greenland (cf. Figure 1). Test site locations were selected to cover various eco- and climatic regions as well as to include major challenges for EO-based surface water mapping, including sites influenced by topography, clouds, canopy shading, fire scars, urban areas, and regions with permanent low backscatter (e.g., flat and impervious areas, sandy surfaces). The sites also included a diversity of waterbodies ranging from large waterbodies (wind and wave effects) to smaller waterbodies of both a permanent and seasonal nature, as well as waterbodies impacted by water constituents and shallow waters influenced by bottom reflectance. The input datasets, made available to all participants, included all Sentinel 1, Sentinel 2, and Landsat 8 images acquired over the test sites from July 2018 to June 2020. Use of ancillary datasets (such as Digital Elevation Model (DEMs) and a priori surface water maps) were allowed, but under the condition they were publicly available, e.g., the Copernicus DEM [15] and JRC-GSWE [4].

IV. Intercomparison of satellite-based algorithms for regional surface water detection (Chapter III)



Figure 1. Location map of the test sites annotated with their dominant eco-region(s).

2.2. Surface Water Detection Models

The following sections provide a high-level summary of the fourteen contributions to the round robin intercomparison. Each contribution is referred to as a model in order to emphasize that the focus on the intercomparison was to evaluate the performance of the underlying data models, i.e., whether the surface water detection was based on optical data only (O), SAR data only (S), or integration of both optical and SAR data (O + S).

Model A [O + S] uses a histogram segmentation method to separate imagery from Sentinel-1, Sentinel-2, and Landsat 8 into water and non-water classes [16,17]. Specifically, it carries out edge detection followed by procedures to help obtain a bimodal distribution on which Otsu's method is carried out to automatically derive an optimal threshold. This model was specifically designed for fast and largescale water detection to assist in flood relief efforts. Similar methods exist that attempt to obtain local thresholds over small sections of each image [18], which can potentially yield more accurate results but at the expense of computational speed. A postprocessing step is applied on the monthly water maps derived separately from optical and SAR imagery, where water pixels are constrained to areas that are hydrologically likely to contain water, with the full timeseries of maps derived from optical imagery included as an additional constraint for the SAR-derived maps. Finally, the optical and SAR-based maps are merged to produce a single water map per month.

Model B [O + S] This surface water detection approach is based on Sentinel-2 imagery as the primary water detection dataset, with the all-weather capabilities of Sentinel-1 SAR imagery being used to "fill-in" cloud-obscured water surfaces. SAR data "in-filling" was restricted to raster cells previously detected as having recorded a surface water content from longer-term data modelling results (circa 2016 and forwards) in order to minimize SAR-generated commission errors in the target month. The water surface modelling procedure is based on a set of decision-tree-generated rules that have been derived from a comprehensive set of water and non-water feature reference points distributed across South Africa. The reference dataset consists of $\pm 60,000$ sample points that represent a wide range of seasonal and geographical variations in both water (i.e., turbidity, depth) and

IV. Intercomparison of satellite-based algorithms for regional surface water detection (Chapter III)

non-water surface conditions with potentially similar spectral characteristics, such as burn scars, terrain shadows, and dark, non-vegetated surfaces from both natural and man-made environments. Collectively, these points ensure full representation of all spectral characteristics required in the water detection modelling process. The monthly surface water datasets represent the median surface water extent for that month, rather than the average or (absolute) maximum extent, as a result of the multivariate image acquisition date compositing approach used to model water features [19,20].

Model C [O + S] uses a random forest classifier to map surface waterbodies pixel by pixel by taking advantage of the strength of both optical and SAR data in an integrated manner [21]. For optical data, the model relies on a maximum value of the NDWI composite created using both Level-1 and L-2 Sentinel-2 data. The model depends on a minimum radar backscatter intensity, from both VV and VH polarizations, of a composite for Sentinel-1 SAR data. Relying composite images minimizes disturbances from clouds, turbidity, and shadows for the optical data and speckles, lake ice, and radar shadows for the SAR data. The model also uses DEM as a feature to remove false positives over a steeper terrain. All the workflows are implemented in Google Earth Engine for ease of transferability and reproducibility.

Model D [O + S] applied a combined histogram-thresholding and edge-detection approach to estimate monthly surface water extent from monthly, cloud-free Sentinel-1, Sentinel-2, and Landsat-8 scenes. Following cloud masking for optical scenes, we applied the Edge-Otsu algorithm to create binary land and water maps for each scene [17,22]. For a complete description and application of the Edge algorithm, see Markert et al., 2020. To initially segment water, histogram-thresholding was performed using the Normalized Difference Water Index (NDWI) index for optical scenes and the VV-median band for SAR scenes within already buffered surface water polygons from Pekel et al., 2016. A second segmentation was applied to full scenes to segment water and non-water, irrespective of initial water polygons. The MERIT DEM [23] was then used to derive a Height Above Nearest Drainage (HAND) model [24] and on regions less than 30 m in height relative to the nearest drainage. Final monthly surface water products combined both optical and SAR water maps by selecting the optical land–water prediction when available, and otherwise selecting the SAR-identified water pixel. Given that cloud-free optical images segment water with higher accuracy than SAR, this approach reduces error during less cloudy periods.

Model E [S] is a fully automated approach that uses dynamic thresholds to classify individual Sentinel-1 scenes. The scene-dependent thresholds to classify water are defined through the use of existing geospatial information of permanent water areas, e.g., data from the Global Surface Water Explorer (GSWE) [4]. The S-1 backscatter values of permanent water areas are derived per scene and are then statistically analyzed by using percentiles to eliminate outliers and a combination of mean and standard deviation to define the individual classification threshold. In opposite to a fixed threshold, this standardized statistical approach allows for the definition of dynamic classification thresholds per scene in order to account for variations in backscatter caused by various factors. The individually classified scenes are then combined to monthly surface water composites, in which false positives (mainly radar shadows) are removed by the use of the Multi-resolution Valley Bottom Flatness (MrVBF) index [25] derived from the Copernicus Digital Elevation Model (DEM). The automated, computationally efficient classification approach has been shown to capture seasonal changes in surface water accurately, but also shows some limitations in non-vegetated sandy areas, in which false positives occur.

Model F [O + S] used combinations of monthly percentile composite images from Sentinel-1 and Normalized Difference Vegetation Index (NDVI), Normalized Difference Water Index (NDWI), Land Surface Water Index (LSWI), Normalized Difference Snow Index (NDSI), red, NIR, and SWIR1 bands from the greenest monthly Sentinel-2 images as covariates for the mapping of monthly surface water extent in Colombia, Mexico, Zambia, and Gabon. For Greenland, covariates from Sentinel-1 were excluded and replaced by

IV. Intercomparison of satellite-based algorithms for regional surface water detection (Chapter III)

monthly minimum NDVI from Sentinel-2 [26]. Training datasets (water–non-water) were generated using a stratified, random sample of points based on Global Surface Water data [4] and visual inspections of spectra profile based on k-means clustering results. Random forest classifier was used for classification.

Model G [S] This approach applies a novel Convolutional Neural Network (CNN) model applied to Sentinel-1 observations to detect surface water. The JRC GSWE product was used as training data, and several finetuning strategies were implemented to improve accuracy of the model in places with complex landcover types. The resulting surface water product has a 10-m spatial resolution, is not impacted by cloud coverage, and can be run in near-real time to detect any surface water changes [27].

Model H [O] uses a thresholding method based on a combination of water indexes (MNDWI > NDVI or MNDWI > EVI) to extract surface water extent from monthly composite Sentinel-2 MSI images. Different from the conventional thresholding method, this algorithm does not need to determine the threshold artificially. To obtain more accurate surface water extent maps, the clouds and cloud shadows pixels, buildup pixels, and snow/ice pixels were removed by auxiliary datasets in preprocessing, and the surface water maps with residual non-water pixels were furtherly denoised in postprocessing. For incomplete monthly surface water extent maps, the surface water frequency map was utilized to fill the gaps caused by clouds and cloud shadows. These methods had been proved effective and accurate in the construction of surface water extent continuous timeseries [28].

Model I [O] uses a multidimensional clustering analysis based on reflectance values and water indices to identify water pixels using optical scenes individually. To achieve high-performance and low memory consumption for high resolution images, this process is applied to a random subsample of the image’s pixels and then coupled with a Naïve Bayes classifier responsible for generalizing the results to the complete scene. The advantage of using an unsupervised approach such as clustering is that the water pixels group is identified automatically by comparing it to other clusters (targets) in the scene. Therefore, the algorithm doesn’t require ancillary data, pretraining, or any threshold calibration, and it is independent of the sensor and the coverage being analyzed. These ideas make it simple to apply the model to a great variety of conditions [29]. As the original algorithm was designed for operational use on single scenes, the monthly water surface has been derived by combining subsequent water masks through an upvote logic that considers as water those pixels that received at least two votes.

Model J [S] This model is based on an unsupervised k-means-clustering algorithm and aims to extract monthly inland waterbody extents over wide areas using multitemporal Sentinel-1 SAR data. To account for slope-induced backscatter differences caused by hills and mountains, due to the slanted acquisition geometry of SAR systems, the model included a radiometric terrain correction, as this step is not applied in the standard Sentinel-1 preprocessing chain. Moreover, the methodology added a multitemporal speckle noise filter which provides better results than a spatial filter applied independently to each SAR image. Seed points for the k-means model are then retrieved by randomly sampling the water layer of the ESA CCI GlobCover Land Cover map [30]. Each sample is represented by a set of temporal features suitable for water characterization in SAR data, such as the mean backscattering value, the maximum value, minimum value, and four “quarter composites” obtained by averaging in time all the Sentinel-1 acquisitions available within each quarter of a year. After the k-means clustering, applied with $k = 4$, the water cluster is selected by considering a majority voting procedure within the multi-polygon water boundaries of the GlobCover map. Since it is based on SAR data, the methodology can be applied in every weather and lighting condition. Being an unsupervised technique, it is quick, robust, and can be applied automatically over any region of the World [31].

Model L [O] uses the simple yet robust band ratio Normalized Difference Vegetation Index (NDVI) on Sentinel-2 images, screened with the cloud mask processor available in

IV. Intercomparison of satellite-based algorithms for regional surface water detection (Chapter III)

ESA's SNAP software. Despite the rather simplistic nature of the NDVI band ratio algorithm, results reported in other studies of this type are encouraging (e.g., [26]). Furthermore, the aim of choosing this approach was to test the application of simple and fast algorithms for processing large amounts of images in a short time. We implemented the processing on the Web Advanced Space Developer Interface (WASDI) to process all images without the need for downloading large data quantities on a personal computer [32].

Model M [O + S] uses an efficient and opensource supervised Random Forest classifier system based on Geographic Object-Based Image Analysis (GEOBIA) [33]. It relies on two main components, which are feature extraction based on attribute profiles and a semi-supervised classification using a Random Forest Algorithm. The first step consists of computing features based on Sentinel-2 L1C without cloud detection (MNDWI) and DEM (SRTM or ArcticDEM for Greenland) and extraction of spatial features (object area). The ground truths are automatically extracted from GlobalSurfaceWater data (Pekel et al., 2016). The output from this model is maps of monthly surface water extent and a confidence index. The same automatic system is applied for all 5 test areas.

Model N [O + S] is based on a combination of different image-binarization techniques applied on monthly aggregated Sentinel-1, Sentinel-2, and Landsat-8 imagery. Dynamic, tile-based thresholding [34,35] is conducted on both SAR and optical inputs. In addition, adaptive thresholding [36] and seeded region growing [37] on each initially detected waterbody is performed on the monthly SAR imagery. Finally, fuzzy-logic classification refinement reduces water lookalikes and misclassifications (e.g., radar shadows) from the SAR-based water masks [38,39].

Model O [O + S] uses a multivariate logistic regression model to estimate monthly surface water extent from the combined usages of Sentinel-1, Sentinel-2, and Landsat-8 imagery. Models that rely upon linear distributions are often simpler and generalize well and, therefore, do not require high-quality training labels. Yet, since land–water classification has some nonlinear exceptions, such as clouds, shadows, and snow, the approach integrates logic-based masking to reduce the impact from problematic areas through specific thresholds or basic decision trees. The final approach has proved to be accurate whilst at the same time maintaining computational efficiency and simplicity that facilitates analysis and understanding at scale [8].

2.3. Validation and Evaluation

These water detection models were evaluated individually and in cross-comparison using independent reference data collected from the test sites. A fundamental premise for sound scientific validation is to use reference data of higher quality than the product to be validated. There are two ways to ensure higher quality in the reference data: (i) by using a reference data source with a better resolution than the data used for production (i.e., verification by higher data) and/or (ii) by using a more accurate measurement or interpretation than being used for production (i.e., verification by higher method). A further requirement on the reference data is the ability to provide sufficient spatial and temporal representation to accurately label each unit in the sample; i.e., the ideal reference data are: (i) available for the entire region of interest, (ii) representative of the attribute at the date of interest, and (iii) available at a low cost. The balance between these criteria is often difficult to achieve and why tradeoffs and compromises may be needed when generating the final set of reference data. In the case of the round robin validation, a two-step approach was followed: (i) sample based validation (pixel based) and labelled using the production imagery (verification by higher method) and (ii) object extraction accuracy (area based) and using PlanetScope data as a reference (verification by higher data). The sample-based validation has the advantage of delivering reference data, which can be directly matched (in space and time) to the validation input, whereas the PlanetScope data offer the advantage of better capturing and, hence, better evaluation of smaller and narrower waterbodies/features. Still, the acquisition and interpretation of PlanetScope data is costly, and their representation is therefore restricted in space and time. In a final step, the

IV. Intercomparison of satellite-based algorithms for regional surface water detection (Chapter III)

temporal consistency of the optical, SAR, and dual sensor-mapping approaches were evaluated by comparing the total areal water extent mapped within each test site and across the monthly timeseries. Each validation and evaluation step is described in more detail below.

2.3.1. Sample Based Validation

Stratified random sampling was used to generate reference points over each 100 × 100 km test site and within three strata across the land–water continuum: permanent water, seasonal water, and non-water. The three strata were generated from the JRC-GSWE long-term water occurrence and defined according to the following thresholds: permanent water > 90%; 0% < seasonal water < 90%, and non-water = 0%. In all test sites, the target class “water” is a rare occurrence. In the case of rare occurrences, statistical equations does not allow for proper estimation of sample sizes, but stratified random sampling affords the option to increase the sample size in classes and/or regions that occupy a small proportion of area to thereby help reduce the standard errors of class/region-specific accuracy estimates [40]. It was our aim to ensure a minimum of 50 samples in each stratum, while using subsequent sample size allocations to provide a proportional allocation of samples in better accordance with the actual area of the different strata within each test site. In addition, the expected variance within each stratum was also considered; i.e., the transitional strata are expected to have the highest variance, and why it has a higher sample allocation. Thus, by taking area and expected variance into account, the following sample allocations were applied for the five test sites (cf. Table 1).

Table 1. Sample size allocations for the 5 test sites used in the round robin.

	Colombia		Gabon		Greenland		Mexico		Zambia	
	<i>per month</i>	<i>total</i>								
Land	140	840	75	450	60	180	140	840	90	540
Transition zone	140	840	150	900	90	270	140	840	190	1140
Water	20	120	60	360	100	300	20	120	40	240
TOTAL	300	1800	285	1710	250	750	300	1800	320	1920

In total, 7,980 samples were allocated across the five test sites and six time periods representing every second month of the year 2019 (January, March, May, July, September, November). Each sample point was assigned to be either water or non-water by two independent and experienced interpreters using blind visual interpretations of monthly Sentinel-1 and -2 composites. To harmonize and achieve consistent reference labelling, a standard validation interface was used to ensure interpreters were looking at same area and using the same reference data and the predefined set of classes. In cases where the interpreters disagreed, a quality manager intervened to seek consensus. If consensus could not be agreed upon, the sample was rejected. For each sample we extracted, the respective water classifications and the final set of samples were used to derive standard metrics for accuracy assessments, i.e., overall accuracy (OA), producer accuracy (PA), and user accuracy (UA). For this analysis, all pixels in the individual round robin classifications not classified as water were considered to be non-water; i.e., the non-water class also included pixels being masked (e.g., due to clouds).

2.3.2. Object Extraction Accuracy

Traditionally, stratified point sampling will, in most instances, under-sample Small Waterbodies (SWB) simply because SWBs only represent a fraction of the total water area, even though they may by far exceed the larger waterbodies in numbers [41]. To deal with the issue of SWBs, we complemented the more conventional stratification, sampling, and confusion matrix-type accuracy assessments with an evaluation of object extraction accuracy based on area-based accuracy metrics and the use of higher spatial resolution but

IV. Intercomparison of satellite-based algorithms for regional surface water detection (Chapter III)

single date (i.e., time-limited) PlanetScope data. An independent reference dataset was created from the classification and interpretation of imagery from Planet. The acquired data was PlanetScope Level 3B (Ortho Scene Products) in 3-m spatial resolution and with 4 spectral bands (RGB, NIR) (<https://www.planet.com/products/planet-imagery/>, accessed on 10 January 2022). The PlanetScope data was acquired within the coverage of each of the test sites and for two areas of approximately 25 km². The exact coverage was determined by size and type of waterbodies, i.e., covering areas with small waterbodies relative to the test site in general and representing both lakes/reservoirs and streams/rivers. For each PlanetScope coverage, we applied a supervised Gradient Boosting (lightGBM) algorithm [42] to generate water masks using the convolution layers derived from spatial filtering of Planet imagery as the explanatory variables and manually derived training samples for water and land (cf. non-water) as the response variable. The Gradient Boosting typically involved a couple of iterations to optimize results, and before finalization, all water masks were manually checked and corrected to ensure high quality. Once analyzed, the PlanetScope data was used to evaluate the object extraction accuracy of the water classifications derived using Sentinel data.

The accuracy evaluation of object extraction is based on object matching, and we focused on two elements related to this, namely: object matching and area-based accuracy measures [43]. The central idea of object matching is to estimate the maximum overlap area by computing the coincidence degree, A_{max} , between two objects.

$$A_{max} = \frac{1}{2} \left(\frac{A_{C,i} \cap A_{R,j}}{A_{C,i}} + \frac{A_{C,i} \cap A_{R,j}}{A_{R,j}} \right)$$

where $A_{C,i}$ denotes the area of the i th-evaluated object, $A_{R,j}$ is the area of the j th reference object, and $A_{C,i} \cap A_{R,j}$ represents the intersection area. For an evaluated object and candidate reference objects, each coincidence degree will be computed. Two objects will be judged as being a matching pair if the area of the coincidence degree is at a maximum, i.e., A_{max} equals 1.

The maximum overlap object matching is complemented by three area-based accuracy measures (i.e., correctness, completeness, and quality). Correctness (A_{cor}) is defined as the ratio of the correctly extracted area (A_C) and the whole extracted area (A_{DC}), whereas completeness (A_{com}) refers to the ratio of the correctly extracted area to the reference area (A_{RC}). The range of correctness and completeness is 0 to 1. If A_C fully corresponds to A_{DC} or A_{RC} , then the value is 1. If there is no overlap between A_C and A_{DC} or A_{RC} , then the value is 0; correctness and completeness interact. For instance, a large A_{DC} leads to a small correctness value, while a small A_{RC} results in a large completeness value. To amend this issue, the quality A_{qual} is designed to provide a measure of quality by balancing correctness and completeness.

$$A_{qual} = \frac{A_C}{A_{DC} + A_{RC} - A_C}$$

The range of quality is 0 to 1. If the water extraction results are the same as the reference data, then the value is 1. If none of the extracted water area overlaps with the reference area, then the value is 0. The advantage of area-based accuracy measures compared to the sample-based validation relates to the fact that the confusion matrix of the latter depends on total pixel number. In contrast, the evaluation results for two cases using area-based accuracy measures are equivalent because it relies only on the evaluation, and reference objects are independent of the total pixel number.

2.3.3. Temporal Consistency Evaluation

The purpose of temporal consistency evaluation is to identify anomalies in sequences of surface water maps. Sudden decreases in surface water can be due not only to drought and high reservoir release but also clouds and lack of valid observation. Flooding, on the other hand, may cause an increase in surface water, but so could cloud shadows and

topographic shading, as well as the impact of low-backscatter areas. More robust water detection algorithms should be able to accurately capture actual water dynamics while minimizing the influence of the other factors.

3. Results

3.1. Water Occurrence

The five test sites used for intercomparison represent very different conditions, which can also be inferred by looking at multiannual water occurrence maps for the respective test sites (cf. Figure 2). As explained in Section 2.1, site variability is, on the one hand, dictated by geographic location (i.e., from tropical to arctic, coastal to inland, and lowland to high land) and, on the other hand, by surface water characteristics. The latter is clearly illustrated in the water occurrence maps, which show the differences between test sites in terms of size and type of waterbodies, as well as the relative distribution of permanent and seasonal water (Figure 2). These different characteristics are important to bear in mind when interpreting the validation results, as they will influence the performance of the individual algorithm.

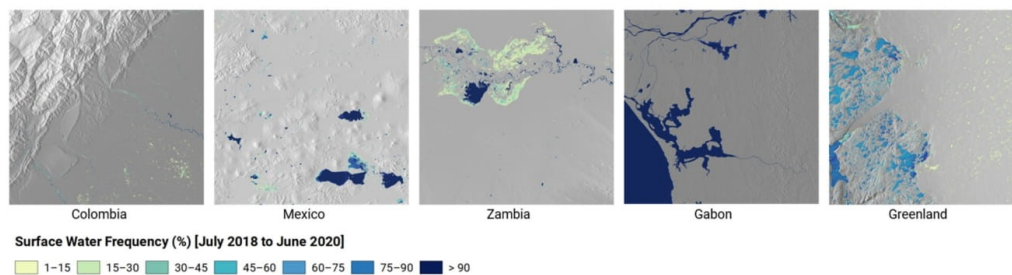


Figure 2. Examples of surface water frequency maps over the 5 test sites and as derived by Model N.

3.2. Sample Based Validation

In Table S1, we provide classification accuracies for the water extraction for all round robin submissions and for each of the three mandatory sites, as well as the optional sites, where relevant. The general performance of all models can be deemed satisfactory, with overall accuracies above or near 90% when looking across the mandatory sites. There is more ambiguity when looking at the performance in terms of user and producer accuracy and at the level of the individual sites.

In Figure 3, the classification accuracies have been grouped (median value) by input data type, i.e., algorithms using both optical and SAR vs. models based on single-sensor inputs (SAR or optical). Figure 3 shows an overall better performance of the combined sensor approach compared to single sensor approaches, although the results are not one-sided when looking at the individual sites or in terms of user and producer accuracies. In Colombia, the combined sensor approach performed best in terms of overall accuracy, but, at the level of UA and PA, the SAR and Optical models, respectively, outperform the combined approach. In Gabon, the SAR approach outperforms the other data models in terms of OA, while in Colombia and Zambia, the optical approach has much higher accuracies for, respectively, PA and UA. In Mexico, OA and UA are almost equal between the data models, but with a noteworthy (+4–5 percentage) drop in producer accuracy for the optical data models compared to the SAR and dual sensor models. The observed differences in UA and PA are closely related to site-specific characteristics. For example, the higher UA accuracies achieved in Gabon and Colombia using SAR are an indication of the benefit SAR adds in a cloud-prone region. In contrast, SAR produces a lower UA in Zambia and Mexico because of commission errors introduced by dry, sandy surfaces. In both

IV. Intercomparison of satellite-based algorithms for regional surface water detection (Chapter III)

Zambia and Mexico, it was also noted that sunglint in certain months caused erroneous cloud masking for certain processors and hence contributed to lowering the PA for the optical data model. In Mexico, the UA for SAR is, however, only marginally lower than for the optical data model, which is impacted by bottom reflectance from shallow waters and turbidity, which both impact the optical properties (cf. spectral signal) of water more than the physical state and, therefore, the sensitivity of SAR backscatter (e.g., roughness). The Zambia site is dominated by the Kafue flats, an extensive wetland ecosystem subject to variable flooding and with a sharp contrast to the surrounding drier landscape, where fire is a major natural factor impacting the landscape. The dynamic nature and many confounding factors (e.g., fires and emergent vegetation) make Zambia a particularly challenging site, and it was also where the dual sensor approach displayed its strongest potential in balancing the individual strengths and weaknesses of optical and SAR data. In Greenland, the topography and light conditions are the main challenges. For optical data, it means higher commission errors (cf. lower UA) due to shading effects and low sun angles. The SAR model is better at dealing with these issues because it works independent of sunlight, and by using ascending and descending SAR scenes, the part of the landscape that can be monitored is increased. Still, the influence of low-backscatter areas (e.g., exposed riverbeds and in snow dominated landscapes) means the SAR data model typically suffers from commission errors and lower PA.

It is important to note that, apart from site-specific characteristics, the UA and PA are also dictated by how individual algorithms have been implemented, e.g., to what extent the individual round robin contributions have favored the importance of commission errors relative to omissions errors. The results will also depend on whether individual scenes are classified and then aggregated to a monthly water map or whether the individual scenes are merged into a monthly composite before water classification. The full accuracy statistics for the individual models is provided as supplementary material (cf. Table S1).

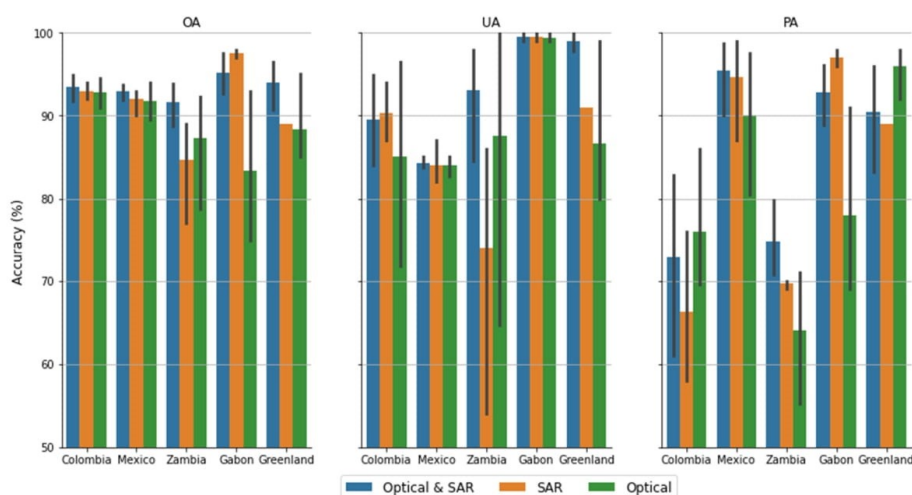


Figure 3. Accuracy statistics from the WorldWater round robin test sites, individually and overall, summarized by model input data type (OA = Overall Accuracy; UA = User Accuracy; PA = Producer Accuracy).

3.3. Object Extraction Accuracy

The 3-m PlanetScope water classification maps used to evaluate object extraction accuracy are shown in Figure 4. Like the full-size test sites, it is important to notice the

IV. Intercomparison of satellite-based algorithms for regional surface water detection (Chapter III)

variability between the sites. Individually, the PlanetScope data represent SWB regions relative to the general water characteristics within their respective test sites, yet, there is variability between sites with, e.g., Zambia having larger waterbodies on average than Colombia.

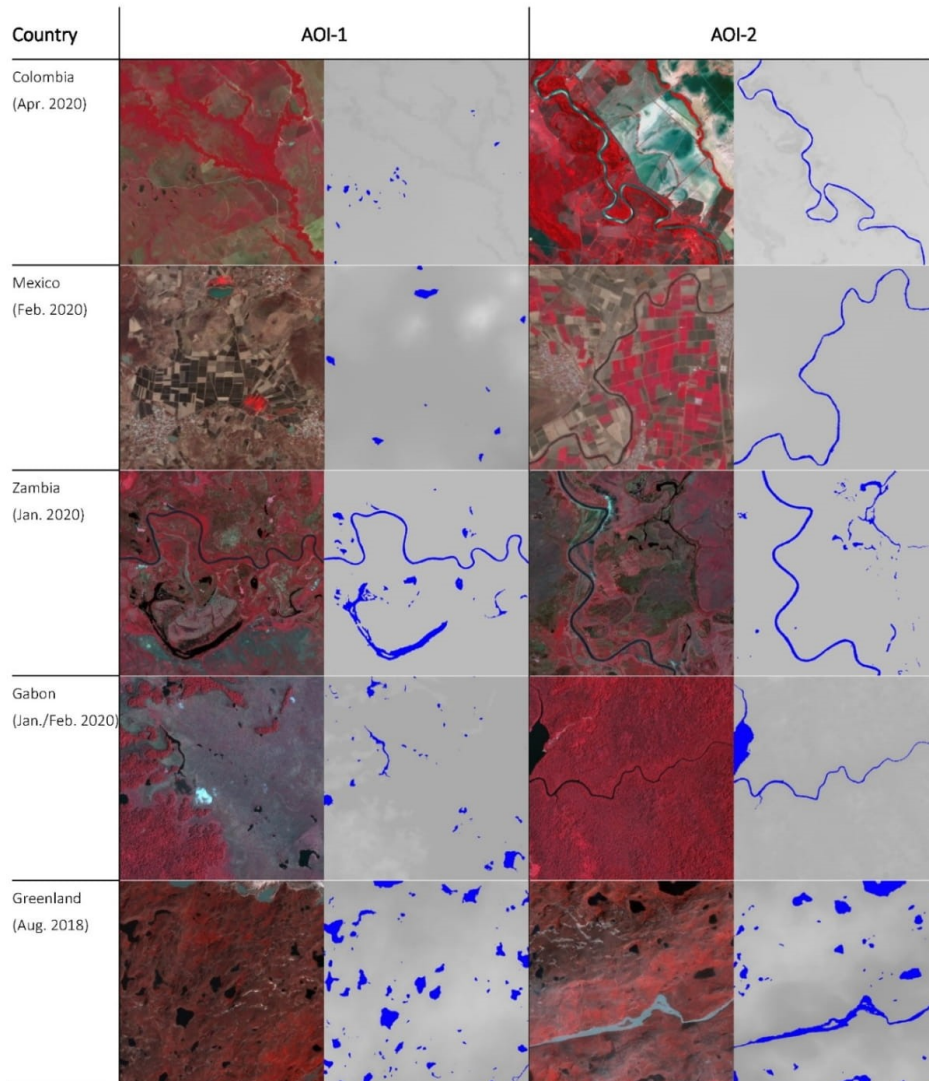


Figure 4. False colour PlanetScope QuickLooks and associated water classifications for each AOI used in the object-based validation approach (Imagery © 2022 Planet Labs Inc.).

Table S2 provides an overview of the summary statistics for object extraction accuracy for each of the three mandatory sites, as well as the optional sites, where relevant. There is a large variability between the individual contributions, and yet, with similar tendency across the sites i.e., the algorithms that integrate optical data perform better than those relying solely on SAR (Figure 5). The lowest overall accuracy is in Colombia, and

IV. Intercomparison of satellite-based algorithms for regional surface water detection (Chapter III)

this is also where the difference between the best optical approaches and the best SAR algorithm is greatest (cf. Figure 5). Figure 5 also shows the highest object extraction accuracy is in Zambia, which, together with Greenland, has the largest share of waterbodies within the test sites (cf. Figure 4). It is also noteworthy the optical data model consistently outperforms the SAR data model in all test sites except for Gabon (Figure 5).

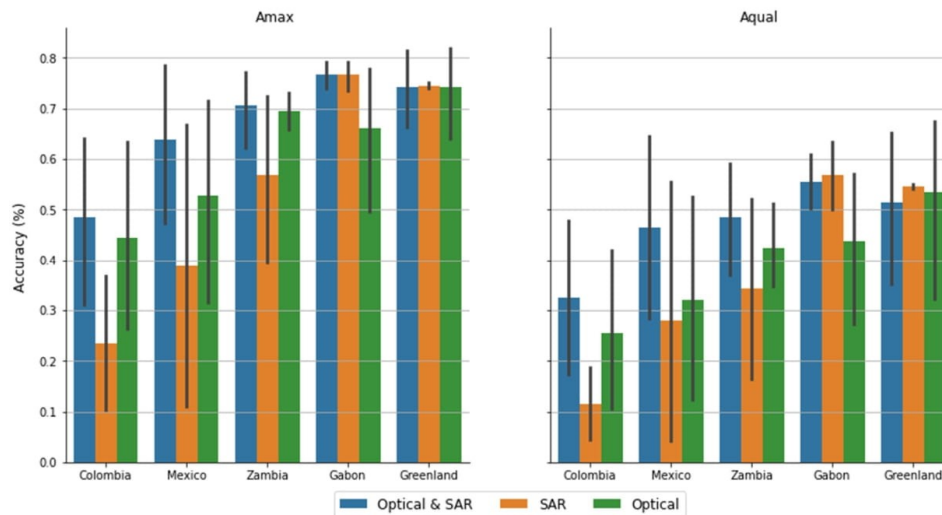


Figure 5. Object accuracy statistics from the WorldWater round robin PlanetScope sites, summarized by country and model input data type.

The findings from the object extraction accuracy analysis indicate that using or integrating optical data into the water detection algorithm is key to achieving accurate water object definitions. How important depends on the average size of the waterbodies and the surrounding landscape. In Colombia, where the average waterbody size/width is smaller compared to other sites, the difference between the optical algorithms and the SAR-only approaches are the largest. This is explained by the characteristics of the input data, with key spectral water detection bands from Sentinel-2 available only in 10-m spatial resolution, while the true spatial resolution of Sentinel-1 is understood to be closer to 20×20 m, although data from the widely used Sentinel-1 Ground Range Detected (GRD) product are delivered with a pixel spacing of 10×10 m. There are also some marked differences between the optical algorithms and the SAR only approaches in Mexico, which is likely caused by the dry environment and a landscape dominated by large tracts of dry, sandy surfaces, as well as the associated challenge for SAR-based water detection [44]. In contrast, the difference between optical and SAR is much less pronounced in Zambia and Gabon, which is likely related to the larger average size of the waterbodies (Zambia) and the dense tropical forest landscape causing a stark land–water contrast (Gabon).

3.4. Temporal Consistency Evaluation

The surface water area (km^2) was calculated over each test site and for each month in the 2-year observation period (cf. July 2018 to June 2020). For each test site, the surface water areas were summarized by input data model type, i.e., optical (O), SAR (S), and the fused date model (O + S). In Figure 6, the average surface water area was then plotted against time with indications of variance (i.e., minimum and maximum observed water extent within a given month) and with some key explanatory variables plotted on the secondary axis.

IV. Intercomparison of satellite-based algorithms for regional surface water detection (Chapter III)

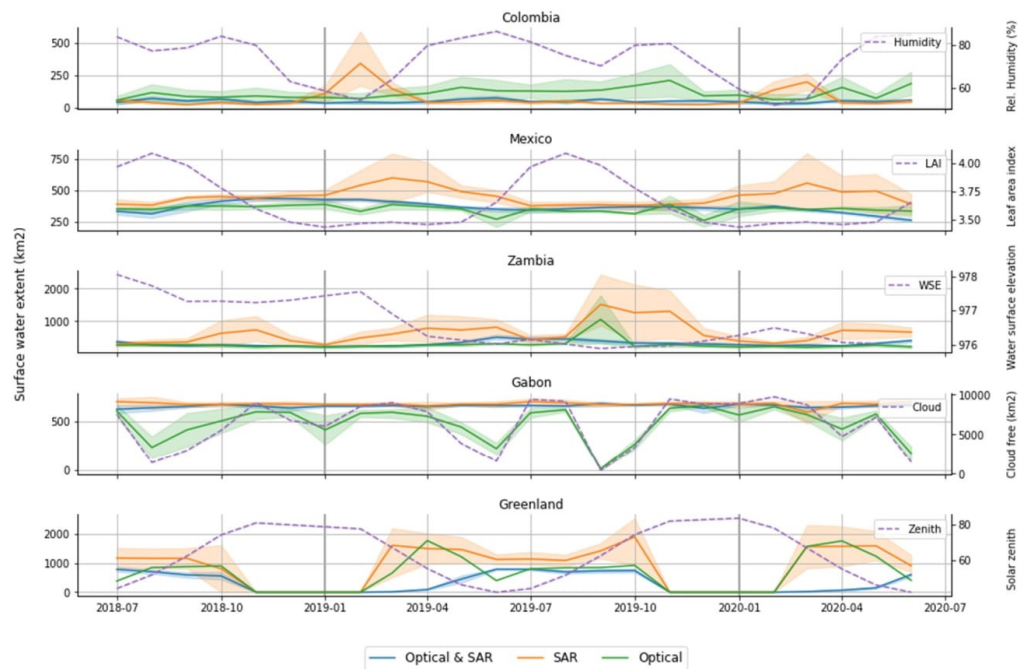


Figure 6. Monthly surface water area trajectories for the individual test sites and per sensor model. For each test site, corresponding timeseries of the key explanatory variables are equally shown, i.e., the Humidity and Leaf Area Index from the ERA-5 monthly averaged reanalysis data [45], water surface elevation from satellite altimetry [46], solar zenith angle, and cloud cover [47].

A comparison of the surface water area temporal development curves shows the variance of the fused Optical–SAR-based algorithms are much less than the single sensor solutions both within and between nearby months. If not directly, then at least indirectly, this indicates the fusing algorithms to be more reliable and have less sensitivity to temporary or seasonal phenomena that can impact water detection, including dry/moist conditions, topographic/canopy shading, and clouds.

In Colombia, the pure optical methods, in general, returns a higher surface water area across the entire timeseries. This can be attributed to false positives from topographic shading and ineffective cloud shadow masking, particularly during the humid season. In Mexico, where clouds and topography are less of a problem, there are hardly any noteworthy peaks/dips in the optical development curves. In Colombia and Mexico, the SAR peaks correspond to the dry seasons when the vegetation cover is low, resulting in an increased influence of low backscatter from dry, sandy surfaces.

In Zambia, the variance observed in both the optical and SAR data predictions is most dominant during the 2019 dry season, which was reported as having been one of the worst droughts in Western Zambia in almost 70 years. The exceptionally low water levels during this period indicates that droughts and receding water lines are likely to have an impact on water classifications. The SAR data are challenged by very dry soils, especially in the southern parts of this site, while wildfires represent another challenge for both the optical and SAR data model, as the burn scars can be difficult to separate from water. In optical imagery, burn scars have low reflectance in the near infrared and visible spectrum, and this can lead to spectral confusion with water. As fire also changes the physical and structural characteristics of the vegetated landscape, it also impacts SAR imagery. After a fire,

IV. Intercomparison of satellite-based algorithms for regional surface water detection (Chapter III)

the backscatter decreases strongly [48], and, as a result, the contrast between land and water will be lessened.

In Gabon, the cloud cover percentage over the test site is, on average, 50%, significantly impacting the optical data model, which returns estimates of water extent that strongly correlate with the cloud cover percentage. In contrast, the SAR and fused sensor approach return a much more consistent timeseries, with no apparent sensitivity to the cloud cover percentage.

Finally, in the case of Greenland, the temporal evaluation shows how limited light conditions in spring and fall (before everything freezes) hamper the optical data model. In essence, our evaluation shows the time window to collect optical imagery is short, but also that it can be extended by integration with SAR data. Using a fused data model in Greenland can also help to even out issues generated by a complex topography (e.g., cast shadows in optical imagery and foreshortening and layover effects in the SAR imagery), as indicated in Table S1.

In Figure 6, a large part of the temporal variation is explained by the performance of the individual contributions both between and within the three different sensor models. The dual sensor model has the least variation and, hence, we argue that it is the more robust in dealing with confounding factors. Figure 7 shows the average monthly surface water area statistics for the top three-performing dual sensor models. Figure 7 illustrates quite well the ability of the dual sensor model to provide consistent timeseries information that captures the seasonality of surface water dynamics in each of the test sites. The strongest seasonality is observed in Colombia and Zambia, which are the two test sites with the largest rainfall gradient. In contrast, Mexico and Gabon have less seasonal variation due to very dry (Mexico) and consistently wet (Gabon) conditions. In Greenland, the seasonality is first and foremost dictated by the temperature, i.e., thawing, and increased melt-water starting around April/May and then frost and total freezing once we enter November.

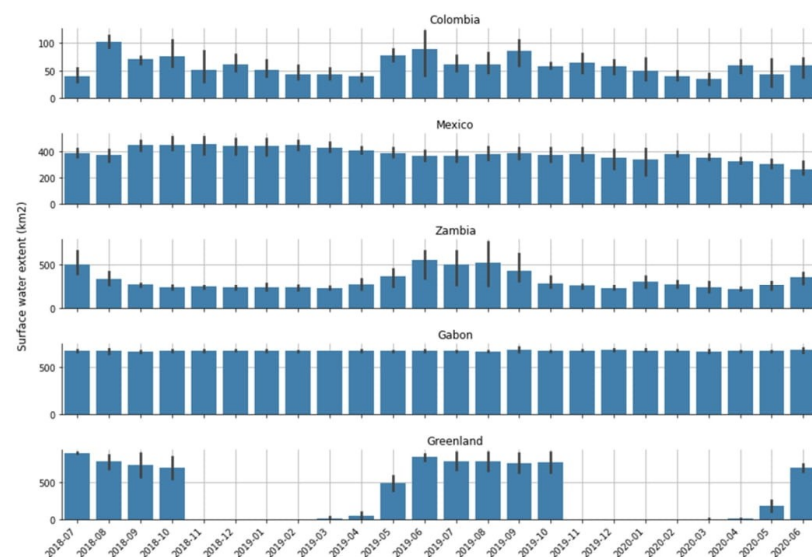


Figure 7. Interannual monthly mean surface water area dynamics and uncertainties (98% CI), as captured by the best-performing dual sensor models (i.e., models A, N, and O).

4. Discussion

The round robin evaluation was conducted over a diverse set of test sites that represented landscapes influenced by several of the known challenges for satellite-based surface water mapping, including topography, clouds, dense and inundated vegetation, fire scars, low-backscatter landcovers, low sun angles, as well as snow and ice. The intercomparison of the different round robin contributions across this diverse set of test sites supports the general hypothesis that fusing optical with SAR data produces a more robust mapping of surface water extent dynamics across bioclimatic gradients. Yet, the findings also show that, at individual locations, the single sensor approach can outperform the fused sensor approach. By example SAR data are the better option in heavily clouded regions (cf. Gabon) while optical data are better in dry regions and in capturing smaller waterbodies. As such the round robin provides key insight to the advantage of the strengths of optical and SAR data while also identifying how a fused sensor model can help address their individual shortfalls. Moreover, the evaluation demonstrates that both supervised and unsupervised learning can provide very good results, and while steps for preprocessing and postprocessing are highly relevant to the outcome, they include many variables that are harder to quantify in terms of their individual contributions to the statistical accuracy. Still, there are several crosscutting factors that impact optical and SAR data in various ways, and which underpin why the dual sensor approach, on an overall level, outperforms single sensor approaches.

Both SAR and optical data can struggle in mountainous areas, as steep slopes can lead to shadow issues and image distortions. Orthorectification and radiometric terrain correction using a DEM are the main direct techniques to obtain the relevant geometric and/or signal correction. Yet, such correction can introduce errors, as globally available DEMs have known quality issues [49], although newer DEMs provide gradual improvements [50]. In complex terrain, shadows cast by mountains and hills will appear very dark in optical imagery, which can cause a confusion between topographic shadows and water. This means extra steps should be taken when mapping water extents to make sure the effect of terrain shadow is minimized. While there are specific methods to deal with this in optical imagery [51], SAR imagery can also be used, e.g., to remove water classified in optical imagery if it is consistently mapped as land in SAR (cf. Model A). SAR imagery is not affected by natural sunlight shadows cast by topography. However, radar sensors are side-looking, meaning they view the Earth's surface from the side of the satellite as it passes by (as opposed to looking directly from above). The side-looking nature of these radar sensors means that they can only see the side of mountains that face their sensors—they cannot see the opposite side of mountains. This is known as radar topographic shadow. Fortunately, radar sensors, such as Sentinel-1, have both ascending and descending orbits, which can collect imagery from east- and west-looking angles. Using ascending and descending imagery together helps to increase the area that can be effectively monitored using radar imagery; however, this does not solve all radar problems related to topography. Areas in deeper canyons and fjords that have a north–south orientation will likely always be in the radar signal shadow, leading to some unavoidable data gaps, and in these cases, sometimes the optical data model can help.

As both SAR and optical data can struggle in mountainous areas, using one sensor to help overcome the other is not always sufficient. Therefore, DEMs are often applied during postprocessing to mask out regions where water formation is unlikely given the topographic conditions, e.g., due to slopes or based on hydrological terrain analysis, such as the Height Above Nearest Drainage (HAND). A range of DEMs have been used for post-processing, including the Shuttle Radar Topography Mission (SRTM) DEM (e.g., Model B, M), ALOS World 3D-30 m (Model F, J), and Copernicus DEM (Model E, N, O). Although the impact on accuracy is not quantified directly, the use of Copernicus DEM is recommended, not only because Copernicus DEM comes out favorably in statistical evaluations against other DEMs [50], but also because of the reference year (2010–2015), which is newer than SRTM (i.e., 2000) and AW3D30 (2006–2011). In essence, this means the

IV. Intercomparison of satellite-based algorithms for regional surface water detection (Chapter III)

Copernicus DEM is more likely to capture and, hence, avoids masking out newly established reservoirs, which have boomed dramatically in the past few decades [52].

Cloud cover is a major limiting factor affecting the usefulness of optical imagery. However, if clouds and their associated shadows can be effectively masked out from each image, the remaining cloud-free data in each image can be used for accurate water classification, yet the frequency of monitoring will depend on the persistency of the cloud cover. While several algorithms are available for automated cloud masking, (e.g., MAJA, Fmask, CFMask, Tmask, IdePix, Sen2Cor, s2cloudless) none are perfect in separating clear observations from those contaminated with clouds and cloud shadows. Too aggressive cloud masking, and many waterbodies may be missed, while failure to adequately mask cloud shadows will introduce many false positives. Often, making a cloud-free optical image will require some form of image compositing and mosaicking. There are several possible ways to do this, e.g., by using the best available pixel by cloudiness (Model O), or through per-pixel band statistics such as mean/median band reflectances (Model N). Model F applies an NDVI Maximum Value Composite (MVC) procedure, which is effective for providing spatially continuous cloud-free imagery [53]. The MVC has been particularly widely adopted in vegetation studies [54], but, since the MVC emphasizes the vegetation signal, it should be used with care for monitoring water dynamics, as seasonally flooded vegetation may risk being masked. Furthermore, and as illustrated by one contribution, a synthetic timeseries can also be constructed by interpolation and gap-filling using the historical water frequency (cf. Model H). Finally, SAR data can also be used to fill in the “cloud” gaps in the optical imagery. However, even if SAR imagery is not affected by clouds, it is impacted by other issues, which can result in spurious water detection, including speckle noise and permanent low-backscatter regions. The reduction of speckle noise is important to improve the usefulness of SAR imagery. The main purpose of the noise reduction technique is to remove speckle noise while still retaining the important features in the images. Widely adopted speckle filters, such as Lee Sigma or Refined Lee, have proved effective; however, depending on the window kernel size, they may compromise the ability to map smaller water features. Therefore, attention has been drawn to other methods, such as the Gamma Map method (Model A, E) and the use of temporal filtering (e.g., mean, median, or minimum backscatter), as a means to better preserve spatial resolution (cf. Model O, N). The further advantage of using temporal filtering is the ability to also suppress the influence of high winds, which can cause wind-roughened waters that, at specific times, can vanish the contrast between open water and dry surfaces and cause Bragg scattering. With SAR data, it can also be difficult to differentiate water from other surfaces with low backscatter, such as asphalt (parking lots, airports, roads), flat rock, and, in some dry regions, sand surfaces. Long timeseries of backscatter measurements can be used to identify such areas but at the expense of computational efficiency, especially for large areas [55]. Another way is to integrate optical data to reduce potential commission errors caused by permanent low-backscatter areas (cf. Models A and O).

As additional examples, the round robin intercomparisons have also shown how the complementary use of optical and SAR data can help suppress the influence of burn scars and, to an extent, the monitoring period in light-constrained, high-latitude regions.

Aside from the challenges discussed above, there are variables and challenges which could not be fully evaluated. Unresolved issues still circulate around inundated vegetation and how to deal with the cryosphere. As the focus in this study was on open inland waters, neither of these issues was investigated. However, future improvements could be performed through the investigation of L-band SAR sensors, which penetrate vegetation better than C-band SAR data (Sentinel-1) and have potential for mapping flooded areas under vegetated canopies [56,57]. In large parts of the world, lake and river ice is an integral part of annual water dynamics, which is why we also recommend looking at scalable solutions for using optical and SAR data to monitor lake and river ice evolution [58,59] and as complementary information for open surface water dynamics.

IV. Intercomparison of satellite-based algorithms for regional surface water detection (Chapter III)

Urban environments represent another challenge from the perspective of both optical and SAR data. For optical images, the main issue is building shadows, whereas SAR data may suffer from layover effects caused by tall buildings, as well as corner reflection (cf. double/triple bouncing). Like topography, the urban challenge is often addressed using postprocess masking, which is sensible, especially for large-area applications, as urban areas represent only a fraction of the overall landscape, and the waterbodies associated with the urban environment even less so. In addition, and as new high resolution and freely available urban footprint layers become available [60], urban masking will gradually improve and integrating them as masking layers can help simplify the water mapping solution.

The results and above discussion point to some inherent limitations to mapping surface water when relying solely on either optical or SAR-based instruments. These limitations can be partly mitigated by using both sensors in a fused approach for surface water extent mapping. However, since the fused mapping approach will likely add to complexity, computational effort, transferability, and automation level of the mapping approach, it is important to consider exact needs and objectives before the appropriation of a specific data model.

However, if monitoring is to be conducted in a region with persistent cloud cover, or if the focus is to monitor during the wet–cloudy season, it may be worth considering if adding optical data will bring the necessary improvement to warrant the additional complexity of an operational solution. In other regions, the status of small farm dams may be the most critical information gap in supporting timely information on potential water shortages. In drier regions or during dry spells, where clouds are not an issue, monitoring should rely on optical data only to maximize the spatial resolution. However, where clouds may be an issue, the integration of SAR data will be critical to reliably monitor the status of small farm reservoirs and dams [22,61]. This reiterates that the best practices for surface water monitoring are often reliant on the study domain. In other words, a case-dependent choice of mapping approach will be needed based on certain criteria, such as ecosystem type, seasonality, climate regime, area size, and requirements for the degree of automation. Moreover, as EO technology becomes more widely adopted and mapping approaches evolve, it is further recommended that cross-comparison exercises, as presented in this paper, be repeated periodically to assess advances in surface water mapping.

5. Conclusions

The availability of satellite missions and constellations for environmental monitoring has continued to grow in the past decades, and combined with the advances in technical infrastructures for big data analysis, it is now within the realm of possibility for countries to implement satellite-based surface water monitoring systems. These systems will be vital to supporting more evidence-based planning and management of water resources and provide an ability to efficiently report and act in response to the global water agenda. By evaluating 14 different EO-based models for surface water detection, we show that single sensor approaches can produce accurate and consistent water maps under ideal conditions, and yet, across a range of challenging environments, the synergistic usage of optical and SAR data delivers more accurate and consistent outputs.

The findings in this paper therefore bear some important perspectives for formulating a new best practice where optical and SAR data are used synergistically to achieve the highest accuracy and most consistent results for monitoring surface water dynamics. While accuracy is a critical concern for selecting a surface water detection model, there are other important aspects, including computational efficiency, simplicity, and ease of implementation, which all contribute to increase understanding, maintainability, and potential scalability. In the end, specific working routines, management objectives, and individual user preferences may all contribute to how users will choose to appropriate EO technology for surface water monitoring. At larger scales across diverse ecological gradients,

IV. Intercomparison of satellite-based algorithms for regional surface water detection (Chapter III)

a synergistic approach should be preferred, but at a local scale, SAR data may be preferred for the effective and timely monitoring of water extent and potential emerging floods during cloudy periods, and similar optical data may be preferred to monitor the status of reservoirs and small waterbodies during drought periods and when clouds are not an issue.

Therefore, rather than advocating for a single “best” approach, we recommend flexibility and options to build and/or adapt surface water detection methods that meet individual user needs in terms of management goals, environmental settings, and scale of study, i.e., ensuring users have options for receiving data in multiple formats or from multiple sources, and with the tools necessary to process these data effectively.

The round robin evaluation presented in this paper has shown that EO datasets, methods, and tools for monitoring surface water dynamics are available and successfully applied in various contexts around the globe. The upcoming challenge will be to make the community aware of these tools and, via practical guidance, illustrate how to get started using EO data and tools to support better water resource monitoring, reporting, and management.

Supplementary Materials: The following supporting information can be downloaded at: www.mdpi.com/2072-4292/14/10/2410/s1, Table S1. Classification accuracies (%) for each of the five round robin test sites. OA = Overall Accuracy; UA = User’s Accuracy, and PA = Producers Accuracy. Table S2. Summary of object extraction accuracies. The accuracy metrics are maximum overlap area (A_{max}) and quality (A_{qual}) as a joint balanced measure of correctness (A_{cor}) and completeness (A_{com}). The overall score is the product between A_{max} and A_{qual} .

Author Contributions: Conceptualization, C.T., M.P., M.C.; methodology, C.T., T.S.; validation, K.J., R.P.M., C.T.; formal analysis and investigation, D.D., M.R., B.D., J.F., M.S., S.W., S.L., H.Z., G.S., L.G., A.M., C.S., V.V., A.H., K.M., M.C.R.C., J.-M.M., D.M., R.R., M.T., H.A., J.H. (Jens Hiestermann), J.H. (Jason Hallowes); data curation, P.R., R.P.M.; writing—original draft preparation, C.T., D.D.; writing—review and editing, J.F., M.S., S.W., S.L., H.Z., G.S., L.G., A.M., C.S., V.V., A.H., K.M., M.C.R.C., J.-M.M., D.M., R.R., M.T., H.A., J.H. (Jens Hiestermann), J.H. (Jason Hallowes), M.C., M.P.; visualization, D.D.; supervision, C.T.; funding acquisition, C.T., M.P. All authors have read and agreed to the published version of the manuscript.

Funding: This study was executed in the context of the WorldWater project, funded by European Space Agency (ESA) under the EO Science for Society programmatic element of the 5th Earth Observation Envelope Programme (EOEP-5, 2017–2021). S. Liu and H. Zhou were funded by the National Key Research and Development Program of China (Grant No. 2018YFE0106500).

Data Availability Statement: The validation data samples used in this study are openly available in Zenodo at <https://doi.org/10.5281/zenodo.6539508>.

Acknowledgments: The WorldWater round robin was organized under the funding and auspices of the European Space Agency and supported by a number of international organizations and initiatives, including CNES, NASA, the European Association of Remote Sensing Companies (EARSC), and the CEOS Ad hoc team on Sustainable Development Goals (CEOS SDG AHT), as well as GEO and their Earth Observations for the Sustainable Development Goals (EO4SDG) initiative. The European Commission and ESA provided the Sentinel data. The USGS and NASA provided the Landsat imagery. The PlanetScope data was provided by Planet Labs Inc. under ESA’s Third-Party Missions scheme.

Conflicts of Interest: The authors declare no conflict of interest.

References

1. UN. United Nations Sustainable Development Goals: Goal 6: Ensure Access to Water and Sanitation for All. 2020. Available online: <https://www.un.org/sustainabledevelopment/water-and-sanitation/> (accessed on 4 April 2022).
2. Long, J. The United Nations’ 2030 Agenda for Sustainable Development and the Impact of the Accounting Industry. *Honor. Coll. Theses* **2019**, 260. Available online: https://digitalcommons.pace.edu/honorscollege_theses/260 (accessed on 4 April 2022).
3. General Assembly of the United Nations. *International Decade for Action: Water for Sustainable Development: 2018–2028*; UN doc A/RES/71/222 (7 February 2017); United Nations: New York, NY, USA, 2017.
4. Pekel, J.F.; Cottam, A.; Gorelick, N.; Belward, A.S. High-resolution mapping of global surface water and its long-term changes. *Nature* **2016**, *540*, 418–422. <https://doi.org/10.1038/nature20584>.

IV. Intercomparison of satellite-based algorithms for regional surface water detection (Chapter III)

5. Pickens, A.H.; Hansen, M.C.; Hancher, M.; Stehman, S.V.; Tyukavina, A.; Potapov, P.; Marroquin, B.; Sherani, Z. Mapping and sampling to characterize global inland water dynamics from 1999 to 2018 with full Landsat time-series. *Remote Sens. Environ.* **2020**, *243*, 111792. <https://doi.org/10.1016/j.rse.2020.111792>.
6. Huang, C.; Chen, Y.; Zhang, S.; Wu, J. Detecting, Extracting, and Monitoring Surface Water From Space Using Optical Sensors: A Review. *Rev. Geophys.* **2018**, *56*, 333–360. <https://doi.org/10.1029/2018RG000598>.
7. Brisco, B. Mapping and monitoring surface water and wetlands with synthetic aperture radar. In *Remote Sensing of Wetlands: Applications and Advances*; Tiner, R.W., Lang, M.W., Klemas, V.V., Eds.; CRC Press: Boca Raton, FL, USA, 2015; pp. 119–136.
8. Druce, D.; Xiao, T.; Lei, X.; Guo, T.; Kittel, C.M.M.; Grogan, K.; Tottrup, C. An optical and SAR based fusion approach for mapping surface water dynamics over mainland China. *Remote Sens.* **2021**, *13*, 1663.
9. Bioresita, F.; Puissant, A.; Stumpf, A.; Malet, J.-P.P. Fusion of Sentinel-1 and Sentinel-2 image time series for permanent and temporary surface water mapping. *Int. J. Remote Sens.* **2019**, *40*, 9026–9049. <https://doi.org/10.1080/01431161.2019.1624869>.
10. Markert, K.N.; Chishtie, F.; Anderson, E.R.; Saah, D.; Griffin, R.E. On the merging of optical and SAR satellite imagery for surface water mapping applications. *Results Phys.* **2018**, *9*, 275–277. <https://doi.org/10.1016/j.rinp.2018.02.054>.
11. van Leeuwen, B.; Tobak, Z.; Kovács, F. Sentinel-1 and-2 based near real time inland excess water mapping for optimized water management. *Sustainability* **2020**, *12*, 2854. <https://doi.org/10.3390/su12072854>.
12. Showstack, R. NEWS Sentinel Satellites Initiate New Era in Earth Observation. *EOS* **2014**, *95*, 239–240.
13. UNFCCC. Paris Agreement. 2015. Available online: http://unfccc.int/files/essential_background/convention/application/pdf/english_paris_agreement.pdf (accessed on 4 April 2022).
14. UNDRR. Sendai Framework for Disaster Risk Reduction. 2015. Available online: <https://www.undrr.org/implementing-sendai-framework/what-sendai-framework> (accessed on 4 April 2022).
15. Airbus. Copernicus DEM Product Handbook. 2019. Available online: https://spacedata.copernicus.eu/documents/20126/0/GEO1988-CopernicusDEM-SPE-002_ProductHandbook_11.00+%281%29.pdf/40b2739a-38d3-2b9f-fe35-1184ccd17694?t=1612269439996 (accessed on 2 March 2021).
16. Donchyts, G.; Schellekens, J.; Winsemius, H.; Eisemann, E.; Van de Giesen, N. A 30 m Resolution Surface Water Mask Including Estimation of Positional and Thematic Differences Using Landsat 8, SRTM and OpenStreetMap: A Case Study in the Murray-Darling Basin, Australia. *Remote Sens.* **2016**, *8*, 386. <https://doi.org/10.3390/rs8050386>.
17. Markert, K.N.; Markert, A.M.; Mayer, T.; Nauman, C.; Haag, A.; Poortinga, A.; Bhandari, B.; Thwal, N.S.; Kunlamai, T.; Chishtie, F.; et al. Comparing Sentinel-1 surface water mapping algorithms and radiometric terrain correction processing in southeast Asia utilizing Google Earth Engine. *Remote Sens.* **2020**, *12*, 2469. <https://doi.org/10.3390/RS12152469>.
18. Chini, M.; Hostache, R.; Giustarini, L.; Matgen, P. A hierarchical split-based approach for parametric thresholding of SAR images: Flood inundation as a test case. *IEEE Trans. Geosci. Remote Sens.* **2017**, *55*, 6975–6988.
19. Thompson, M.; Hiestermann, J.; Eady, B.; Hallows, J. Frankly My Dear I Give a Dam! Or Using Satellite Observation to Determine Water Resource Availability in Catchments. 2018. Available online: http://sbdvdc.ekodata.co.za/downloads/SANCIAHS_paper.pdf (accessed on 6 May 2022).
20. Department of Science and Innovation Republic of South Africa. mzansiAmanzi—A Monthly Outlook of Water in South Africa. Available online: <https://www.water-southafrica.co.za/> (accessed on 6 May 2022).
21. Wangchuk, S.; Bolch, T. Mapping of glacial lakes using Sentinel-1 and Sentinel-2 data and a random forest classifier: Strengths and challenges. *Sci. Remote Sens.* **2020**, *2*, 100008. <https://doi.org/10.1016/j.srs.2020.100008>.
22. Vanthof, V.; Kelly, R. Water storage estimation in ungauged small reservoirs with the TanDEM-X DEM and multi-source satellite observations. *Remote Sens. Environ.* **2019**, *235*, 111437.
23. Yamazaki, D.; Ikeshima, D.; Neal, J.C.; O’Loughlin, F.; Sampson, C.C.; Kanae, S.; Bates, P.D. MERIT DEM: A new high-accuracy global digital elevation model and its merit to global hydrodynamic modeling. *AGU Fall Meet. Abstr.* **2017**, *2017*, H12C-04.
24. Nobre, A.D.; Cuartas, L.A.; Hodnett, M.; Rennó, C.D.; Rodrigues, G.; Silveira, A.; Saleska, S. Height Above the Nearest Drainage—a hydrologically relevant new terrain model. *J. Hydrol.* **2011**, *404*, 13–29.
25. Gallant, J.C.; Dowling, T.I. A multiresolution index of valley bottom flatness for mapping depositional areas. *Water Resour. Res.* **2003**, *39*, 12. <https://doi.org/10.1029/2002WR001426>.
26. Fan, X.; Liu, Y.; Wu, G.; Zhao, X. Compositing the Minimum NDVI for Daily Water Surface Mapping. *Remote Sens.* **2020**, *12*, 700. <https://doi.org/10.3390/rs12040700>.
27. Guzder-Williams, B.; Alemohammad, H. Surface Water Detection from Sentinel-1. In Proceedings of IEEE International Geoscience and Remote Sensing Symposium IGARSS, Brussels, Belgium, 11–16 July 2021.
28. Zhou, H.; Liu, S.; Hu, S.; Mo, X. Retrieving dynamics of the surface water extent in the upper reach of Yellow River. *Sci. Total Environ.* **2021**, *800*, 149348.
29. Cordeiro, M.C.R.; Martinez, J.-M.; Peña-Luque, S. Automatic water detection from multidimensional hierarchical clustering for Sentinel-2 images and a comparison with Level 2A processors. *Remote Sens. Environ.* **2021**, *253*, 112209.
30. Defourny, P.; Kirches, G.; Brockmann, C.; Boettcher, M.; Peters, M.; Bontemps, S.; Lamarche, C.; Schlerf, M.; Santoro, M. Land cover CCI: Product User Guide Version 2.0. 2017. Available online: http://maps.elie.ucl.ac.be/CCI/viewer/download/ESACCI-LC-Ph2-PUGv2_2.0.pdf (accessed on 4 April 2022).
31. Marzi, D.; Gamba, P. Inland Water Body Mapping Using Multitemporal Sentinel-1 SAR Data. *IEEE J. Sel. Top. Appl. Earth Obs. Remote Sens.* **2021**, *14*, 11789–11799. <https://doi.org/10.1109/JSTARS.2021.3127748>.

IV. Intercomparison of satellite-based algorithms for regional surface water detection (Chapter III)

32. Schumann, G.J.P.; Campanella, P.; Tasso, A.; Giustarini, L.; Matgen, P.; Chini, M.; Hoffmann, L. An Online Platform for Fully-Automated EO Processing Workflows for Developers and End-Users Alike. In Proceedings of the 2021 IEEE International Geoscience and Remote Sensing Symposium IGARSS, Brussels, Belgium, 11–16 July 2021; pp. 8656–8659.
33. Merciol, F.; Fauqueur, L.; Damodaran, B.B.; Rémy, P.-Y.; Desclée, B.; Dazin, F.; Lefèvre, S.; Masse, A.; Sannier, C. Geobia at the terapixel scale: Toward efficient mapping of small woody features from heterogeneous vhr scenes. *ISPRS Int. J. Geo-Inf.* **2019**, *8*, 46.
34. Ludwig, C.; Walli, A.; Schleicher, C.; Weichselbaum, J.; Riffler, M. A highly automated algorithm for wetland detection using multi-temporal optical satellite data. *Remote Sens. Environ.* **2019**, *224*, 333–351.
35. Martinis, S.; Twele, A.; Voigt, S. Towards operational near real-time flood detection using a split-based automatic thresholding procedure on high resolution TerraSAR-X data. *Nat. Hazards Earth Syst. Sci.* **2009**, *9*, 303–314.
36. Bradley, D.; Roth, G. Adaptive thresholding using the integral image. *J. Graph. Tools* **2007**, *12*, 13–21.
37. Adams, R.; Bischof, L. Seeded region growing. *IEEE Trans. Pattern Anal. Mach. Intell.* **1994**, *16*, 641–647.
38. Martinis, S.; Kersten, J.; Twele, A. A fully automated TerraSAR-X based flood service. *ISPRS J. Photogramm. Remote Sens.* **2015**, *104*, 203–212.
39. Twele, A.; Cao, W.; Plank, S.; Martinis, S. Sentinel-1-based flood mapping: A fully automated processing chain. *Int. J. Remote Sens.* **2016**, *37*, 2990–3004. <https://doi.org/10.1080/01431161.2016.1192304>.
40. Olofsson, P.; Foody, G.M.; Herold, M.; Stehman, S.V.; Woodcock, C.E.; Wulder, M.A. Good practices for estimating area and assessing accuracy of land change. *Remote Sens. Environ.* **2014**, *148*, 42–57. <https://doi.org/10.1016/j.rse.2014.02.015>.
41. Downing, J.A.; Prairie, Y.T.; Cole, J.J.; Duarte, C.M.; Tranvik, L.J.; Striegl, R.G.; McDowell, W.H.; Kortelainen, P.; Caraco, N.F.; Melack, J.M. The global abundance and size distribution of lakes, ponds, and impoundments. *Limnol. Oceanogr.* **2006**, *51*, 2388–2397.
42. Ke, G.; Meng, Q.; Finley, T.; Wang, T.; Chen, W.; Ma, W.; Ye, Q.; Liu, T.-Y. Lightgbm: A highly efficient gradient boosting decision tree. *Adv. Neural Inf. Process. Syst.* **2017**, *30*, 3146–3154.
43. Cai, L.; Shi, W.; Miao, Z.; Hao, M. Accuracy assessment measures for object extraction from remote sensing images. *Remote Sens.* **2018**, *10*, 303. <https://doi.org/10.3390/rs10020303>.
44. Martinis, S.; Kuenzer, C.; Wendleder, A.; Huth, J.; Twele, A.; Roth, A.; Dech, S. Comparing four operational SAR-based water and flood detection approaches. *Int. J. Remote Sens.* **2015**, *36*, 3519–3543.
45. Climate Data Store. ERA5 Climate Reanalysis. Available online: <https://cds.climate.copernicus.eu/> (accessed on 27 March 2022).
46. U.S. Department of Agriculture. Global Reservoirs and Lakes Monitor (G-REALM). Available online: https://ipad.fas.usda.gov/cropexplorer/global_reservoir/ (accessed on 22 March 2022).
47. European Union/ESA/Copernicus/SentinelHub. Sentinel-2: Cloud Probability. Available online: https://developers.google.com/earth-engine/datasets/catalog/COPERNICUS_S2_CLOUD_PROBABILITY#description (accessed on 22 March 2022).
48. Siegert, F.; Ruecker, G. Use of multitemporal ERS-2 SAR images for identification of burned scars in south-east Asian tropical rainforest. *Int. J. Remote Sens.* **2000**, *21*, 831–837. <https://doi.org/10.1080/014311600210632>.
49. Uuemaa, E.; Ahi, S.; Montibeller, B.; Muru, M.; Knoch, A. Vertical Accuracy of Freely Available Global Digital Elevation Models (ASTER, AW3D30, MERIT, TanDEM-X, SRTM, and NASADEM). *Remote Sens.* **2020**, *12*, 3482. <https://doi.org/10.3390/rs12213482>.
50. Guth, P.L.; Geoffroy, T.M. LiDAR point cloud and ICESat-2 evaluation of 1 second global digital elevation models: Copernicus wins. *Trans. GIS* **2021**, *25*, 2245–2261.
51. Tottrup, C. Forest and land cover mapping in a tropical highland region. *Photogramm. Eng. Remote Sens.* **2007**, *73*, 1057.
52. Zarfl, C.; Lumsdon, A.E.; Berlekamp, J.; Tydecks, L.; Tockner, K. A global boom in hydropower dam construction. *Aquat. Sci.* **2015**, *77*, 161–170.
53. Holben, B.N. Characteristics of maximum-value composite images from temporal AVHRR data. *Int. J. Remote Sens.* **1986**, *7*, 1417–1434.
54. Pettorelli, N.; Vik, J.O.; Mysterud, A.; Gaillard, J.-M.; Tucker, C.J.; Stenseth, N.C. Using the satellite-derived NDVI to assess ecological responses to environmental change. *Trends Ecol. Evol.* **2005**, *20*, 503–510.
55. Schlaffer, S.; Matgen, P.; Hollaus, M.; Wagner, W. Flood detection from multi-temporal SAR data using harmonic analysis and change detection. *Int. J. Appl. Earth Obs. Geoinf.* **2015**, *38*, 15–24. <https://doi.org/10.1016/j.jag.2014.12.001>.
56. Tsyganskaya, V.; Martinis, S.; Marzahn, P.; Ludwig, R. SAR-based detection of flooded vegetation—a review of characteristics and approaches. *Int. J. Remote Sens.* **2018**, *39*, 2255–2293. <https://doi.org/10.1080/01431161.2017.1420938>.
57. Tsyganskaya, V.; Martinis, S.; Marzahn, P.; Ludwig, R. Detection of temporary flooded vegetation using Sentinel-1 time series data. *Remote Sens.* **2018**, *10*, 1286.
58. Wang, X.; Feng, L.; Gibson, L.; Qi, W.; Liu, J.; Zheng, Y.; Tang, J.; Zeng, Z.; Zheng, C. High-Resolution Mapping of Ice Cover Changes in Over 33,000 Lakes Across the North Temperate Zone. *Geophys. Res. Lett.* **2021**, *48*, e2021GL095614.
59. Scott, K.A.; Xu, L.; Pour, H.K. Retrieval of ice/water observations from synthetic aperture radar imagery for use in lake ice data assimilation. *J. Great Lakes Res.* **2020**, *46*, 1521–1532. <https://doi.org/10.1016/j.jglr.2020.08.018>.
60. Esch, T.; Marconcini, M.; Felbier, A.; Roth, A.; Heldens, W.; Huber, M.; Schwinger, M.; Taubenböck, H.; Müller, A.; Dech, S. Urban footprint processor—Fully automated processing chain generating settlement masks from global data of the TanDEM-X mission. *IEEE Geosci. Remote Sens. Lett.* **2013**, *10*, 1617–1621.
61. Perin, V.; Tulbure, M.G.; Gaines, M.D.; Reba, M.L.; Yaeger, M.A. A multi-sensor satellite imagery approach to monitor on-farm reservoirs. *Remote Sens. Environ.* **2022**, *270*, 112796.

V. Multi-annual yield model at the field level for subsistence farming in Burkina Faso (Chapter IV)

Schwarz, M., Ouédraogo, A. W., Traoré, I., Müller, C., Sié, A., Barteit, S., Mank, I., Siegert, F., Sauerborn, R., Franke, J. (2022) Satellite-based multi-annual yield models for major food crops at the household field level for nutrition and health research: a case study from the Nouna HDSS, Burkina Faso. *International Journal of Applied Earth Observation and Geoinformation*. Manuscript submitted for publication.

Satellite-based multi-annual yield models for major food crops at the household field level for nutrition and health research: a case study from the Nouna HDSS, Burkina Faso

Maximilian Schwarz^{1,2~*}, Windpanga Aristide Ouédraogo^{3,4~}, Issouf Traoré^{3,5}, Charlotte Müller⁴, Ali Sié³, Sandra Barteit⁴, Isabel Mank^{4,6}, Florian Siegert^{1,2}, Rainer Sauerborn⁴⁺, Jonas Franke¹⁺

¹ Remote Sensing Solutions GmbH, Dingolfinger Str. 9, 81673 Munich, Germany; schwarz@rssgmbh.de (M.S.); franke@rssgmbh.de (J.F.); siegert@rssgmbh.de (F.S.)

² Department of Biology, Ludwig-Maximilians-University Munich, Großhaderner Str. 2, 82152 Planegg-Martinsried, Germany

³ Centre de Recherche en Santé de Nouna (CRSN), Institut National de Santé Publique (INSP), Rue Namory Keita, BP 02, Nouna, Burkina Faso; windparis2007@yahoo.fr (A.W.O.); t_issouf2000@yahoo.fr (I.T.); sieali@yahoo.fr (A.S.)

⁴ Heidelberg Institute of Global Health (HIGH), Faculty of Medicine and University Hospital, Heidelberg University, Im Neuenheimer Feld 130.3, 69120 Heidelberg, Germany; charlotte.mueller@uni-heidelberg.de (C.M.); barteit@uni-heidelberg.de (S.B.); isabel.mank@uni-heidelberg.de (I.M.); rainer.sauerborn@uni-heidelberg.de (R.S.)

⁵ Institut de Formations Initiale et Continue (IUFIC), Université Thomas Sankara, 12 BP 417 Ouagadougou 12, Burkina Faso

⁶ German Institute for Development Evaluation (Deval), Fritz-Schaeffer-Str. 26, 53113 Bonn

*Correspondence: schwarz@rssmbh.de, Tel.: +49-89-48954765

~Shared first authorship

+Shared last authorship

Abstract

Increasing frequencies of climate change-induced extreme weather like prolonged droughts pose significant challenges for small-scale subsistence farmers in sub-Saharan Africa, who rely on the yearly harvest by more than 80% of their nutritional needs. However, yield estimates at the field and household level (mean field size < 2 ha), that can be applied without continuously collected in-situ data, are still lacking. Statistical models for region-wide food crop yield estimations based on high-resolution satellite data at the field level may generate better insights on how to address health risks like child undernutrition in low-resource contexts where the burden is greatest and projected to aggravate in future climate projections. Our study developed crop-specific, satellite-based yield models using a novel three-year data set of in-situ yield measurements as exemplified for a rural region in Burkina Faso. The aim of the model is to reduce the need for in-situ field data collection while still assuring accurate yield estimates at the field level. The model employed LASSO regression and was based on monthly vegetation index composites from Sentinel-2 and weekly accumulated Climate Hazards Group InfraRed Precipitation with Station (CHIRPS) rainfall data. Our yield modeling results suggest that an increase in training data capturing a wider range of yields over three years led to more robustness to overfitting and, therefore, better model fits. R^2 values ranged from 0.62 (Maize) to 0.3 (Sorghum) for the three-year yield models, with normalized root mean square error (nRMSE) values ranging from 12% - 16%. An additional plausibility check confirmed the validity of our models, as we compared the magnitude of our yield estimation with national yield statistics for Burkina Faso. We showed that the models based on three-year in-situ data can capture parts of the inter-year variability in yields, which enables the proposed models to be applied to future years without the need for additional in-situ measurements. Our advances in predicting yield estimates at the field level enable a linkage between household-level yields, socioeconomic indicators, nutritional status of children, and the health status of the household members. A further application is linking high-resolution yield data to farmers' productivity losses from increasing heat under climate change.

Keywords: food crop yield, child nutrition, health, climate change, food security, sub-Saharan Africa

1. Introduction

Increasing temperatures, shifting rainfall patterns, and shorter frequencies of extreme weather events such as floods and droughts are already affecting food security (Mbow et al. 2019) and particularly child undernutrition (Belesova et al. 2019a). According to the United Nations Committee on World Food Security (CFS), these climate stressors act in tandem with factors such as population growth (CFS 2009). According to the Global Climate Risk Index 2021, five out of ten countries that suffered the most from climate change-related extreme weather events between 2000 and 2019 are located in Africa (Eckstein et al. 2021). In 2020, over 768 million people worldwide faced hunger, while 21% of Africa's population was affected. In Western Africa, 18.1% of children suffered from undernutrition in 2020, including Burkina Faso (FAO et al. 2021). The effects of climate change on food availability are especially apparent in subsistence farming settings, where people eat almost exclusively what they have harvested from their own fields. The agricultural sector employs nearly 80% of the working population and generates around 30% of the country's GDP (The World Bank 2020; Dabat et al. 2012). Droughts are one of the most frequent and hazardous climate change-related events. It is the main cause of crop failure and loss of agricultural varieties, which in turn increases the risk of undernutrition (Belesova et al. 2019a; Kogan et al. 2019). Increasingly common causes of crop failure and low yields are sequential torrential rainfalls that flood fields for days, thus damaging the crop plants (Licht 2022; Wang et al. 2022).

The government supports subsistence farmers in two ways: First, (i) through weather-indexed crop insurance. Using remote sensing for quantifying each subscriber household's yields to determine, whether they are eligible for benefit payments can prove useful. This is currently tested as part of an early warning and responses system by the Burkinian government. Second (ii), farmers are supported in the diversification of agricultural production, better partial integration of agriculture into markets, and development of domestic and foreign markets. To support food self-sufficiency and smallholder farmers in the development of agricultural strategies, it is essential to constantly monitor crop yields at the household field level.

Since the majority of crop types show a correlation with vegetation indices (VI), e.g., the normalized difference vegetation index (NDVI), multi-temporal satellite data is well suited to estimate yields (Groten 1993; Doraiswamy et al. 2003; Bolton and Friedl 2013;

Huang et al. 2019). Vallentin et al. (2022) showed that high-resolution satellite remote sensing images like Sentinel-2 improve the correlation between yield and satellite data compared to lower-resolution sensors. While most studies to date have focused on large industrialized farming systems using simulations (Jin et al. 2017; Jain et al. 2016) or regression models based on different VIs or the leaf area index (Lambert et al. 2018; Meroni et al. 2013; Mkhabela et al. 2011; Schwalbert et al. 2018), there are very few studies on yield estimates at the household level. Jain et al. (2016) used high-resolution SkySat data to simulate yield for smallholder wheat fields, while Lambert et al. (2017) and Karst, Mank et al. (2020) explored Sentinel-2 data with a 10 meter (m) spatial resolution to estimate yields at the household field level. However, due to highly variable biotic and abiotic factors affecting crop yield, especially in the scenario of a changing climate, studies that are based solely on data from *one* phenological cycle, cannot adequately address and assess the yield variability, which is also shown in Belesova et al. (2018). Therefore, *multi-annual* assessments are needed to develop yield estimating approaches that account for a range of inter-annual yield variabilities. This would enable yield quantification without the need for further labor-intensive and costly ground truthing.

This study aims to develop a valid yield model for various food crops using a unique three-year in-situ yield data set. Through satellite-based crop yield models, we want to reduce labor-, time-, and cost-intensive data collection crop yield on the ground (Paliwal and Jain 2020), while assuring accurate yield estimates at the household field level (mean field size < 2 ha). The presented work is nested in a larger research unit that focuses on aspects including food security and child undernutrition (Mank et al. 2020; Beiersmann et al. 2012), children's health (Belesova et al. 2017, 2018; Belesova et al. 2019b), and heat stress (Kjellstrom et al. 2016; Sahu et al. 2013) (www.cch-africa.de).

2. Material and Methods

2.1. Study area

The study area is located in the Kossi province of the Boucle du Mouhoun Region in rural northwestern Burkina Faso (Figure 1). One-third of the province is under health and

V. Multi-annual yield model at the field level for subsistence farming in Burkina Faso (Chapter IV)

nutritional surveillance of the Nouna Health and Demographic Surveillance System (NHDSS) since 1992 (Sié et al. 2010).

The study area is characterized by a dry tropical climate of the Sudano-Sahelian type. The rainfall pattern is characterized by two seasons, a long dry season (October to May) and a short-wet season (June to September). The yearly amount of rainfall averages 700 mm. More than 30% of the annual rain falls in August (213 mm).

More than 80% of households depend on small-scale subsistence farming which is rain-fed agriculture. Nine crop types are dominant in the region: millet, sorghum, maize, peanuts, beans, cotton, sesame, fonio, and rice, which cover more than 90% of the cultivated area (Grace et al. 2014). The use of chemical fertilizers or insecticides and herbicides is limited.

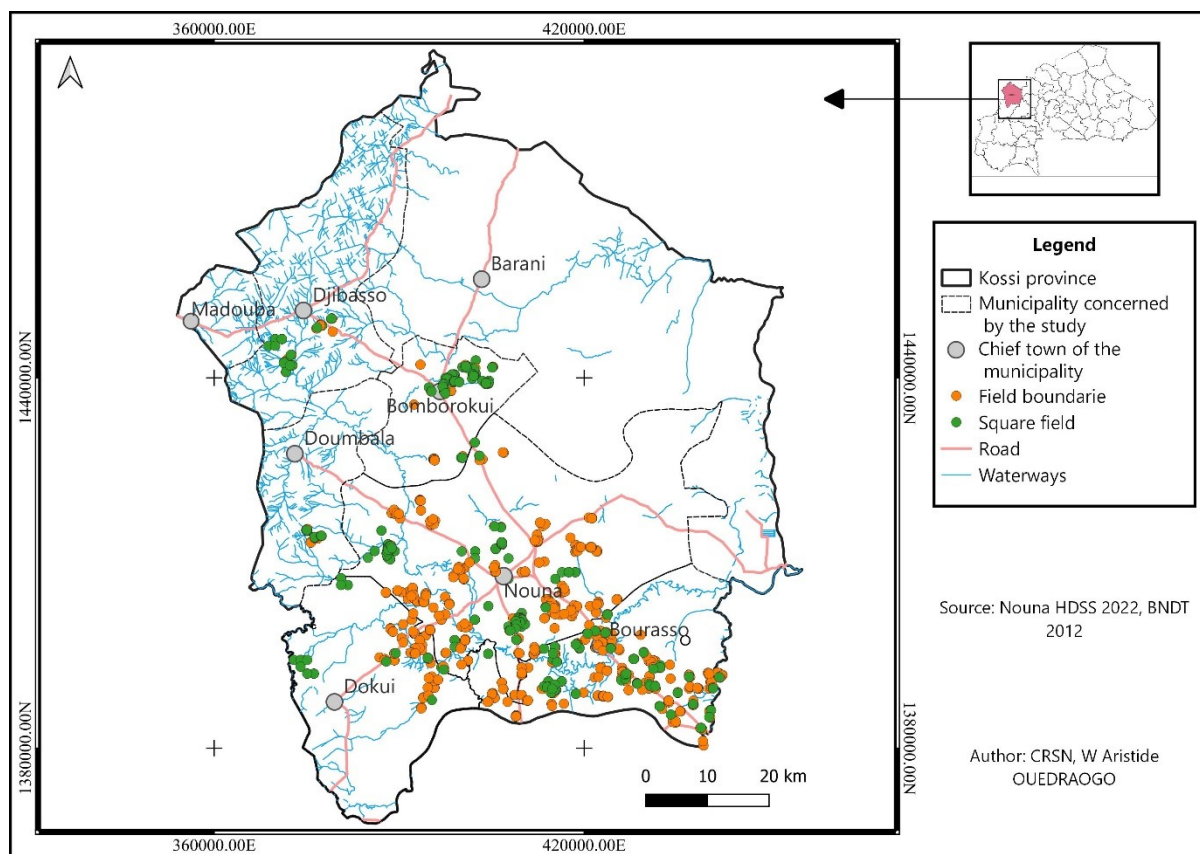


Figure 1: Study area (Health Demographic Surveillance System (HDSS)) with the collected field boundaries and yield measurements (yield squares) in the Kossi province.

2.2. In-situ data and satellite data

2.2.1 Field Data

An essential component of this study was the collection of field data for the five main food crops maize, millet, sorghum, beans, and sesame over a period of three years (2018, 2020, and 2021). Seven agricultural surveyors were trained for the sampling of field boundaries using GPS devices and the installation, monitoring, and harvesting of yield squares. The fields were selected with the intention of maximizing variation between them so as to represent the full range of variability in the entire study area. Yield squares for each field were randomly selected (Figure 2). Generally, the sampling followed a protocol from the Agriculture Ministry (DPSAA 2011). Every field was assigned a unique identifier, so that each field could be linked to individual households. For each type of crop, we targeted a sample size of $n \geq 25$ yield squares per year to satisfy the robustness of the model. In addition, woody vegetation within the studied fields was manually mapped in GIS using Google Earth and masked out of the sampled field boundaries as they can have negative impacts on harvest estimates based on remote sensing data (Lambert et al. 2018). From June to December of each year, data was collected during the rainy season until the harvest of all selected crops. The field sampling followed the established methodology of Karst, Mank, et al. (2020) (see Karst, Mank, et al. (2020) for further details).

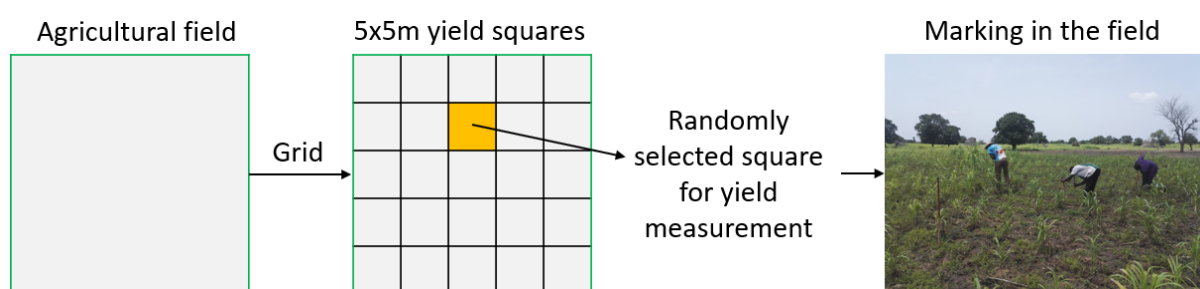


Figure 2: Schematic representation of in-situ yield measurements. Each field, that was selected for in-situ measurements, was divided into 5x5m squares using a grid. The yield square, for which the harvest was measured, was randomly selected and then marked and protected in the field by circumferences. Picture copyright by Isabel Mank.

2.2.2 *Processing of remote sensing data*

For each crop growing season in the study years 2018, 2020, and 2021, all available Sentinel-2 images at a 10m spatial resolution were used at Level-1C and preprocessed including an atmospheric correction using the Sen2Cor version 2.10. Monthly maximum NDVI composites were created for the preprocessed Sentinel-2 reflectance images, which best represent the phenology of farming systems (Hasenbein et al. 2022). For each monthly composite, three vegetation indices, namely the normalized difference vegetation index (NDVI), the normalized difference red edge index (NDRE), and the normalized difference water index (NDWI) were calculated. All of these indices have proven their suitability for monitoring vegetation and estimating yields (Lambert et al. 2017; Gao 1996). All 10 monthly composites for each VI and year were then used as input variables (30 variables in total) for the linear regression model, from which pixel values at the respective sampled harvest squares were extracted (Figure 3).

2.2.3 *Rainfall Data*

Rainfall data helped to explain the variability of vegetation indices as there is a strong correlation between green plant health and rainfall (Greve et al. 2011). Since the crops of interest in this study are exclusively rainfed, rainfall and vegetation indices times series were used to monitor crop growth. We used daily CHIRPS (Climate Hazards Group InfraRed Precipitation with Station data) data as rainfall data for the model (Funk et al. 2015). For each of the three years 2018, 2020, and 2021, daily rainfall data for each calendar week of the crop growing season, including all preceding weeks for that week, were accumulated (e.g., calendar week three contains the rainfall sum of calendar weeks one, two, and three). Each calendar week from March onwards was used as an input variable for the model (except November and December as the months of harvest) (35 variables in total) (Figure 3). In addition, daily rainfall data from one of the five weather stations in the Nouna HDSS (at the CRSN in Nouna) as part of the research unit on climate change and health in sub-Saharan Africa (www.cch-africa.de) were used to analyze the results.

2.3. Methodology of the crop yield model

We used the LASSO (Least Absolute Shrinkage and Selection Operator) regression instead of a stepwise multiple linear regression used in previous studies (Karst, Mank, et al. (2020)). LASSO regression addresses two common problems in regression analyses: (i) overfitting in terms of the number of predictors included in the model and (ii) overestimating, how well the model explains the observed variability with the included variables (Tibshirani 1996). It aims to find the model with the smallest prediction error and identifies the variables and their corresponding regression coefficients for each model by ‘shrinking’ the regression coefficients towards zero. The LASSO regression constrains the model complexity by requiring the sum of absolute regression coefficient values to be smaller than a preset value (lambda (λ)) (Ranstam and Cook 2018). Hence, LASSO aims to minimize the sum of squares with constraint $\sum |\beta_j| \leq t$. Statistically, it is written as:

$$\sum_{i=1}^n \left(y_i - \sum_j x_{ij} \beta_j \right)^2 + \lambda \sum_{j=1}^p |\beta_j| \quad (1)$$

for a linear regression model with y_i ($i = 1, 2, \dots, N$) as the response variable and the p -vector of regressors x_{ij} ($j = 1, 2, \dots, p$) with its β_j coefficients for the i th observation (Tibshirani 1996; Chintalapudi et al. 2022).

Generally, the best lambda is determined using a k -fold cross-validation (Ranstam and Cook 2018). The k -fold cross-validation also helps to reduce overfitting since the analysis is not limited to using a single subset for the internal validation (Ranstam and Cook 2018). In this study, we used a 5-fold cross-validation to have at least five field samples in each fold. Since the data fed into each fold was selected randomly, we computed the 5-fold cross-validation 1000 times. Each iteration yielded an optimal lambda value for the final LASSO regression model. To determine the overall optimal lambda, we calculated an index based on the ratio of R^2 and the Root Mean Square Error (RMSE), where the highest index value identifies the model with the best fit and its corresponding lambda value. To account for outliers, we identified the optimal model using the 95th percentile of the index. This process was repeated for each crop type, resulting in crop-dependent yield models (Figure 3). For each crop type, we ran a model with only one year of training data, corresponding to each year of 2018, 2020, and 2021, and a model using all three years of data. A single-year model was only possible if the training data had more than 25 per crop

V. Multi-annual yield model at the field level for subsistence farming in Burkina Faso (Chapter IV)

type per year. Finally, the three-year models were applied to all sampled field boundaries to predict yield estimates.

We verified the goodness of fit of the different models with statistical measures and validated the plausibility of the model results by comparing them to national yield statistics for Burkina Faso provided by the Food and Agriculture Organization (FAO) via their FAOSTAT database (FAO 2022).

Figure 3 provides the schematic workflow of our method.

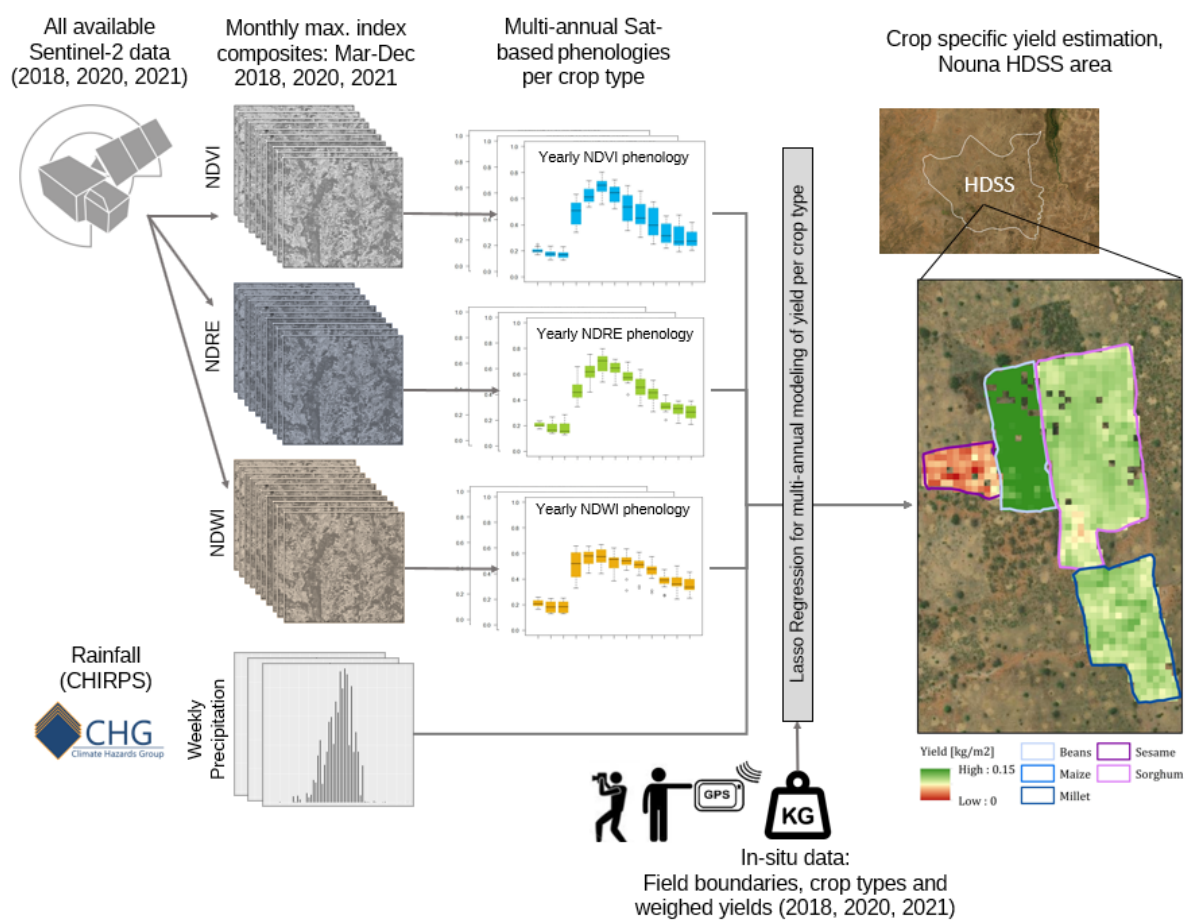


Figure 3: Schematic workflow diagram of the multi-annual crop yield model. Left to right: Preprocessing of Sentinel-2 imagery, from which monthly composites of the NDVI, NDRE, and NDWI were derived. These datasets were used as model predictors together with weekly rainfall sums for all three years 2018, 2020, and 2021. The model was trained and validated through cross-validation with the reference data from the 5x5m harvest squares. Finally, the model predicted yield estimates for all sampled field boundaries in the study area.

3. Results

3.1 Summary of the in-situ field sampling

Table 1 shows the number of in-situ measured harvest squares (411 in total) and field boundaries (1027 in total) per crop type in the years 2018, 2020, and 2021. The most significant and dominant food crops, namely sorghum, millet, and maize, were monitored in all three years, while sesame and beans were observed less frequently. Also, in 2021 the number of field boundaries increased to predict yield estimates for a wide range of fields when applying the final models. Other differences in numbers of the sample sizes mainly occurred due to data cleaning.

Table 1: Number of sampled yield squares and field boundaries per crop type in the years 2018, 2020, and 2021.

	2018		2020		2021		Total	
	Yield plots	Boundaries						
Maize	33	44	29	35	23	136	85	215
Millet	45	44	30	30	29	163	104	237
Sorghum	57	61	35	36	28	175	120	272
Beans	31	52	0	0	12	84	43	136
Sesame	0	0	30	33	29	134	59	167
Total	166	201	124	134	121	692	411	1027

3.2 Results of the weighed yields for each crop type

On the one hand, boxplots of the weighed yields showed that millet, sorghum, and sesame had higher weighted values in 2020, whereas maize and beans had the highest yields in

2018 (Figure 4). On the other hand, yields were overall low in 2021. For millet and maize, there was substantial inter-annual variability in production, as reflected by the upper quartile ranges of the boxplots. Especially in 2018, maize showed exceptionally higher yield values. The yields of other crops such as sorghum, beans, and sesame, seem more consistent from year to year.

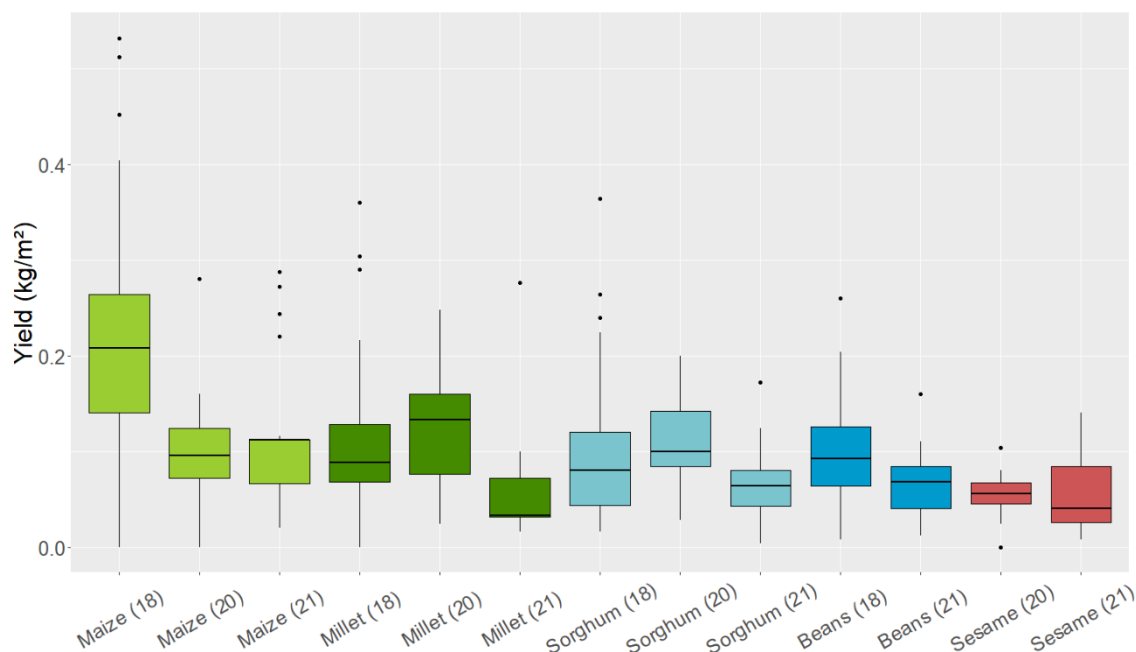


Figure 4: Boxplot analysis of the in-situ yield measurements showing the difference in yield per crop type over the three years 2018 (18), 2020 (20), and 2021 (21). In-situ data for beans and sesame were only available for two of the three years

3.3 Exemplary phenology of monthly NDVI values for Sorghum

Figure 5 depicts the monthly distribution of NDVI values derived from pixels lying inside all sampled and monitored sorghum field boundaries over three years. The NDVI trend of sorghum was chosen as an example. Figure 5 visualizes that the monthly VI composites reflect the phenology of the crop while also displaying inter-annual differences. From June onwards, NDVI values are increasing when the crops develop and increase in photosynthetically active biomass, reaching peak values in September. During the dry season (January to June), the interquartile range is very low, reflecting low variability in the vegetation, whereas during the rainy season (July to October) this variability is substantial, with high deviations from the mean. With the onset of ripening and

senescence of the crops, the NDVI values rapidly decline between October and the harvest months (November/December). In 2018, the NDVI values were generally higher with an earlier onset than in 2020 and especially than in 2021.

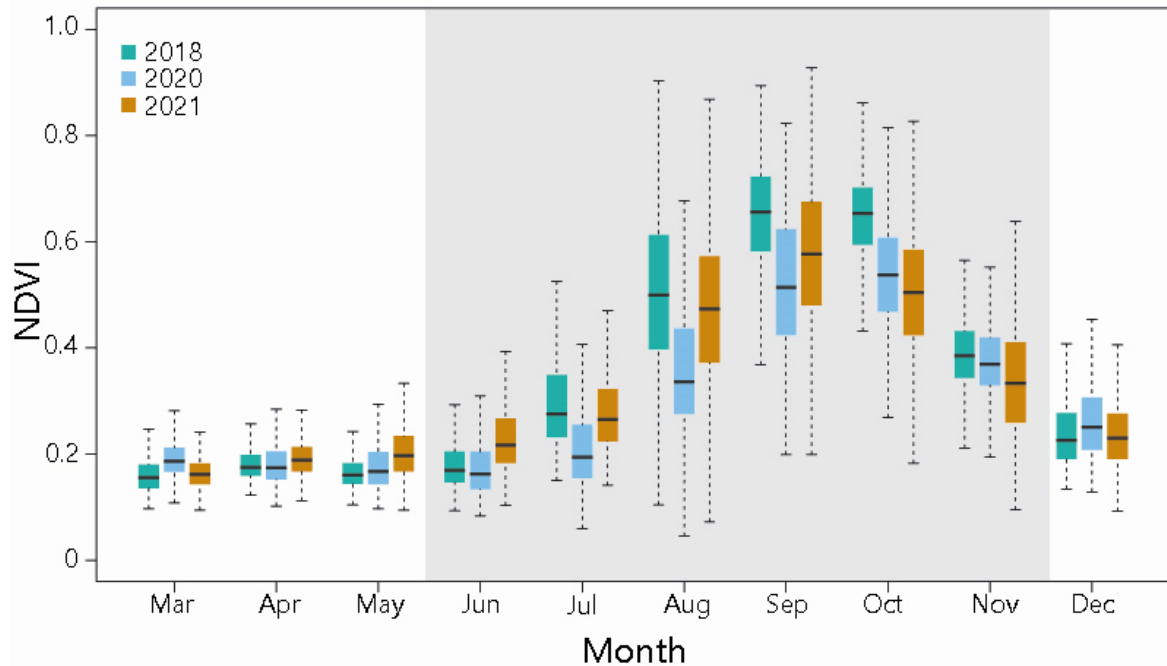


Figure 5: Exemplary yearly time series of the Normalized Difference Vegetation Index (NDVI) for sorghum for the three years 2018, 2020, and 2021. The crop cycle during the rainy season is displayed in grey. Sowing period: June, Period of growth: July-October, Harvesting: October-November.

3.4. Rainfall extremes and flooding in 2021

In order to interpret the lower yields in 2021, as observed in the field data (Figure 4) and the phenology shown by the NDVI (Figure 5), rainfall data must be incorporated. While the temporal rainfall pattern was in line with historic averages, shown by the onset of rainfall in May, the amount of rainfall was comparably low until early August (Figure 6). Then, about 67 % of the total yearly rain fell in a five-week window between week two of August and week two of September. In the latter interval, the highest weekly rainfall amounts were observed. Two extreme rainfall events at the end of August and the beginning of September (recorded by the weather station in Nouna) caused severe floodings (see Sentinel-2 examples in Figure 7) of fields. Additionally, the comparison

V. Multi-annual yield model at the field level for subsistence farming in Burkina Faso (Chapter IV)

of the rainfall pattern shows the inter-annual variability of rainfall patterns. These patterns of inter-annual variability can also be observed in yields (Figure 4).

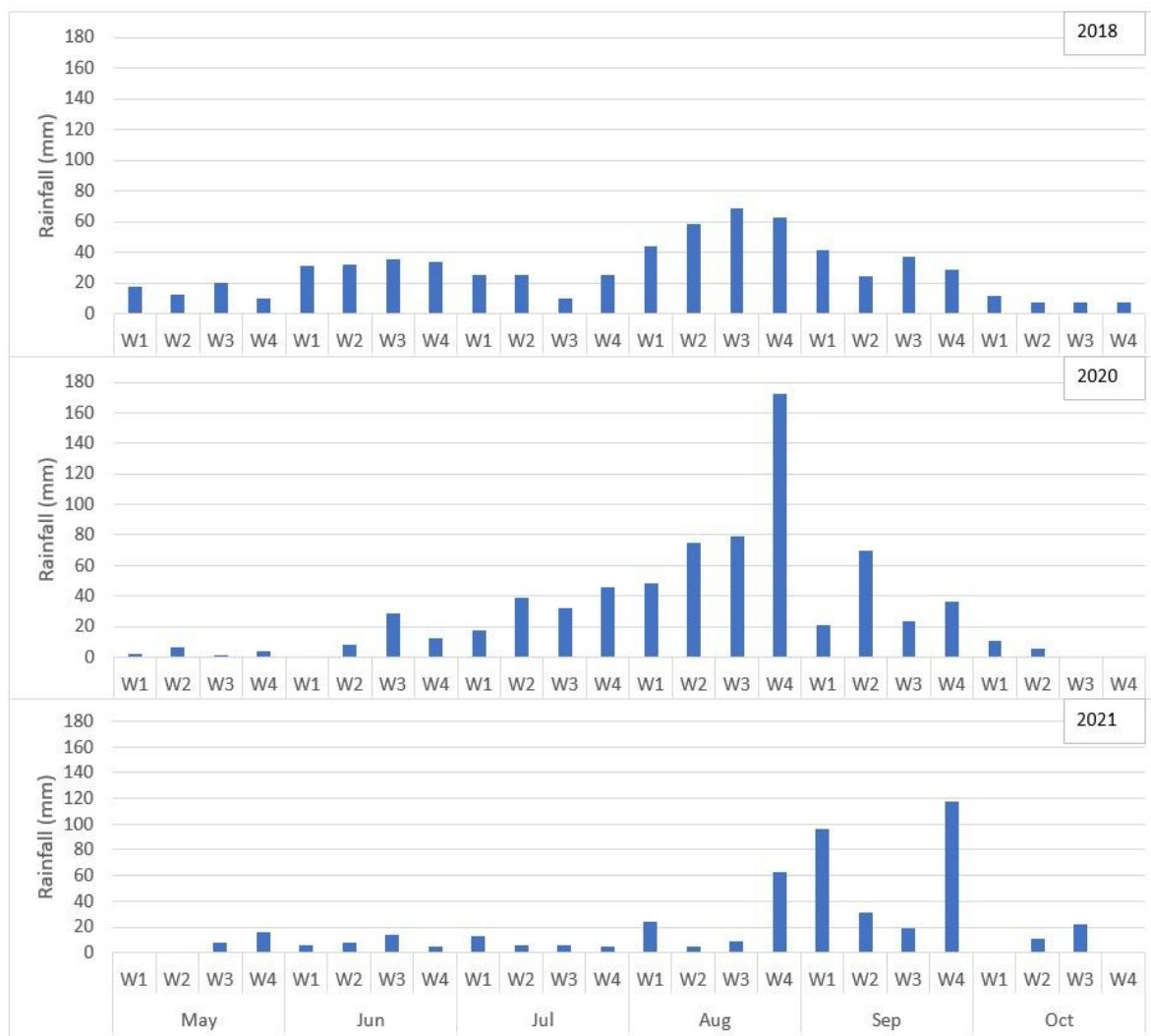


Figure 6: Distribution of weekly rainfall at Nouna weather station in 2018, 2020, and 2021. Nearly 70% of the annual rainfall occurred in a five-week from August – September in 2021 following a long period of unusually low rainfall.

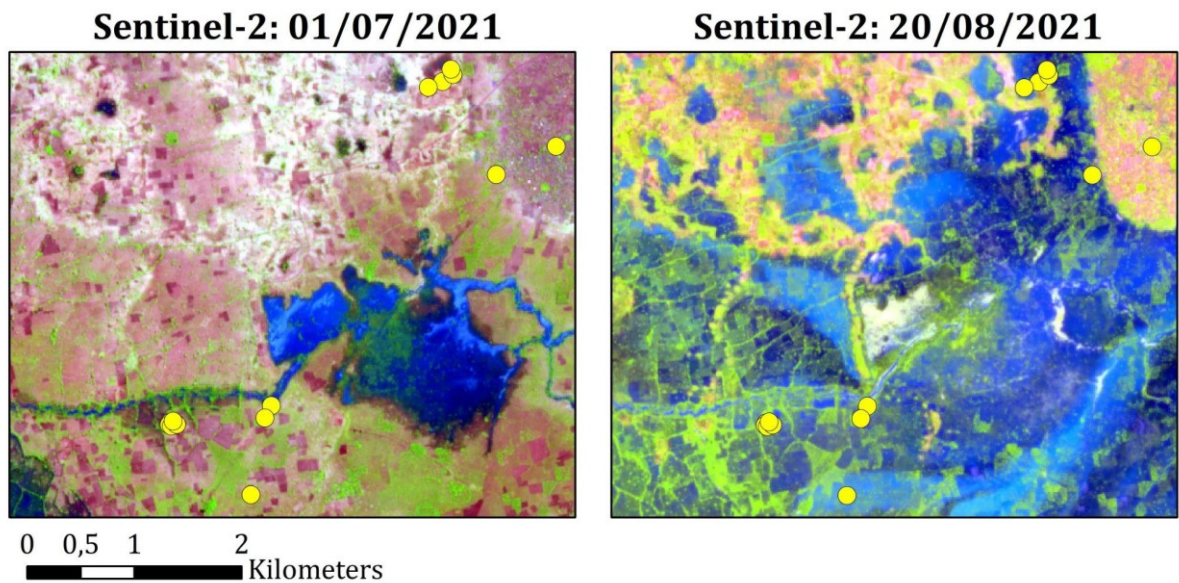


Figure 7: Pre-flooding Sentinel-2 image (left: end of sowing season) and post-flooding image (right: middle of the growing period) after two weeks of heavy rainfall (see Figure 5) with locations of yield sampling plots (yellow dots) in a subset of the study area. Flooded areas are visible in blue. Color representation: R: SWIR, G: NIR, B: Red.

3.5. Results of the crop-specific yield models

For each crop type, an individual model was developed with varying results in terms of goodness of fit but also in terms of included predictors from the LASSO regression (Table 2). Maize yield models showed good R^2 values in general, for the yearly models (2018 and 2020) as well as for the multi-annual model. For 2021, there were not enough reference yield plots (<25) to conduct a model. The best model for maize was the model for 2018, while the multi-annual model was showing better results than 2020. Comparing the results of the multi-annual models, maize showed the highest R^2 of 0.62, while sesame, beans, millet, and sorghum showed R^2 values of 0.59, 0.54, 0.32, and 0.30, respectively. For millet and sorghum, the yearly models performed much better than the multi-annual models in most cases. However, overfitting is a bigger problem in the yearly models (e.g., millet 2020 and 2021), which is indicated by a high drop-off of the adjusted R^2 compared to the original R^2 . This shows, that the three-year models are more robust against overfitting by taking a wider range and distribution of measured crop yields through the inter-annual variability into account. As the normalized RMSE (nRMSE) compares the RMSE to the range of the in-situ measurements, it is an additional indicator to describe the model error in percent. Reasonable low nRMSE values for all crop type

V. Multi-annual yield model at the field level for subsistence farming in Burkina Faso (Chapter IV)

models were found (between 13% and 16% nRMSE) proving the statistical goodness of fit together with the R^2 and adjusted R^2 .

Table 2: Results of the crop-dependent yield models for each year as well as for the multi-annual yield model. The table includes the number of yield reference samples per crop type (N), the number of used predictor variables, the resulting R^2 and adjusted R^2 of the model as well as the RMSE and normalized RMSE that can be interpreted together with the range of measured yields.

Crop type	Statistic parameters	2018	2020	2021	3-year model
Maize	N	32	28	23	83
	<i>No. of predictors</i>	10	9	-	13
	R^2	0.78	0.52	-	0.62
	<i>Adj. R^2</i>	0.68	0.28	-	0.55
	<i>RMSE (kg/m²)</i>	0.056	0.033	-	0.065
	<i>Range (kg/m²)</i>	0.456	0.256	-	0.512
	<i>nRMSE (%)</i>	12.28	12.89	-	12.70
Millet	N	44	30	29	103
	<i>No. of predictors</i>	9	24	21	7
	R^2	0.46	0.95	0.64	0.32
	<i>Adj. R^2</i>	0.32	0.71	-0.44	0.27
	<i>RMSE (kg/m²)</i>	0.053	0.013	0.029	0.056
	<i>Range (kg/m²)</i>	0.328	0.224	0.260	0.344
	<i>nRMSE (%)</i>	16.16	5.80	11.15	16.28
Sorghum	N	57	35	28	120
	<i>No. of predictors</i>	6	12	3	11
	R^2	0.41	0.56	0.23	0.30

V. Multi-annual yield model at the field level for subsistence farming in Burkina Faso (Chapter IV)

	<i>Adj. R²</i>	0.34	0.32	0.13	0.23
	<i>RMSE (kg/m²)</i>	0.050	0.029	0.032	0.047
	<i>Range (kg/m²)</i>	0.348	0.172	0.168	0.360
	<i>nRMSE (%)</i>	14.37	16.86	19.05	13.06
Beans	<i>N</i>	31	0	12	43
	<i>No. of predictors</i>	9	-	-	10
	<i>R²</i>	0.59	-	-	0.54
	<i>Adj. R²</i>	0.41	-	-	0.40
	<i>RMSE (kg/m²)</i>	0.033	-	-	0.034
	<i>Range (kg/m²)</i>	0.252	-	-	0.252
	<i>nRMSE (%)</i>	13.10	-	-	13.49
		<i>N</i>	0	28	29
Sesame	<i>No. of predictors</i>	-	22	13	17
	<i>R²</i>	-	0.84	0.65	0.59
	<i>Adj. R²</i>	-	0.14	0.35	0.41
	<i>RMSE (kg/m²)</i>	-	0.007	0.023	0.019
	<i>Range (kg/m²)</i>	-	0.080	0.132	0.132
	<i>nRMSE (%)</i>	-	8.75	17.42	14.39

3.6. Results of the extrapolated three-year crop yield models

Figure 8 illustrates an excerpt of the results of the three-year individual crop yield models with a 10m spatial resolution applied to predict yield estimates for all sampled field boundaries in 2021. The final model results of the three-year models (Figure 8) display the intra-field yield as well as the inter-year variability of crops. Additionally, differences

in productivity (kg/m^2) between the different crop types are displayed in Figure 8. For example, it shows, that beans have the highest yield per m^2 (dark green), while sesame is showing the lowest yield values per m^2 , which reflects the observation made in the field (Figure 4).

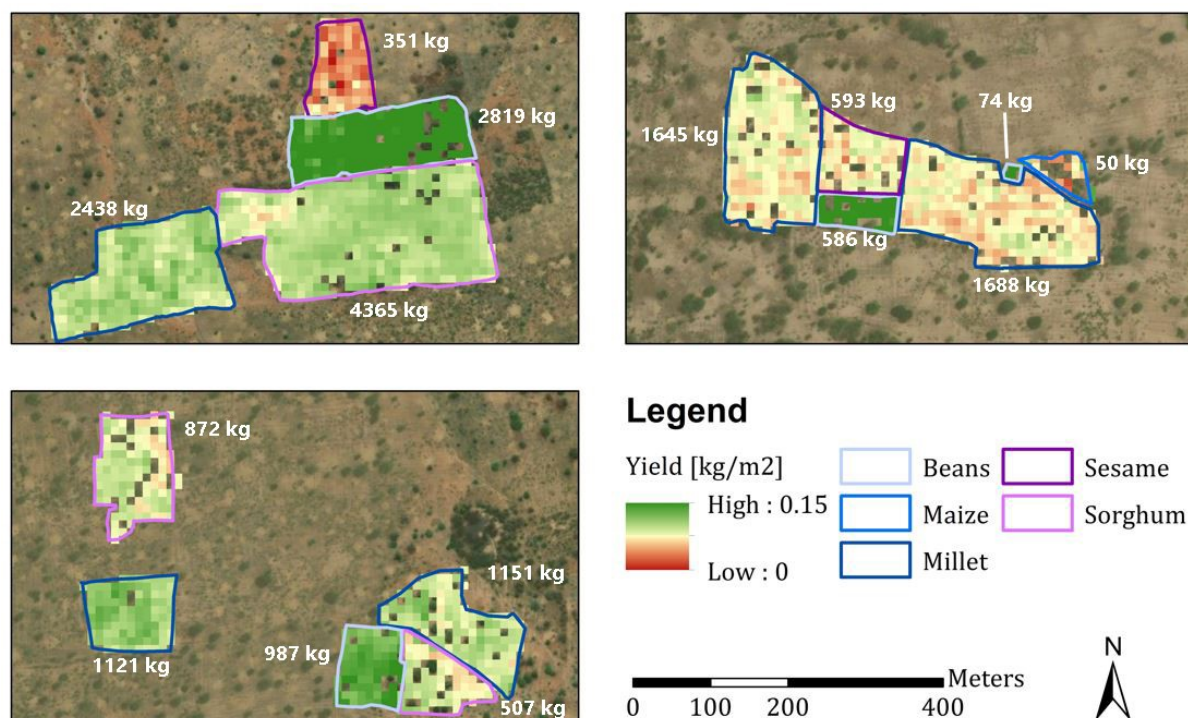


Figure 8: Results of the extrapolation of the crop-specific three-year models to exemplary fields in the Nouna HDSS area in the year 2021 (zoomed to three different exemplary areas). The colored outlines of the fields indicate the crop type according to the color scheme in the legend. Red to green variations within the fields represent the predicted yield estimates in kg/m^2 for each pixel, where the same range was used for all five crop types. Numbers in kg on the side of each field show the total predicted yield for each field. Transparent pixels are masked out from the analysis because of the presence of other woody vegetation. Background: True color imagery, ESRI Basemaps.

3.7. Plausibility check of the model results

In a last step, an additional plausibility check was done by comparing the model results with national yield statistics for Burkina Faso provided by the FAO through their FAOSTAT database (FAO 2022). We used this dataset to verify the plausibility of the model. The FAOSTAT database only contained data until 2020. We assumed consistent conditions for 2021, given national yield statistics for the prior three years showed little variation. Comparing the magnitude of the productivity provided by FAOSTAT to the mean productivity estimates provided by our model, we found similar values in the

V. Multi-annual yield model at the field level for subsistence farming in Burkina Faso (Chapter IV)

magnitude of the numbers, underlining that our multi-annual crop yield model is plausible.

Table 3: Yield estimates of the three-year yield model per crop type for 2021 in comparison to the national yield in Burkina Faso in 2020 reported by the FAO. The statistics show the results of yield estimates for all sampled field boundaries for 2021.

Crop type	Modeled mean total yield per field (t)	Mean field size (ha)	Modeled mean yield (t/ha) (2021)	FAO yield (t/ha) (2020)
Maize	0.39	0.32	1.40	1.69
Millet	0.78	1.09	0.76	0.81
Sorghum	0.77	1.18	0.75	0.99
Beans	0.43	0.30	1.62	1.35
Sesame	0.81	1.46	0.60	0.60

4. Discussion

This study demonstrated the validity of a multi-year crop yield model in comparison to single-year models with the aim to reduce the need for in-situ field data collection while assuring accurate yield estimates at the household field level. It is important to mention that the in-situ measurements are also related to uncertainties that have been reported by Karst, Mank, et al. (2020).

Results of the model application of the three-year model for exemplary fields of the study area in 2021 well represented the inter- and intra-variability of the fields. Comparing the field sizes together with the productivity between the crop types led to the conclusion, that crops with higher productivity were cultivated on smaller fields and crops with low productivity were grown on larger fields.

Overall, the multi-year models were more robust against overfitting compared to the single-year models as proven by the adjusted R^2 . Single-year models with less training data tend to pick too many variables for the final model on some occasions compared to the multi-year model, which led to overfitting. A good example are the models for millet,

where the single-year models had a higher R^2 than the final model, but had 24 (2020) and 21 (2021) predictor variables included. Therefore, the adjusted R^2 values had a higher drop-off from the original R^2 than in the three-year model. While the R^2 measures of the three-year were comparably lower, the model still provided good measures in nRMSE and the magnitude of the mean yield per ha compared to the national yield statistics of the FAO, which proves the model's plausibility. Differences between the single and multi-year models were also the differential variation of rainfall over the different periods of the growing period. The agricultural calendar (date of sowing, etc.) varies according to the arrival of the first rains and we made the hypothesis of equal use of production factors, like fertilizers, because we are dealing with small-scale subsistence farmers in our research observatory. Concluding, the models based on a single year of training data tend to be more accurate in predicting yields for the same year, however, the three-year models are more robust against overfitting and can better reflect the inter-annual variability of yields. This enables the three-year models to be applicable in future years without the need for new in-situ measurements.

Differences occur not only between the single and multi-year models but also between the model results of the different crop types, where some crop yield models outperform others. Some of the crops were more affected by flooding and extreme weather events in 2021 than other crops, which could have led to lower yields in 2021 and higher discrepancies within the training data. However, future detailed research would be needed for a definite statement. Another major finding of this study was that more field samples (training data) did not necessarily result in better model performance (see maize and sorghum in Table 2).

Comparing the size of yield (t/ha) to the national figures provided by FAOSTAT, it was determined that all models produced plausible outcomes. Furthermore, by providing yield estimates at the field level, our model closes the gap of yield statistics not being available at the household level. By linking the respective fields to the individual households, yield estimations at the household level can be provided through our model. With our three-year observation of the in-situ measurements, we are capable of also capturing inter-annual variability. As can be seen in Belesova et al. (2019b), a three-year window captures large parts of the variability as more than two consecutive years with stable productivity were very rare between 1984 and 2012. This is also shown by the highly

varying rainfall patterns from the years 2018, 2020, and 2021 (Figure 6). We, therefore, assume, that this three-year period of training data is enough to capture the variability in the yield estimates to be valid for future applications without the need for additional in-situ data. To determine a fixed threshold on how many years is sufficient to capture most of the inter-annual variability is not possible from our study, however, and would require additional future research.

Our study demonstrates the novelty of using a three-year in-situ dataset that reduces the need for future ground truthing. We found comparable results to our models in Lambert et al. (2018) reporting R^2 regression values between 0.4 and 0.8 for cotton, maize, millet, and sorghum in Mali for the year 2016. However, their regression results are only based on the more homogeneous fields and the peak Leaf Area Index (LAI) as their sole predictor. Morel et al. (2014) found similar results with an R^2 between 0.21 and 0.53, albeit for sugarcane on Reunion Island but also using only one predictor, namely the NDVI. Karst, Mank, et al. (2020) conducted a similar study in the same study area and reported comparable results using only one year of training data (2018), the same data was incorporated in our study. By additionally extending the training data set of in-situ measurements to three years our study extends their findings. Overall, the multi-year model showed, that it is possible to generate more robust models with increasing and more balanced training data sets. More research would be welcome to prove our model results with in-situ measurements being sampled as validation datasets in the upcoming years. Additionally, a study on automated cropland and crop type classification using the sampled field boundaries as reference data is underway and would help to extrapolate the models to the whole study area. In the long term, we aim to estimate crop production by the household from the cadaster of fields in the Nouna HDSS area.

Multiple potential benefits exist for both future HDSS interventions and research using household field level valid and “automated” low-cost remote sensing-based food crop yields. Some examples are given below:

- (i) in the area of agricultural research including but not limited to yield effects of changing field practices or increased inputs, irrigation – both modern, where feasible, and traditional such as the Zai practice (Sorgho et al. 2020a; Sorgho et al. 2020b);

- (ii) in the field of child undernutrition from harvest failures, a large proportion (estimated 75%) of which are driven by increasing climate variability (Belesova et al. 2019a);
- (iii) the effect of heat on lower work productivity of farmers. Evidence from studies indicate that increased heat reduced the work productivity of farmers and endangered their health (e.g., Crowe et al. 2010). A study of the impact of heat on crop yields is currently underway in Burkina Faso, based on a preliminary study by Lang et al. (2022).

This will enable us to contribute to connecting the science of remote sensing, with the fields of agriculture and human health and nutrition.

5. Conclusion

We developed satellite-based crop-specific models to predict yield estimates at the household field level using a unique dataset of three-year yield measurements from rural Burkina Faso. According to our knowledge, this is the first study to successfully develop a model on household plot level for subsistence farming in sub-Saharan Africa to predict yield estimates using a multi-annual training dataset, which is the first step toward a low-cost solution for future applications in yield monitoring at the household field level. Our results indicate, that models are more robust against overfitting when increasing the number of years of training data and therefore including inter-annual variability. Our model was validated by the fact that the magnitudes of the anticipated yield estimates coincided with the magnitudes of the national yield numbers. The value of numerous years of training data for incorporating inter-annual variations of biotic and abiotic yield-influencing factors was demonstrated. The crop yield models based on multi-annual data could be applied to upcoming years without the need for additional in-situ measurements (ground truthing). This is especially important to fight food security under a changing climate, that comes with additional challenges. To tackle health aspects like child undernutrition on a household level, high-resolution yield estimates at the household field level are fundamental, which allow us to predict nutritional shortages at the individual farmer and household level.

CRedit author statement:

Maximilian Schwarz: Methodology, Software, Formal analysis, Data curation, Validation, Visualization, Writing-Original Draft **Windpanga Aristide Ouédraogo:** Investigation, Data curation, Writing – Original Draft, Visualization **Issouf Traoré:** Investigation, Data curation, Writing – Original Draft, Visualization **Charlotte Müller:** Writing – Original Draft **Ali Sié:** Supervision **Sandra Barteit:** Writing – Review & Editing, Funding acquisition **Isabel Mank:** Investigation, Data curation, Writing – Review & Editing **Florian Siegert:** Writing – Review & Editing, Supervision **Rainer Sauerborn:** Conceptualization, Writing – Review & Editing, Supervision, Project administration, Funding acquisition **Jonas Franke:** Conceptualization, Writing – Review & Editing, Supervision, Funding acquisition.

Funding: The authors wish to thank the German Research Foundation (Deutsche Forschungsgemeinschaft) for supporting this work as part of a Deutsche Forschungsgemeinschaft–funded research unit (Forschungsgruppe FOR 2936). We acknowledge financial support by the German Research Foundation (Deutsche Forschungsgemeinschaft) within the funding programme Open Access Publishing, by the Baden-Württemberg Ministry of Science, Research and the Arts and by Ruprecht-Karls-Universität Heidelberg. The funders did not have a role in the design, data collection and analysis, decision to publish, or writing of the manuscript.

Acknowledgments: We would like to express our gratitude to the people of the Nouna HDSS area for their time and support in conducting this research. We also thank the local Agricultural Service and its members and the Nouna team for their input and support during and beyond the data collection.

Data statement: All Data will be made available on request. Climate Hazards Group InfraRed Precipitation with Station data (CHIRPS) data information and data access can be obtained at <https://www.chc.ucsb.edu/data/chirps>. Satellite-based Sentinel-2 data information and data access can be found at <https://sentinel.esa.int/web/sentinel/sentinel-data-access>.

References

Beiersmann, C.; Bountogo, M.; Tiendrébeogo, J.; Louis, V. R.; Gabrysch, S.; Yé, M. et al. (2012): Malnutrition in young children of rural Burkina Faso: comparison of survey data from 1999 with 2009. In

V. Multi-annual yield model at the field level for subsistence farming in Burkina Faso (Chapter IV)

Tropical medicine & international health : TM & IH 17 (6), pp. 715–721. DOI: 10.1111/j.1365-3156.2012.02985.x.

Belesova, Kristine; Agabiirwe, Caroline Noel; Zou, Margaret; Phalkey, Revati; Wilkinson, Paul (2019a): Drought exposure as a risk factor for child undernutrition in low- and middle-income countries: A systematic review and assessment of empirical evidence. In *Environment international* 131, p. 104973. DOI: 10.1016/j.envint.2019.104973.

Belesova, Kristine; Gasparrini, Antonio; Sié, Ali; Sauerborn, Rainer; Wilkinson, Paul (2017): Household cereal crop harvest and children's nutritional status in rural Burkina Faso. In *Environmental health : a global access science source* 16 (1), p. 65. DOI: 10.1186/s12940-017-0258-9.

Belesova, Kristine; Gasparrini, Antonio; Sié, Ali; Sauerborn, Rainer; Wilkinson, Paul (2018): Annual Crop-Yield Variation, Child Survival, and Nutrition Among Subsistence Farmers in Burkina Faso. In *American journal of epidemiology* 187 (2), pp. 242–250. DOI: 10.1093/aje/kwx241.

Belesova, Kristine; Gornott, Christoph; Milner, James; Sié, Ali; Sauerborn, Rainer; Wilkinson, Paul (2019b): Mortality impact of low annual crop yields in a subsistence farming population of Burkina Faso under the current and a 1.5°C warmer climate in 2100. In *The Science of the total environment* 691, pp. 538–548. DOI: 10.1016/j.scitotenv.2019.07.027.

Bolton, Douglas K.; Friedl, Mark A. (2013): Forecasting crop yield using remotely sensed vegetation indices and crop phenology metrics. In *Agricultural and Forest Meteorology* 173, pp. 74–84. DOI: 10.1016/j.agrformet.2013.01.007.

CFS (2009): Reform of the Committee on World Food Security: Final Version. Committee on World Food Security. Rome. Available online at <http://www.fao.org/3/k7197e/k7197e.pdf>, checked on 8/1/2022.

Chintalapudi, Nalini; Angeloni, Ulrico; Battineni, Gopi; Di Canio, Marzio; Marotta, Claudia; Rezza, Giovanni et al. (2022): LASSO Regression Modeling on Prediction of Medical Terms among Seafarers' Health Documents Using Tidy Text Mining. In *Bioengineering (Basel, Switzerland)* 9 (3). DOI: 10.3390/bioengineering9030124.

Crowe, Jennifer; Moya-Bonilla, José Manuel; Román-Solano, Bryan; Robles-Ramírez, Andrés (2010): Heat exposure in sugarcane workers in Costa Rica during the non-harvest season. In *Global health action* 3. DOI: 10.3402/gha.v3i0.5619.

Dabat, Marie-Hélène; Lahmar, Rabah; Guissou, Richard (2012): La culture du niébé au Burkina Faso : une voie d'adaptation de la petite agriculture à son environnement ? In *Autrepart* N° 62 (3), pp. 95–114. DOI: 10.3917/autr.062.0095.

Doraiswamy, Paul C.; Moulin, Sophie; Cook, Paul W.; Stern, Alan (2003): Crop Yield Assessment from Remote Sensing. In *photogramm eng remote sensing* 69 (6), pp. 665–674. DOI: 10.14358/PERS.69.6.665.

V. Multi-annual yield model at the field level for subsistence farming in Burkina Faso (Chapter IV)

DPSAA (2011): Rapport General du Module Pluvial. Phase 2. Edited by Direction de la Prospective et des Statistiques Agricoles et Alimentaires (DPSAA). Ministère de l'Agriculture et de l'Hydraulique: Ouagadougou, Burkina Faso.

Eckstein, David; Künzel, Vera; Schäfer, Laura (2021): Global Climate Risk Index 2021. Who Suffers Most Extreme Weather Events? Weather-Related Loss Events in 2019 and 2000-2019. Bonn: Germanwatch Nord-Süd Initiative e.V.

FAO (2022): FAOSTAT. Available online at <https://www.fao.org/faostat/en/#data/>, checked on 8/5/2022.

FAO; IFAD; UNICEF; WFP; WHO (2021): The State of Food Security and Nutrition in the World 2021. Transforming food systems for food security, improved nutrition and affordable healthy diets for all. Rome: FAO (2021).

Funk, Chris; Peterson, Pete; Landsfeld, Martin; Pedreros, Diego; Verdin, James; Shukla, Shraddhanand et al. (2015): The climate hazards infrared precipitation with stations—a new environmental record for monitoring extremes. In *Scientific data* 2, p. 150066. DOI: 10.1038/sdata.2015.66.

Gao, Bo-cai (1996): NDWI—A normalized difference water index for remote sensing of vegetation liquid water from space. In *Remote Sensing of Environment* 58 (3), pp. 257–266. DOI: 10.1016/S0034-4257(96)00067-3.

Grace, Kathryn; Brown, Molly; McNally, Amy (2014): Examining the link between food prices and food insecurity: A multi-level analysis of maize price and birthweight in Kenya. In *Food Policy* 46, pp. 56–65. DOI: 10.1016/j.foodpol.2014.01.010.

Greve, Michelle; Lykke, Anne Mette; Blach-Overgaard, Anne; Svenning, Jens-Christian (2011): Environmental and anthropogenic determinants of vegetation distribution across Africa. In *Global Ecology and Biogeography* 20 (5), pp. 661–674. DOI: 10.1111/j.1466-8238.2011.00666.x.

Groten, S. M. E. (1993): NDVI—crop monitoring and early yield assessment of Burkina Faso. In *International Journal of Remote Sensing* 14 (8), pp. 1495–1515. DOI: 10.1080/01431169308953983.

Hasenbein, Katrin; Abdel-Rahman, Elfatih M.; Adan, Mariam; Gachoki, Stella Muthoni; King'ori, Eunice; Dubois, Thomas; Landmann, Tobias (2022): Availability of Sentinel-2-based time-series observations: which vegetation phenology-based metrics perform best for mapping farming systems in complex landscapes? In *Remote Sensing Letters* 13 (7), pp. 695–707. DOI: 10.1080/2150704X.2022.2068985.

Huang, Jianxi; Gómez-Dans, Jose L.; Huang, Hai; Ma, Hongyuan; Wu, Qingling; Lewis, Philip E. et al. (2019): Assimilation of remote sensing into crop growth models: Current status and perspectives. In *Agricultural and Forest Meteorology* 276-277, p. 107609. DOI: 10.1016/j.agrformet.2019.06.008.

Jain, Meha; Srivastava, Amit; Balwinder-Singh; Joon, Rajiv; McDonald, Andrew; Royal, Keitasha et al. (2016): Mapping Smallholder Wheat Yields and Sowing Dates Using Micro-Satellite Data. In *Remote Sensing* 8 (10), p. 860. DOI: 10.3390/rs8100860.

V. Multi-annual yield model at the field level for subsistence farming in Burkina Faso (Chapter IV)

Jin, Zhenong; Azzari, George; Burke, Marshall; Aston, Stephen; Lobell, David (2017): Mapping Smallholder Yield Heterogeneity at Multiple Scales in Eastern Africa. In *Remote Sensing* 9 (9), p. 931. DOI: 10.3390/rs9090931.

Karst, Isabel G.; Mank, Isabel; Traoré, Issouf; Sorgho, Raissa; Stückemann, Kim-Jana; Simboro, Séraphin et al. (2020): Estimating Yields of Household Fields in Rural Subsistence Farming Systems to Study Food Security in Burkina Faso. In *Remote Sensing* 12 (11), p. 1717. DOI: 10.3390/rs12111717.

Kjellstrom, Tord; Briggs, David; Freyberg, Chris; Lemke, Bruno; Otto, Matthias; Hyatt, Olivia (2016): Heat, Human Performance, and Occupational Health: A Key Issue for the Assessment of Global Climate Change Impacts. In *Annual review of public health* 37, pp. 97–112. DOI: 10.1146/annurev-publhealth-032315-021740.

Kogan, Felix; Guo, Wei; Yang, Wenze (2019): Drought and food security prediction from NOAA new generation of operational satellites. In *Geomatics, Natural Hazards and Risk* 10 (1), pp. 651–666. DOI: 10.1080/19475705.2018.1541257.

Lambert, Marie-Julie; Blaes, Xavier; Traore, Pierre Sibiry; Defourny, Pierre (2017): Estimate yield at parcel level from S2 time serie in sub-Saharan smallholder farming systems. In IEEE Staff (Ed.): 2017 9th International Workshop on the Analysis of Multitemporal Remote Sensing Images (MultiTemp). 2017 9th International Workshop on the Analysis of Multitemporal Remote Sensing Images (MultiTemp). Brugge, Belgium, 6/27/2017 - 6/29/2017. Piscataway: IEEE, pp. 1–7.

Lambert, Marie-Julie; Traoré, Pierre C. Sibiry; Blaes, Xavier; Baret, Philippe; Defourny, Pierre (2018): Estimating smallholder crops production at village level from Sentinel-2 time series in Mali's cotton belt. In *Remote Sensing of Environment* 216, pp. 647–657. DOI: 10.1016/j.rse.2018.06.036.

Lang, Morin; Mendt, Stefan; Paéz, Valeria; Gunga, Hanns-Christian; Bilo, Grzegorz; Merati, Giampiero et al. (2022): Cardiac Autonomic Modulation and Response to Sub-Maximal Exercise in Chilean Hypertensive Miners. In *Frontiers in physiology* 13, p. 846891. DOI: 10.3389/fphys.2022.846891.

Licht, Mark (2022): Flooding Impacts on Corn Growth & Development. Iowa State University. Available online at <https://crops.extension.iastate.edu/encyclopedia/flooding-impacts-corn-growth-development>, checked on 9/16/2022.

Mank, Isabel; Vandormael, Alain; Traoré, Issouf; Ouédraogo, Windpanga Aristide; Sauerborn, Rainer; Danquah, Ina (2020): Dietary habits associated with growth development of children aged < 5 years in the Nouna Health and Demographic Surveillance System, Burkina Faso. In *Nutrition journal* 19 (1), p. 81. DOI: 10.1186/s12937-020-00591-3.

Mbow, C.; Rosenzwei, C.; Barioni L. G.; Benton, T. G.; Herrero M.; Krishnapillai, M. et al. (2019): Food Security. In P. R. Shukla, J. Skea, E. Calvo Buendia, V. Masson-Delmotte, H.-O. Pörtner, Roberts D. C. et al. (Eds.): *Climate Change and Land: an IPCC special report on climate change, desertification, land*

V. Multi-annual yield model at the field level for subsistence farming in Burkina Faso (Chapter IV)

degradation, sustainable land management, food security, and greenhouse gas fluxes in terrestrial ecosystems: IPCC.

Meroni, Michele; Marinho, Eduardo; Sghaier, Nabil; Verstrate, Michel; Leo, Olivier (2013): Remote Sensing Based Yield Estimation in a Stochastic Framework — Case Study of Durum Wheat in Tunisia. In *Remote Sensing* 5 (2), pp. 539–557. DOI: 10.3390/rs5020539.

Mkhabela, M. S.; Bullock, P.; Raj, S.; Wang, S.; Yang, Y. (2011): Crop yield forecasting on the Canadian Prairies using MODIS NDVI data. In *Agricultural and Forest Meteorology* 151 (3), pp. 385–393. DOI: 10.1016/j.agrformet.2010.11.012.

Morel, Julien; Todoroff, Pierre; Bégué, Agnès; Bury, Aurore; Martiné, Jean-François; Petit, Michel (2014): Toward a Satellite-Based System of Sugarcane Yield Estimation and Forecasting in Smallholder Farming Conditions: A Case Study on Reunion Island. In *Remote Sensing* 6 (7), pp. 6620–6635. DOI: 10.3390/rs6076620.

Paliwal, Ambica; Jain, Meha (2020): The Accuracy of Self-Reported Crop Yield Estimates and Their Ability to Train Remote Sensing Algorithms. In *Front. Sustain. Food Syst.* 4, Article 25. DOI: 10.3389/fsufs.2020.00025.

Ranstam, J.; Cook, J. A. (2018): LASSO regression. In *British Journal of Surgery* 105 (10), p. 1348. DOI: 10.1002/bjs.10895.

Sahu, Subhashis; Sett, Moumita; Kjellstrom, Tord (2013): Heat exposure, cardiovascular stress and work productivity in rice harvesters in India: implications for a climate change future. In *Industrial health* 51 (4), pp. 424–431. DOI: 10.2486/indhealth.2013-0006.

Schwalbert, Rai A.; Amado, Telmo J.C.; Nieto, Luciana; Varela, Sebastian; Corassa, Geomar M.; Horbe, Tiago A.N. et al. (2018): Forecasting maize yield at field scale based on high-resolution satellite imagery. In *Biosystems Engineering* 171, pp. 179–192. DOI: 10.1016/j.biosystemseng.2018.04.020.

Sié, Ali; Louis, Valérie R.; Gbangou, Adjima; Müller, Olaf; Niamba, Louis; Stieglbauer, Gabriele et al. (2010): The Health and Demographic Surveillance System (HDSS) in Nouna, Burkina Faso, 1993-2007. In *Global health action* 3. DOI: 10.3402/gha.v3i0.5284.

Sorgho, Raissa; Mank, Isabel; Kagoné, Moubassira; Souares, Aurélia; Danquah, Ina; Sauerborn, Rainer (2020a): “We Will Always Ask Ourselves the Question of How to Feed the Family”: Subsistence Farmers’ Perceptions on Adaptation to Climate Change in Burkina Faso. In *International journal of environmental research and public health* 17 (19). DOI: 10.3390/ijerph17197200.

Sorgho, Raissa; Quiñonez, Carlos A. Montenegro; Louis, Valérie R.; Winkler, Volker; Dambach, Peter; Sauerborn, Rainer; Horstick, Olaf (2020b): Climate Change Policies in 16 West African Countries: A Systematic Review of Adaptation with a Focus on Agriculture, Food Security, and Nutrition. In *International journal of environmental research and public health* 17 (23). DOI: 10.3390/ijerph17238897.

V. Multi-annual yield model at the field level for subsistence farming in Burkina Faso (Chapter IV)

The World Bank (2020): Burkina Faso Agricultural Productivity and Food Security Project. Available online at <https://www.gafspfund.org/sites/default/files/inline-files/Burkina-Faso-Agricultural-Productivity-and-Food-Security-Project.pdf>, checked on 8/1/2022.

Tibshirani, Robert (1996): Regression Shrinkage and Selection via the Lasso. In *Journal of the Royal Statistical Society. Series B (Methodological)* 58 (1), pp. 267–288. Available online at <http://www.jstor.org/stable/2346178>, checked on 5/20/2022.

Vallentin, Claudia; Harfenmeister, Katharina; Itzerott, Sibylle; Kleinschmit, Birgit; Conrad, Christopher; Spengler, Daniel (2022): Suitability of satellite remote sensing data for yield estimation in northeast Germany. In *Precision Agric* 23 (1), pp. 52–82. DOI: 10.1007/s11119-021-09827-6.

Wang, Xi; Liu, Zhanyan; Chen, Huili (2022): Investigating Flood Impact on Crop Production under a Comprehensive and Spatially Explicit Risk Evaluation Framework. In *Agriculture* 12 (4), p. 484. DOI: 10.3390/agriculture12040484.

VI. Synthesis

1. General Discussion

Climate change-related risks are threatening rural livelihoods in Africa. Decreasing crop production, reduced livestock health or an increased malnutrition rate among children are some of the effects that have already been observed and additionally worsened by natural hazards such as floods and droughts (IPCC, 2022). Weather and climate extreme events are projected to increase even further in the future (IPCC, 2013, 2022). This will lead to growing pressure on food production (IPCC, 2022). Besides smallholder farmers, pastoralists are also set to face food insecurity as the livestock's vulnerability to drought was already evident (Djouidi et al., 2013; Masike & Ulrich, 2018). Conflicts between farmers and herders present an additional risk and have already increased over the past years as conflicts due to drought and water tensions are widespread in the Sahel (Ayana et al., 2016; Puig Cepero et al., 2021). The studies presented in this thesis address these climate change-related food security and health risks from various perspectives.

The first study (Chapter I) herein presented a regional transferable drought probability model based on remote sensing data with a spatial resolution of 1km. By doing so it addressed the gap between global drought monitoring systems with a low spatial resolution (e.g., Huntington et al., 2017; Vogt et al., 2018) and local drought models (e.g., H. Wu & Wilhite, 2004), which are not spatially transferable. Additionally, to the study area presented in Chapter I, the modeling framework was successfully transferred and applied in Chad, the Central African Republic (CAR), and Germany, which is not presented here. This further proved the capability of the model to be easily transferred to other areas and capture regional drought conditions. Other regional drought models have also been developed. Shen et al. (2019) for example developed a deep learning model based on remote sensing data that showed good results and applicability for meteorological and agricultural droughts but was only tested in the Henan Province of China. Monteleone et al. (2020) even developed a new drought index (PPVI) providing also the advantage of being spatially transferable. The index presented in their study however was only evaluated in Haiti. While the herein (Chapter I) presented modeling framework has proven to be regionally transferable it is also lacking information on soil moisture for example, which could further improve the model. Nevertheless, this regional drought probability model can furthermore be used as an early warning alert when

drought conditions begin to show up in different regions. Through the model results and its time series analyses regions at risk, which face more often and severe droughts, can be addressed to reduce their vulnerability to drought. On the other hand, areas with historically fewer droughts can be identified and used by agriculture for example. The presented drought vulnerability approach though comes with some limitations as the study only used globally available data sets and therefore missed some important information like water availability. Nevertheless, the results of this study help to monitor droughts, which is the first step toward reducing vulnerability and drought impacts.

Water availability plays a crucial role along with drought in rural livelihoods practicing agricultural or livestock farming. Therefore, the detection of surface water and surface water monitoring systems are important, also to reach the Sixth Sustainable Development Goal (SDG) (Long, 2019). Chapter III, in this context, presented a round-robin intercomparison of different EO-based surface water detection and classification algorithms. As many different algorithms can be found in the literature, this study helped to find most accurate methods – such as those that combine radar and optical data. Additionally, this study provides the information needed when searching for the right algorithm or application as for example the implementation time or computational costs also play a crucial role in choosing the right option. One of the presented algorithms of this study was also used as one of the input parameters for the environmental suitability maps for transhumance (Chapter II). Fresh water is needed for both agriculture and transhumance. For agriculture, it is mainly used for irrigation purposes, while open water locations represent resting points for the livestock herds during their seasonal movements. By performing time series analyses of the monthly surface water classifications, it can be additionally separated between temporary, seasonal, and permanent water bodies. Therefore, the surface water locations and types of water bodies can be also used as one of many information inputs when planning transhumance corridors to ensure food security and to secure livelihoods of herders. These locations can be also used to equally distribute natural water resources to minimize conflicts due to water tensions as they are already widespread in the Sahel (Ayana et al., 2016; Puig Cepero et al., 2021).

Chapter II tries to address these conflicts by analyzing the environmental suitability for transhumance based on high-resolution satellite data. Previous research on that topic is scarce. One of the very few studies for example used MODIS data with a lower spatial resolution to analyze the green-up and senescence times of forage patches (Brottem et al.,

2014; Butt et al., 2011). A landcover change analysis that revealed increasing pressure on transhumance was performed by Ellison et al. (2021), while McGuirk and Nunn (2020) provided insights on the impact of droughts on conflicts. However, all these studies did not address concepts that can directly support transhumance. Mertz et al. (2016) stated that improved information on weather and natural resources as support for transhumance needs to be passed together with multiple options for herd movements to effectively minimize conflicts. Since then, this left an open research question that this study (Chapter II) addressed. To provide multiple options, environmental monitoring systems need to be set in place and can be combined with the spatial modeling of transhumance routes. As this has not been done very often in the context of transhumance, D'Abramo et al. (2021) provide an example as they modeled paths for pastoralists in Argentina. While their results also had some limitations, they found the modeled paths to be beneficial in identifying critical areas for mobility and to develop information-based policies to regulate management strategies. While this has not been done in the Sahel outside the presented study, Chapter II goes beyond that by providing additional spatial information to reduce farmer-herder-related conflicts. By analyzing high-resolution Sentinel-2 and Sentinel-1 data, several earth observation-based products like surface water availability or rangeland productivity were derived. These products represent the basis for the monthly environmental suitability maps for transhumance, which provide timely information on favorable or unfavorable areas. The suitability maps can help herders to find forage areas that provide enough fodder for the animals and therefore directly tackle food insecurity in SSA. By adding additional information on agricultural land and its farming systems (rainfed vs. irrigated agriculture), urban areas, or protected areas, the transhumance suitability maps can also be used as a possible planning tool for agricultural expansion that also considers transhumance corridors. This could reduce conflicts if space for corridors needed by the pastoralists for their seasonal movements is granted. On top of that, theoretical optimum movement paths along the highest environmental suitability values were modeled. While these paths do not represent reality, as other aspects like traditional paths also factor in (D'Abramo et al., 2021), they can be used by local authorities for potential safe corridors with enough natural resources to improve conflict prevention. The whole framework presented in Chapter II is also regionally transferable to other regions in the Sahel as additional information or weights through expert knowledge can be incorporated into the calculation of the suitability maps, depending on

the region. In general, the findings of this study can help to tackle food insecurity by finding forage areas through the monitoring of rangeland and can lead to a decision support tool for conflict prevention measures. Additionally, the results could help the herders to continue practicing livestock farming as many of them are settling down. The analysis can furthermore be combined with drought monitoring, as drought-related conflicts are widespread (Ayana et al., 2016), to be used as an early warning system and to identify grazing land with less severe drought conditions.

The last study (Chapter IV) focused on smallholder farmers, that once were sharing their land with pastoralists during the dry season and therefore complemented each other (Ikhuoso et al., 2020). The study presents a satellite-based agricultural yield model for the major food crops in Nouna, Burkina Faso at the field level. Previous studies have for example modeled yield estimates with lower resolution data by MODIS at the country level (Petersen, 2018) or also used high-resolution Sentinel-2 data but predicted yield estimates at farm-to-community scales (Lambert et al., 2018). Yield predictions at the field level though, provide crucial information for food security and health-related issues like malnutrition (Karst et al., 2020). Therefore Karst et al. (2020) developed a high-resolution agricultural yield model based on Sentinel-2 data to provide yield estimates at the field level. While the study in this thesis follows their general methodology, it goes beyond by utilizing a unique three-year training data set. Within the study, general yield models for the main food crops based on three years of training data were developed and compared to the single-year models. This comparison was used to determine whether it is possible to generate an accurate general yield model based on multi-year training data to lower the need for cost- and labor-intensive field data (Paliwal & Jain, 2020). The results showed that the three-year models capture inter-year variability of yields and therefore can be used to predict yield estimates in upcoming years. Additionally, through incorporating a wider range of yield values over multiple years, the models were more robust against overfitting than the single year models. Yield monitoring provides the first step needed to implement adaptation measures for agriculture to tackle food insecurity under a changing climate. Widespread intercropping though is still a challenge in yield modeling as the presented model was limited to mono-cropped fields. Overall, this study addresses food security issues through yield estimates and a possible forecast of one or two months before harvest depending on the crop type. Yield estimates at the field level are also important inputs for studies on prevention measures and health care as for

example Belesova et al. (2018) analyzed annual crop yield variations in context with nutrition and health. By providing yield estimates at a higher level (field level) such studies can be enhanced by the work presented in this thesis. Additionally, the study presented in Chapter IV can be combined with the regional drought model in Chapter I and the surface water algorithm in Chapter III for the spatial analysis of the impacts of droughts and flooding and potential yield losses. Therefore, potential food security issues could be addressed before the harvest.

While addressing these climate change-related risks to food security, health, and the livelihood of rural communities in Africa from different perspectives, all these studies relate to each other in a certain way. The following section provides an overview of how the used satellite data can be combined and used efficiently. For example, the same satellite data (Sentinel-2) was used for the agricultural yield model and the environmental suitability maps for transhumance (in combination with Sentinel-1). This could enable a monitoring system for both agricultural practices, where the processed satellite data could be used effectively in multiple ways. Additionally, the drought model could also be tested on a local scale, based on yield predictions by the model presented in Chapter II, and therefore could also use Sentinel-2 data on a finer scale. Food security is dependent on vegetation health and also water availability for the planted crops and livestock, which are both impacted by droughts. All studies could therefore be combined as drought monitoring is important for both pastoralists and smallholder subsistence farmers. Surface water locations represent irrigation potential and on the other hand, are used by herders as resting points for their cattle. Floodings, their extent, and the following potential yield losses can also be observed by the surface water detection algorithm in Chapter III. In total, all this information can be combined to support both, smallholder farmers and transhumant herders. The gathered information can be used as a planning tool for agricultural expansion, the planning of corridors for the seasonal movements of pastoralists, and the protection of rangeland to achieve a peaceful coexistence between farmers and herders with enough land and natural resources for both communities. This could not only reduce conflicts but also help both farming practices to adapt to climate change and to tackle food insecurity and health risks. Furthermore, all of the presented methods are scalable. The drought model has already been proven to be regionally transferable beyond the presented study in Chapter I and could be applied to bigger areas. The environmental suitability maps could also be expanded to the whole Sahel with

regional adaptations, where future investigations of regional varying input parameters are needed. Lastly, the agricultural yield model is also scalable to all fields in the area and could be applied and tested in other sub-Saharan countries.

2. Future research

Despite the advances in all the topics presented, future research still needs to be done. The drought model presented in Chapter I for example could be tested on a local scale with high-resolution satellite data to predict drought probabilities also at the field level for agricultural purposes. It could then be investigated if the drought and crop yield model could be used in a combination to predict yields together with current drought conditions. Since drought conditions are usually long-lasting, early estimates in which direction the projected harvest of the current year trends could be made for example. The same accounts for the suitability maps, where the drought model could be used in addition to the environmental suitability maps as an input to an early warning system on conflicts. The analysis of the environmental suitability maps and the modeled theoretical optimal movement paths could also be enhanced by GPS livestock tracking data to better understand the mobility of transhumant pastoralists. Cooperation with local people could potentially lead to new rangeland possibilities or new corridors. Additionally, the analysis of multiple years could show if the inter-annual variability of the environmental suitability plays an important role in movement patterns and conflict numbers. The framework should also be tested in other areas leading to an investigation of whether the environmental suitability maps could be scaled to the whole Sahel zone. While the agricultural yield model already enhanced previous studies by using a unique three-year training data set, it should be investigated how many years of training data are needed to capture enough inter-annual variability to make long-lasting future predictions without the need of additional field sampling campaigns. Furthermore, an accurate land cover classification, which also provides information on different crop types, could be used to apply the model to all agricultural fields in the study area. This would furthermore reduce the need for GPS sampled field boundaries. An accurate classification though would be needed as currently, available cropland classifications overestimate cropland areas by up to 170% (Samasse et al., 2018). The agricultural yield models could also be used to evaluate, plan and recommend different adaptation measures. As agriculture represents a

major source of livelihood in most rural communities in SSA, adaption to climate change plays a major role to ensure food security (Kogo et al., 2021). Potential adaptation measures could lead to the enhancement of the resilience of the agricultural sector, the protection of livelihoods, and lower vulnerabilities associated with food insecurity. Possible adaptations at the farm level range from crop management practices like diversified crop cultivars or the staggering of planting dates to spread risk and mitigate against food shortages, to drought-tolerant cultivars, conservation agricultural practices like rainwater harvesting for irrigation, and soil fertility management. Diversified livelihoods like mixed crop-livestock farming systems or off-farm employment could be additional options (Kogo et al., 2021). Carr et al. (2022) state that a combination of fertilizers and adopting cropping practices are needed to enhance crop production. By combining the information on used adaptation measures with time series data of the modeled yield estimates, effective adaptation strategies can be identified.

REFERENCES

- Abdul Mumin, Y., & Abdulai, A. (2022). Informing Food Security and Nutrition Strategies in Sub-Saharan African Countries: An Overview and Empirical Analysis. *Applied Economic Perspectives and Policy*, 44(1), 364–393. <https://doi.org/10.1002/aep.13126>
- Abdulai, A., & Birachi, E. A. (2009). Choice of Coordination Mechanism in the Kenyan Fresh Milk Supply Chain. *Review of Agricultural Economics*, 31(1), 103–121. <https://doi.org/10.1111/j.1467-9353.2008.01428.x>
- Abdul-Rahaman, A., & Abdulai, A. (2020). Vertical coordination mechanisms and farm performance amongst smallholder rice farmers in northern Ghana. *Agribusiness*, 36(2), 259–280. <https://doi.org/10.1002/agr.21628>
- AGRA. (2017). African Agriculture Status Report: The Business of Smallholder Agriculture in Sub-Saharan Africa. Nairobi, Kenya. Alliance for a Green Revolution in Africa (AGRA). <https://agra.org/wp-content/uploads/2017/09/Final-AASR-2017-Aug-28.pdf>
- Aliber, M [M.], & Hart, T. G. B. (2009). Should subsistence agriculture be supported as a strategy to address rural food insecurity? *Agrekon*, 48(4), 434–458. <https://doi.org/10.1080/03031853.2009.9523835>
- Aliber, M [Michael], Swardt, C. de, Du Toit, A., Mbhele, T., & Mthethwa, T. (2005). Trends and policy challenges in the rural economy: Four provincial case studies. HSRC research monograph, 3-105. HSRC Press; Chicago. <http://www.loc.gov/catdir/enhancements/fy0643/2006376975-d.html>
- Anderegg, W. R. L., Flint, A., Huang, C.-Y., Flint, L., Berry, J. A., Davis, F. W., Sperry, J. S., & Field, C. B. (2015). Tree mortality predicted from drought-induced vascular damage. *Nature Geoscience*, 8(5), 367–371. <https://doi.org/10.1038/ngeo2400>
- Anjum, S. A., Xie, X [Xiao-yu], Wang, L., Saleem, M. F., Man, C., & Lei, W. (2011). Morphological, physiological and biochemical responses of plants to drought stress. *African Journal of Agricultural Research* (6), 2026–2032.
- Asner, G. P., Knapp, D. E., Cooper, A. N., Bustamante, M. M. C., & Olander, L. P. (2005). Ecosystem structure throughout the Brazilian Amazon from Landsat observations and automated spectral unmixing. *Earth Interactions*, 9, 1–31.
- Assefa, B. T., Chamberlin, J., Reidsma, P., Silva, J. V., & van Ittersum, M. K. (2020). Unravelling the variability and causes of smallholder maize yield gaps in Ethiopia. *Food Security*, 12(1), 83–103. <https://doi.org/10.1007/s12571-019-00981-4>
- Ayana, E. K., Ceccato, P., Fisher, J. R. B., & DeFries, R. (2016). Examining the relationship between environmental factors and conflict in pastoralist areas of East Africa. *The Science of the Total Environment*, 557-558, 601–611. <https://doi.org/10.1016/j.scitotenv.2016.03.102>

REFERENCES

- Bachmair, S., Svensson, C., Prosdocimi, I., Hannaford, J., & Stahl, K. (2017). Developing drought impact functions for drought risk management. *Natural Hazards and Earth System Sciences*, 17(11), 1947–1960. <https://doi.org/10.5194/nhess-17-1947-2017>
- Bates, B., & Kundzewicz, Z. W., Wu, S., Palutikof, J. P. (Eds.) (2008). IPCC Technical Paper 6. Climate Change and Water (1st ed.). Technical Paper of the Intergovernmental Panel on Climate Change, 5-185. IPCC Secretariat. Geneva. <http://www.ipcc.ch/pdf/technical-papers/climate-change-water-en.pdf>
- Bégué, A., Leroux, L., Soumaré, M., Faure, J.-F., Diouf, A. A., Augusseau, X., Touré, L., & Tonneau, J.-P. (2020). Remote Sensing Products and Services in Support of Agricultural Public Policies in Africa: Overview and Challenges. *Frontiers in Sustainable Food Systems*, 4, Article 58. <https://doi.org/10.3389/fsufs.2020.00058>
- Belesova, K., Gasparini, A., Sié, A., Sauerborn, R., & Wilkinson, P. (2018). Annual Crop-Yield Variation, Child Survival, and Nutrition Among Subsistence Farmers in Burkina Faso. *American Journal of Epidemiology*, 187(2), 242–250. <https://doi.org/10.1093/aje/kwx241>
- Benami, E., Jin, Z., Carter, M. R., Ghosh, A., Hijmans, R. J., Hobbs, A., Kenduiywo, B., & Lobell, D. B. (2021). Uniting remote sensing, crop modelling and economics for agricultural risk management. *Nature Reviews Earth & Environment*, 2(2), 140–159. <https://doi.org/10.1038/s43017-020-00122-y>
- Benjaminsen, T. A., & Ba, B. (2009). Farmer-herder conflicts, pastoral marginalisation and corruption: a case study from the inland Niger delta of Mali. *Geographical Journal*, 175(1), 71–81. <https://doi.org/10.1111/j.1475-4959.2008.00312.x>
- Benjaminsen, T. A., Maganga, F. P., & Abdallah, J. M. (2009). The Kilosa Killings: Political Ecology of a Farmer - Herder Conflict in Tanzania. *Development and Change*, 40(3), 423–445. <https://doi.org/10.1111/j.1467-7660.2009.01558.x>
- Berninger, A. L. (2020). Biomass Estimation in Indonesian Tropical Forests Using Active Remote Sensing Systems [Dissertation], 10-25. Ludwig-Maximilians-University, Munich.
- Bobrowsky, P. T. (2013). *Encyclopedia of Natural Hazards* (1st ed.). Springer Netherlands. <https://doi.org/10.1007/978-1-4020-4399-4>
- Bolton, D. K., & Friedl, M. A. (2013). Forecasting crop yield using remotely sensed vegetation indices and crop phenology metrics. *Agricultural and Forest Meteorology*, 173, 74–84. <https://doi.org/10.1016/j.agrformet.2013.01.007>
- Borengasser, M., Hungate, W. S., & Watkins, R. L. (2008). *Hyperspectral remote sensing: Principles and applications* (1st Edition), 1-128. CRC Press. <https://doi.org/10.1201/9781420012606>
- Bradstock, R. A., Cohn, J. S., Gill, A. M., Bedward, M., & Lucas, C. (2009). Prediction of the probability of large fires in the Sydney region of south-eastern Australia using fire weather. *International Journal of Wildland Fire*, 18(8), 932. <https://doi.org/10.1071/WF08133>

- Brottem, L., Turner, M. D., Butt, B., & Singh, A. (2014). Biophysical Variability and Pastoral Rights to Resources: West African Transhumance Revisited. *Human Ecology*, 42(3), 351–365. <https://doi.org/10.1007/s10745-014-9640-1>
- Butt, B., Turner, M. D., Singh, A., & Brottem, L. (2011). Use of MODIS NDVI to evaluate changing latitudinal gradients of rangeland phenology in Sudano-Sahelian West Africa. *Remote Sensing of Environment*, 115(12), 3367–3376. <https://doi.org/10.1016/j.rse.2011.08.001>
- Cabot, C. (2017). Climate Change and Farmer–Herder Conflicts in West Africa. In C. Cabot (Ed.), *Hexagon Series on Human and Environmental Security and Peace. Climate Change, Security Risks and Conflict Reduction in Africa* (Vol. 12, pp. 11–44). Springer Berlin Heidelberg. https://doi.org/10.1007/978-3-642-29237-8_2
- Cairns, J. E., Chamberlin, J., Rutsaert, P., Voss, R. C., Ndhlela, T., & Magorokosho, C. (2021). Challenges for sustainable maize production of smallholder farmers in sub-Saharan Africa. *Journal of Cereal Science*, 101, 103274. <https://doi.org/10.1016/j.jcs.2021.103274>
- Campbell, J., & Wynne, R. (2011). *Introduction to Remote Sensing* (R. H. Wynne, Ed.) (Fifth edition), 3–239. Guilford Publications.
- Carr, T. W., Mkuhlani, S., Segnon, A. C., Ali, Z., Zougmore, R., Dangour, A. D., Green, R., & Scheelbeek, P. (2022). Climate change impacts and adaptation strategies for crops in West Africa: a systematic review. *Environmental Research Letters*, 17(5), 53001. <https://doi.org/10.1088/1748-9326/ac61c8>
- Carrão, H., Naumann, G [Gustavo], & Barbosa, P [Paulo] (2016). Mapping global patterns of drought risk: An empirical framework based on sub-national estimates of hazard, exposure and vulnerability. *Global Environmental Change*, 39, 108–124. <https://doi.org/10.1016/j.gloenvcha.2016.04.012>
- Chang, C.-T., Wang, H.-C., & Huang, C.-Y. (2017). Assessment of MODIS-derived indices (2001–2013) to drought across Taiwan's forests. *International Journal of Biometeorology*, 62, 1–14. <https://doi.org/10.1007/s00484-017-1482-2>
- Chapman, S., Birch, C. E., Marsham, J. H., Part, C., Hajat, S., Chersich, M. F., Ebi, K. L., Luchters, S., Nakstad, B., & Kovats, S. (2022). Past and projected climate change impacts on heat-related child mortality in Africa. *Environmental Research Letters*, 17(7), 74028. <https://doi.org/10.1088/1748-9326/ac7ac5>
- Chirwa, E. W. (2006). *Commercialisation of Food Crops in Rural Malawi: Insights from the Household Survey: Working Paper No. 2006/04*, 1–21. Zomba, Malawi. University of Malawi Chancellor College, Department of Economics.
- Ciais, P [Ph], Reichstein, M., Viovy, N., Granier, A., Ogée, J., Allard, V., Aubinet, M., Buchmann, N., Bernhofer, C., Carrara, A., Chevallier, F., Noblet, N. de, Friend, A. D., Friedlingstein, P., Grünwald, T., Heinesch, B., Keronen, P., Knohl, A., Krinner, G., . . . Valentini, R. (2005). Europe-wide reduction in primary productivity caused by the heat and drought in 2003. *Nature*, 437(7058), 529–533. <https://doi.org/10.1038/nature03972>

REFERENCES

- Cloude, S. (2010). *Polarisation: Applications in remote sensing* (1st ed.). Oxford University Press.
- D'Abramo, S. L., Gonzalez, P. N., Perez, S. I., & Bernal, V. (2021). Modelling the Routes of Seasonal Transhumance Movement in North Neuquén (Patagonia). *Human Ecology*, 49(4), 415–428. <https://doi.org/10.1007/s10745-021-00246-9>
- Dabanli, I. (2018). Drought Risk Assessment by Using Drought Hazard and Vulnerability Indexes. *Natural Hazards and Earth System Sciences Discussions*, [preprint], 1–15. <https://doi.org/10.5194/nhess-2018-129>
- Detges, A. (2016). Local conditions of drought-related violence in sub-Saharan Africa. *Journal of Peace Research*, 53(5), 696–710. <https://doi.org/10.1177/0022343316651922>
- Di Wu, Qu, J. J., & Hao, X. (2015). Agricultural drought monitoring using MODIS-based drought indices over the USA Corn Belt. *International Journal of Remote Sensing*, 36(21), 5403–5425. <https://doi.org/10.1080/01431161.2015.1093190>
- Diallo, A. (1978). *Transhumance: Comportement, Nutrition et Productivité d'un Troupeau Zébus de Diafarabé*. Bamako, 37-74. Ministère de l'Education Nationale, Direction de l'Enseignement Supérieur et de la Recherche Scientifique, Centre Pédagogique Supérieur.
- Diermanse, F. L. M., Mens, M. J. P., Macian-Sorribes, H., & Schasfoort, F. (2018). A stochastic model for drought risk analysis in The Netherlands. *Hydrology and Earth System Sciences Discussions*, [preprint], 1–20. <https://doi.org/10.5194/hess-2018-45>
- Djoudi, H., Brockhaus, M., & Locatelli, B. (2013). Once there was a lake: vulnerability to environmental changes in northern Mali. *Regional Environmental Change*, 13(3), 493–508. <https://doi.org/10.1007/s10113-011-0262-5>
- Dracup, J. A., Lee, K. S., & Paulson, E. G. (1980). On the definition of droughts. *Water Resources Research*, 16(2), 297–302. <https://doi.org/10.1029/WR016i002p00297>
- ECOWAS (1998). Decision A/DEC.5/10/98. Relating to the regulations on transhumance between ECOWAS Member States. *Official Journal of the Economic Community of West African States (ECOWAS)*, 35, 3-7. <https://ecpf.ecowas.int/wp-content/uploads/2016/01/Decision-1998-English.pdf>
- Edame, G. E., Ekpenyong, A., Fonta, W. M., & Duru, E. (2011). Climate change, food security and agricultural productivity in Africa: Issues and policy directions. *International Journal of Humanities and Social Science*, 1(21), 205–233.
- Ellison, J., Brinkmann, K., Diogo, R. V. C., & Buerkert, A. (2022). Land cover transitions and effects of transhumance on available forage biomass of rangelands in Benin. *Environment, Development and Sustainability*, 22, 12276–12310. <https://doi.org/10.1007/s10668-021-01947-3>
- ESA. (2022). Sentinel-2 Overview. <https://sentinel.esa.int/web/sentinel/missions/sentinel-2/overview>
- European Space Agency. (2022). Radar Course 3. Electromagnetic Spectrum. <https://earth.esa.int/eogateway/missions/ers/radar-courses/radar-course-3>

- Fafchamps, M. (1992). Cash Crop Production, Food Price Volatility, and Rural Market Integration in the Third World. *American Journal of Agricultural Economics*, 74, 90–99.
- FAO. (2012). Factsheet: Smallholders and Family Farmers, 1-2. https://www.fao.org/fileadmin/templates/nr/sustainability_pathways/docs/Factsheet_SMALLHOLDERS.pdf
- FAO. (2021). Small family farmers produce a third of the world's food: New FAO research focuses on contributions of farmers with fewer than two hectares. FAO. <https://www.fao.org/newsroom/detail/Small-family-farmers-produce-a-third-of-the-world-s-food/en>
- FAO, IFAD, UNICEF, WFP, & WHO. (2019). *The State of Food Security and Nutrition in the World 2019. Safeguarding against economic slowdowns and downturns*, 3-118. Rome. FAO.
- FAO, IFAD, UNICEF, WFP, & WHO. (2020). *The State of Food Security and Nutrition in the World 2020*, 1-60. FAO. <https://doi.org/10.4060/ca9692en>
- FAO, & NDMC. (2008). A Review of Drought Occurrence and Monitoring and Planning Activities in the Near East Region, 1-5. <http://www.ais.unwater.org/ais/pluginfile.php/516/course/section/175/Drought%20Occurrence%20and%20Activities%20in%20the%20Near%20East.pdf>
- Farooq, M., Wahid, A., Kobayashi, N., Fujita, D., & Basra, S. M. A. (2009). Plant drought stress: effects, mechanisms and management. *Agronomy for Sustainable Development*, 29(1), 185–212. <https://doi.org/10.1051/agro:2008021>
- Fernandez-Gimenez, M. E., & Le Febre, S. (2006). Mobility in pastoral systems: Dynamic flux or downward trend? *International Journal of Sustainable Development & World Ecology*, 13(5), 341–362. <https://doi.org/10.1080/13504500609469685>
- Fernández-Giménez, M. E. (2002). Spatial and Social Boundaries and the Paradox of Pastoral Land Tenure: A Case Study From Postsocialist Mongolia. *Human Ecology*, 30(1), 49–78. <https://doi.org/10.1023/A:1014562913014>
- Flannigan, M. D., & Harrington, J. B. (1988). A Study of the Relation of Meteorological Variables to Monthly Provincial Area Burned by Wildfire Canada. *Journal of Applied Meteorology* (27), 441–452.
- Franke, J., Barradas, A. C. S., Borges, M. A., Menezes Costa, M., Dias, P. A., Hoffmann, A. A., Orozco Filho, J. C., Melchiori, A. E., & Siegert, F. (2018). Fuel load mapping in the Brazilian Cerrado in support of integrated fire management. *Remote Sensing of Environment*, 217(1), 221–232. <https://doi.org/10.1016/j.rse.2018.08.018>
- Frelat, R., Lopez-Ridaura, S., Giller, K. E., Herrero, M [Mario], Douchamps, S., Andersson Djurfeldt, A., Erenstein, O., Henderson, B., Kassie, M., Paul, B. K., Rigolot, C., Ritzema, R. S., Rodriguez, D., van Asten, P. J. A., & van Wijk, M. T. (2016). Drivers of household food availability in sub-Saharan Africa based on

REFERENCES

- big data from small farms. *Proceedings of the National Academy of Sciences of the United States of America*, 113(2), 458–463. <https://doi.org/10.1073/pnas.1518384112>
- Gao, B. (1996). NDWI—A normalized difference water index for remote sensing of vegetation liquid water from space. *Remote Sensing of Environment*, 58(3), 257–266. [https://doi.org/10.1016/S0034-4257\(96\)00067-3](https://doi.org/10.1016/S0034-4257(96)00067-3)
- Gatti, L. V., Gloor, M., Miller, J. B., Doughty, C. E., Malhi, Y., Domingues, L. G., Basso, L. S., Martinewski, A., Correia, C. S. C., Borges, V. F., Freitas, S., Braz, R., Anderson, L. O., Rocha, H., Grace, J., Phillips, O. L., & Lloyd, J. (2014). Drought sensitivity of Amazonian carbon balance revealed by atmospheric measurements. *Nature*, 506(7486), 76–80. <https://doi.org/10.1038/nature12957>
- The Global Economy. (2019). Employment in Agriculture. https://www.theglobaleconomy.com/rankings/Employment_in_agriculture/
- Grolleaud, M. (2020). Post-harvest losses: Discovering the full story. Overview of the Phenomenon of Losses During the Post-harvest System, Ch. 2-3. FAO. <https://www.fao.org/3/AC301E/AC301e00.htm>
- Groten, S. M. E. (1993). NDVI—crop monitoring and early yield assessment of Burkina Faso. *International Journal of Remote Sensing*, 14(8), 1495–1515. <https://doi.org/10.1080/01431169308953983>
- Gulácsi, A., & Kovács, F. (2015). Drought Monitoring With Spectral Indices Calculated From Modis Satellite Images In Hungary. *Journal of Environmental Geography*, 8(11-20). <https://doi.org/10.1515/jengeo-2015-0008>
- Haile, G. G., Tang, Q., Hosseini-Moghari, S.-M., Liu, X., Gebremicael, T. G., Leng, G., Kebede, A., Xu, X., & Yun, X. (2020). Projected Impacts of Climate Change on Drought Patterns Over East Africa. *Earth's Future*, 8(7), 1-23. <https://doi.org/10.1029/2020EF001502>
- Hazaymeh, K., & Hassan, Q. K. (2016). Remote sensing of agricultural drought monitoring: A state of art review. *AIMS Environmental Science*, 3(4), 604–630. <https://doi.org/10.3934/environsci.2016.4.604>
- Heim, R. R. (2002). A Review of Twentieth-Century Drought Indices Used in the United States. *Bulletin of the American Meteorological Society*, 83(8), 1149–1166. <https://doi.org/10.1175/1520-0477-83.8.1149>
- Huang, J., Gómez-Dans, J. L., Huang, H., Ma, H., Wu, Q., Lewis, P. E., Liang, S., Chen, Z., Xue, J.-H., Wu, Y., Zhao, F., Wang, J., & Xie, X [Xianhong] (2019). Assimilation of remote sensing into crop growth models: Current status and perspectives. *Agricultural and Forest Meteorology*, 276-277, 107609. <https://doi.org/10.1016/j.agrformet.2019.06.008>
- Hulme, M., & Kelly, M. (1993). Exploring the links between Desertification and Climate Change. *Environment: Science and Policy for Sustainable Development*, 35(6), 4-45. <https://doi.org/10.1080/00139157.1993.9929106>
- Huntington, J. L., Hegewisch, K. C., Daudert, B., Morton, C. G., Abatzoglou, J. T., McEvoy, D. J., & Erickson, T. (2017). *Climate Engine: Cloud Computing and Visualization of Climate and Remote Sensing*

- Data for Advanced Natural Resource Monitoring and Process Understanding. *Bulletin of the American Meteorological Society*, 98(11), 2397–2410. <https://doi.org/10.1175/BAMS-D-15-00324.1>
- IFC. (2013). *Working with Smallholders: A Handbook for Firms Building Sustainable Supply Chains*, 1-117. The World Bank. <https://www.ifc.org/wps/wcm/connect/647f85fc-6ad7-4315-aad8-4967075a304b/Handbook+-+Working+with+Smallholders.pdf?MOD=AJPERES&CVID=ka-TX8j>
- Ikhuoso, O. A., Adegbeye, M. J., Elghandour, M., Mellado, M., Al-Dobaib, S. N., & Salem, A. (2020). Climate change and agriculture: The competition for limited resources amidst crop farmers-livestock herding conflict in Nigeria - A review. *Journal of Cleaner Production*, 272(1), 1–9. <https://doi.org/10.1016/j.jclepro.2020.123104>
- Inter-resaux. (2017). Pastoral livestock farmin in Sahel and West Africa: 5 preconceptions put to the test, 3-17. <https://www.inter-reseaux.org/wp-content/uploads/int-17-broch-pastoralismeuk-bd.pdf>
- IPCC (2007). *Climate Change 2007: Synthesis Report. Contribution of Working Groups I, II and III to the Fourth Assessment Report of the Intergovernmental Panel on Climate Change* [Core Writing Team, Pachauri, R.K., Reisinger, A. (eds.)], pp. 104. IPCC. Geneva. Switzerland
- IPCC. (2013). Summary for Policymakers.4-29. In IPCC (Ed.), *Climate Change 2013: The Physical Science Basis. Contribution of Working Group I to the Fifth Assessment Report of the Intergovernmental Panel on Climate Change*. Cambridge University Press.
- IPCC. (2014). Summary for policymakers, 1-32. In: *Climate Change 2014: Impacts, Adaptation, and Vulnerability. Part A: Global and Sectoral Aspects. Contribution of Working Group II to the Fifth Assessment Report of the Intergovernmental Panel on Climate Change*. Cambridge, UK, New York, NY, USA. Cambridge University Press.
- IPCC. (2022). Summary for Policymakers. In H.-O. Pörtner, D. C. Roberts, M. Tignor, E. S. Poloczanska, K. Mintenbeck, A. Alegria, M. Craig, S. Langsdorf, S. Löschke, V. Möller, A. Okem, & B. Rama (Eds.), *Climate Change 2022: Impacts, Adaptation and Vulnerability.: Contribution of Working Group II to the Sixth Assessment Report of the Intergovernmental Panel on Climate Change* (pp. 3–33). Cambridge University Press.
- Jayne, T. S., Mather, D., & Mghenyi, E. (2010). Principal Challenges Confronting Smallholder Agriculture in Sub-Saharan Africa. *World Development*, 38(10), 1384–1398. <https://doi.org/10.1016/j.worlddev.2010.06.002>
- Jayne, T. S., Yamano, T., Weber, M. T., Tschirley, D., Benfica, R., Chapoto, A., & Zulu, B. (2003). Smallholder income and land distribution in Africa: implications for poverty reduction strategies. *Food Policy*, 28(3), 253–275. [https://doi.org/10.1016/S0306-9192\(03\)00046-0](https://doi.org/10.1016/S0306-9192(03)00046-0)
- Jones, H. G., & Corlett, J. E. (1992). Current topics in drought physiology. *The Journal of Agricultural Science*, 119(03), 291–296. <https://doi.org/10.1017/S0021859600012144>

REFERENCES

- Jones, S. (2005). Transhumance Re-Examined. *The Journal of the Royal Anthropological Institute*, 11(2), 357–359.
- Kaptué, A. T., Prihodko, L., & Hanan, N. P. (2015). On greening and degradation in Sahelian watersheds. *Proceedings of the National Academy of Sciences of the United States of America*, 112(39), 12133–12138. <https://doi.org/10.1073/pnas.1509645112>
- Karst, I. G., Mank, I., Traoré, I., Sorgho, R., Stückemann, K.-J., Simboro, S., Sié, A., Franke, J., & Sauerborn, R. (2020). Estimating Yields of Household Fields in Rural Subsistence Farming Systems to Study Food Security in Burkina Faso. *Remote Sensing*, 12(11), 1717. <https://doi.org/10.3390/rs12111717>
- Ketiem, P., Makeni, P., M., Maranga, E., K., & Omondi, P., A. (2017). Integration of climate change information into drylands crop production practices for enhanced food security: A case study of Lower Tana Basin in Kenya. *African Journal of Agricultural Research*, 12(20), 1763–1771. <https://doi.org/10.5897/AJAR2016.11506>
- Kim, D.-G., Grieco, E., Bombelli, A., Hickman, J. E., & Sanz-Cobena, A. (2021). Challenges and opportunities for enhancing food security and greenhouse gas mitigation in smallholder farming in sub-Saharan Africa. A review. *Food Security*, 13(2), 457–476. <https://doi.org/10.1007/s12571-021-01149-9>
- Kogan, F. N. (1997). Global Drought Watch from Space. *Bulletin of the American Meteorological Society*, 78(4), 621–636. [https://doi.org/10.1175/1520-0477\(1997\)078%3C0621:GDWFS%3E2.0.CO;2](https://doi.org/10.1175/1520-0477(1997)078%3C0621:GDWFS%3E2.0.CO;2)
- Kogo, B. K., Kumar, L., & Koech, R. (2021). Climate change and variability in Kenya: a review of impacts on agriculture and food security. *Environment, Development and Sustainability*, 23(1), 23–43. <https://doi.org/10.1007/s10668-020-00589-1>
- Lambert, M.-J., Blaes, X., Traore, P. S., & Defourny, P. (June 2017). Estimate yield at parcel level from S2 time serie in sub-Saharan smallholder farming systems. In I. Staff (Ed.), 2017 9th International Workshop on the Analysis of Multitemporal Remote Sensing Images (MultiTemp) (pp. 1–7). IEEE. <https://doi.org/10.1109/Multi-Temp.2017.8035204>
- Lambert, M.-J., Traoré, P. C. S., Blaes, X., Baret, P., & Defourny, P. (2018). Estimating smallholder crops production at village level from Sentinel-2 time series in Mali's cotton belt. *Remote Sensing of Environment*, 216, 647–657. <https://doi.org/10.1016/j.rse.2018.06.036>
- Le Toan, T., Beaudoin, A., Riom, J., & Guyon, D. (1992). Relating forest biomass to SAR data. *IEEE Transactions on Geoscience and Remote Sensing*, 30(2), 403–411. <https://doi.org/10.1109/36.134089>
- Leonhardt, M. (2017). Regional Policies and Response to Manage Pastoral Movements within the ECOWAS Region: Study on behalf of the International Organization for Migration (IOM), within the framework of the Support to Free Movement of Persons and Migration in West Africa (FMM West Africa) Project, 1-21. Abuja, Nigeria. https://publications.iom.int/system/files/pdf/iom_ecowas_pastoralism.pdf

- Leroux, L., Castets, M., Baron, C., Escorihuela, M.-J., Bégué, A., & Lo Seen, D. (2019). Maize yield estimation in West Africa from crop process-induced combinations of multi-domain remote sensing indices. *European Journal of Agronomy*, 108, 11–26. <https://doi.org/10.1016/j.eja.2019.04.007>
- Lidzhegu, Z., & Kabanda, T. (2022). Declining land for subsistence and small-scale farming in South Africa: A case study of Thulamela local municipality. *Land Use Policy*, 119, 106–170. <https://doi.org/10.1016/j.landusepol.2022.106170>
- Lillesand, T. M., & Kiefer, R. W [Raphl W.]. (1994). *Remote sensing and image interpretation* (3rd ed.), pp. 750. John Wiley & Sons, Inc.
- Lillesand, T. M., Kiefer, R. W [Ralph W.], & Chipman, J. W. (2004). *Remote sensing and image interpretation* (5th ed.), pp. 761. Wiley.
- Lillesand, T. M., Kiefer, R. W [Ralph W.], & Chipman, J. W. (2015). *Remote sensing and image interpretation* (Seventh edition), pp. 736. Wiley.
- Lo, C. P. (1987). *Applied remote sensing*, pp. 393. New York.
- Loeper, W. von, Musango, J., Brent, A., & Drimie, S. (2016). Analysing challenges facing smallholder farmers and conservation agriculture in South Africa: A system dynamics approach. *South African Journal of Economic and Management Sciences*, 19(5), 747–773. <https://doi.org/10.4102/sajems.v19i5.1588>
- Long, J. (2019). The United Nations' 2030 Agenda for Sustainable Development and the Impact of the Accounting Industry, 5-27. Honors College Theses. https://digitalcommons.pace.edu/honorscollege_theses/260/
- Maass Wolfenson, K. D. (2013). Coping with the food and agriculture challenge: smallholders' agenda: Preparations and outcomes of the 2012 United Nations Conference on Sustainable Development (Rio+20), 15-30. Rome. https://www.fao.org/fileadmin/templates/nr/sustainability_pathways/docs/Coping_with_food_and_agriculture_challenge__Smallholder_s_agenda_Final.pdf
- Maisongrande, P., Kuhlmann, J., Boulet, G., Lobo, A., Henry, P., & Hafeez, M. (2007). ENSO Impact on the Australian vegetation. A satellite diagnostic from 1998-2006, 2583–2589.
- Marty, A. (1993). La gestion de terroirs et les éleveurs : un outil d'exclusion ou de négociation? *Revue Tiers Monde*, 134, 327–344.
- Masike, S., & Ulrich, P. (2018). Vulnerability of traditional beef sector to drought and the challenges of climate change: The case of Kgatleng District, Botswana. *Journal of Geography and Regional Planning*, 1(1), 12–18. <http://www.academicjournals.org/JGRP>
- McDowell, N. G., & Allen, C. D. (2015). Darcy's law predicts widespread forest mortality under climate warming. *Nature Climate Change*, 5(7), 669–672. <https://doi.org/10.1038/nclimate2641>
- McGuirk, E., & Nunn, N. (2021). Transhumant Pastoralism, Climate Change, and Conflict in Africa. Working Paper 28243, 1-41 Cambridge, MA. <https://doi.org/10.3386/w28243>

REFERENCES

- Mertz, O., Rasmussen, K., & Rasmussen, L. V. (2016). Weather and resource information as tools for dealing with farmer–pastoralist conflicts in the Sahel. *Earth System Dynamics*, 7(4), 969–976. <https://doi.org/10.5194/esd-7-969-2016>
- Mishra, A. K., & Singh, V. P. (2010). A review of drought concepts. *Journal of Hydrology*, 391(1-2), 202–216. <https://doi.org/10.1016/j.jhydrol.2010.07.012>
- Moeletsi, M. E., Mellaart, E., Mpandeli, N. S., & Hamandawana, H. (2013). The Use of Rainfall Forecasts as a Decision Guide for Small-scale Farming in Limpopo Province, South Africa. *The Journal of Agricultural Education and Extension*, 19(2), 133–145. <https://doi.org/10.1080/1389224X.2012.734253>
- Monteleone, B., Bonaccorso, B., & Martina, M. (2020). A joint probabilistic index for objective drought identification: the case study of Haiti. *Natural Hazards and Earth System Sciences*, 20(2), 471–487. <https://doi.org/10.5194/nhess-20-471-2020>
- Motta, P., Porphyre, T., Hamman, S. M., Morgan, K. L., Ngwa, V. N., Tanya, V. N., Raizman, E., Handel, I. G., & Bronsvort, B. M. (2018). Cattle transhumance and agropastoral nomadic herding practices in Central Cameroon. *BMC Veterinary Research*, 14(1), 214. <https://doi.org/10.1186/s12917-018-1515-z>
- Mpandeli, S., & Maponya, P. (2014). Constraints and Challenges Facing the Small Scale Farmers in Limpopo Province, South Africa. *Journal of Agricultural Science*, 6(4), 135. <https://doi.org/10.5539/jas.v6n4p135>
- Myers, S. S., Smith, M. R., Guth, S., Golden, C. D., Vaitla, B., Mueller, N. D., Dangour, A. D., & Huybers, P. (2017). Climate Change and Global Food Systems: Potential Impacts on Food Security and Undernutrition. *Annual Review of Public Health*, 38, 259–277. <https://doi.org/10.1146/annurev-publhealth-031816-044356>
- Naumann, G [G.], Barbosa, P [P.], Garrote, L., Iglesias, A., & Vogt, J. (2014). Exploring drought vulnerability in Africa: an indicator based analysis to be used in early warning systems. *Hydrology and Earth System Sciences*, 18(5), 1591–1604. <https://doi.org/10.5194/hess-18-1591-2014>
- Niang, I., Ruppel, O. C., Abdrabo, M. A., Essel, A., Lennard, C., Padgham, J., & Urquhart, P. (2014). Africa. In: *Climate change 2014: Impacts, Adaptation and Vulnerability. Contribution of Working Group II to the Fifth Assessment Report of the Intergovernmental Panel on Climate Change*, 1199-1265. Cambridge. Cambridge University Press.
- OECD/SWAC. (2014). *An atlas of the Sahara-Sahel: Geography, economics and security. West African studies*, 22-219. OECD Publishing. <https://doi.org/10.1787/9789264222359-en>
- Olsen, V. M., Fensholt, R., Olofsson, P., Bonifacio, R., van Butsic, D., Druce, D., Ray, D., & Prishchepov, A. V. (2021). The impact of conflict-driven cropland abandonment on food insecurity in South Sudan revealed using satellite remote sensing. *Nature Food*, 2(12), 990–996. <https://doi.org/10.1038/s43016-021-00417-3>

- Oteros-Rozas, E., Martín-López, B., González, J. A., Plieninger, T., López, C. A., & Montes, C. (2014). Socio-cultural valuation of ecosystem services in a transhumance social-ecological network. *Regional Environmental Change*, 14(4), 1269–1289. <https://doi.org/10.1007/s10113-013-0571-y>
- Overpeck, J., & Udall, B. (2010). Climate change. Dry times ahead. *Science (New York, N.Y.)*, 328(5986), 1642–1643. <https://doi.org/10.1126/science.1186591>
- Owringi, M. A., Adamowski, J., Rahnamaei, M., Mohammadzadeh, A., & Sharifan, R. A. (2011). Drought Monitoring Methodology Based on AVHRR Images and SPOT Vegetation Maps. *Journal of Water Resource and Protection*, 03(05), 325–334. <https://doi.org/10.4236/jwarp.2011.35041>
- Painter, T., Sumberg, J., & Price, T. (1994). Your 'Terroir' and my 'Action Space': implications of differentiation, mobility and diversification for the 'Approche Terroir' in Sahelian West Africa. *Africa: Journal of the African Institute*, 64(4), 447–464. <https://doi.org/10.2307/1161368>
- Paliwal, A., & Jain, M. (2020). The Accuracy of Self-Reported Crop Yield Estimates and Their Ability to Train Remote Sensing Algorithms. *Frontiers in Sustainable Food Systems*, 4, Article 25. <https://doi.org/10.3389/fsufs.2020.00025>
- Penning de Vries, F. W. T., & Djitéye, M. A. (1982). La productivité des pâturages sahéliens: une étude des sols, des végétations et de l'exploitation de cette ressource naturelle, pp. 525. Centre for Agricultural Publishing and Documentation.
- Petersen, L. (2018). Real-Time Prediction of Crop Yields From MODIS Relative Vegetation Health: A Continent-Wide Analysis of Africa. *Remote Sensing*, 10(11), 1726. <https://doi.org/10.3390/rs10111726>
- Puig Cepero, O., Desmidt, S., Detges, A., Tondel, F., van Ackern, P., Foong, A., & Volkholz, J. (2021). Climate Change, Development and Security in the Central Sahel, 9-75. Cascades Report. London. <https://www.cascades.eu/wp-content/uploads/2021/06/Climate-Change-Development-and-Security-in-the-Central-Sahel.pdf>
- Reddy, A. R., Chaitanya, K. V., & Vivekanandan, M. (2004). Drought-induced responses of photosynthesis and antioxidant metabolism in higher plants. *Journal of Plant Physiology*, 161(11), 1189–1202. <https://doi.org/10.1016/j.jplph.2004.01.013>
- Rezaei, E. E., Ghazaryan, G., González, J., Cornish, N., Dubovyk, O., & Siebert, S. (2021). The use of remote sensing to derive maize sowing dates for large-scale crop yield simulations. *International Journal of Biometeorology*, 65(4), 565–576. <https://doi.org/10.1007/s00484-020-02050-4>
- Richards, J. A. (2009). Remote sensing with imaging radar. *Signals and communication technology*, 1-320. ISBN: 978-3-642-02020-9. Springer.
- Roberts, D. A., Dennison, P. E [P. E.], Gardner, M. E., Hetzel, Y., Ustin, S. L., & Lee, C. T. (2003). Evaluation of the potential of hyperion for fire danger assessment by comparison to the airborne visible/infrared imaging spectrometer. *IEEE Transactions on Geoscience and Remote Sensing*, 41(6), 1297–1310. <https://doi.org/10.1109/TGRS.2003.812904>

REFERENCES

- Roberts, D. A., Smith, M. O., & Adams, J. B. (1993). Green vegetation, nonphotosynthetic vegetation, and soils in AVIRIS data. *Remote Sensing of Environment*, 44(2-3), 255–269. [https://doi.org/10.1016/0034-4257\(93\)90020-X](https://doi.org/10.1016/0034-4257(93)90020-X)
- Rojas, O., Vrieling, A., & Rembold, F. (2011). Assessing drought probability for agricultural areas in Africa with coarse resolution remote sensing imagery. *Remote Sensing of Environment*, 115(2), 343–352. <https://doi.org/10.1016/j.rse.2010.09.006>
- Saigusa, N., Ichii, K., Murakami, H., Hirata, R., Asanuma, J., Den, H., Han, S.-J., Ide, R., Li, S.-G., Ohta, T., Sasai, T., Wang, S.-Q., & Yu, G.-R. (2010). Impact of meteorological anomalies in the 2003 summer on Gross Primary Productivity in East Asia. *Biogeosciences*, 7(2), 641–655. <https://doi.org/10.5194/bg-7-641-2010>
- Salack, S., Klein, C., Giannini, A., Sarr, B., Worou, O. N., Belko, N., Bliefernicht, J., & Kunstman, H. (2016). Global warming induced hybrid rainy seasons in the Sahel. *Environmental Research Letters*, 11(10), 104008. <https://doi.org/10.1088/1748-9326/11/10/104008>
- Saleska, S. R., Didan, K., Huete, A. R., & da Rocha, H. R. (2007). Amazon forests green-up during 2005 drought. *Science (New York, N.Y.)*, 318(5850), 612. <https://doi.org/10.1126/science.1146663>
- Samasse, K., Hanan, N., Tappan, G., & Diallo, Y. (2018). Assessing Cropland Area in West Africa for Agricultural Yield Analysis. *Remote Sensing*, 10(11), 1785. <https://doi.org/10.3390/rs10111785>
- Schaaf, C., & Wang, Z. (2015). MCD43A3 MODIS/Terra+Aqua BRDF/Albedo Daily L3 Global - 500m V006. <https://doi.org/10.5067/MODIS/MCD43A3.006>
- Scheffran, J., Link, P. M., & Schilling, J. (2019). Climate and Conflict in Africa, 1-38. *Oxford Research Encyclopedia of Climate Science*. Oxford University Press. <https://doi.org/10.1093/acrefore/9780190228620.013.557>
- Schowengerdt, R. A. (2007). *Remote sensing: Models and methods for image processing* (3rd ed.), 1-45. Academic Press.
- Serdeczny, O., Adams, S., Baarsch, F., Coumou, D., Robinson, A., Hare, W., Schaeffer, M., Perrette, M., & Reinhardt, J. (2017). Climate change impacts in Sub-Saharan Africa: from physical changes to their social repercussions. *Regional Environmental Change*, 17(6), 1585–1600. <https://doi.org/10.1007/s10113-015-0910-2>
- Shackleton, R. T. (2020). Loss of land and livelihoods from mining operations: A case in the Limpopo Province, South Africa. *Land Use Policy*, 99(14), 104825. <https://doi.org/10.1016/j.landusepol.2020.104825>
- Shah, M., Fischer, G., & van Velthuisen, H. (2008). *Food security and sustainable agriculture: The challenges of climate change in Sub-Saharan Africa*. Laxenburg: International Institute for Applied System Analysis.

- Sheahan, M., & Barrett, C. B. (2017). Ten striking facts about agricultural input use in Sub-Saharan Africa. *Food Policy*, 67, 12–25. <https://doi.org/10.1016/j.foodpol.2016.09.010>
- Sheffield, J., & Wood, E. F. (2007). Characteristics of global and regional drought, 1950–2000: Analysis of soil moisture data from off-line simulation of the terrestrial hydrologic cycle. *Journal of Geophysical Research*, 112(D17), 7449. <https://doi.org/10.1029/2006JD008288>
- Shen, R., Huang, A., Li, B., & Guo, J. (2019). Construction of a drought monitoring model using deep learning based on multi-source remote sensing data. *International Journal of Applied Earth Observation and Geoinformation*, 79, 48–57. <https://doi.org/10.1016/j.jag.2019.03.006>
- Shettima, A. G., & Tar, U. A. (2008). Farmer-Pastoralist Conflict in West Africa: Exploring the Causes and Consequences. *Information, Society and Justice*, 1.2, 163–184. <https://doi.org/10.3734/isj.2008.1205>
- Sivakumar, M. V. K., Motha, R. P., Wilhite, D. A. [Donald A.], & Wood, D. A. (2011). Agricultural Drought Indices. Proceedings of the WMO/UNISDR Expert Group Meeting on Agricultural Drought Indices, 2-172. WMO Expert Group Meeting, 2-4 June 2010 in Murcia (Spain).
- Steinbach, S., Cornish, N., Franke, J., Hentze, K., Strauch, A., Thonfeld, F., Zwart, S. J., & Nelson, A. (2021). A New Conceptual Framework for Integrating Earth Observation in Large-scale Wetland Management in East Africa. *Wetlands*, 41(7), 5256. <https://doi.org/10.1007/s13157-021-01468-9>
- Sultan, B., Defrance, D., & Iizumi, T. (2019). Evidence of crop production losses in West Africa due to historical global warming in two crop models. *Scientific Reports*, 9(1), 12834. <https://doi.org/10.1038/s41598-019-49167-0>
- Tannehill, I. R. (1949). Drought-Its Causes and Effects. *Journal of the South African Forestry Association*, 18(1), 83–84. <https://doi.org/10.1080/03759873.1949.9630655>
- Thompson, J., Millstone, E., Scoones, I., Ely, A., Marshall, F., Shah, E., & Stagl, S. (2007). Agri-food System Dynamics: pathways to sustainability in an era of uncertainty: STEPS Working Paper 4, 1-54. Brighton: STEPS Centre.
- Thorlakson, T., & Neufeldt, H. (2012). Reducing subsistence farmers' vulnerability to climate change: evaluating the potential contributions of agroforestry in western Kenya. *Agriculture & Food Security*, 1(15). <https://doi.org/10.1186/2048-7010-1-15>
- Thornton, P. K., van de Steeg, J., Notenbaert, A., & Herrero, M. [M.] (2009). The impacts of climate change on livestock and livestock systems in developing countries: A review of what we know and what we need to know. *Agricultural Systems*, 101(3), 113–127. <https://doi.org/10.1016/j.agry.2009.05.002>
- Tilman, D., Balzer, C., Hill, J., & Befort, B. L. (2011). Global food demand and the sustainable intensification of agriculture. *Proceedings of the National Academy of Sciences of the United States of America*, 108(50), 20260–20264. <https://doi.org/10.1073/pnas.1116437108>
- Touré, I., Ickowicz, A., Wane, A., Garba, I., Gerber, P., & Eds. (2012). Atlas of trends in pastoral systems in the Sahel – Atlas des évolutions des systèmes pastoraux au Sahel, 2-32. Centre for International

REFERENCES

Cooperation in Agricultural Research for Development (CIRAD); United Nations Food and Agriculture Organization of the United Nations (FAO).

Towler, E., & Lazrus, H. (2016). Increasing the usability of drought information for risk management in the Arbuckle Simpson Aquifer, Oklahoma. *Climate Risk Management*, 13, 64–75. <https://doi.org/10.1016/j.crm.2016.06.003>

Turner, M. D., Ayantunde, A. A., Patterson, K. P., & Patterson III, E. D. (2011). Livelihood transitions and the changing nature of farmer-herder conflict in Sahelian West Africa. *The Journal of Development Studies*, 47(2), 183–206. <https://doi.org/10.1080/00220381003599352>

United Nations. (2017). *World Population Prospects: Data Booklet - 2017 Revision*, 1-18. https://population.un.org/wpp/Publications/Files/WPP2017_DataBooklet.pdf

van Dijk, A. I. J. M., Beck, H. E., Crosbie, R. S., Jeu, R. A. M. de, Liu, Y. Y., Podger, G. M., Timbal, B., & Viney, N. R. (2013). The Millennium Drought in southeast Australia (2001-2009): Natural and human causes and implications for water resources, ecosystems, economy, and society. *Water Resources Research*, 49(2), 1040–1057. <https://doi.org/10.1002/wrcr.20123>

van Ittersum, M. K., van Bussel, L. G. J., Wolf, J., Grassini, P., van Wart, J., Guilpart, N., Claessens, L., Groot, H. de, Wiebe, K., Mason-D'Croz, D., Yang, H., Boogaard, H., van Oort, P. A. J., van Loon, M. P., Saito, K., Adimo, O., Adjei-Nsiah, S., Agali, A., Bala, A., . . . Cassman, K. G. (2016). Can sub-Saharan Africa feed itself? *Proceedings of the National Academy of Sciences of the United States of America*, 113(52), 14964–14969. <https://doi.org/10.1073/pnas.1610359113>

Verhoeven, G. J. (2017). The reflection of two fields – Electromagnetic radiation and its role in (aerial) imaging. *AARGnews*, 55, 3-18. <https://doi.org/10.5281/zenodo.3534245>

Vermote, E. F., Roger, J. C., & Ray, J. P. (2015). *MODIS Surface Reflectance User's Guide - Collection 6*, 4-29. MODIS Land Surface Reflectance Science Computing Facility. https://lpdaac.usgs.gov/documents/306/MOD09_User_Guide_V6.pdf

Vogt, J. V., Naumann, G [G.], Masante, D., Spinoni, J., Cammalleri, C., Erian, W., Pischke, F., Pulwarty, R., & Barbosa, P [P.]. (2018). *Drought Risk Assessment. A conceptual Framework*, 5-49. (JRC113937, EUR 29464 EN). Publications Office of the European Union. Luxembourg. ISBN 978-92-79-97469-4, doi:10.2760/057223

Westerling, A. L., Hidalgo, H. G., Cayan, D. R., & Swetnam, T. W. (2006). Warming and earlier spring increase western U.S. Forest wildfire activity. *Science (New York, N.Y.)*, 313(5789), 940–943. <https://doi.org/10.1126/science.1128834>

Wiggins, S. (2009). *Can the smallholder model deliver poverty reduction and food security for a rapidly growing population in Africa?* FAC Working Paper No. 08, 4-18. Brighton. Future Agricultures Consortium Secretariat. https://opendocs.ids.ac.uk/opendocs/bitstream/handle/20.500.12413/2338/FAC_Working%20_Paper_08.pdf

- Wilhite, D. A [Donald A.] (Ed.). (2000a). *Drought: A global assessment* (2nd ed.), pp. 752. Routledge. <https://doi.org/10.4324/9781315830896>
- Wilhite, D. A [Donald A.]. (2000b). *Preparing for Drought: A Methodology*. In D. A. Wilhite (Ed.), *Routledge hazards and disasters series. Drought: A global assessment* (2nd ed., pp. 89–104). Routledge.
- Wilhite, D. A [Donald A.], Svoboda, M. D., & Hayes, M. J. (2007). Understanding the complex impacts of drought: A key to enhancing drought mitigation and preparedness. *Water Resources Management*, 21(5), 763–774. <https://doi.org/10.1007/s11269-006-9076-5>
- Wu, H., & Wilhite, D. A [D. A.] (2004). An Operational Agricultural Drought Risk Assessment Model for Nebraska, USA. *Natural Hazards*, 33, 1–21.
- Wu, J., Zhou, L [Lei], Liu, M., Zhang, J [Jie], Leng, S., & Diao, C. (2012). Establishing and assessing the Integrated Surface Drought Index (ISDI) for agricultural drought monitoring in mid-eastern China. *International Journal of Applied Earth Observation and Geoinformation*, 23, 397–410. <https://doi.org/10.1016/j.jag.2012.11.003>
- Yebra, M., Dennison, P. E [Philip E.], Chuvieco, E., Riaño, D., Zylstra, P., Hunt, E. R., Danson, F. M., Qi, Y., & Jurdao, S. (2013). A global review of remote sensing of live fuel moisture content for fire danger assessment: Moving towards operational products. *Remote Sensing of Environment*, 136(11), 455–468. <https://doi.org/10.1016/j.rse.2013.05.029>
- Zhang, Y., Peng, C., Li, W., Fang, X., Zhang, T., Zhu, Q., Chen, H [Huai], & Zhao, P. (2013). Monitoring and estimating drought-induced impacts on forest structure, growth, function, and ecosystem services using remote-sensing data: recent progress and future challenges. *Environmental Reviews*, 21(2), 103–115. <https://doi.org/10.1139/er-2013-0006>
- Zhao, M., & Running, S. W. (2010). Drought-induced reduction in global terrestrial net primary production from 2000 through 2009. *Science (New York, N.Y.)*, 329(5994), 940–943. <https://doi.org/10.1126/science.1192666>
- Zhou, L [Lei], Wu, J., Zhang, J [Jianhui], Leng, S., Liu, M., Zhang, J [Jie], Zhao, L., Zhang, F., & Shi, Y. (2013). The Integrated Surface Drought Index (ISDI) as an Indicator for Agricultural Drought Monitoring: Theory, Validation, and Application in Mid-Eastern China. *IEEE Journal of Selected Topics in Applied Earth Observations and Remote Sensing*, 6(3), 1254–1262. <https://doi.org/10.1109/JSTARS.2013.2248077>
- Zhou, L [Leocadia], Kori, D. S., Sibanda, M., & Nhundu, K. (2022). An Analysis of the Differences in Vulnerability to Climate Change: A Review of Rural and Urban Areas in South Africa. *Climate*, 10(8), 118. <https://doi.org/10.3390/cli10080118>
- Zhou, L [Liming], Tian, Y., Myneni, R. B., Ciaï, P [Philippe], Saatchi, S., Liu, Y. Y., Piao, S., Chen, H [Haishan], Vermote, E. F., Song, C., & Hwang, T. (2014). Widespread decline of Congo rainforest greenness in the past decade. *Nature*, 509(7498), 86–90. <https://doi.org/10.1038/nature13265>

REFERENCES

Zhuo, W., Huang, J., Zhang, X., Sun, H., Zhu, D., Su, W., Zhang, C., & Liu, Z. (2016). Comparison of five drought indices for agricultural drought monitoring and impacts on winter wheat yields analysis. *Agro-Geoinformatics (Agro-Geoinformatics)*, 2016 Fifth International Conference on 18-20 July 2016, 1–6. <https://doi.org/10.1109/Agro-Geoinformatics.2016.7577702>

STATEMENT AND DECLARATION OF HONOR

Eidesstattliche Erklärung

Ich versichere hiermit an Eides statt, dass die vorgelegte Dissertation von mir selbständig und ohne unerlaubte Hilfe angefertigt ist.

München, den.....17.10.2022..... Maximilian Schwarz.....

(Unterschrift)

Erklärung

Hiermit erkläre ich, *

- dass die Dissertation nicht ganz oder in wesentlichen Teilen einer anderen Prüfungskommission vorgelegt worden ist.
- dass ich mich anderweitig einer Doktorprüfung ohne Erfolg **nicht** unterzogen habe.
- ~~dass ich mich mit Erfolg der Doktorprüfung im Hauptfach
und in den Nebenfächern
..... bei der Fakultät für
..... der
(Hochschule/Universität) unterzogen habe.~~
- ~~dass ich ohne Erfolg versucht habe, eine Dissertation einzureichen oder mich der
Doktorprüfung zu unterziehen.~~

München, den17.10.2022..... Maximilian Schwarz.....

(Unterschrift)

*) Nichtzutreffendes streichen

CURRICULUM VITAE

Personal Information

Name	Maximilian Schwarz
Date of Birth	April 19 th 1994
Place of Birth	Munich, Germany
email	schwarz@rssgmbh.de

Education

2019 - 2022 Doctoral student at the Ludwig-Maximilians-University (LMU), Munich, and research associate and project engineer at the Remote Sensing Solutions GmbH, Munich,

Doctoral thesis title: *“Satellite based monitoring of environmental related factors affecting rural livelihoods, food security and health risks in Africa”*

2016 - 2019 Studies of Climate and Environmental Sciences at the University of Augsburg,

Graduation: Master of Science,

Master thesis title: *“Satellitenbasierte Modellierung globaler Dürrewahrscheinlichkeiten und Dürreerisiken” (Satellite based modelling of global drought probabilities and drought risk)*

2012 - 2016 Studies of Geography and Meteorology at the Ludwig-Maximilians-University, Munich,

Graduation: Bachelor of Science,

Bachelor thesis title: *“Auswertung satellitenbasierter Langzeitreihen zur Stickstoffdioxidbelastung globaler Megacities” (Evaluation of satellite-based long-term series on nitrogen dioxide pollution of global megacities)*

2005 - 2012 Gymnasium Fürstenried West, München,

Graduation: Abitur

Publications in peer-reviewed journals:

Schwarz, M., Landmann, T., Cornish, N., Wetzel, K.-F., Siebert, S., Franke, J. (2020) A Spatially Transferable Drought Hazard and Drought Risk Modeling Approach Based on Remote Sensing Data. *Remote Sensing*, 12(2), 237. DOI: <https://doi.org/10.3390/rs12020237>.

Schwarz, M., Landmann, T., Jusselme, D., Zambrano, E., Danzeglocke, J., Siebert, F., Franke, J. (2022) Assessing the Environmental Suitability for Transhumance in Support of Conflict Prevention in the Sahel. *Remote Sensing*, 14(5), 1109. DOI: <https://doi.org/10.3390/rs14051109>.

Tottrup, C., Druce, D., Meyer, R.P., Christensen, M., Riffler, M., Dulleck, B., Rastner, P., Jupova, K., Sokoup, T., Haag, A., Cordeiro, M.C.R., Martinez, J.-M., Franke, J., **Schwarz, M.**, Vanthof, V., Liu, S., Zhou, H., Marzi, D., Rudiyanto, R., Thompson, M., Hiestermann, J., Alemohammad, H., Masse, A., Sannier, C., Wangchuk, S., Schumann, G., Giustarini, L., Hallows, J., Markert, K., Paganini, M. (2022) Surface Water Dynamics from Space: A Round Robin Intercomparison of Using Optical and SAR High-Resolution Satellite Observations for Regional Surface Water Detection. *Remote Sensing*, 14(10), 2410. DOI: <https://doi.org/10.3390/rs14102410>.

Schwarz, M., Ouédraogo, A. W., Traoré, I., Müller, C., Sié, A., Barteit, S., Mank, I., Siebert, F., Sauerborn, R., Franke, J. (2022) Satellite-based multi-annual yield models for major food crops at the household field level for nutrition and health research: a case study from the Nouna HDSS, Burkina Faso. *International Journal of Applied Earth Observation and Geoinformation*. Manuscript submitted for publication.

Impact factor of the journals:

Journal	5-year Impact Factor	Impact Factor 2022
Remote Sensing	5.786 (2021)	5.349
International Journal of Applied Earth Observation and Geoinformation	6.488 (2021)	7.672

Oral presentations and posters:

Schwarz, M., Landmann, T., Cornish, N., Wetzel, K.-F., Siebert, S., Franke, J. (2021) A Spatially Transferable Drought Hazard and Drought Risk Modeling Approach Based on Remote Sensing Data. *EGU General Assembly. 4th – 8th May 2020. Virtual Event.*

Schwarz, M., Landmann, T., Cornish, N., Wetzel, K.-F., Siebert, S., Franke, J. (2021) A Spatially Transferable Drought Hazard and Drought Risk Modeling Approach Based on Remote Sensing Data. *6th Nile Basin Development Forum. 22nd February – 29th April 2021. Virtual Event.*

Lohberger, S., **Schwarz, M. (Presenter)**, Kuonath, K., Roßberg, T., Abdel-Rahman, E., Mudereri, B., Kimathi, E., Senagi, K., Landmann, T., Franke, J., Schmitt, M., Siegert, F. (2022) Analysis of Sentinel-2 timeseries densification for crop type assessment in sub-Saharan Africa. *ESA Living Planet Symposium 23 – 27th May 2022 at Bonn, Germany.*

Schaefer, A., **Schwarz, M.**, Jusselme, D. Rossner, G., Franke, J. (2022) Earth Observation-Based Monitoring of Environmental-Related Transhumance Patterns in Support of Conflict Prevention in the Sahel. *Webinar 20th April 2022.*